Dayna Nielson
Editor

Geographic Information Systems (GIS)

Techniques, Applications and Technologies

NOVA

GEOGRAPHIC INFORMATION SYSTEMS (GIS)

TECHNIQUES, APPLICATIONS AND TECHNOLOGIES

ENGINEERING TOOLS, TECHNIQUES AND TABLES

Additional books in this series can be found on Nova's website under the Series tab.

Additional e-books in this series can be found on Nova's website under the e-book tab.

GEOGRAPHIC INFORMATION SYSTEMS (GIS)

TECHNIQUES, APPLICATIONS AND TECHNOLOGIES

DAYNA NIELSON
EDITOR

Copyright © 2014 by Nova Science Publishers, Inc.

For permission to use material from this book please contact us:
Telephone 631-231-7269; Fax 631-231-8175
Web Site: http://www.novapublishers.com

NOTICE TO THE READER

Additional color graphics may be available in the e-book version of this book.

Published by Nova Science Publishers, Inc. † New York

CONTENTS

PREFACE

Geographic Information Systems (GIS) has emerged as a powerful tool for solving complex problems due to its capabilities to integrate, visualize, and analyze geographic data across domains and disciplines. An urgent need for balancing fundamental human needs with ecological capacity has compelled us to utilize geospatial technology for the sustainable future. This volume showcases GIS applications in transportation, water management, agriculture, seismology, archeology, and community development. Part I highlights different GIS techniques: network analysis to optimize solid waste collection; spatio-temporal analysis of phone-call records to explore human mobility; spatial interpolation and overlay to assess water quality. Part II illustrates GIS applications in planning for future and reconstructing the past: how GIS is used to aid asset-building processes for sustainable community development, enhance the transport planner's toolbox through visualization of transportation activities, and determine likely land pathways to transport megaliths. Part III exhibits integration of geospatial technology (GIS, GPS, remote sensing) for environmental monitoring and sustainable management of natural resources. Geospatial technologies are coupled with modeling to automate the pesticide spraying process and forecast pests; analyze the spatial patterns of seismicity; identify flood prone areas and assess groundwater potential. This volume provides a snapshot of current developments in the geospatial fields, and will be valuable to academics and practitioners in geography, planning, and sustainability science.

Table of Contents
I. Techniques

Chapter 1 - The management of solid waste in the City of Altoona, Pennsylvania, USA is unique in that a department responsible for the design and collection of solid waste is non-existent. Further, the city does not contract any particular company for collection. Rather, the city utilizes a freedom to choose system where residents can choose from any one of twenty companies for their solid waste collection. The Intermunicipal Relations Committee (IRC) is the local organization responsible for overseeing and enforcing waste and recycling regulations within the city. The freedom to choose system is highly inefficient. The sheer number of companies operating within the city makes it difficult for the IRC to enforce regulations as each company's customers are scattered throughout the city. On any particular day, several collection trucks could be driving through the same neighborhood. This result in lengthy collection times and unnecessary miles traveled. This research utilizes the GIS spatial analyst vehicle routing problem (VRP) function to model the current freedom to choose collection system and determine total collection times, miles traveled, and number of trips to the transfer station. Two alternative collection scenarios are proposed and modeled. Results indicate the inefficiencies associated with current collection when compared to two

alternate scenarios. A controlled collection scenario reduces miles traveled by 70 percent and collection time by 44 percent. Greater savings of 76 and 50 percent occur with the improved efficiency scenario. Results confirm the wasteful miles traveled and man hours worked, thus demonstrating the need for city officials to implement changes that would bring savings to collection companies, customers, and the environment.

Chapter 2 - Sustainability—balancing fundamental human needs with ecological resilience—has been embraced as an overarching policy goal. And communities have been called to participate in the process of attaining that ideal. Community-based organizations (CBOs) can benefit from using GIS in building community assets and developing sustainability initiatives. However, GIS, has not been used widely for these purposes in CBOs yet. In this chapter, the author illustrates how geographic information (such as maps) can be useful in community development drawing from community GIS projects, and explain how theories of sustainability and spatial thinking can be utilized in community-based efforts towards sustainability. CBOs can monitor and assess community sustainability by (a) organizing relevant indicators into the capital framework (theories of sustainability), and (b) exploring spatial distribution, interactions, relationships, and changes in sustainability-related issues using GIS (spatial thinking). The framework presented here can be applied to promote effective use of geospatial tools for community sustainability.

Chapter 3 - The spatio-temporal visualization and analysis techniques play important roles in geographic information systems and knowledge discovery. In this research, the authors introduce three spatio-temporal analytical techniques including spatio-temporal visualization, space-time kernel density estimation, and spatio-temporal autocorrelation-analysis for exploring human mobility and urban structure patterns. These spatio-temporal analytics can help to answer questions like: Where are the spatio-temporal hotspots of human activities? How to explore spatio-temporal patterns in three-dimension GIS? Experiments are conducted using a large scale of phone-call detailed records in urban space.

Expeditions on the spatio-temporal functionality and techniques contribute to the GIScience community for the future development of Space-Time GIS; and more broadly, it has potential to be applied in other disciplines, e.g., environmental, urban and social sciences.

Chapter 4 - Crop Protection is besides agricultural engineering, plant breeding and fertilization an indispensable part of modern agriculture. Still, even though not substitutable, there is a downside. The use of pesticides and therefore the application of chemicals into the environment bear substantial

risks for both nature as well as human beings. Geographical Information Systems (GIS) can help making crop protection more sustainable. This chapter describes two possible examples of how GIS is used by the Central Institute for Decision Support Systems (DSS) in Crop Protection (German acronym ZEPP) to support farmers in Germany with their pesticide applications.

The first example describes a DSS that creates machine readable application maps using a web based GIS application. Application maps offer the possibility to automate the pesticide spraying process. The maps created by the DSS include legal buffer zones to water bodies and protected terrestric structures, e.g. hedges, where spraying of pesticides is prohibited. Provided that a tractor with Global Navigation Satellite System (GNSS) and a pesticide sprayer with section control is available, an automated application is possible. Once the sprayer moves into an area of the field that is a buffer zone, the respective section is switched of automatically. The DSS helps farmers to comply with legal rules and to prevent the contamination of the environment.

The second example describes how GIS is used in pest forecast systems. With the help of GIS it is possible to obtain results with higher accuracy for disease and pest simulation models. Pest forecast systems developed by ZEPP use GIS to interpolate geographical factors like temperature and relative humidity such getting meteorological data for every km^2 in Germany. The interpolated data and the parameter precipitation, taken by radar measured precipitation data are used as input for the simulation models. The output of these models is presented as spatial risk maps in which areas of maximum risk of the disease outbreak, infection pressure or pest appearances are displayed. The modern presentation methods of GIS lead to an easy interpretation and further-more promote the use of the system by farmers.

Chapter 5 - The spatial pattern of urban transport activities has become a focus of recent academic enquiry and planning policy concerns. This is largely driven by the rapid urban growth and increased transport pressure in major international cities and the demand for improved transport infrastructure and services. This article focuses on the application of Geographical Information Systems (GIS) techniques in exploring geographic patterns of major urban transport activities at both urban and regional scales. The first part in this article develops GIS methods to analyse geographical pattern of commuting transport at a regional level. The methodology uses multiple spatial O-D transport data at regional geographical units and applies disaggregated spatial techniques to identify spatial patterns of commuting distance and traffic flow and the changes in these patterns over time. The second part of the article demonstrates the application of GIS techniques in exploring tempo-spatial

patterns of public bicycle trips in urban areas. A GIS technique called flow map is developed to explore tempo-spatial patterns of public bicycle under different calendar event and climatic conditions. The paper demonstrates how the results from the GIS techniques may form part of an evidence base for the transport planner with the potential to inform future development to enhance the efficiency, and how the application of GIS techniques will enhance the planner's toolbox whilst responding the transport planning issues.

Chapter 6 - Limited evidence has led to considerable debate about land routes and methods to move megaliths chosen for sculpture by prehistoric societies. The current research is investigating the question using Geographic Information System (GIS) to determine likely land pathways to transport megaliths over 100 kilometres in Mesoamerica by Preclassic Olmec society. Access was restricted and the terrain included floodplains, seasonal rivers and extensive swamps. Analyses were derived from digitised survey maps using slope gradient tools initially from ARCVIEW 3.2 and finally ARC10. Although compatibility issues arose with this combination as the authors describe, tools of both versions provided a starting point between stones' source from which to then define a pathway across the challenging terrain.

Chapter 7 - This chapter presents a tool for studying natural disasters, such as seismic and impact events, using real data from Catalogs of earthquakes (EC) and Earth's impact structures (EISC) [1]. It is ENDDB [2] (the Earth's Natural Disasters DataBase), a new version of a geoinformation system (GIS). The algorithms implemented in ENDDB allow visualizing a selected part of a current catalog in a pseudo-3D background map. With its mathematical support, the ENDDB system can plot frequency dependences of magnitudes or sizes (crater diameters) of events from various samples, as well as other distributions of integrated parameters in time and space, or their relationships with one another.

The expert earthquake database (EEDB). There existed an earlier GIS version, an EEDB system [3], which had a wide range of seismological applications. It was gradual transition from a conventional GIS (originally created by the authors) to a high-tech expert system updated by including successively various mathematical methods for earthquake data processing, new parameters of seismic regime, and advanced representation tools. The realized algorithms [4] allow the user to compute and visualize maps and diagrams of seismicity parameters (slope of magnitude-recurrence curves, seismic quiescence, earthquake density, etc.), to reveal clustering of events, and remove aftershocks. Modifications and versions of GIS-EEDB for

different geodynamic regions [5] are illustrated in the chapter with case studies of seismic anomalies.

Visualization and analysis of EISC data. Applying the EEDB system software to EISC data [1] (in the new GIS system, called Earth's Impact Structures Catalog (EISC) [6]) allows gaining insights into spatial patterns of impact structures. In addition, the shapes of craters are constrained using a shaded relief model based on NASA data arrays of SRTM (Shuttle Radar Topography Mission) and ASTER GDEM (Global Digital Elevation Model), and the technology of digital mapping. Thus typical elements of impact craters morphology have been systematized and can be used as indicators of the crater origin [7].

Gravity data and new applications of GIS ENDDB. The reliability of geomorphically expressed diagnostic indicators of crater shapes was checked against geophysical features revealed by gravity data, namely, the presence of tail-shaped negative gravity anomalies produced by large impact craters. By mapping gravity anomalies, using their shaded relief model and "Global marine gravity" data (V18.1), the authors can verify the gravity patterns associated with impact cratering and check their validity as tracers of bolide trajectories. Gravity data also have seismological implications and can be used to identify seismic blocks, lineaments, and other structures detectable with GIS ENDDB mathematical tools and thus to analyze the spatial patterns of seismicity.

Chapter 8 - Water quality evaluation is an overall process of evaluating physical, chemical and biological nature of water in relation to natural quality, human effects and intended uses particularly uses which may affect human health and the health of the ecosystem itself. Interpretation of enormous water quality data in a convenient manner for visual inspection is an important but often underestimated or omitted step in a water quality evaluation program. Recently, need of modern approaches and tools for interpreting water quality is emphasized for efficient water quality management. Geographic Information System (GIS), with an ability of capturing, storing, analyzing, manipulating, retrieving and displaying spatial data, has emerged as a powerful tool for decision-making in several areas including environmental field. This chapter aims at highlighting the role of GIS in synthesising, compiling, presenting and interpreting chemical data of both surface and ground waters. Firstly, few relevant fundamental terms and process of water quality evaluation are defined and/or described. Thereafter, the chapter contains theoretical procedure for applying GIS to assess spatial change or variability in water quality by characterizing extent and patterns of

contamination. In general, a water quality monitoring network consists of a group of point locations with known chemical attributes of water. GIS helps converting the point values into areal information through spatial interpolation.

Hence, an overview of spatial interpolation techniques is provided, together with the methodologies for employing geostatistical modelling (kriging) and inverse distance weighting techniques and for computing spatial statistics (mean, median, standard deviation and coefficient of variation). The major application of GIS in past groundwater studies has been for assessing groundwater vulnerability.

Therefore, the concept of groundwater vulnerability along with its historical perspective is described and different GIS-based overlay and index methods used for groundwater vulnerability assessment are summarized. Methodologies for applying different GIS methods in evaluating the groundwater vulnerability are illustrated through flowcharts.

The major tools for describing groundwater vulnerability in GIS framework include DRASTIC, modified DRASTIC, DRAMIC, GOD, AVI, SINTACS, EPIK, GLA, PI and COP.

Furthermore, the development of GIS-based water quality index for evaluating water quality is discussed. Finally, combined use of GIS and multivariate statistical analysis techniques in delineating water quality zones is discussed. It is concluded that GIS is a promising geospatial tool which offers efficient framework for sustainable management of freshwater resources.

Chapter 9 - Flood hazard has become the most frequent natural disaster and has provoked global responsiveness. Due to its devastating nature, many lives have been lost, natural ecology degraded, disrupted social and economic activities and destroyed properties worth billions of dollars. Such over-whelming effect is felt more in urban centers especially those located in coastal regions. Estimating flood risk was a complex multi-faceted problem due to the level and amount of knowledge in systematic disciplines such as geography, geomorphology, climatology, hydrology, hydraulic engineering and urban planning that need to be combined.

Presently, this problem has been surmount with the introduction of geographic information system (GIS) which when properly integrated with remote sensing technique, has the capability to transform the manner and way of modeling flood risk and extracting spatial information to support decision making processes.

The substantive objective of this chapter is to examine the formidability of using high resolution remote sensing data and GIS techniques to assess and identify flood prone areas before occurrence in Lagos State-large coastal city

of Nigeria. The GIS-based flood risk methodology so-developed for a littoral urban region proved to be helpful in extracting flood prone areas based on elevation from SRTM digital elevation model (DEM) and proximity to source of hazard. Such risk areas were then classified into magnitudes of potential risk and five classes were identified-very high, high, moderate, low and very low. This extracted flood mask was further used to estimate the proportion of agricultural land and urban land likely to be affected in the event of a flood episode. To support grass root policy, the areal calculation was disaggregated into local government area territory. Furthermore, land use/ land cover data of the study region was extracted from Landsat image using a supervised classification method based on maximum likelihood algorithm. The extracted potential flood risk masks were overlaid on the land cover data so as to assess the likely impact of flood on the various land uses-agricultural land use and urban land use. In the same way, the identified flood prone area masks were entered into Google earth engine for the purpose of quick visual impression and mapping the flood vulnerable areas by neighborhood and road infrastructures. The five-class vulnerability feature was then overlaid on the local administrative map data loaded with the projected population figure of the study region. From here the vulnerable population was estimated by Local Government Area (LGA). The results of the study show that GIS technique is a formidable tool for flood risk analysis, mitigation and pre-hazard planning. This can be seen from the series of thematic maps that were generated which were used to develop a large GIS-assisted database. It is evident that the database so-generated will facilitate flood risk management and provide an effective framework that will support policy formulation.

Chapter 10 - Detection of favorable zones for sustainable groundwater supply in terrains underlying by crystalline rocks needs to integrate two approaches: Remote Sensing and GIS. Landsat ETM+ images are processed by using ERDAS IMAGINE 9.2 and ASTER images by ArcGIS 9.3. Parameters controlling groundwater accumulation such as: rainfall, lineaments, lithology, slopes, and drainage network are evaluated in terms of 5 potential classes namely: very good potentials, good; moderate; low and very low potential and integrated in the GIS tool. The resulting map shows that 5% of the study area presents a very good groundwater potential and this part is mainly concentrated in the south part of the study area and on the MTZ, very low potentials constitute 13% of the area located essentially in the north part of the study area and particularly on granites. Combination of results generated by the GIS with NDVI and the borehole productivities shows that, generally good groundwater potentials are well correlated with high vegetal activities in

dry season except in areas affected by forest fires which are frequent in the region. High borehole productivities (11.5 -30m^3/H) are observed in zone presenting high groundwater potential resulting from the GIS tool and very low borehole productivities (0.6-2.5m^3/H) are shown in the north part of the study area corresponding to the low and very low groundwater potentials. Good, moderate and low groundwater potentials represent respectively 18, 33 and 30% of the total investigated surface area. This integrated approach combining Use of RS, GIS and hydrodynamic parameters such as borehole productivities can contribute to improve Knowledge of groundwater resources investigation in context of hard rock aquifers of the south-eastern of Senegal and can reduce the high rates of failed wells. So, RS and GIS can be used as an efficient tools for assessing groundwater potential at large scale.

Chapter 1

APPLICATION OF VEHICLE ROUTING PROBLEM FOR SUSTAINABLE WASTE COLLECTION: CASE STUDY OF ALTOONA, PENNSYLVANIA

Timothy J. Dolney[*]

The Pennsylvania State University, Altoona College
Ivyside Park, Altoona, Pennsylvania, US

ABSTRACT

The management of solid waste in the City of Altoona, Pennsylvania, USA is unique in that a department responsible for the design and collection of solid waste is non-existent. Further, the city does not contract any particular company for collection. Rather, the city utilizes a freedom to choose system where residents can choose from any one of twenty companies for their solid waste collection. The Intermunicipal Relations Committee (IRC) is the local organization responsible for overseeing and enforcing waste and recycling regulations within the city. The freedom to choose system is highly inefficient. The sheer number of companies operating within the city makes it difficult for the IRC to enforce regulations as each company's customers are scattered throughout the city. On any particular day, several collection trucks could be driving through the same neighborhood. This result in lengthy

---

[*] Phone: 1-814-949-5454, Email: tjd15@psu.edu.

collection times and unnecessary miles traveled. This research utilizes the GIS spatial analyst vehicle routing problem (VRP) function to model the current freedom to choose collection system and determine total collection times, miles traveled, and number of trips to the transfer station. Two alternative collection scenarios are proposed and modeled. Results indicate the inefficiencies associated with current collection when compared to two alternate scenarios. A controlled collection scenario reduces miles traveled by 70 percent and collection time by 44 percent. Greater savings of 76 and 50 percent occur with the improved efficiency scenario. Results confirm the wasteful miles traveled and man hours worked, thus demonstrating the need for city officials to implement changes that would bring savings to collection companies, customers, and the environment.

INTRODUCTION

The issue of sustainability has garnered a lot of attention in the past few years. This is primarily due to concerns about the unintended social, economic, and environmental consequences of rapid population growth, economic growth, and consumption of our natural resources (US EPA, 2012). Unsustainable solid waste disposal and collection is one area of concern that is pushing the environment towards potential risk. Solid waste collection is regularly performed by trucks with diesel engines that average 5.1 miles per gallon (mpg) and use 220 gallons of fuel per year during idling (Gaines et al., 2006). The trucks emit several emissions to the environment that are proportional to both route time (including stops) and route distance. Routing strategies are central to minimizing emissions. A poorly designed urban solid waste collection system has enormous impact on labor, operational and transport costs, and on society in general due to road contamination and negative effects on public health and the environment (Arribas et al., 2010). Fortunately, geographic information system (GIS) technology exists to assist decision makers in improving their waste management strategies.

GIS technology has been applied to many different areas of waste collection to assist in the design and execution of successful waste management systems. These include GIS to assist in the overall design of waste collection systems (Pandey et al., 2012; Kanchanabhan et al., 2011;

Arribas et al., 2010; Zheng and Pan, 2010; Karadimas and Loumos, 2008; Lopez et al., 2008; Salhofer et al., 2007; Sharholy et al., 2007;Ghose et al., 2006) and siting of landfills (Yesilnacar et al., 2012; Nazari et al., 2012; Vasilijevic et al., 2012; Sumathi et al., 2008; Kontos et al., 2003; Leao et al., 2001). The most notable application of GIS for waste collection is route optimization to improve routing strategies and reduce vehicle emissions.

Jovicic et al. (2011) used ArcGIS network analyst functionality to estimate the potential for reducing fuel consumption and thus the emission of carbon dioxide (CO_2) through the communal vehicles route optimization. Results indicated an approximate annual savings of 1,700 miles for one collection vehicle within the City of Kragujevac, Serbia. Further, the most fuel-economical route was extracted and compared with the original route, and with the routes extracted from criterions concerning the traffic time and shortest distance. According to available information for the City of Kragujevac and the results from this study, it was estimated that the total savings could be 20% in costs and the associated emissions. Bhambulkar (2010) also used ArcGIS network analyst to identify best routing for municipal solid waste that cannot be collected by standard waste collection trucks, due to size and other prohibitive obstacles in the municipality of Nagpur, India. Optimal routing was cost effective and less time consuming when compared with the existing route with a monthly savings of 14%.

Tavares et al. (2009) used GIS 3D route modeling software for waste collection and transportation to optimize driving routes and minimize fuel consumption in the city of Praia, Cape Verde. Their model accounted for road inclination and vehicle weight. Using ArcGIS software, the most fuel economical route was calculated, yielding cost savings of 8-12% for fuel consumption even though the most economical route was 1.8% longer that the shortest route. Karamidas et al. (2008) performed research using GIS to optimize the number and position of the waste bins in the Municipality of Athens, Greece. The number of waste bins decreased from 162 to 112 (30% reduction). This reduction also presents great savings in energy usedduring waste collection. Apaydin and Gonullu (2008) applied a shortest path model to Trabzon City, Turkey in order to optimize solid waste collection and minimize emissions. The optimized route decreased the route distance and route time by 24.6% and 44.3% for nine routes in 26 districts. Further, emissions of (CO_2), nitrogen oxide (NOx), hydrocarbons (HC), carbon monoxide (CO), and particulate matter (PM) decreased 831.4, 12.8, 1.2, 0.4, and 0.7 grams per route.

Karadimas et al. (2007) employed the ant colony system algorithm for monitoring, simulating, testing, and optimizing costs for different scenarios of solid waste management systems. A GIS tool supported the municipal solid waste management system by using parameters such as waste bin locations, road network topology, and population density. Further research is required to test the proposed model on an extended area. Apaydin and Gonullu (2007) published results of their research in route optimization for solid waste collection in the city of Trabzon, Turkey. The city of Trabzon is as large as the city of Kragujevac, Serbia and has 185,000 inhabitants. For 39 districts in the city, a shortest path model was used in order to optimize solid waste collection and hauling processes, as minimum cost was aimed. The Route View ProTM software as an optimization tool was used for that purpose and the success was around 4−59% for distance and 14−65% for time. The total benefit was 24% in total costs or about 18.014 $ monthly. Lakshumi et al. (2006) presented the results of study for the city of Chennai, India which has a population of 4.5 million. The aim was to determinate the optimal route for solid waste collection and to compare the cost of new optimized and present routes. The commercial software package ArcGIS was used with savings in length of 41.5% in day shift and 44% in night shift for one particular route.

One of the earliest applications of GIS for waste collection vehicle routing was performed by Chang et al. (1997). They applied a revised multi-objective programing model associated with GIS spatial analysis capabilities to analyze and visualize optimal paths, and allocate vehicles and labor within a waste collection network. They were able to analyze alternate solid waste collection strategies under different planning scenarios to evaluate different planning scenarios in the network to quickly gain a general understanding of the impact of policy changes in the waste collection system. Among the authors conclusions were that GIS will increasingly be relied on to support solid waste management issues in the future.

Other studies have relied on other methodologies aside from GIS functionality. Kim et al. (2006) and Sahoo et al. (2005) each report on the development of a waste collection vehicle routing problem with time windows (VRPTW) algorithm intended to reduce the number of vehicles and total traveling time. The VRP is typically utilized in the waste collection industry to reduce the number of vehicles and total traveling time. The authors also considered route compactness since a solution with better route compactness has fewer crossovers among routes. Their algorithm was successfully implemented and deployed for real life commercial waste collection problems at Waste Management (WM), Inc., the leading provider of comprehensive

waste management services in North America. Specifically, the algorithm was embedded in WasteRoute (Sahoo et. al, 2005), a comprehensive enterprise-wide web-based route management application that takes into account WM's specific routing considerations. WasteRoute was deployed across North America beginning March 2003 and immediately brought savings. The authors illustrated one example of savings in the city of Elgin, Illinois, USA. Before WasteRoute, the city required ten 9-hour routes with a productivity of 57.06 yards/hour. By utilizing Waste Route, the city now requires nine 9-hour routes and increased its productivity to 63.40 yards/hour. The authors estimate that WM could reduce 984 routes over the subsequent year for a savings of $18US million. In the end, WasteRoute reduced WM's operational costs by organizing routes to minimize overlap and thereby reduce the number of vehicles WM needed to serve its customers, and by sequencing stops along a route to make the best use of fuel, driver schedules, and disposal trips.

Ghiani et al. (2005) conducted a study of solid waste collection in the municipality of Castrovillari, Italy in an attempt to reduce the amount of money allocated to waste collection. The focus was on residential collection routes that were manually formed by a supervisor. They modeled waste collection as an arc routing problem (ARP); designing a set of vehicle routes traversing a specified subset of required arcs and/or edges of a graph, with or without side constraints. The objective is to minimize the total distance traveled by the vehicles. GIS was unavailable to the city for the research resulting in the authors having to collect data about travel times on the road network and estimate solid waste daily levels for each street. The outcome was a computerized system developed in Visual C language that eliminated overtime and achieved an annual reduction of approximately 8 percent in total cost. More detailed costs were generated that corresponded to three collection vehicles: a reduction in distance traveled equal to 10.6% (i.e. 18 km/day) equivalent to a savings of 7000 Euro per year; a reduction in work time equal to 13.5% (i.e. 2 h 10 s); overtime elimination, equivalent to an additional saving of 5000 Euro per year; and a better workload distribution among vehicles. These improvements were primarily the result of better allocation of containers to vehicles. The authors feel that if applied by other Italian municipalities, this kind of analysis could save hundreds of millions of Euro every year.

Simonetto and Borenstein (2007) developed a decision support system (DSS) called SCOLDSS to support the operational planning of solid waste collection. The system specifically supports the following tasks: reducing the amount of solid waste destined to the landfill; assuring a waste input

percentage at each sorting unit; assigning vehicles to collection trips; defining their route; and estimating the work capacity (productivity) of sorting units, in relation to the waste arrival and processing (separation). The system basically aids the solid waste collection operational management through the generation, analysis, and assessment of possible operational scenarios for this type of collection. The system was developed using the Borland Delphi environment and the commercial software Arena to carry out the simulations. Results from the system were validated using real data from the solid waste collection in the city of Porto Alegre, Brazil. By using the system, it is possible to obtain a mean reduction of 8.82% in the distance (43.8 km less) to be covered by the collection vehicles and a reduction of 17.89% in the weekly number of trips. The distances covered weekly would decrease 262.8 km, leading to an annual reduction estimated at 13,665 km. Concerning the number of trips, the current mean is 27.3 trips per day (163.8 per week). Using SCOLDSS, the average number of trips would be 134.9 weekly trips (reduction of 17.89%), which would result in an annual reduction of 1502 trips. These results outperform the current operation planning deployed. The authors feel the system has great potential as an effective support tool to be used in real world solid waste systems.

El-Hamouz (2008) demonstrates how advantageous the application of a logistical management strategy can be used for rescheduling municipal solid waste collection systems, reallocating street solid waste containers, and minimizing vehicle routing. The author used real field data to test the methods in Tubas, West Bank. The application was tested by the private sector for 1 month. The new system proved to be successful in terms of greater efficiency, coverage and quality of service. The total cost of collection was found to be US$21 per ton of solid waste. These reduced collection costs to a level that is socially acceptable (US$3.75/family/month) as well as economically and environmentally sound.

The City of Altoona, Pennsylvania, USA and its solid waste collection system, or lack thereof, is a perfect candidate for a GIS-based solid waste collection strategy. The current collection system is highly inefficient with too many solid waste companies and too many miles traveled. This article presents the application of GIS for residential solid waste collection in the City of Altoona to demonstrate the system's inefficiencies and also present alternate scenarios that improve the collection process. Information for this research specific to solid waste collection in the city was obtained from several sources including: the Executive Director of the Intermunicipal Relations Committee (IRC), the Director of the Blair County Department of Solid Waste and

Recycling (defunct as of 10/2012), Gannett Fleming, Inc. Technical Assistance Study, solid waste collection companies, and City of Altoona residents (including the author). The IRC is a council of governments (COG) consisting of the City of Altoona and other surrounding townships and boroughs. It was initially established as the Intermunicipal Recycling Committee in 1990 to address the needs of member municipalities related to recycling and composting required by Pennsylvania Act 101 of 1988. The name was changed in 1997 to reflect a desire by the member municipalities to undertake other intermunicipal issues. They are currently the only organization that enforces regulations related to solid waste collection in the city.
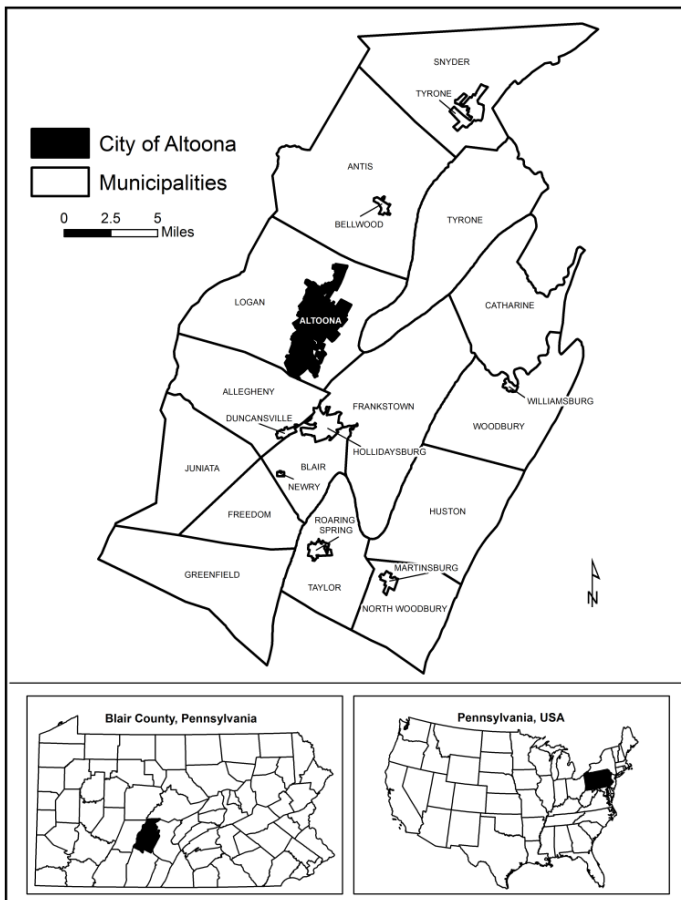

Figure 1. City of Altoona, Pennsylvania, USA.

2. STUDY AREA

2.1. Solid Waste Collection

The City of Altoona, Pennsylvania is one of twenty-four municipalities located in Blair County (Figure 1). It has a population of 46,320 with 19,473 households spread across 9.91 square miles of land (US Census Bureau, 2012). The city's inefficient solid waste collection problem emanates from a "freedom to choose" system where residents choose their own solid waste company because the city has no department of solid waste management nor do they contract a single company for waste collection. As a result, 20 independent companies operate within the city collecting solid waste and recyclables. Their customer base is not concentrated in one particular area of the city but rather is scattered throughout the city. As a result, any particular neighborhood could have several separate companies collecting solid waste throughout the day. Such a system has a trickledown effect as the sheer number of companies leads to a number of environmental and policy issues. The only positive aspect of solid waste collection within the city is that residents are required to participate in curbside recycling of newspaper, other mixed paper, cardboard, glass, plastic bottles, aluminum cans, and steel cans. Companies working within the city are required to properly recycle these materials and adhere to ordinances set by the city and IRC. It's worth noting that the only municipality in Blair County that contracts their solid waste collection to a single company is the borough of Tyrone. Not coincidentally, monthly costs in Tyrone are more than $8US cheaper per household than the average cost in the City of Altoona.

2.2. Inefficient Solid Waste Collection

In 2006, Gannett Fleming, Inc. performed a study that evaluated recycling and solid waste collection in the City of Altoona and surrounding townships. They concluded that the freedom to choose system as it existed was expensive, inefficient, and impossible to enforce (Gannett Fleming, 2006). Based on the report, Altoona City Council was prepared to contract a single company for solid waste collection within the city. This would reduce the cost per household to $14.00US (25-35 percent savings) when compared to the current $22.00US average fee per month paid by Altoona residents for private subscription service at that time. However, a small minority of Altoona

residents voiced opinions of their constitutional right to choose their own trash company. Altoona City Council promptly folded and residents are still free to choose with today's costs generally $22.00US or more per household. The only positive outcome from this initiative was the division of the city into four separate areas, each with weekly uniform collection days (Figure 2). Collection days are named according to the main section of the city where collection occurs on that particular day. For instance, households that live in the Juniata section of Altoona have solid waste collection on Thursday. Subsequent figures presented in this article represent Thursday collection in the Juniata section of Altoona. Uniform collection days have improved the ability to monitor curbside collection, something the IRC or county office were never able to do before because recycling could be set-out on any of twelve days over a two week collection cycle.
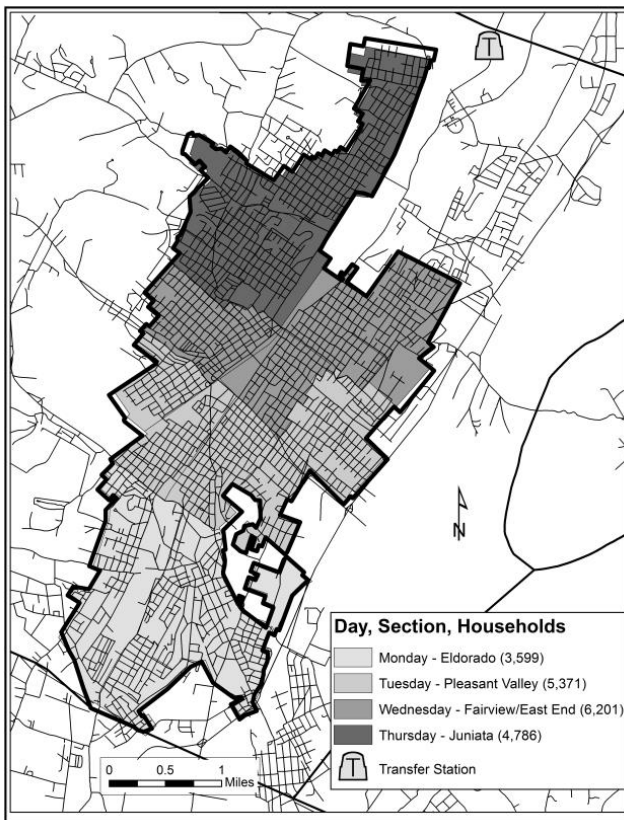

Figure 2. City of Altoona Solid Waste Collection Areas.

Collection companies also realize how inefficient the collection system is but obviously remain quiet as their business benefits by getting a share of customers whether a large or small amount. This was evident when attempts were made to contact each of the 20 companies to gather general information about their collection strategies. Questions included but were not limited to: do you use any route logistics when collecting solid waste, what is the size of your solid waste hauler, and do you conduct 100 percent recycling? Many were reluctant to answer questions as they feel any information provided will lead to their demise. Few did provide insight into their operations. All company names were kept confidential for this research.

While this system allows residents freedom to choose their solid waste company, it testifies to an unawareness or denial of the high cost of the current system, both environmentally and financially. First, several collection trucks frequenting the same neighborhoods creates unnecessary and additional vehicle emissions. This problem is exasperated by some companies using more than one vehicle, one truck for solid waste collection and one for recyclables. Thus, the number of collection trucks passing through a neighborhood on collection days could potentially be greater than 20. This process is even more inefficient when one considers that solid waste collection companies are generally clueless about routing strategies. Under the best circumstances they are driving a few blocks between stops. The average distance between stops in single-collector systems is measured in feet, but is usually measured in blocks in a system like Altoona's. Routes also include trips to the transfer station once the trucks are filled. None of the companies interviewed for this study have scientifically approached the issue and systematically derived a route that minimizes mileage, intersection crossing, and traffic congestion. It's been suggested that companies have little incentive to invest time and money into route logistics. Rather, if a route is inefficient resulting in higher gas costs, it is easier for the company to raise customer's monthly bill.

Second, the increased truck traffic also generates noise pollution throughout the day. Companies can begin collecting at 5AM and can continue working until 6PM. Trucks themselves are loud but the noise is manifested when workers use the hydraulic system to compact the solid waste. Although they can collect until 6PM, most try and finish before the transfer stations close at 3PM. Those that collect later in the day have no place to take their solid waste and it remains in trucks overnight, sometimes parked in areas not permitted. Being that some begin collecting at different times and locations, trucks continually pass through neighborhoods during the day. Increased truck

traffic can also lead to road degradation. Last, City of Altoona residents are paying more for the freedom to choose system than if the city had one or two contracted companies.

Aside from the freedom to choose, two other benefits have been identified with this system. First, elderly residents have difficulty preparing their trash for curbside collection and the company they subscribed with for 25-plus years understands their need. Upon arriving at their residence, workers will walk to the back door to retrieve their trash and place it in the hauler. Some companies even advertise on their collection trucks the phrase "elderly friendly." Many elderly fear they will lose this privilege if the city contracts a required company for all residential collection. However, if the city were to, the few companies interviewed for this research indicated they would be willing to assist elderly or handicapped customers. Special contractual provisions (for a small additional charge) could also be added for those that needed or desired backdoor pickup. Second, most companies do not have restrictions on the amount of solid waste residents can place out for pick-up. Many residents said they can place large amounts of garbage out for pick-up (seven or eight bags) and their company will collect it all. Companies do not want to place restrictions on amounts for fear they will lose business to other companies. Aside from the cost, residents are the primary beneficiary of the current system. Each company also benefits by getting a share of the customer base. Regardless, there are too many companies participating in solid waste collection and the benefits residents receive negatively impact the environment. The situation also demonstrates how local governments fail to use GIS as a planning tool.

This research presents the use of GIS as an assessment and planning tool for a case study of solid waste collection in the City of Altoona. The city lends itself as a unique study area compared to others in the academic literature due to the sheer number of collection companies and the lack of systematic planning amongst them. Jovicic et al. (2011) states there is no universal solution for the optimization of solid waste management as each locale's characteristics must be taken into consideration as unique. Utilizing the GIS network analyst function of Vehicle Routing Problem (VRP) and data obtained from the IRC, the purpose of this research is two-fold. First, GIS was used to model the current *freedom to choose* system to assess collection time, miles traveled, and number of trips to the transfer station. The design of the current collection systems likely results in wasted miles traveled and lengthy collection times. Therefore, the second part of this research used GIS to model alternate collection scenarios that potentially improve the freedom to choose

system and provide greater efficiency. Rather than adopt the approach taken by other studies and use VRP to only solve for the optimal routing strategy, this research differs by proposing and modeling an alternate scenario that utilizes several collection companies but remains efficient.

3. DATA AND METHODS

This research design utilized the Vehicle Routing Problem (VRP) function through ESRI's ArcGIS network analyst. The VRP is a type of network analysis tool for routing a fleet of vehicles to service a set of orders with the goal of minimizing some objective (e.g., operating cost), while satisfying certain constraints. These constraints may include time windows, multiple route capacities, travel duration constraints, route zone and route seed point constraints, specialties constraints, and paired order constraints (ESRI GIS Dictionary - http://support.esri.com/ en/knowledgebase/GISDictionary/term/ vehicle%20routing%20problem). Several studies have utilized VRP within GIS for the purpose of assessing and designing improved waste collection strategies (Jovicic et al., 2011; Bhambulkar2010; Kim et al., 2006 Sahoo et al., 2005). Further, ArcGIS is readily available and is the most popular GIS software package used within many state and local governments in the United States. Local governments could apply this research design to their solid waste collection strategies. VRP's user-interface within ArcGIS is user-friendly and allows users to define a variety of inputs. Given these reasons and the availability of data from the IRC, VRP within ArcGIS was chosen as the methods to analyze waste collection in the City of Altoona.

For this research, the solid waste collection companies represent the fleet of vehicles serving a set of orders comprised of residential households and their solid waste. Constraints include time windows for companies to begin and end collection, amount of solid waste per household, household collection time, capacity of solid waste collection trucks, and typical road constraints (speed limits, turn restrictions, traffic congestion) imposed by the road network. The VRP provides output that includes driving directions, total distance traveled, and total travel time.

Applying the VRP to solid waste collection in the City of Altoona required several data and methodology considerations:

- *residential locations* - represented through GIS polygon parcel data obtained from the Blair County Assessment Office. Structured query statements were used to select residential land use types to serve as household collection points.
- *solid waste collection companies* – the IRC provided an address list of the 20 companies and their locations were geocoded in ArcMap.
- *transfer stations* - The City of Altoona utilizes two transfer stations that are within 0.5 mile of each other. Addresses of each were obtained and geocoded using ArcMap. Their geographic center was calculated to serve as the city's lone transfer station for this research. The transfer station illustrated in Figure 2 is the geographic center of the two primary transfer stations.
- *streets*– in order to model the street network as close to reality, StreetMap Premium for ArcGIS was obtained. It is an enhanced street dataset based on commercial street data from NAVTEQ and TomTom that works with ESRI's ArcGIS software to provide geocoding, routing, and high-quality display. The data allows one to generate the shortest or fastest distance, point-to-point, or multistop routes with driving directions. One-way and turn restriction information is taken into consideration to ensure the most accurate routes and directions. The data also includes historical traffic data that summarizes the average roadway travel speed for more accurate arrival time projections and avoidance of congestion based on day and time.
- *amount of solid waste* – the IRC provided the 2011 solid waste collection totals for each of the 20 companies operating within the city (Table 1). Based on these totals, the average amount of solid waste generated per household each week in the City of Altoona is 50.2 lbs. This number was rounded to 50.0 lbs per household.
- *collection time* – this research accounted for total collection time between 5AM-3PM. Variables include street travel time, time collecting and loading each household's solid waste, and time at transfer station. Collection time begins at 5AM when the collection truck leaves company headquarters, not when it arrives at the first household. This is an unfortunate input in the VRP model that cannot be altered. Collection time ends at 3PM with the transfer station the last stop for each company regardless if the collection truck is full or not. This ensures the truck does not sit overnight with solid waste onboard. The Gannett Fleming, Inc. Technical Assistance Study (2006) found the average household stop within the city is 30 seconds.

This is the same amount of time used by Arribas et al. 2010.(Anecdotal evidence would indicate that this collection time is actually much longer with some smaller companies due to trucks that do not compact waste efficiently or a single employee doing both driving and collecting of solid waste.) According to workers at the local transfer stations, the amount of time spent unloading a full truck varies between 5-15 minutes depending on the number of other trucks present. This research uses an average time of 10 minutes for each visit to the transfer station.

- *solid waste collection truck size* –the size of each company's solid waste collection truck varies from the smallest of a 2cubic yard loader to the largest of 25 cubic yards. Varying sizes of 11, 12, 14, and 20 cubic yard loaders also exist. Because so few companies were willing to cooperate when contacted, the size of each hauler was visually estimated and placed into one of three size categories:

  - ✓ Mini – 4 cubic yard loader = 1.0 tons (2,000 lbs) of solid waste
  - ✓ Mid – 12 cubic yard loader = 4.5 tons (9,000 lbs) of solid waste
  - ✓ Large – 25 cubic yard loader = 10.5 Tons (21,000 lbs) of solid waste

Based on solid waste hauler size and amount of solid waste per household, the approximate number of households each can collect prior to capacity is 40 houses for a mini-hauler, 180 houses for a mid-hauler, and 420 houses for a large hauler.

3.1. Vehicle Routing Problem

These data and methods were used in conjunction with the VRP to assess the current collection system and also propose more efficient collection scenarios. Figure 3 illustrates of a layout of the VRP model as it relates to solid waste collection within the city. Even though some companies utilize more than one truck to collect solid waste, this research models one collection truck per company on each collection day. Three separate collection scenarios for the City of Altoona were modeled: current collection, controlled collection, and improved efficiency. The current collection scenario models all 20 independent companies as they collect solid waste on each of the four collection days.

Table 1. Solid Waste Company Collection Statisticsfor Year 2011

No.	Solid Waste Company	Number Customers	Percent of Customers	Recyclable Waste in Tons	Non-Recyclable Waste in Tons	TOTAL Solid Waste in Tons
1	Company A	4,841	24.3%	601.52	8,064.43	8,665.94
2	Company B	396	2.0%	15.32	727.71	743.03
3	Company C	440	2.2%	0.00	884.83	884.83
4	Company D	2,794	14.0%	98.83	1,140.82	1,239.65
5	Company E	1,100	5.5%	23.01	742.85	765.86
6	Company F	44	0.2%	0.12	3.25	3.37
7	Company G	66	0.3%	0.17	9.95	10.12
8	Company H	352	1.8%	24.00	3,495.67	3,519.67
9	Company I	528	2.6%	3.25	378.34	381.58
10	Company J	352	1.8%	46.04	2,055.44	2,101.48
11	Company K	968	4.9%	0.00	715.44	715.44
12	Company L	352	1.8%	0.00	634.51	634.51
13	Company M	968	4.9%	24.01	749.36	773.38
14	Company N	2,310	11.6%	51.48	1,976.20	2,027.68
15	Company O	176	0.9%	4.00	38.10	42.10
16	Company P	440	2.2%	3.01	363.85	366.85
17	Company Q	1,496	7.5%	70.53	503.85	574.37
18	Company R	792	4.0%	10.00	285.44	295.44
19	Company S	1,320	6.6%	89.58	2,077.62	2,167.20
20	Company T	220	1.1%	6.50	170.57	177.07
	TOTAL	19,957	100.0%	1,071.36	25,018.22	26,089.58

Even though each company's customer list is not readily available, the number of customers they serve within the city are recorded by the IRC (Table 1). To allocate the correct number of customers to each solid waste collector, a "select random polygons" tool for use in ArcGIS's ArcToobox was obtained from the North Carolina, United States Department of Agriculture (USDA). They developed the tool for use in soil survey updates and evaluations.
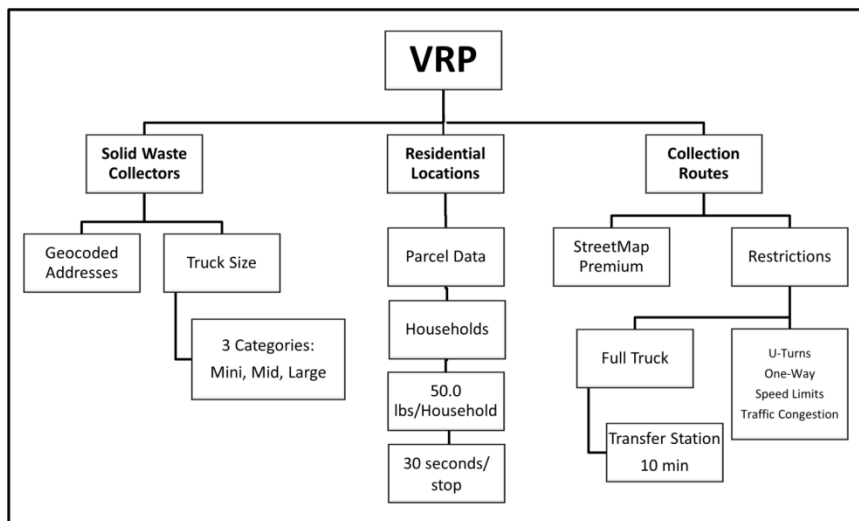
Figure 3. Layout of VRP Model and Inputs for Modeling Solid Waste Collection.

Given a polygon data-set, the user can specify the number of random polygons to be selected.

The tool was applied to the parcel data to assign residential locations (customers) on each of the four collection days to the 20 companies (Figure 4). The randomness of the tool mimics reality in that there is no systematic structure in residents choosing their solid waste collection company. All residential locations in each of the four collection areas were assigned to a particular company. No residential location is served by more than one company.

The controlled collection scenario models six solid waste companies in each of the four collection areas. Residential locations serving as solid waste collection points are equally divided into six geographic clusters (Figure 5). The purpose of this scenario is to give local companies with the larger number of customers an equal share of customers. One of the concerns city officials have about contracting solid waste collection to only one or two companies is that approximately 18 companies would lose their customer base, thus hurting local businesses. As a compromise, this scenario utilizes six companies with residential locations clustered rather than spread across the city. Identifying clusters in GIS can be performed using the Cluster and Outlier Analysis or Hot Spot Analysis tools given a weighted variable for the data.
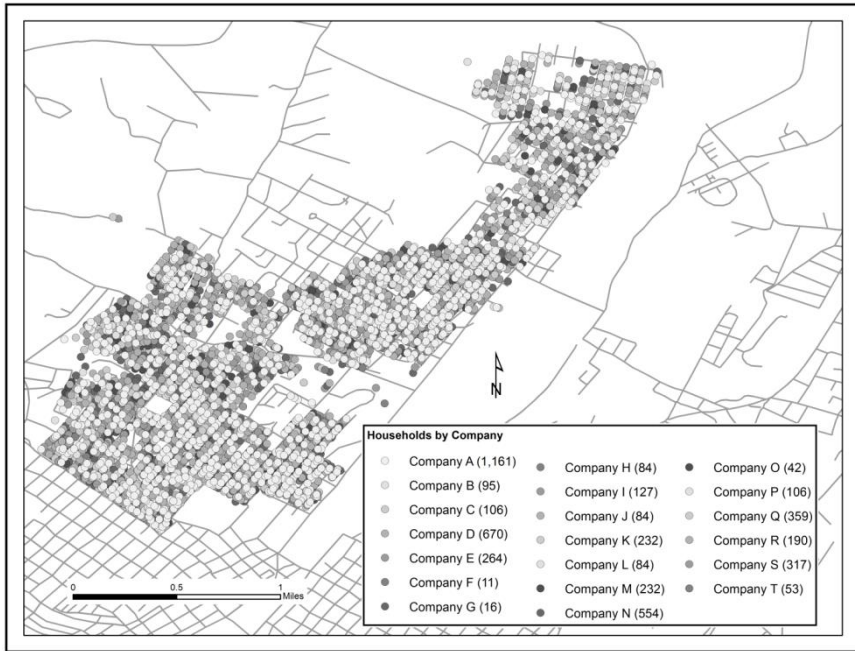
Figure 4. Distribution of Customers for Thursday, Juniata Collection – Scenario 1.

However, this research is unable to use these tools for cluster identification as the lone weighted variable that can be used, amount of waste per household, is the same for all households (50.0 lbs per household. As a result, clusters were visually determined. Based on the current data available, an alternate method to identifying clusters could be based on the amount of waste to be collected and truck size. Large haulers would get a greater number of clustered households than mid-sized haulers. In the end, the purpose of this scenario is to demonstrate how clustering a company's customer base can potentially reduce miles travelled and collection time.

The improved efficiency scenario determines the maximum number of 25 cubic yard solid waste collection trucks needed to service each of the four collection days. A 25 cubic yard truck was selected to maximize the amount of solid waste that can be collected which ultimately reduces collection time and distance traveled. Rather than contract solid waste collection to one or several companies, officials want to explore the option of the city performing collection with their own trucks and city workers. This scenario would provide officials with an approximation of how many trucks are needed to service the city and the amount of time needed for collection. This scenario was modeled

with VRP using one 25 cubic yard truck serving all residential locations on a particular collection day in the 10-hour collection time frame. Once the time frame limit was reached, the number of residential locations serviced was determined and then removed from the data-set.

The model was then run again for the remaining residential locations on that particular collection day. This process was repeated until all locations for each collection day were serviced, thus providing the total number of 25 cubic yards trucks needed to service each collection day in the required time frame. Output from the VRP model for all scenarios includes: driving directions, time collection begins and ends, total collection time (hours:minutes), total distance traveled (miles), and number of trips to the transfer station.

Driving directions could greatly benefit solid waste collection companies by providing drivers with an optimal route serving residential locations that could reduce miles traveled and fuel consumption.
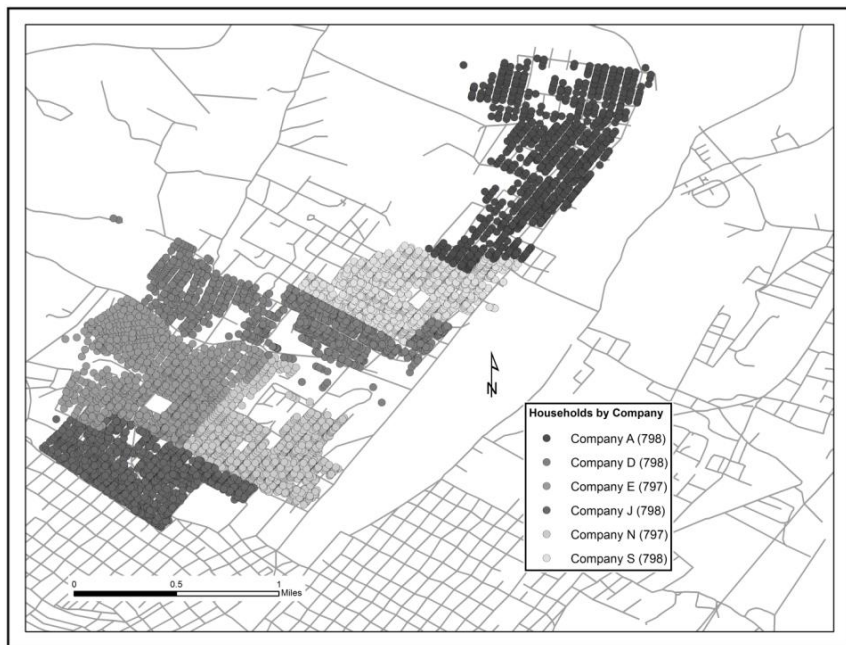

Figure 5. Distribution of Customers for Thursday (Juniata) Collection – Scenario 2.

4. RESULTS

The City of Altoona has 19,957 residential locations that generate approximately 997,850 pounds of solid waste each week. Monday collection in Eldorado contains the fewest households with 3,599. Conversely, Wednesday collection in Fairview contains the greatest number with 6,201. This represents a 72 percent increase in households compared to Eldorado. Several companies with a large number of Fairview residential customers expressed frustration regarding the difficulty in completing all their stops prior to the 3PM deadline. This demonstrates the need for a more efficient collection system as driving several blocks between households and crisscrossing the city results in wasted work time.

City-wide, Company A serves the largest number of households at24.3 percent. Three companies (A, D, and N) serve half of all households. The remaining 50 percent is comprised of several companies with only 1 to 2 percent of households and three companies (F, G, and O) serving less than one percent. This exemplifies the large amount of unnecessary waste collection traffic as several solid waste companies have few customers that could otherwise be served by companies with a larger number of customers.

4.1. Scenario 1

Table 2 presents results from modeling Scenario 1 – current collection – in the four collection areas. Monday collection represents the longest number of miles traveled (1,266.8 miles) of all four collection days. Conversely, Monday has the least amount of collection hours (64 hours and 46 minutes).The transfer station being located furthest from Monday collection area has an influence on the former while the fewest number of households has an influence on the latter. Wednesday collection in Fairview neighborhoods has the greatest number of households resulting in the longest collection time of 74 hours and 50 minutes. This represents a 15 percent increase in collection time from the least on Monday. The greatest number of trips to the transfer station (52) also occurs on Wednesday. With the transfer station nearby, the fewest miles travelled (820.7 miles) occurs during Thursday collection. This represents a 35 percent decrease from the longest distance on Monday. Overall, results suggest that the greatest distance traveled coincides with increasing distance from the transfer station and the longest hours of operation corresponds with increasing number of households.

Table 2. Scenario 1 – Current Collection – Solid Waste Collection Statistics

CMPY	SIZE	Monday - Eldorado					Tuesday - Pleasant Valley					Wednesday - Greenwood					Thursday - Juniata				
		HHs	HR	MIN	DIST	TRANS	HHs	HR	MIN	DIST	TRANS	HHs	HR	MIN	DIST	TRANS	HHs	HR	MIN	DIST	TRANS
A	Large	873	8	59	127.2	3	1,303	11	28	100.5	4	1,504	12	25	97.5	4	1,161	9	10	67.2	3
B	Mid	71	1	33	31.4	1	107	1	46	27.2	1	123	1	44	25.2	1	95	1	31	24.0	1
C	Mid	79	1	29	23.7	1	118	1	44	25.1	1	137	1	40	20.9	1	106	1	22	18.2	1
D	Mid	504	7	29	128.5	3	752	8	18	87.6	5	868	8	19	76.9	5	670	7	53	89.6	4
E	Mid	198	3	7	52.5	2	296	3	32	39.6	2	342	3	39	38.8	2	264	3	4	34.5	3
F	Mini	8	0	38	18.0	1	12	0	31	10.5	1	14	0	31	10.0	1	11	0	20	6.4	1
G	Mini	12	0	18	38.0	1	18	0	36	11.3	1	21	0	35	11.0	1	16	0	28	8.8	1
H	Large	63	1	39	34.3	1	95	1	49	30.7	1	109	1	50	30.5	1	84	1	39	28.3	1
I	Large	95	2	48	96.6	1	142	3	9	95.1	1	164	3	13	94.9	1	127	2	56	85.8	1
J	Large	63	1	29	31.2	1	95	1	44	28.4	1	109	1	42	26.6	1	84	1	31	25.1	1
K	Mini	175	6	24	135.6	5	261	5	57	88.0	7	301	6	2	82.8	8	232	4	29	59.3	6
L	Mid	63	1	30	32.2	1	95	1	43	32.4	1	109	1	41	26.9	1	84	1	22	22.4	1
M	Mini	175	6	31	129.3	5	261	4	32	47.1	7	301	5	52	79.9	8	232	4	34	60.2	6
N	Mid	417	6	7	110.8	4	622	6	55	74.0	4	718	6	56	64.7	4	554	6	14	63.8	5
O	Mid	32	1	5	23.2	1	47	1	11	24.0	1	55	1	15	24.5	1	42	1	6	23.0	1
P	Mid	79	1	29	28.3	1	118	2	52	45.7	3	137	3	2	44.7	4	106	2	20	34.6	3
Q	Mid	270	4	16	73.7	3	403	4	59	59.0	3	465	5	8	55.8	3	359	3	50	40.6	3
R	Mid	143	3	2	64.7	2	213	3	37	66.6	2	246	3	30	60.7	2	190	2	55	54.0	2
S	Large	238	2	49	40.9	1	355	3	37	39.1	1	410	3	50	37.9	1	317	3	9	33.9	1
T	Mini	40	2	4	46.7	2	59	2	1	45.0	2	68	1	56	42.7	2	53	1	48	41.0	2
TOTAL		3,599	64	46	1,266.8	40	5,371	72	1	976.9	49	6,201	74	50	952.9	52	4,786	70	55	820.7	47
Total Time: 282 Hours and 32 Minutes Total Distance: 4,017.3 miles Total Trips to Transfer Station: 188																				

NOTE: CMPY: Company, HHs = Number of Households, HR = Hours, MIN = Minutes, DIST = Distance Travelled, TRNS = Trips to Transfer Station, S1 = Scenario 1.

With the greatest number of customers, Company A has the longest collection times on each of the four days. One positive is their large hauler, thus reducing trips to the transfer station. On two occasions (Tuesday and Wednesday), they violate the 10-hour collection time and would need a minimum of two trucks to complete their route in the allotted time. With the exception of Tuesday and Wednesday, Company A does not travel the longest distances. Company K, with only 175 households, covers the longest distance of 135.6 miles on Monday.

A combination of a mini hauler and lengthy distance from transfer station not only results in a long total travel distance but a collection time of approximately 6 hours and 24 minutes for 175 households. Company D covers the longest distance of 89.6 miles on Thursday. This is a result of the large number of households they serve and their mid-size hauler. Other companies require a lesser amount of time to complete their routes– 8 to 9 companies finish within 2 hours. Companies F and G finish in less than an hour. Multiple companies make one trip to the transfer station with a truck that does not once reach capacity.

When interpreting results, Company I is an anomaly because its headquarters are approximately 65 miles (1 hour 20 minutes) from the City of Altoona. This time and distance is part of their total solid waste collection time and travel distance. One wonders why a company with less than three percent of customers travels such a distance to collect solid waste. The freedom to choose system virtually allows anyone to collect in the city if they follow a few regulations.

4.2. Scenario 2

Results for Scenario 2 are very similar to current collectionwith the greatest number of miles traveled on Monday and longest collection time on Wednesday (Table 3).

However, the design of controlled collection has greatly reduced miles travel and collection time for all four collection days. The combined total distance traveled on all four collection days decreased from 4,017.3 miles to 1,173.6 miles, a 70 percent decrease. Thursday collection in Juniata has the largest decrease in miles traveled with a 73.8 percent reduction (820.7 miles to 215.1 miles). The combined total collection time for all four collection days decreased 44 percent from 282 hours and 32 minutes to 156 hours and 2 minutes.

Monday and Thursday collection each reduced collection time by 50 percent with Wednesday collection having the smallest reduction at 38 percent. The controlled collection scenario would reduce the overall number of trips to the transfer station across all four collection days by 52 percent (188 to 90).

4.3. Scenario 3

Results from the improved efficiency scenario illustrate the maximum amount of 25-yard collection trucks required for each of the four collection days. The number of trucks ranges from a low of three during Monday collection to ahigh of five on Wednesday (Table 4).

This is a substantial reduction compared to current 20 solid waste collection trucks of varying sizes. Compared to Scenario 1, the combined number of miles traveled decreases by 76.7 percent (4,017.3 miles to 973.3 miles). Each of the four collection days reduced their miles traveled by at least 70 percent with Monday collection in Eldorado the largest reduction at 80.5 percent less. Similarly, the combined total collection time was reduced by 49.6 percent (282 hours and 32 minutes to 142 hours and 20 minutes).

Monday collection with the least number of households has the largest decrease in collection time (59.0%) while Wednesday collection with the greatest number of houses has the smallest decrease (41.9%). The combined number of trips to the transfer station decreased from 118 to 56, a 70.2 percent reduction. The single largest decrease occurs on Thursday collection where the number of trips to the transfer station decreases from 47 to 12 (75.4 percent decrease).

Improved efficiency also improves Scenario 2. The combined number of miles traveled is 20.1 percent less (1,173.6 to 973.3 miles). The percent reduction ranges from 6.6 percent (Thursday) to 30.0 percent (Monday). The former contains the greatest number of households and the latter the least.

There is a 12.6 percent reduction in collection time − 156 hours and 2 minutes to 136 hours and 24 minutes. The largest occurs during Thursday collection in Juniata (20.4 percent) and the least during Wednesday collection in Fairview (5.5 percent). Scenario 3 requires 38.9 percent fewer trips to the transfer station than Scenario 2 (90 to 55).

Table 3. Scenario 2 – Controlled Collection – Solid Waste Collection Statistics

CMPY	SIZE	Monday - Eldorado					Tuesday - Pleasant Valley					Wednesday - Fairview					Thursday - Juniata				
		HHs	HR	MIN	DIST	TRNS	HHs	HR	MIN	DIST	TRNS	HHs	HR	MIN	DIST	TRNS	HHs	HR	MIN	DIST	TRNS
A	Large	600	4	37	34.3	2	896	6	44	45.1	3	1,034	7	8	41.1	3	798	5	14	25.0	2
D	Mid	599	6	9	62.7	4	895	7	56	65.3	5	1,034	7	54	53.2	6	798	6	38	47.9	5
E	Mid	600	6	1	86.9	4	895	7	31	58.0	5	1,034	8	2	53.1	6	797	6	36	47.2	5
J	Large	600	4	48	47.4	2	895	6	25	39.7	3	1,034	7	19	46.5	3	798	5	28	31.1	2
N	Mid	600	5	46	89.0	4	895	7	35	58.9	5	1,034	7	59	53.6	6	797	6	21	41.1	5
S	Large	600	4	33	32.4	2	895	6	33	41.1	3	1,034	7	37	50.2	3	798	5	8	22.8	2
Total		3,599	31	54	352.7	18	5,371	42	44	308.1	24	6,201	45	59	297.7	27	4,786	35	25	215.1	21
% Reduction S1			50.7%		72.2%	55.0%		40.7%		68.5%	51.0%		38.6%		68.8%	48.1%		50.1%		73.8%	55.3%
TOTAL S2		Total Time: 156 Hours and 2 Minutes					Total Distance: 1,173.6 miles					Total Trips to Transfer Station: 90									
% Reduction S1		Total Time: 44.8% Less					Total Distance: 70.8% Less					Total Trips to Transfer Station: 52.1% Less									

NOTE: S2 = Scenario 2.

Table 4. Scenario 3 – Improved Efficiency – Solid Waste Collection Statistics

CMPY	SIZE	Monday - Eldorado					Tuesday - Pleasant Valley					Wednesday - Fairview					Thursday - Juniata				
		HHs	HR	MIN	DIST	TRNS	HHs	HR	MIN	DIST	TRNS	HHs	HR	MIN	DIST	TRNS	HHs	HR	MIN	DIST	TRNS
A	Large	1,370	10	0	96.1	4	1,409	10	0	59.7	4	1,430	10	0	62.7	4	1,398	9	0	54.6	3
A	Large	1,370	10	0	92.1	4	1,409	10	0	66.5	4	1,430	10	0	64.0	4	1,398	9	0	58.2	3
A	Large	859	6	32	58.8	3	1,409	10	0	63.3	4	1,430	10	0	61.2	4	1,398	9	0	51.7	3
A	Large	----	----	----	----	----	1,144	8	14	50.0	3	1,430	10	0	64.0	4	592	7	16	44.2	3
A	Large	----	----	----	----	----	----	----	----	----	----	481	3	27	26.1	2	----	----	----	----	----
Total		3,599	26	32	247.0	11	5,371	38	14	239.5	15	6,201	43	27	278.0	18	4,786	34	16	208.7	12
% Reduction S1			59.0%		80.5%	72.5%		46.9%		75.5%	69.4%		41.9%		70.8%	65.4%		60.2%		78.9%	76.6%
% Reduction S2			16.8%		30.0%	38.9%		10.5%		22.3%	37.5%		5.5%		6.6%	33.3%		20.4%		19.6%	47.6%
TOTAL S3		Total Time: 136 Hours and 24 Minutes					Total Distance: 973.3 miles					Total Trips to Transfer Station: 55									
% Reduction S1		Total Time: 51.7% Less					Total Distance: 76.7% Less					Total Trips to Transfer Station: 70.7% Less									
% Reduction S2		Total Time: 12.6% Less					Total Distance: 20.1% Less					Total Trips to Transfer Station: 38.9% Less									

5. DISCUSSION

By modeling the current collection system and proposing two alternate scenarios, results confirm the initial hypothesis that the current collection system is highly inefficient and can be improved. This is most evident through the long collection time, lengthy distance traveled, and substantial number of trips to the transfer station on each collection day. The obvious problem with the current collection system is the number of solid waste companies and the varying number of customers each serves. Manifesting the problem is the size of the collection truck used by several companies, particularly those with a mini hauler that serve too few or too many households. For instance, Companies F and G serve such a low percentage of households that each finishes collection in less than an hour on each day. They are accounting for unnecessary miles traveled and trips to the transfer station that could otherwise be served by larger companies. Conversely, Companies K and M with a mini hauler serve a larger percentage of customers. This requires several trips to the transfer station translating to a much longer collection time and distance traveled. For comparison purposes, Company E with only 23 more households than Company K requires approximately half the time, distance, and trips to transfer station because it utilizes a mid-size hauler. However, the same argument can be made against Companies I and K that have large haulers but only serve a few households. Regardless of how one analyzes current collection, the system is highly inefficient from the number of solid waste collectors, most truck sizes, number of miles traveled, collection time, and the number of trips to the transfer station. Fortunately, this research proposed and demonstrated alternate scenarios that greatly improve upon these variables regardless which scenario is chosen.

Scenario 2 – Controlled Collection improves current collection by 50 percent in all variables with the exception of total collection time. This reduction cannot solely be attributed to decreasing the number of solid waste collectors to six but also because their households were geographically clustered. With each collector serving a particular cluster, the amount of driving across the entire city was reduced. The only driving outside their cluster involved trips to the transfer station. This translated to a 70 percent reduction in the combined total distance traveled on each of the four collection days. The elimination of mini-size haulers also reduces miles traveled. The elimination of several companies and geographic clustering of customers presented in Scenario 2 is a similar approach instituted by the City of Portland, Oregon, USA twenty years ago. Solid waste, recycling, and composting

collection services are provided to residents under a franchise system that limits the number of companies authorized to provide service. The city assigns each company a section of the city and also regulates the rates companies are allowed to charge, determined through a comprehensive rate study (Hong, Adams, and Love 1993; Hong and Adams 1999; City of Portland 2012). This structure has allowed the City of Portland to promote high quality solid waste, recycling, and composting collection services while simultaneously maximizing recycling participation and recovery.

A downfall to implementing Scenario 2 is that 14 independent solid waste companies would lose their customer base in the City of Altoona and this could impact the local economy by possibly putting small collection companies out of business. However, a reduction in the number of companies could potentially save households approximately $7.50US per month. This translates to a savings of 1.75US million dollars each year (19,473 households * 12 months * $7.50US). Households could invest this savings back into local economy. With Scenario 2, one must weigh the elimination of collection companies against reducing collection times and distances which ultimately improves air and noise pollution and road degradation.

There are two local companies that work within the City of Altoona that have multiple large sized haulers. Scenario 3, improved efficiency, provides a realistic solution for these companies to complete solid waste collection within the city. Implementing this scenario would reduce collection time, distance traveled, and trips to transfer station by 51.7, 76.6, and 70.7 percent compared to Scenario 1. These savings are among the highest found in academic literature related to GIS optimization of solid waste collection. The largest savings were noted in the study performed by Apaydin and Gonullu (2008). They applied a shortest path model within GIS to Trabzon City, Turkey and noted a decrease of 44.3 and 24.6 percent in route time and route distant for nine routes in 26 districts. The differences in savings between this research and Apaydin and Gonullu (2008) can be attributed to either model design or the current collection system in the City of Altoona is among the most unorganized.

Results from this research demonstrate that city officials must address solid waste collection. At a minimum they should implement a collection system similar to Scenario 2. This not only provides savings in terms of collection time and distance traveled, it will allow officials to better monitor and enforce curbside collection, especially recyclables. Solid waste companies and city residents could then be held more accountable. Also, the exact locations of each company's customers are known with scenarios 2 and 3. This

provides the advantage of using the VRP model to establish driving directions for each company that provides the optimal collection route by minimizing travel time.

5.1. Limitations

Modeling is an effective approach to better understanding how certain phenomena behave when, in reality, it is impossible to obtain that understanding through actual implementation or real operations. A review of the academic literature confirms that GIS network analyst is an established approach to analyze and improve upon solid waste collection strategies. However, it should be noted that models can only offer one realization of many possible scenarios under a specific set of conditions set forth by the model's assumptions. This research attempted to minimize any assumptions through field work and data collected by the IRC. Some assumptions could have been avoided had local companies been willing to provide information on their collection strategy. This research assumes a uniform amount of 50 pounds of solid waste per household each week. While no one can estimate the amount of waste per household, this amount is based on the total amount of solid waste each company brings to the transfer stations. The totals are specific to the City of Altoona and provide the most accurate representation.

Solid waste collection trucks were placed into three categories of mini (2 cubic yard loader), mid (12 cubic yard loader), and large (25 cubic yard loader). However, some companies have multiple trucks of varying sizes, including 14- and 20-yard loaders. The three categories best represent the truck fleet observed. Even if the truck size of every company was confirmed, there are several factors that affect the amount of solid waste a full truck can haul. First is the age of the truck. New trucks pack much better than older trucks due to hydraulic fatigue in older trucks. Truck maintenance is also important as neglecting to grease fittings on a weekly basis weakens the compactors ability to compact solid waste. A second factor is how households choose to place their solid waste on curbside for pick-up. Waste placed in trash cans and bins without a lid is prone to fill with rainwater or snow. Wet refuse is much heavier but compacts much better. Last are the employees on the routes. The more often they compact the waste in the truck the better compaction weight one gets. Some employees only compact when the hopper is completely filled thus reducing the amount of waste the truck can haul. Even

if the size of each company's hauler were known, these factors make it difficult to quantify the total amount of solid waste each could hold.

One final assumption to consider is the application of VRP to Scenario 1. The primary goal of VRP is to service each household by minimizing the overall collection time for each solid waste collection company. Thus, Scenario 1 results are based on the optimal collection route when in reality, most if not all companies are driving completely different routes. The only way to truly model current collection is for companies to share their collection strategies and customer lists. Until then, results from the VRP model as it relates to current collection cannot be validated as reality.

CONCLUSION

Solid waste management system planning has received wide attention from environmental planners because of its complex coordination of various management strategies. One issue is how to effectively distribute the collection crew size and vehicles in a metropolitan region. This research applied the VRP function to solid waste collection in the City of Altoona, Pennsylvania, USA.

Focus was placed on understanding the current collection strategy and proposing two alternate scenarios. Results indicate the current collection strategy with 20 separate collection companies and a fragmented customer base is highly inefficient in terms of collection time, distance traveled, and number of trips to the transfer station. Each of the alternate scenarios greatly improves upon current collection in all areas. Controlled collection scenario with six collection companies and clustered customers offers a savings of approximately 70 percent in distance traveled and 44 percent in collection time.

Additional savings were demonstrated with the improved efficiency scenario as distance traveled and collection time were 76 and 50 percent less than current collection. Improved efficiency provides further savings compared to controlled collection as the distance and time traveled is 20 and 12 percent less.

Savings in terms of distance traveled and collection time are significant for a city's operating budget as the cost of waste collection is a very large part of the operating budget. The two alternate scenarios demonstrate that optimization of waste collection service can significantly reduce collection time and distance traveled. This translates to financial savings for collection

companies who can then pass savings onto the customer. In the end, results from each scenario emphasize the need for city officials to make changes to the current collection system. It is my hope city officials will adopt one of the proposed scenarios in the near future.

ACKNOWLEDGMENTS

REFERENCES

Apaydin, O., & Gonullu, M.T.(2007). Route Optimization for Solid Waste Collection: Trabzon (Turkey) Case Study. *Global NEST Journal*, 9(1), 6-11.

Arribas, C.A., Blazquez, C.A., & Lamas, A. (2010). Urban solid waste collection system using mathematical modeling and tools of geographic information systems. *Waste Management and Research*, 28, 355-363.

Bhambulkar, A. V. (2010). Municipal Solid Waste Collection Routes Optimized with ArcGIS Network Analyst. *International Journal of Advanced Engineering Sciences and Technologie*s, 11(1), 202-207.

Chang, N.B., Lu, H. Y., & Wei, Y.L. (1997). GIS technology for vehicle routing and scheduling in solid waste collection systems. *Journal of Environmental Engineering*,123, 901-910.

City of Portland.(2012). Residential Solid Waste and Recycling Rate Study. Bureau of Planning and Sustainability Solid Waste and Recycling, http://www.portlandoregon.gov/bps/article/404493, 18pp.

El-Hamouz, A.M. (2008). Logistical management and private sector involvement in reducing the cost of municipal solid waste collection service in the Tubas area of the West Bank. *Waste Management*, 28, 260-271.

Gaines, L., Vyas, A., & Anderson, J.L. (2006). Estimation of Fuel Use by Idling Commercial Trucks. Abstract. 85th Annual Meeting of the Transportation Research Board. Washington, D.C. January 22-26. *TRB 85th Annual Meeting Compendium of Papers*.

Gannett Fleming, Inc. (2006). Logan Township Evaluation of Recycling and Solid Waste Collection. http://www.portal.state.pa.us/portal/server.pt?open=18&objID=505233&mode=2, 15 pp.

Ghiani, G., Guerriero, F., Improta, G., & Musmanno, R. (2005). Waste collection in Southern Italy: solution of a real-life arc routing problem. *International Transactions in Operational Research*, 12, 135-144.

Ghose, M.K., Dikshit, A.K., & Sharma. S.K. (2006). A GIS based transportation model for solid waste disposal – A case study on Asanol municipality. *Waste Management, 26*, 1287-1293.

Hong, S., & Adams, R.M. (1999). Household Responses to Price Incentives for Recycling: some Further Evidence. *Land Economics*, 75(4), 505-514.

Hong, S., Adams, R.M., & Love, H.A., (1993). An Economic Analysis of Household Recycling of Solid Wastes: The Case of Portland, Oregon. *Journal of Environmental Economics and Management*, 25, 136-146.

Jovicic, N.M., Boskovic, G.B., Vujic, G.V., Jovicic, G.R., Despotovic, M.Z., Milovanovic, D.M., & Gordic, D.R.(2011). Route Optimization to Increase Energy Efficiency and Reduce Fuel Consumption of Communal Vehicles. *Thermal Science*, 14, 67-78.

Kanchanabhan, T.E., Mohaideen, J.A., Srinivasan, S., &Sundaram, V.L.K. (2011). Optimum municipal solid waste collection using geographical information system (GIS) and vehicle tracking for Pallavapuram municipality. *Waste Management & Research*,29(3), 323-339.

Karadimas, N.V., & Loumos, V.G. (2008). GIS-based modeling for the estimation of municipal solid waste generation and collection. *Waste Management & Research*,26, 337-346.

Karadimas, N., Doukas, N., Kolokathi, M., & Defteraiou, G. (2008). Routing Optimization Heuristic Algorithms for Urban Solid Waste Transportation Management. *WSEAS Transaction on Computers*, 7(12), 2022-2031.

Karadimas, N., Papatzelou, K., & Loumos, V. (2007). Optimal solid waste collection routes identified by the ant colony system algorithm. *Waste Management & Research*,25, 139-147.

Kim, B.I., Kim, S., & Sahoo, S. (2006). Waste collection vehicle routing problem with time windows. *Computers & Operations Research*, 33, 3624-3642.

Kontos, T., Komilis, D.P., & Halvadakis, C.P. (2003). Siting MSW landfills on Lesvos island with a GIS-based methodology. *Waste Management & Research*,21, 262-277.

Leao, S., Bishop, I., & Evans, D. (2001). Assessing the demand of solid waste disposal in urban region by urban dynamics modeling in a GIS environment Resources. *Conservation and Recycling*,33(4), 289-313.

Lopez, J.V., Aguilar, M., Fernández-Carrión, S.,& Jiménez del Valle, A. (2008). Optimizing the collection of used paper from small businesses through GIS techniques: the Leganés case (Madrid, Spain). *Waste Management*,28, 282-293.

Lakshumi, A., Ramiya, A., & Ssthya, R. (2006). Optimal Route Analysis for Solid Waste Disposal Using GIS. Proceedings on CD, International Conference of Land Registration and Cadastre – MAP India, New Delhi, India.

Nazari, A., Salarirad, M.M., & Bazzazi, A.A. (2012). Landfill site selection by decision-making tools based on fuzzy multi-attribute decision-making method. *Environmental Earth Sciences*, 65(6), 1631-1642.

Pandey, P.C., Sharma, L.K., & Nathawat, M.S.(2012). Geospatial strategy for sustainable management of municipal solid waste for growing urban environment. *Environmental Monitoring and Assessment*, 184(4), 2413-2419.

Sahoo, S., Kim, S,. Kim, B.I., Kraas, B., & Popov Jr., A. (2005). *Routing Optimization for Waste Management. Interfac*es, 35(1), 24–36.

Salhofer, S., Wassermann, G., & Binner, E. (2007). Strategic environmental assessment as an approach to assess waste management systems. *Experiences from an Austrian case study*, 22(5), 610-618.

Sharholy, M., Ahmad, K., Vaishya, R. C.,& Grupta, R.D. (2007). Municipal solid waste characteristics and management in Allahabad, India. *Waste Management,* 27, 490-496.

Simonetto, E., & Borenstein, D. (2007).A decision support system for the operational planning of solid waste collection. *Waste Management*, 27, 1286-1297.

Sumathi, V.R., Natesan, U., &Sarkar, C. (2008). GIS-based approach for optimized siting of municipal solid waste landfill. *Waste Management*, 28(11), 2146-2160.

Tavares, G., Zsigraiova, Z., Semiao, V., & Carvalho, M.G. (2009). Optimisation of MSW collection routes for minimum fuel consumption using 3D GIS modeling. *Waste Management*, 29(3), 1176-1185.

U.S. Census Bureau: State and County QuickFacts. (2012). Data derived from Population Estimates, American Community Survey, Census of Population and Housing, County Business Patterns, Economic Census, Survey of Business Owners, Building Permits, Consolidated Federal Funds Report, Census of Government. http://quickfacts.census.gov/qfd/states/42/4202184.html

United States Environmental Protection Agency (US EPA). 2012. Sustainability. http://www.epa.gov/sustainability/basicinfo.htm

Vasilijevic, T.Z., Srdjevic, Z., Bajcetic, R., & Miloradov, M.V. (2012). GIS and the Analytic Hierarchy Process for Regional Landfill Site Selection in Transitional Countries: A Case Study From Serbia. *Environmental Management,* 49(2), 445-458.

Yesilnacar, M.I., Suzen, M.L., Kaya, B.S., & Doyuran, V.(2012). Municipal solid waste landfill site selection for the city of Sanliurfa-Turkey: an example using MCDA integrated with GIS. *International Journal of Digital Earth*, 5(2), 147-164.

Zheng, G.L., & Pan W. B., (2010). A GIS Based Mode Research for Urban Industrial Solid Waste Management and Exchanges. *Conference on Environmental Pollution and Public Healt*h, 1-2, 393-397.

Chapter 2

CONCEPTUAL FRAMEWORK FOR USING GIS IN BUILDING COMMUNITY CAPITAL TOWARDS SUSTAINABILITY

Sungsoon Hwang[*]

Department of Geography, DePaul University, Chicago, Illinois, US

ABSTRACT

Sustainability—balancing fundamental human needs with ecological resilience—has been embraced as an overarching policy goal. And communities have been called to participate in the process of attaining that ideal. Community-based organizations (CBOs) can benefit from using GIS in building community assets and developing sustainability initiatives. However, GIS, has not been used widely for these purposes in CBOs yet. In this chapter, I illustrate how geographic information (such as maps) can be useful in community development drawing from community GIS projects, and explain how theories of sustainability and spatial thinking can be utilized in community-based efforts towards sustainability. CBOs can monitor and assess community sustainability by (a) organizing relevant indicators into the capital framework (theories of sustainability), and (b) exploring spatial distribution, interactions, relationships, and changes in sustainability-related issues using GIS (spatial thinking). The framework presented here can be applied to promote effective use of geospatial tools for community sustainability.

[*] shwang9@depaul.edu.

1. INTRODUCTION

This chapter presents how GIS can be used to help build community capital towards sustainability. Community capital is an existing community asset or resource that can be leveraged to improve quality of life in the community and bring about desired social change (Kretzmann & McKnight, 1993; Roseland & Connelly, 2005). Community-based organizations (CBOs) work to build and enhance various forms of community capital, including environmental capital, physical capital, human capital, political capital, financial capital, social capital, and cultural capital (Green & Haines, 2012). The community can take a crucial role in sustainable development (United Nations [UN], 1992, Section III), and data and tools relevant to sustainable community development have exploded due to advances in information and communications technology (ICT). Given this, it is timely and important to consider how GIS can assist community-based efforts to progress toward sustainability.

GIS can aid the process of building community capital because spatial elements are present in various stages of community development from public participation and community organizing to community visioning. CBOs use geographic information (GI) (such as maps, geospatial data, and tools) to (a) support the activities of their staff members (administrative use of GI); (b) investigate conditions and plan for the provision of services (strategic use of GI); (c) plan specific action around a particular issue (tactical use of GI); and (d) persuade and organize more people to get involved in community issues and activities either through recruitment or grant-seeking (organizing) (Craig & Elwood, 1998). As sustainability emphasizes the balance of environmental, economic, and social goals, there is a need to better understand how different forms of capital interact with each other and how building specific community capital contributes to overall community sustainability.

To assess whether a community is on a sustainable path, it is necessary to monitor the increase or decrease of total stocks of capital over time as well as the dynamics of human-environmental interaction unique to the community (Daly, 1973). One can analyze how different forms of capital—natural capital, built capital, human capital, and social capital—are related or in balance to assess sustainability using the capital framework in an information system (Meadows, 1998). This framework has advantages because it attempts to integrate different forms of capital, and enables an analysis of sustainability condition (strong and weak sustainability) informed by economic theories of sustainability (Solow, 1986; Pearce & Atkinson, 1993). The capital framework

is criticized, however, for problems of data availability and lack of attention to intra-generational equity (UN, 2007).

One can now objectively monitor aspects of sustainability that have been elusive to measure (e.g., indicators that fall into natural capital and social capital) through recent developments in geospatial technology, including hyperspectral and radar remote sensing, sensor networks, ubiquitous GPS tracking, and GeoWeb 2.0. Along with increased quantity and quality of data, GIS can provide a platform to integrate data from various sources across different geographic scales (global to local) and investigate the changing nature of the planet (National Research Council [NRC], 1997; NRC, 2010). As society continues to improve access to data across various domains (social to environmental) over space and time, it is likely that spatial thinking (NRC, 2006) will play an important role in turning big data into knowledge in conjunction with relevant analytics and tools. Visual images can condense a large amount of data and present a message effectively enough to change behaviors (Sheppard, 2005). GIS is well suited to supporting the complex task of assessing sustainability (Graymore et al., 2009).

Research shows that CBOs do not use GI as effectively as they should because they lack organizational capabilities, continuity, and connections (social networks) to deploy GIS; nor is their use of GI is well aligned with organizational contexts and structure (Sieber, 2000; Elwood & Ghose, 2001; Esnard, 2007). CBOs do not use GI simply because they don't know how to use GIS or what they can do with GIS, and also because they are not *compelled* to pose geographic questions. They are not compelled to discern geographic elements in planning and conducting their activities because they are rarely aware of the value of GI or trained to think spatially. In other words, CBOs' (and the general public's) inadequate appreciation of geospatial concepts in part contributes to underutilization of GI. Geographic concepts and GIS are conducive to sustainability discourse (Wilbanks, 1994; Whitehead, 2006; Hwang, 2013), and thus it is necessary to promote the use of GI in CBOs' efforts toward sustainable development. The purpose of this chapter is to demonstrate the utility of GI in building community capital and to present a conceptual framework to help CBOs to think spatially and increase the efficacy of their sustainability initiatives.

This chapter is organized into three sections. In Section 2, I discuss the role of GIS in building community capital, largely illustrated by community-based service-learning GIS projects. Then I present how to organize different forms of capital to assess sustainability in community following the capital framework in Section 3. I discuss the typology of geospatial inquiries suited to

exploring sustainability-related issues in Section 4. Spatial thinking used to assess sustainability following the capital framework can guard against losing sight of holistic, context-specific, and dynamic notions of sustainability.

2. BUILDING COMMUNITY CAPITAL WITH GIS

In this section I present case studies in which GIS was applied to building community capital. The section is organized into different forms of community capital—namely, natural capital, built capital, human capital, and social capital—to connect with the capital framework presented in the next section. The case studies presented in this section are drawn from service-learning projects that students enrolled in the GIS program at DePaul University conducted in partnership with CBOs or non-profit organizations in the Chicagoland area from 2007 to 2013. The names of the partner CBOs are shown in italics in this section.
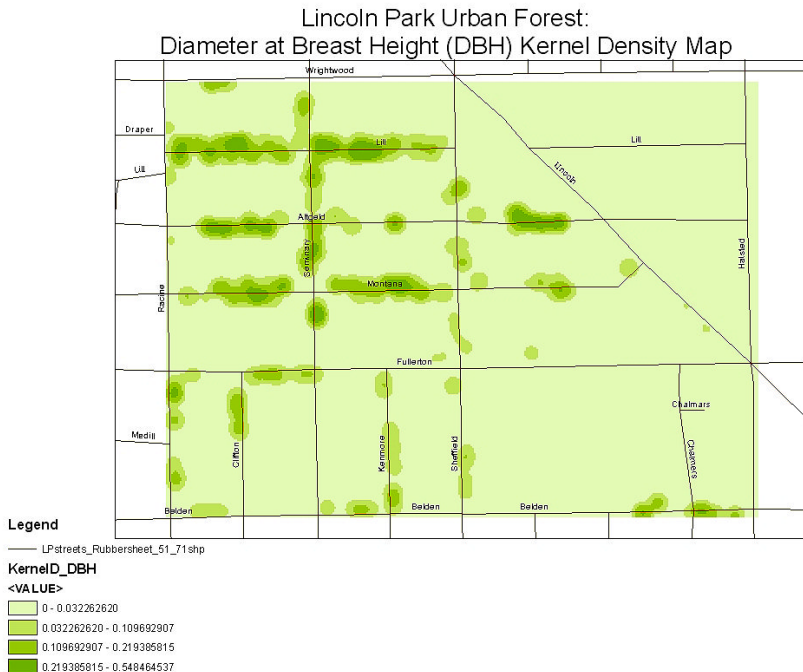
Figure 1. Kernel density map of healthy trees in Lincoln Park, Chicago (2007).

Natural Capital

Natural capital is a community's base of natural resources including air, water, land, flora, and fauna. Natural resources provide ecosystem service (e.g., flood control, waste assimilation) and are extracted as an input of production (e.g., fossil fuel, timber, tourism) (Green & Haines, 2011). GIS students surveyed the location and health (measured as diameter at breast height [DBH]) of trees in a Chicago neighborhood using GPS receivers (Frye et al., 2007).
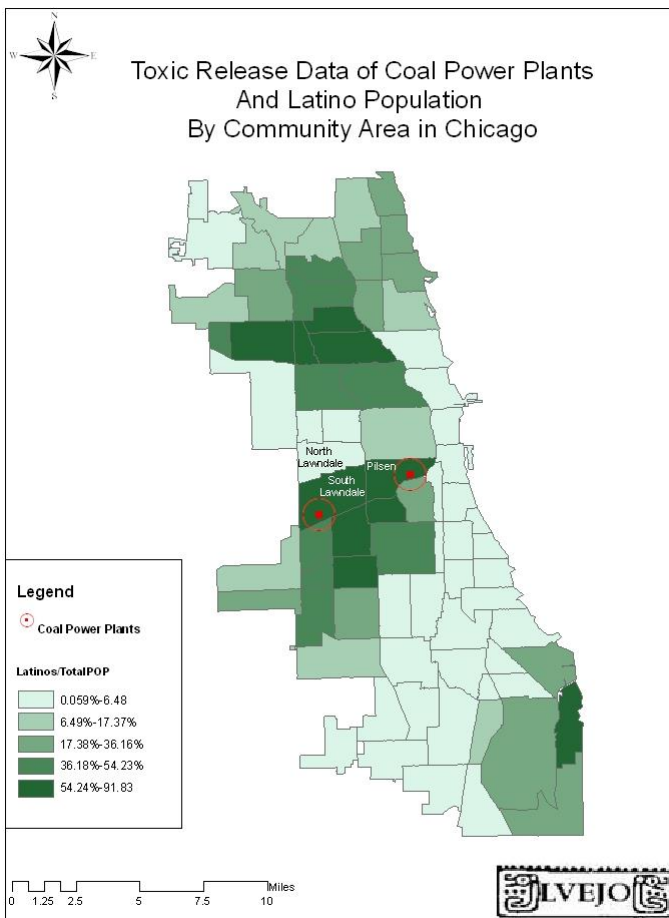
Figure 2. Coal power plants and percent of Latino population by community areas in Chicago (2009).

Figure 1 shows the kernel density of trees weighted by DBH in Lincoln Park. In the map, the darker the shade, the greater the concentration of healthy trees. The map indicates that trees are less healthy in non-residential areas around major roads with much vehicular traffic (the southern part of the map) than in highly residential areas (the northwestern part of the map). This project demonstrates how vehicle emissions affect tree health.

GIS students in collaboration with *Little Village Environmental Justice Organization* (LVEJO) examined whether communities with a large Latino population were more likely to have a power plant and what related health effects might be (Becerra et al., 2009). Figure 2 shows that coal power plants are located in predominantly Latino communities in Chicago.
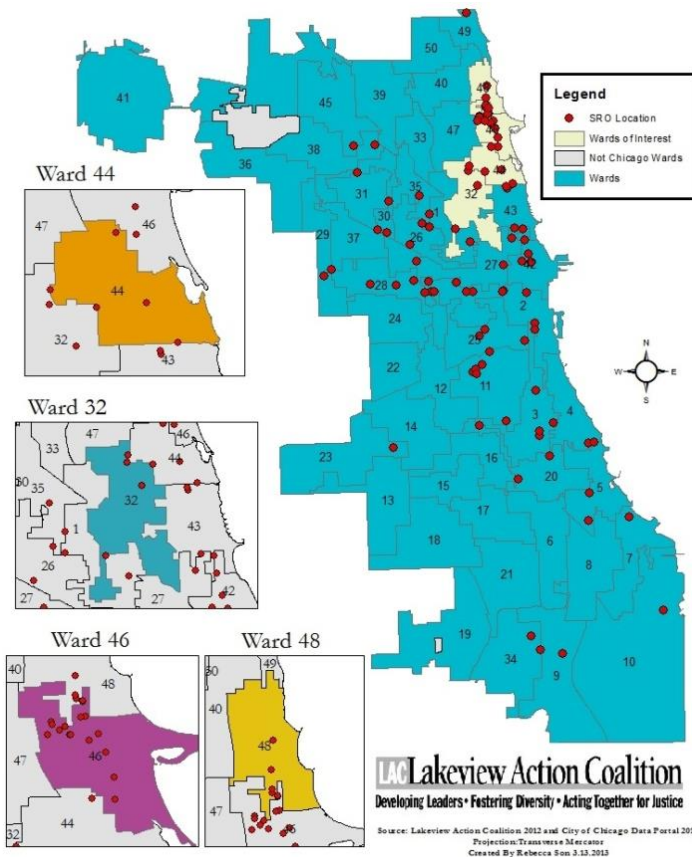
Figure 3. Single room occupancy housing in Chicago (2012).

Built Capital

Built capital includes the buildings, infrastructure (roads, bridges, sewers), and other physical features (railroad tracks, vacant land) in the community. Affordable housing has been a major concern among CBOs, particularly in low-income communities. Single room occupancy housing (SRO's), one source of affordable housing, has been on the verge of being converted to condos in Chicago. GIS students helped *Lakeview Action Coalition* locate SROs and other affordable housing stocks using GIS mapping (Cameron et al., 2013). Figure 3 shows where SROs are located, and in what wards they are concentrated in the North Side of Chicago. CBOs can use this kind of map to protest against market pressure that would potentially displace low-income populations and to determine where to focus their organizing efforts.

Figure 4. Bike infrastructure in Little Village, Chicago as of October 2010.

Driving is a predominant way of getting around in Little Village, Chicago. In the process of a grant application, *Enlace Chicago* surveyed the transportation infrastructure and traffic patterns by different modes of transportation in Little Village. They used GIS to demonstrate the need for

alternative modes of transportation (e.g., bicycling, public transportation) as a means to mitigate traffic congestion. Figure 4 shows bike meters and racks mapped by GIS students as of October 2010 in Little Village (Carlstrom & Vasquez, 2010). Figure 5 represents the relative share of traffic by different modes of transportation at major road intersections surveyed by GIS students as of March 2011 in Little Village (Boyter et al., 2011). The figure shows that cars dominate the traffic (80%) while public transportation (city buses) accounts for 1% of traffic.
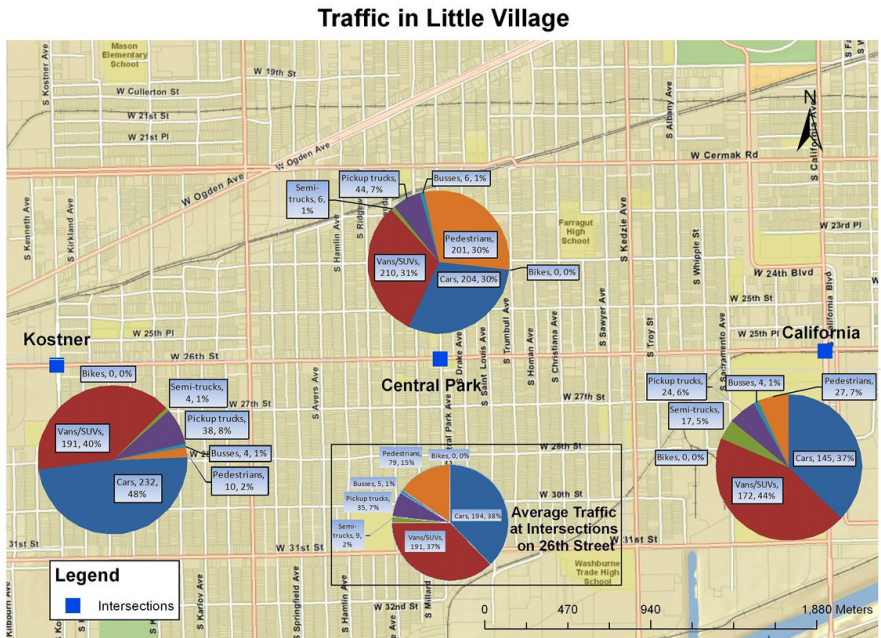
Figure 5. Survey of traffic in major road intersections in Little Village, Chicago as of March 2011.

Existing community assets such as vacant lots can be used as public space for youth education. *Camp Bufferfly* wanted to determine the availability of space that can be potentially used for green youth education with GIS. GIS students identified vacant lots, brown field sites, youth centers, and community gardens using GIS to address the needs of *Camp Butterfly* in the Bronzeville community (Chaffin et al., 2012). This project demonstrates how built capital can be utilized in relation to building human capital in the community.

Human Capital

Human capital, as an essential community asset, refers to the characteristics of individuals performing within the labor market, including educational background, work experience, and health. Since human capital is closely related to the economic health of a community, many CBOs implement workforce development programs. Immigrants in particular do not fully participate in the labor market due to their lack of language skills. *Chicago Federation of Labor*'s Workers Assistance Committee (CFL-WAC) provides maps of free ESL (English as a Second Language) centers to those who lack English skills (Brost et al., 2007).
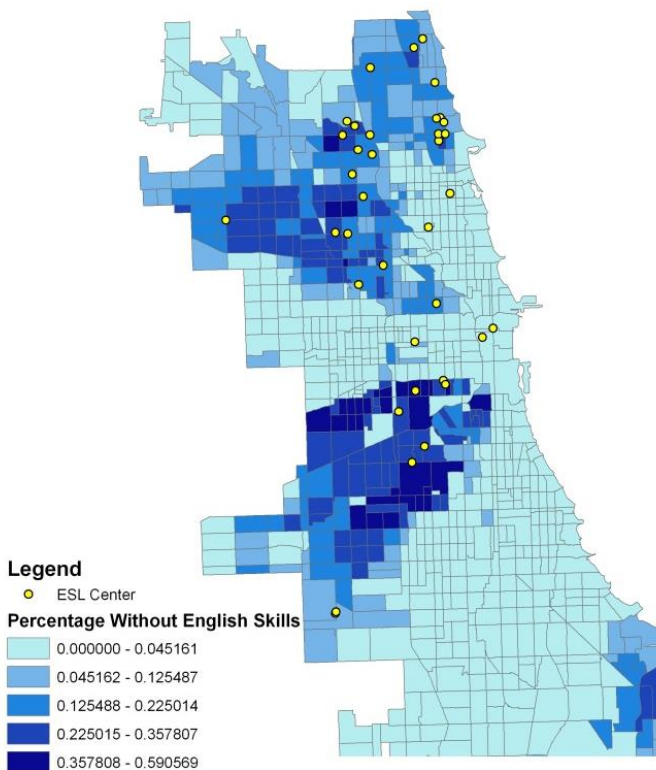
Figure 6. ESL centers and population without English skills in Chicago (2007).

Figure 6 shows where free ESL centers are located and where those without English skills are concentrated at tract levels in Chicago. The figure indicates that the far western and southeastern parts of Chicago do not have enough ESL services for the high proportion of those who need such services while other areas are relatively well-served by ESL centers.

Adequate access to child care can be greatly instrumental in supporting workforce development. *Illinois Action for Children* used GIS to identify so-called "child care deserts" in Cook County to determine where the supply of child care falls short of the likely demand using GIS (Stoll et al., 2009). For this task, GIS students calculated the difference between children likely in need of child care and the slots available in child care centers in each tract. Figure 7 shows how a tract performs relative to other tracts in meeting child care needs. In the map areas shaded brown or dark red represent child care deserts where the demand far exceeds the supply of child care.

The child obesity rate is nearly three times the national average in Humboldt Park, Chicago. In the wake of this significant community health issue, *Puerto Rican Cultural Center* wanted to assess access to healthy food and to inventory community assets that can be utilized to address this community health issue. Students surveyed and mapped community assets and the nutritional value of food venues. Figure 8 shows religious institutions, community assets (community gardens, farmers markets, and health and fitness programs), and grocers and restaurants categorized by nutritional value (produce options, limited produce options, no produce options) in Humboldt Park (Stutsman et al., 2010). Figure 9 shows what areas are within walking distance (500 meters) of grocery stores with fresh produce options (Knight et al., 2011). While there are various food venues in Humboldt Park, food venues with high nutritional value are not widely accessible.

Chicago Public Schools (CPS) launched the Safe Haven, Safe Summer program in partnership with faith-based communities. The program offers free educational programs to help keep youth away from crime particularly in low-income neighborhoods. GIS can be used to determine where the programs might be needed. *Enlace Chicago* used GIS to assess violent crimes committed near schools in connection with the area's youth population to determine potential demand for the Safe Haven program in Little Village. The percent of youth was mapped in Figure 10 to help identify potential demand, and the map was compared to available crime data nearby (Luna et al., 2012).

The locations of emergency food providers (such as food pantries) were mapped to assist Little Village and Pilsen residents who seek food assistance (Robidoux et al., 2011). Figure 11 can help identify where underserved areas

are and determine how emergency food assistance can be coordinated at different times and locations.
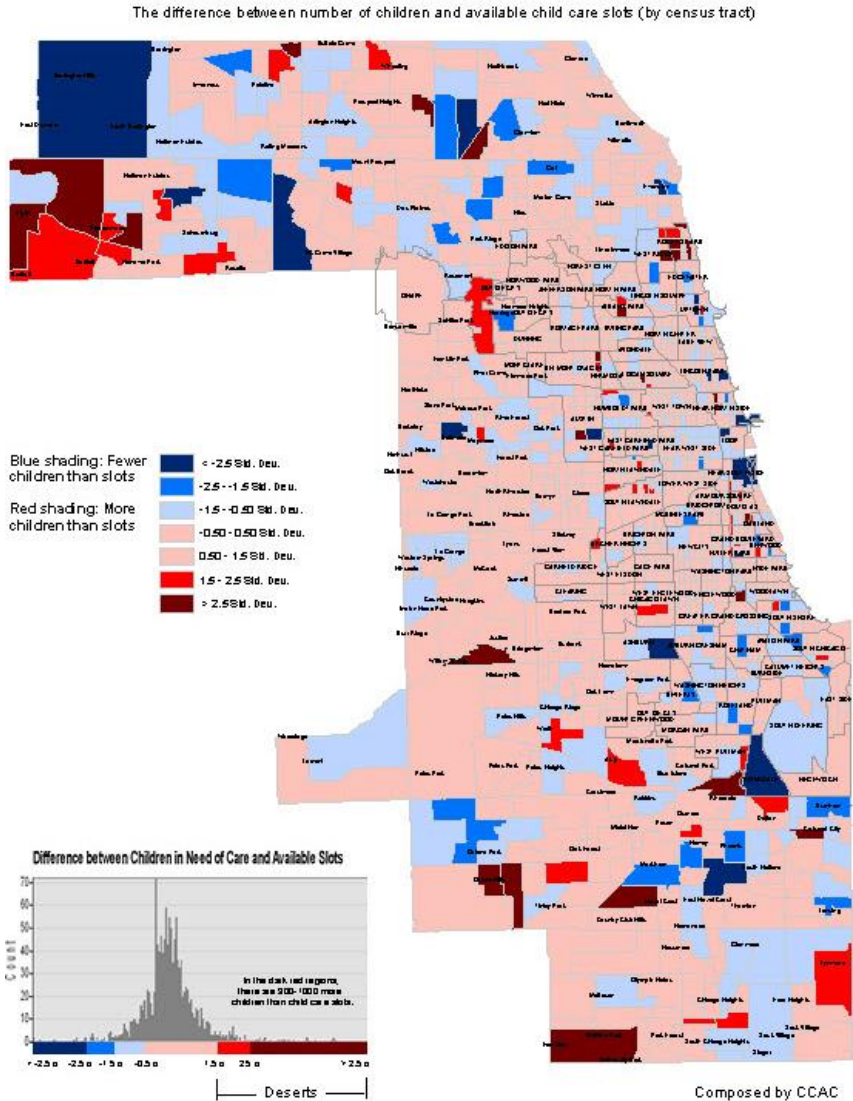
Figure 7. Child Care Deserts in Cook County (2009).
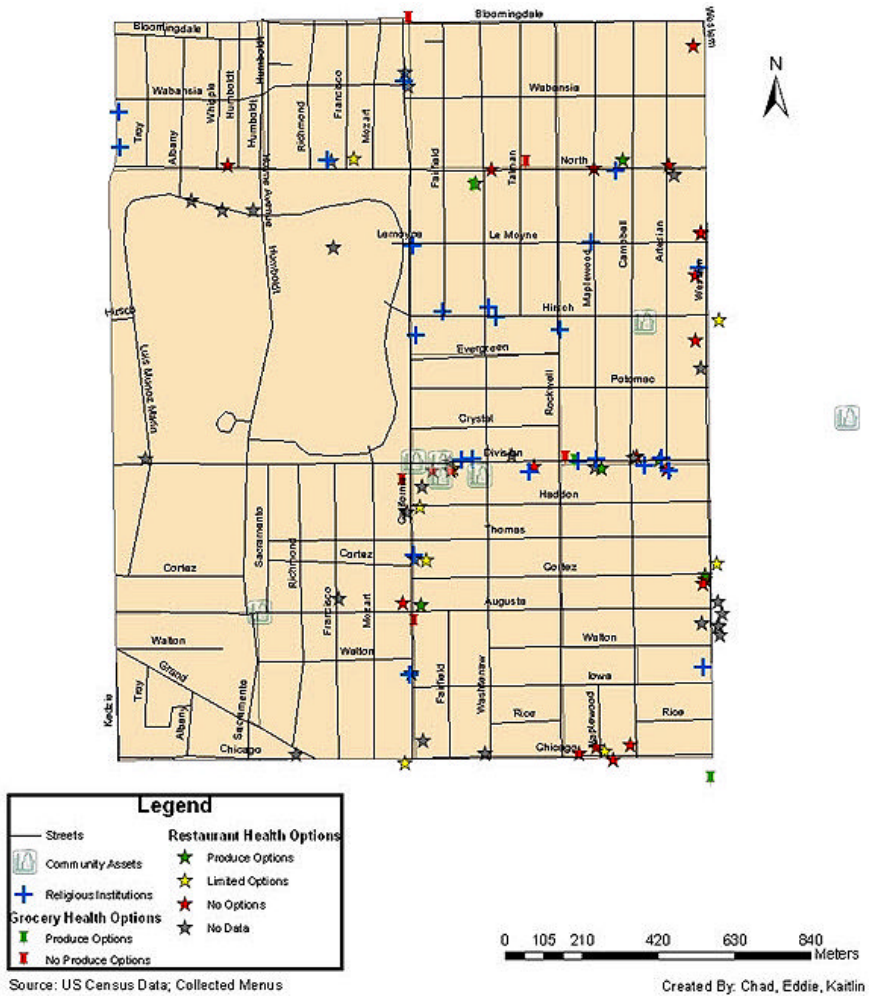
Figure 8. Community assets & food vendors in Humboldt Park (2010).

The Cook County Sheriff's Office runs a Boot Camp program to provide inmates in Cook County Jail with physical and job training. *Chicago Federation of Labor*'s Workers Assistance Committee (CFL-WAC) helps prepare graduates of the Boot Camp for the job market and their return to their communities. GIS was used to examine what communities the Boot Camp participants return to and what the characteristics of those communities are (Ambuehl et al., 2008). This mapping project suggests that if a participant returns to neighborhoods with high crime, unemployment, or poverty, then a participant is more likely to re-engage in criminal activity. This project

provides empirical support for the detrimental influences of negative social capital on human capital and opportunity structures (neighborhood effects) (Sampson et al., 2002).

Figure 9. Areas within 500 meters from grocery stores with fresh produce in Humboldt Park (2011).
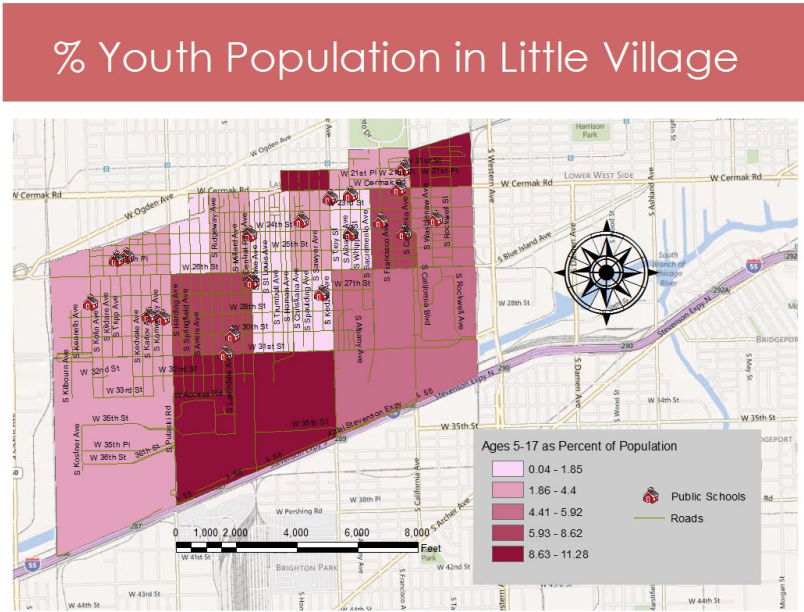
Figure 10. Percent of youth population in Little Village (2012).
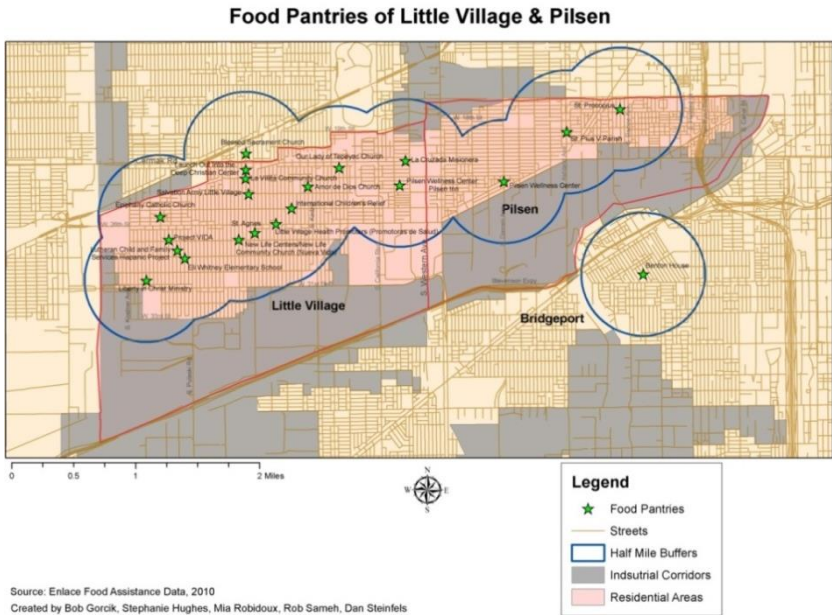
Figure 11. Food pantries of Little Village & Pilsen in Chicago (2011).

Social Capital

Social capital refers to the characteristics of a collection of individuals that are deemed to influence the quality of social relationships in a community, such as social trust, norm, and cohesion. In a society with large stocks of positive social capital, rules will be enforced fairly and therefore those who promote common interests can be rewarded properly. Social capital is developed over time in a way that is unique to the community. What constitutes social capital is subject to debate, but political engagement, corruption, crime, and volunteerism are widely used as measures of social capital (Narayan & Cassidy, 2001).

Many non-profit organizations strive to reach a large number of communities in accomplishing their missions. For example, *Chicago Fair Trade* (CFT) wanted to monitor progress towards increasing the number of fair trade outlets in Chicago. GIS students created a map (Figure 12) that shows where those outlets are located, and which community areas lack fair trade outlets (Barron et al., 2011). CFT used the map to determine where they should focus their outreach efforts. *Institute of Cultural Affairs* (ICA) collected sustainability initiatives in Chicago's 77 community areas for circa 2012 with the help of student interns. Students in the GIS program mapped sustainability initiatives in the process (Paschen et al., 2012). ICA created interactive maps to facilitate sharing knowledge and resources based on common interests towards community sustainability (ICA, 2013).

In addition to its community outreach and information sharing purposes, GIS can help build other subcategories of social capital—namely, political capital, financial capital, and cultural capital. CBOs need to build and increase political capital, access to decision making, in a community to accomplish their missions effectively. CBOs do so by analyzing the local power structure, exposing power relations, and educating the public on pertinent issues. GIS can help exhibit uneven distribution of power and its consequences in the community concerning environmental justice, zoning changes, site proposals, and so on. GIS has long been advocated as a tool for public participation due to its ability to help engage the public and to help build common understanding on issues. CBOs make spatial narratives to advance their agendas using GIS (Elwood, 2006).

Latino Policy Forum mapped the Latino voting age population by election districts (Figure 13) to devise place-based strategies for mobilizing their constituencies (Hernandez et al., 2013). *LVEJO* exposed uneven power relations manifested in spatial distribution of hazardous waste sites (Becerra et

al., 2009). *Active Transportation Alliance* (formerly known as Chicagoland Bicycle Federation) identified bicycle crash hot spots (Figure 14) using GIS to raise awareness of bicyclers' safety issues and to make evidence-based recommendations for promoting bicycling (Weiss & Rygh, 2007).
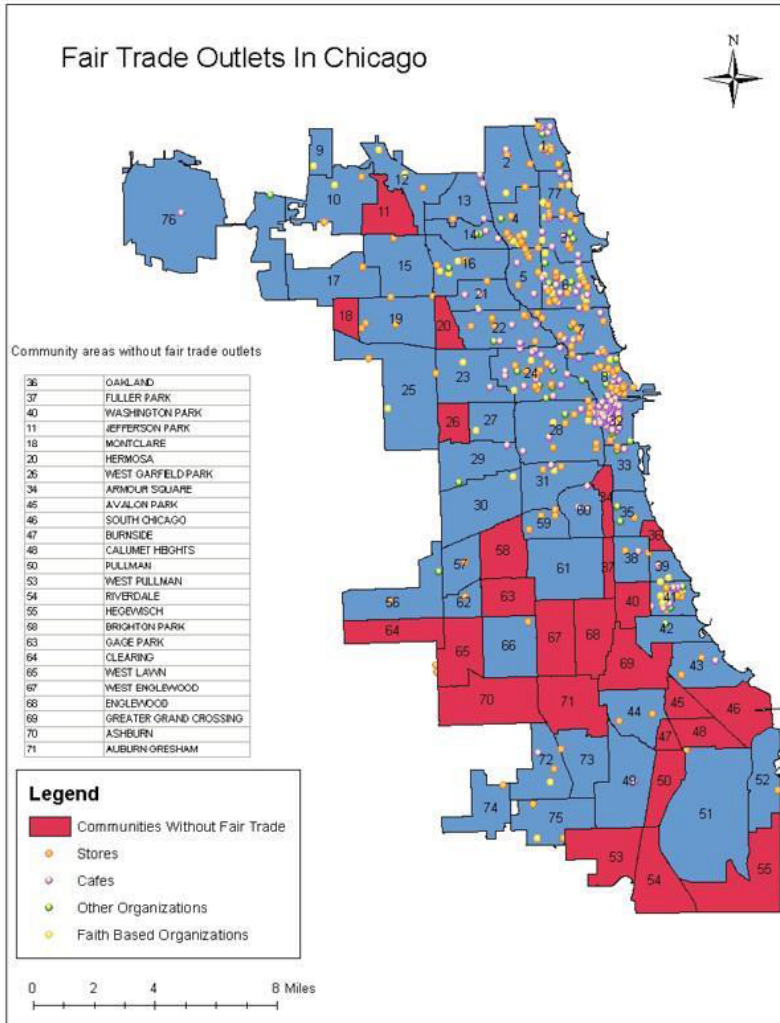
Figure 12. Fair trade outlets in Chicago (2011).

While access to financial capital is crucial to economic development, credit markets do not respond well to the needs of poor communities. The poor and minority often experience discriminatory and predatory lending, but lack

the resources to meet their credit needs. Underserved communities have been vulnerable to market volatility as observed during the recent recession. CBOs protest against unfair lending practices and work to build local credit markets while navigating the available policy tools.
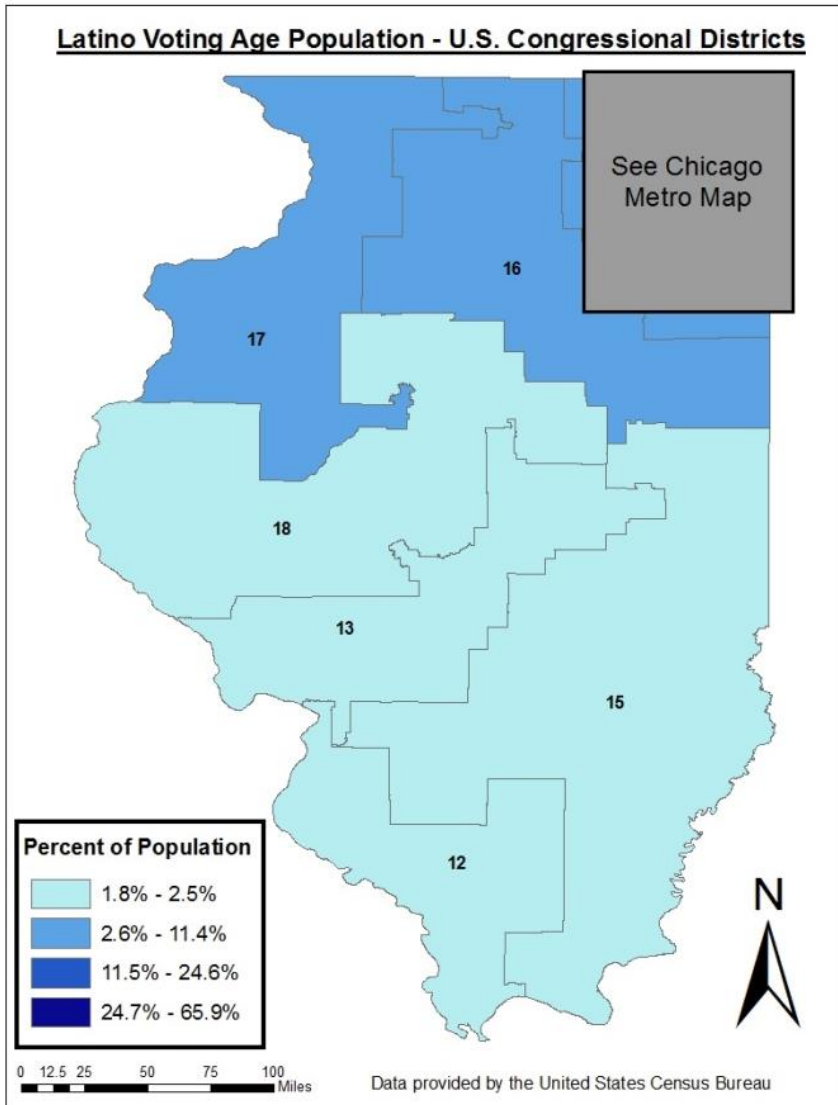
Figure 13. Continued on next page.
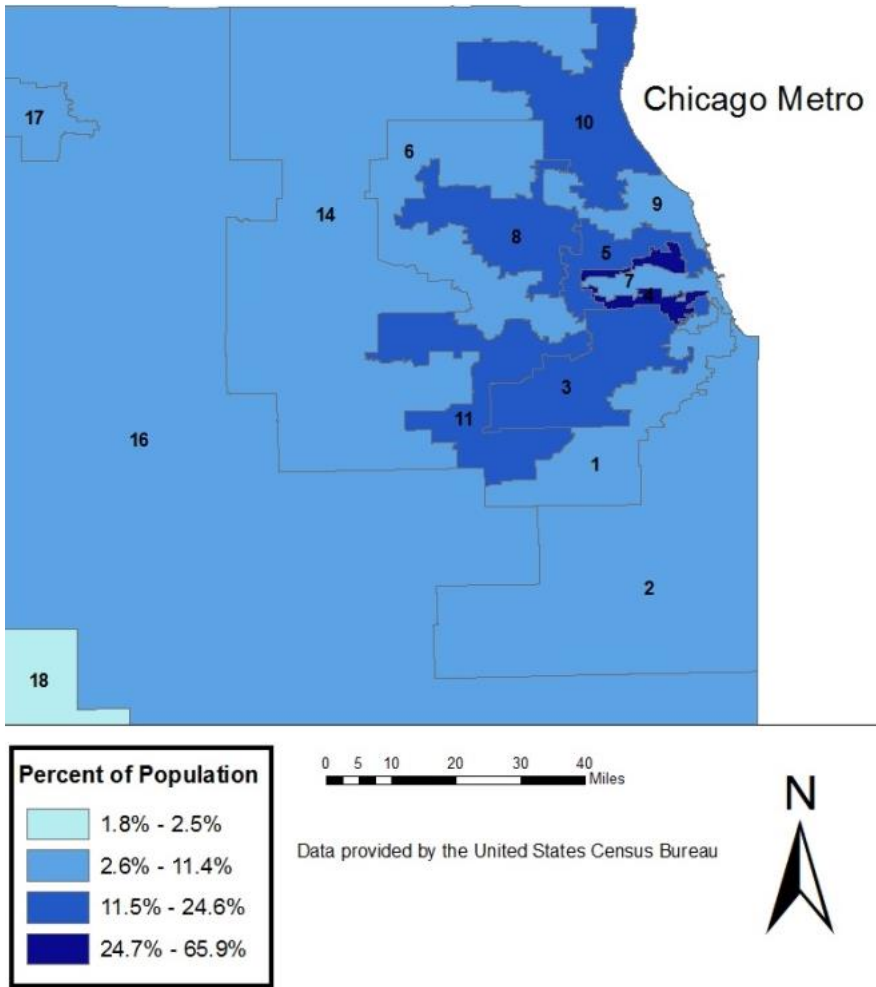
Figure 13. Latino voting age population by U.S. Congressional Districts in Illinois (2010).

Latino Policy Forum assessed the impact of foreclosures on the Latino population using data provided through the Home Mortgage Disclosure Act (HMDA). They used GIS as a visual tool to demonstrate the uneven impact on the Latino population (McConnaughhay et al., 2013). Figure 15 shows that foreclosure auctions were largely concentrated in predominantly Latino communities during 2010 - 2012.
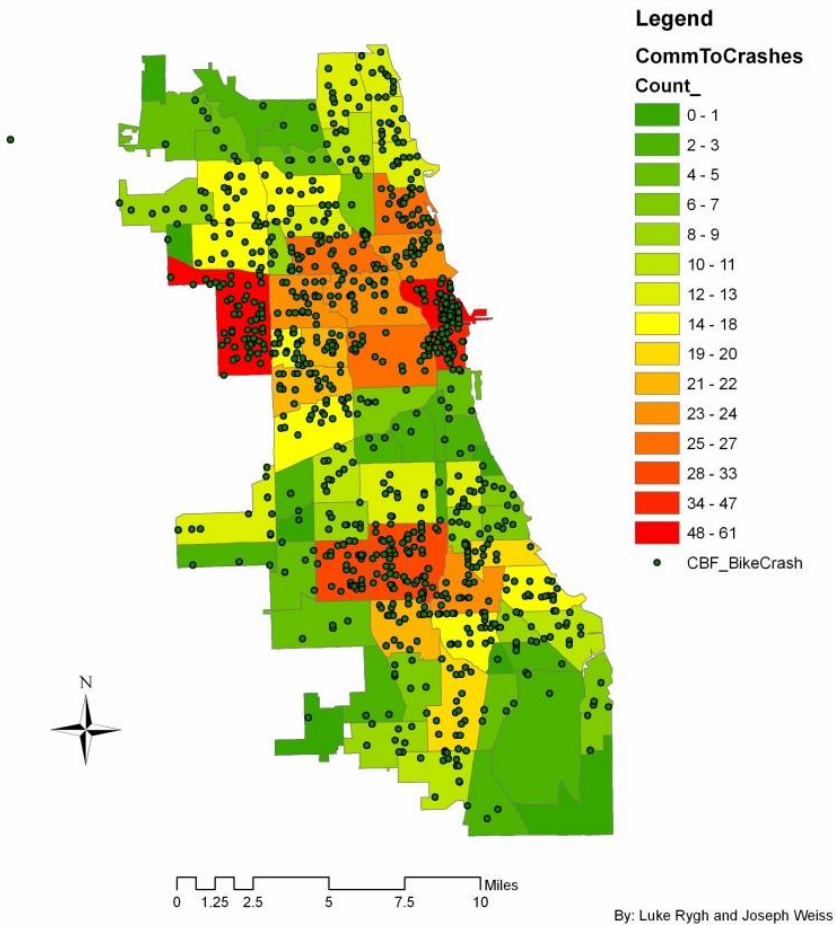
Figure 14. Number of bicycle crashes by community areas in Chicago (2005).

A growing number of CBOs (and governments) have relied on enhancing cultural capital as a strategy to revitalize the local economy and promote a sense of community. Their activities include hosting art-related events, designating historic and conservation districts, and attracting "creative classes" (Florida, 2014). *Bronzeville Visitor Information Center* believes that the cultural assets scattered around Bronzeville can be leveraged to promote tourism and generate local job opportunities. GIS was utilized to map cultural assets as a source for developing cultural art tours in the community (Nieciak et al., 2012) (Figure 16).
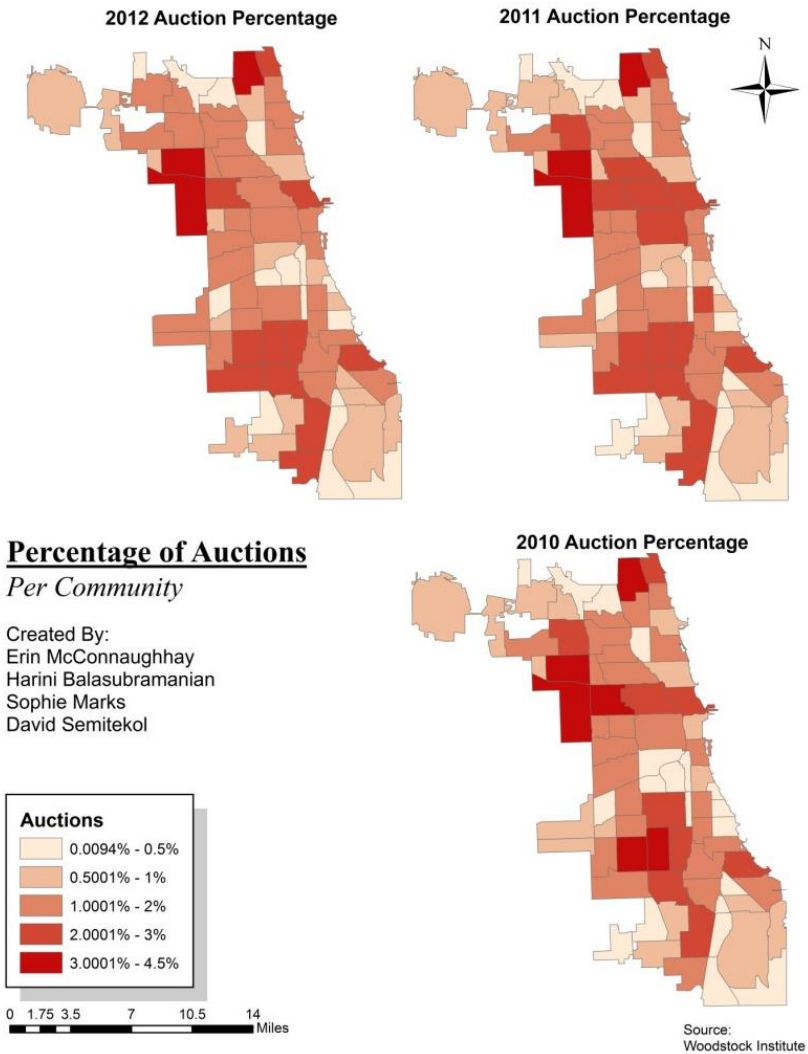
Figure 15. Percent of auctions from 2010 to 2012 by Chicago's community areas.

Different forms of capital are not necessarily mutually exclusive, but rather mutually reinforce one another. For example, workforce development and civic education (human capital) affects social trust (social capital). Affordable housing (built capital) cannot be developed without the proper use of financial capital (access to credit) (Green & Haines, 2012). Characteristics of social capital unique to community can affect the rate in which innovation drives economic development (e.g., Silicon Valley) (NRC, 1997).

CBOs can benefit from an improved understanding of the relationships among different forms of capital. This can lead to designs for smart programs that target environmental, social, and economic sustainability goals in a balanced manner. Urban agriculture or community gardens initiatives are good examples of integrated programs designed to develop the workforce and address food security issues while reducing carbon footprint at the same time.

Figure 16. Tourism maps for Bronzeville, Chicago: cultural assets in Zone 1 (2012).

It appears that CBOs develop both specialized and integrated programs these days. For instance, CBOs can offer financial advice and technology training to community members facing the foreclosure crisis and joblessness in the community. While this (specialization of programs) is a welcome trend, more integrated programs that cut across natural and human systems are needed as sustainability increasingly becomes a new political ideal. This section suggests that thus far CBOs have been less active in developing programs related to natural capital than in those related to man-made capital. This, however, seems to be changing. According to the ICA (2013), there were over 900 sustainability initiatives in Chicago's 77 community areas as of Fall 2013. It should be noted, however, that there is ambiguity over what are considered sustainability initiatives, and the quality of the sustainability initiatives data posted on the ICA's website is not verified. CBOs can apply the capital framework to analyze the interaction among different forms of capital and devise integrated programs toward sustainability.

3. ASSESSING COMMUNITY SUSTAINABILITY USING THE CAPITAL FRAMEWORK

There is increasing recognition that we ought to live within ecological means so that we do not compromise the capabilities of future generations to meet their own needs (Brudtland, 1987). The concept of sustainability has arisen from debates on how to balance the goal of economic and social development with environmental conservation. A consensus on human modification of the environment has emerged among the scientific community as scientists call for collective action to prepare for climate change (Solomon, 2007). More and more communities are compelled to participate in the collaborative process towards sustainable development as communities recognize that sustainability is essential to their survival. Community-based sustainability initiatives, however, have been barely informed by theories of sustainability or supported by tools for assessing sustainability.

Capital Theory of Sustainability

Economic theories of sustainability extend the concept of capital to include nature. Natural capital has two components: resource capital and environmental quality (Purvis & Grainger, 2005). Resource capital refers to the *stocks* of all natural resources that are either renewable (e.g., forests, fisheries) or non-renewable (e.g., fossil fuels). Environmental quality refers to the condition of environmental *sinks* such as land, water, and air that provide an assimilative function.

Critical natural capital is capital that is essential to support life and thus should be maintained under any circumstances favoring present and future generations (Brand, 2009); examples include areas of tropical forests with high biodiversity and carbon stocks. Theories state that a development path is strongly sustainable if critical natural capital does not decline (Solow, 1986) and is weakly sustainable if total stocks of capital (natural, built, human, and social capital) do not decline (Pearce & Atkinson, 1993). The difference between so-called strong and weak sustainability condition comes from different views on the relations between economy and environment.

If environment subsumes economy, sustainability means maintenance of critical natural capital (that is, strong sustainability) since all man-made capital (built, human, and social capital) depends on natural capital. If environment

does not necessarily subsume economy but rather is interdependent on economy, sustainability means maintenance of total stocks of capital (that is, weak sustainability) since improvement in man-made capital (such as development of alternative energy, enforcement of pollution tax) can offset some decline in natural capital.

The first view is significant in that it specifies the minimal necessary condition of sustainability and inspires environmentalists to action. This view, however, neglects the human dimension and what constitutes critical natural capital is subject to debate. That is, the view does not recognize the potential of man-made capital to improve natural capital. The Green Belt Movement in Kenya illustrates the role of man-made capital that mutually reinforces natural capital—how communities organize themselves to choose the path to preserve natural resources by planting trees to educate the workforce and improve the quality of life in their communities.

The second view suggests that one can minimize consumption of natural resources while finding solutions, leaving room for human efforts. However, it is unrealistic to presume perfect substitutive relationships among natural capital and man-made capital since some critical natural capital simply has no substitute. A more realistic view is to preserve critical natural capital while acknowledging the tradeoff relations that exist between natural capital and man-made capital. Therefore, sustainability cannot be assessed without an understanding of this nature-society relation. The capital theory of sustainability provides a calculus for integrating natural and human systems (i.e., natural capital and man-made capital in economic terms), and offers a starting point to assess sustainability in an integrative manner. Once the concept of sustainability is theorized, aspects of sustainability can be measured to assess sustainability objectively.

Developing and Organizing Sustainability Indicators Informed by Capital Theory

What is measured can be managed. Without indicators, it would be hard to monitor progress toward sustainability. Sustainability indicators should serve as a pointer to symptoms of system (e.g., Biochemical Oxygen Demand or BOD to monitor the self-cleansing of water), and an orientor of systems (e.g., the rate of fossil fuel exploitation/rate of alternative energy development) (Meadows, 1998). Additionally, good sustainability indicators should be integrative (i.e., should portray linkages among the environmental, economic,

and social dimensions of sustainability) and be distributional (i.e., should measure intra-generational equity in addition to inter-generational equity) (Maclaren, 1996). Many sustainability indicators are global or national in scope; fewer have been developed at the community level. Research recognizes that developing sustainability indicators at the community level involves collaborative and adaptive learning processes (Valentin & Spangenberg, 2000; Reed et al., 2006). Little research examines the role of technology (such as GIS) in this process.

Sustainability indicators can be organized into natural capital, built/human capital, and human/social capital according to Daly (1973). An advantage of organizing sustainability indicators this way is that the framework can be tied to the capital theory discussed above (UN, 2007). Humans have modified natural ecosystems by exploiting resource *stocks* and depositing waste into *sinks*. At the same time, technology and political economy, the realm of human dimensions, can be deployed to minimize detrimental environmental effects. Sustainability indicators can be organized so that the dynamics of human-environmental interaction can be monitored and examined. The framework is *hierarchical* in that it acknowledges the fundamental quality of natural capital as the foundation of human economy, and is *integrative* in that it emphasizes the interaction between natural capital and man-made capital in relation to sustainability of the planet.

The Daly Triangle (Daly, 1973) provides an idealized view of the capital framework (Figure 17). The triangle is premised on the idea that the economy is ultimately built to fulfill human well-being and all other forms of capital ultimately rest on natural capital. Therefore, well-being can be seen as ultimate ends and natural capital can be seen as ultimate means. Built capital, human capital, and social capital play a crucial role in rendering the ultimate means to be sustainably used and the ultimate ends to be sufficiently satisfied (Meadows, 1998). The commonly held view of economic growth overlooks environmental costs and the productive nature of well-functioning governance. In other words, the Daly Triangle attempts to revise the economic system from the system that only accounts for built and human capital as means; to the system also accounts for human/social capital as ends that need be in balance with natural capital.

Using the Capital Framework to Assess Community Sustainability

Once sustainability indicators are organized into four tiers following the Daly Triangle, one can monitor progress toward community sustainability by posing the following three questions; the questions focus on the sufficiency of ultimate ends, channeling from ultimate means to ultimate ends, and the sustainability of ultimate means (Meadows, 1998).

- Are ultimate ends sufficiently realized?
- How efficiently are ultimate means translated into ultimate ends?
- Is natural capital (ultimate means) sustainably used?

The first question regards what "fundamental human needs" are in the face of an unsustainable pattern of consumption and production and whether there are any barriers to fulfilling human potential (e.g., social injustice, human rights issues) in contemporary society. The second question is concerned with how institutions function to induce the private sector or civil society to use natural resources efficiently and minimize human impacts. For example, do institutions enact policy frameworks that internalize (or account for) environmental costs to correct potential market failure? Examples include pollution taxes, congestion charges, and energy efficiency standards that meet community needs and enable adaptation to climate change. The third question can be posed to determine whether the rate of natural resource usage exceeds the rate of regeneration of stocks, and whether the rate of waste emissions exceeds the rate of recovering the absorptive capacities of sinks.

While the capital framework has some theoretical utility, it encounters problems when put into practice in policy-setting and community development. The integrative nature of the framework may render the tasks of developing indicators overwhelming. There is an ongoing debate over the relationship between economy and environment and what constitutes critical natural capital, which does not encourage practitioners to utilize this framework. Finally, the framework is not explicit about intra-generational equity. GIS can help address some of these problems to be discussed later.

We are still in the process of building a consensus on best practices for measuring and assessing sustainability and we do not understand the emergent and complex properties of the dynamic human-environmental interaction yet (Clark & Dickinson, 2003). As we make this journey, geospatial technology

can play a significant role in improving scientific understanding and building a consensus that will shape the path towards sustainability.
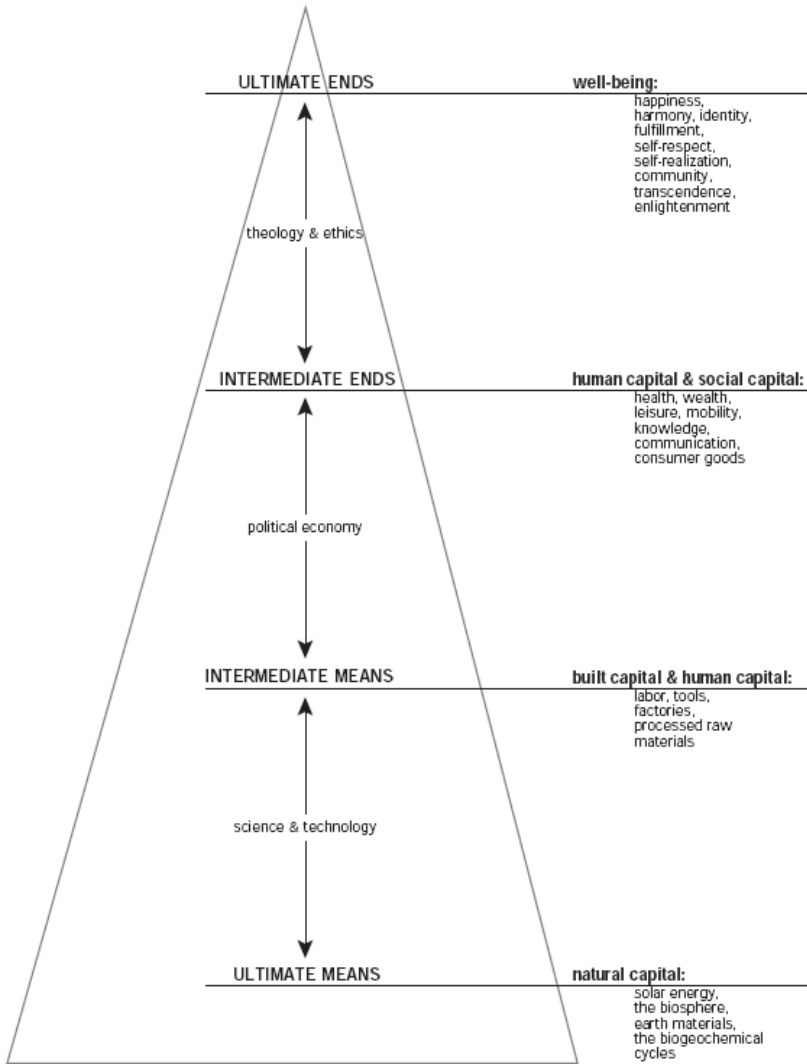
Figure 17. Daly Triangle: the capital framework for organizing sustainability indicators (Meadows, 1998).

4. ASSESSING COMMUNITY SUSTAINABILITY SPATIALLY WITH GIS

GIS is particularly useful for sustainability assessment since it can integrate data in various domains across natural systems (water, air, land) and human systems (political, social, economic characteristics). GIS can be used to capture aspects of sustainability that have been elusive to measure—such as natural capita and social capital—through hyperspectral remote sensing, ubiquitous GPS tracking, and social media. In addition, visualization of multidimensional data in GIS can compress large amounts of information and convey information effectively. With GIS, one can monitor change and analyze spatial distribution and the relationships of entities. This (integration, visualization, and analysis of appropriate data) can facilitate the collaborative learning process of identifying issues related to sustainability, particularly through open platforms like GeoWeb 2.0. GIS can help address the limitations of the capital framework discussed earlier (i.e., integration of large data, lack of understanding of the society-nature relation, lack of attention to distributional aspects of sustainability). Despite the potential of GIS discussed above, GI has been underutilized due to an inadequate understanding of spatial concepts (Marsh et al., 2007).

Here I present a typology of geospatial inquiries applicable to sustainability-related issues. This is intended to address an inadequate appreciation of spatial concepts and to guide GIS users to think more spatially about sustainability. GIS can address the following five questions (Hwang, 2013). Working definitions of those geospatial inquiries are provided below:

- Spatial Distribution (SD): where things are in a place/region
- Spatial Interactions (SI): how things interact between places/regions
- Spatial Relationships (SR): where things are related across domains in a place/region
- Spatial Comparisons (SC): where things differ among places/regions
- Temporal Relationships (TR): how things change in places/regions

Here *thing* is used as an umbrella term to refer to objects (spatially discrete phenomena such as land parcels and roads), fields (spatially continuous phenomena such as temperature and elevation), and events (dynamic geographic phenomena such as earthquakes and crime incidents) (Goodchild et al., 2007). The term *place/region* is a domain-specific multi-

scalar construct; for instance, climatic regions can be defined specifically for the climactic domain at varying geographic scales.

SD involves recognizing the identity of a spatial entity (e.g., what is a watershed?) and identifying the location (or extent) of the spatial entity (e.g., where is a watershed?) and spatial distribution of variables (e.g., precipitation in a watershed). SI involves recognizing how entities are connected among places/regions (e.g., how does city A interact with city B?). SI is equivalent to the concept of flow and movement from one place/region to another. SR concerns noting how entities of one domain are associated with those of another (e.g., how is a runoff level associated with land cover types in a watershed?). SR is equivalent to the concept of correlation. SC focuses on differences between places/regions (or idiosyncrasy of locality) whereas SI focuses on connections between places/regions. TR examines changes in where things are, how things interact, how things are related, and how things differ. Figure 18 depicts five geospatial inquiries in the geographic matrix (Berry, 1964) that synthesizes subject matters of geography—characteristics (rows of the matrix) of regions (columns of the matrix) over time (tiers of the matrix).
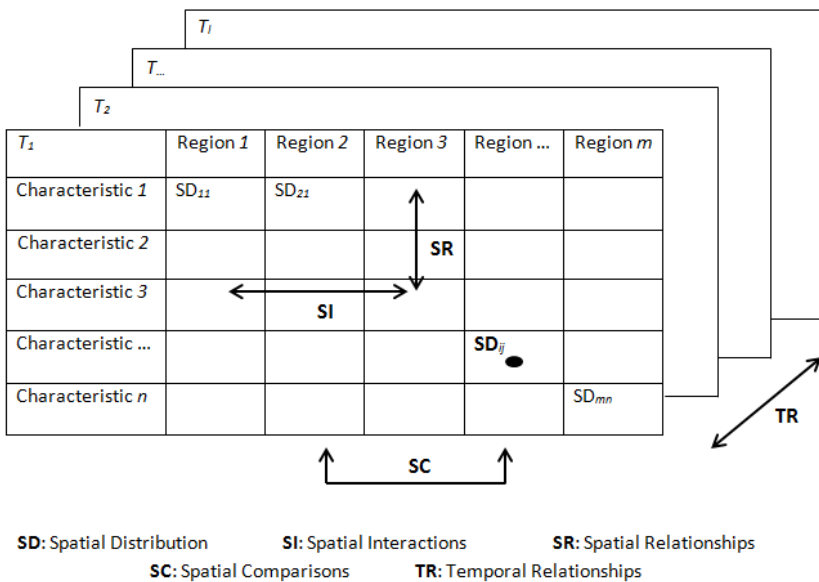
Figure 18. Geospatial inquiries in the geographic matrix (Hwang, 2013).

Geospatial inquiries begin with describing the spatial distribution of objects, fields, and events. Performing spatial interaction tasks (e.g., seeing how air pollution diffuses, how water flows along streams, and where food comes from) is important to understanding how places are interconnected. Engaging in spatial relationships inquiry encourages one to make connections across domains (interdisciplinary thinking) and better understand cross-cutting concepts of sustainability, "improving the quality of human life while living within the carrying capacity of supporting ecosystems" (IUCN, 1991). Spatial comparisons inquiry is instrumental in revealing place-specific characteristics. Temporal relationships inquiry is appropriate for investigating the intrinsically dynamic nature of sustainability of the biosphere.

CONCLUSION

In this chapter I propose that CBOs can use GIS to (a) help build different forms of community capital; (b) assess community sustainability as an interaction and a composite of different forms of capital; and (c) explore directional (inter-generational equity), distributional (intra-generational equity), and relational (integrative) aspects of sustainability. That is, one can better understand the dynamic society-nature relationship and monitor progress toward sustainability by applying spatial thinking to the capital framework in the GIS platform. The chapter illustrates the value of geographic information in community development and reviews how economic theories and geospatial tools can help foster community sustainability.

CBOs will develop more environmentally-informed programs as public awareness of sustainability increases. The trend will accelerate with an improved ability to monitor the features and functions of natural ecosystems. The use of remotely sensed imagery or sensor networks in the field will allow us to monitor conditions of vegetation, chlorophyll in the ocean, climatic conditions, flooding, and water contamination in a timely fashion. Increasingly user-friendly geospatial tools will help us monitor these changes in an easy-to-understand manner. With further developments in spatial data infrastructure (Williamson et al., 2004) including the recent climate initiatives by the White House (2014), this future scenario will be realized soon.

REFERENCES

Ambuehl, A., Barreiro, L., Chaffin, J., & Lydum, D. (2008, June). CFL and the Boot Camp Way to Succeed. Retrieved from http://gis.depaul.edu/shwang/cgis/Spr0708_Bootcamp.pdf.

Barron, C., Jones, M., Formentini, B., Marshall, E., & Birza, V. (2011, March). Chicago Fair Trade. Retrieved from http://gis.depaul.edu/shwang/cgis/Win1011_CFT.pdf.

Becerra, M., Armstrong, M., Foley, L., & Loomis, N. (2009, March). Environmental Justice: Mapping Coal Power Plants in Illinois and Chicago. http://gis.depaul.edu/shwang/cgis/Win0809_LVEJO.pdf.

Berry, B. J. L. (1964). Approaches to Regional Analysis: A Synthesis. *Annals of the Association of American Geographers*, *54*(1), 2–11. doi:10.1111/j.1467-8306.1964.tb00469.x.

Boyter, K., Fendrich, D., Svoboda, A., Vorobel, J., & Wiegand, A. (2011, March). Transportation in Little Village: Why People Move The Way They Do. http://gis.depaul.edu/shwang/cgis/Win1011_EC_TR.pdf.

Brand, F. (2009). Critical natural capital revisited: Ecological resilience and sustainable development. *Ecological Economics*, *68*(3), 605–612. doi:10.1016/j.ecolecon.2008.09.013.

Brost, J., Levy, L., & Nikokiris, G. (2007, November). English As A Second Language: Community Service Project. Retrieved from http://gis.depaul.edu/shwang/cgis/Aut0708_CFL.pdf.

Brundtland, G. (1987). Our Common Future: Report of the 1987 World Commission on Environment and Development.

Cameron, D., Wood, D., Farhan, H., Pinkley, K., & Son, R. (2013, March). Mapping Affordable Housing in Chicago. Retrieved from http://gis.depaul.edu/shwang/cgis/Win1213_LAC.pdf.

Carlstrom, Z., & Vasquez, A. (2010, November). Bikes, Bikers and Infrastructure. http://gis.depaul.edu/shwang/cgis/Aut1011_EC.pdf.

Chaffin, M., Kohler, F., Siddick, S., & Burgess, P. (2012, March). Potential Green Spaces In Proximity to Camp Butterfly. Retrieved from http://gis.depaul.edu/shwang/cgis/Win1112_CB.pdf.

Clark, W. C., & Dickson, N. M. (2003). Sustainability science: The emerging research program. *Proceedings of the National Academy of Sciences*, *100*(14), 8059–8061. doi:10.1073/pnas.1231333100.

Craig, W. J., & Elwood, S. A. (1998). How and Why Community Groups Use Maps and Geographic Information. *Cartography and Geographic Information Systems*, *25*(2), 95–104. doi:10.1559/152304098782594616.

Daly, H. E. (1973). Toward a steady-state economy. *CERN Document Server*. Retrieved April 6, 2014, from http://cds.cern.ch/record/275371.

Elwood, S. (2006). Beyond Cooptation or Resistance: Urban Spatial Politics, Community Organizations, and GIS-Based Spatial Narratives. *Annals of the Association of American Geographers*, *96*(2), 323–341. doi:10.1111/j.1467-8306.2006.00480.x.

Elwood, S., & Ghose, R. (2001). PPGIS in Community Development Planning: Framing the Organizational Context. *Cartographica: The International Journal for Geographic Information and Geovisualization*, *38*(3), 19–33. doi:10.3138/R411-50G8-1777-2120.

Esnard, A.-M. (2007). Institutional and organizational barriers to effective use of GIS by community-based organizations. *URISA Journal*, *19*(2), 13–21.

Florida, R. (2014). *The rise of the creative class, revisited*. New York: Basic Books.

Frye, K., Nyerges, M., Baer, E., Metz, A., & Wagenblast, A. (2007, March). Lincoln Park Tree Health Study. Retrieved from http://gis.depaul.edu/ shwang/cgis/Win0607_LPTree.pdf.

Goodchild, M. F., Yuan, M., & Cova, T. J. (2007).Towards a general theory of geographic representation in GIS. *International Journal of Geographical Information Science*, *21*(3), 239–260. doi:10.1080/13658810600965271.

Graymore, M. L. M., Wallis, A. M., & Richards, A. J. (2009). An Index of Regional Sustainability: A GIS-based multiple criteria analysis decision support system for progressing sustainability. *Ecological Complexity*, *6*(4), 453–462. doi:10.1016/j.ecocom.2009.08.006.

Green, G. P., & Haines, A. (2012). *Asset building & community development*. Thousand Oaks, Calif.: SAGE.

Hernandez, A., Peacock, T., & LaPiana, S. (2013, March). Tracking Latino Population Density and Voting Age Population in Illinois. Retrieved from http://gis.depaul.edu/shwang/cgis/Win1213_LPF_LVAP.pdf.

Hwang, S. (2013). Placing GIS in sustainability education. *Journal of Geography in Higher Education*, *37*(2), 276–291. doi:10.1080/ 03098265.2013.769090.

Institute of Cultural Affairs. (2013, October). Accelerate 77 - View the Map. Retrieved April 7, 2014, from http://www.accelerate77.net/map/view-the-map.

IUCN (International Union for Conservation of Nature). (1991). *Caring for the earth: A strategy for sustainable living*.

Knight, E., Berggren, M., Causton, D., & Fernandez, B. (2011, March). Fresh Produce and Health Care Access in Humboldt Park. Retrieved from http://gis.depaul.edu/shwang/cgis/Win1011_PRCC.pdf.

Kretzmann, J. P., & McKnight, J. L. (1993). *Building communities from the inside out a path towards finding and mobilizing a community assets*. Chicago, Ill: ACTA Publ.

Luna, A., Gonzalez, L., Rodriguez, B., Mariscal, R., & Gorman, K. (2012, March). Moving Towards Revitalization and Safety: An Analysis of Little Village. http://gis.depaul.edu/shwang/cgis/Win1112_EC.pdf.

Maclaren, V. W. (1996). Urban Sustainability Reporting. *Journal of the American Planning Association*, *62*(2), 184–202.doi:10.1080/01944369608975684.

Marsh, M., Golledge, R., & Battersby, S. E. (2007). Geospatial Concept Understanding and Recognition in G6–College Students: A Preliminary Argument for Minimal GIS. *Annals of the Association of American Geographers*, *97*(4), 696–712. doi:10.1111/j.1467-8306.2007.00578.x.

McConnaughhay, E., Balasubramanian, H., Semiteko, D., & Marks, S. (2013, March). Comparing Foreclosure Rates to Latino Populations by Chicago Community Areas. Retrieved from http://gis.depaul.edu/shwang/cgis/Win1213_LPF_LF.pdf.

Meadows, D. (1998). Indicators and Information Systems for Sustainable Developmnet. The Sustainability Institute. Retrieved April 7, 2014, from https://www-auth.uwrf.edu/SCISCD/upload/Indicators-Information.pdf.

Narayan, D., & Cassidy, M. F. (2001). A Dimensional Approach to Measuring Social Capital: Development and Validation of a Social Capital Inventory. *Current Sociology*, *49*(2), 59–102. doi:10.1177/0011392101049002006.

National Research Council (1997). Rediscovering geography: new relevance for science and society. Washington, D.C: National Academies Press.

National Research Council (2006). *Learning to think spatially*. Washington, D.C: National Academies Press.

National Research Council (2010). *Understanding the changing planet: strategic directions for the geographical sciences*. Washington, D.C: National Academies Press.

Nieciak, J., Sullivan, C., Collins, P., & Friloux, C. (2012, March). Mapping community assets in Bronzeville. Retrieved from http://gis.depaul.edu/shwang/cgis/Win1112_BVIC.pdf.

Paschen, M., Yoshimura-Rank, M., Groos, N., & McNeese, C. (2012, March). Accelerate 77: Accelerating Green Initiatives in Chicago's 77 Community

Areas. Retrieved from http://gis.depaul.edu/shwang/cgis/Win1112_ ICA.pdf.

Pearce, D. W., & Atkinson, G. D. (1993). Capital theory and the measurement of sustainable development: an indicator of "weak" sustainability. *Ecological Economics*, *8*(2), 103–108. doi:10.1016/0921-8009(93)900 39-9.

Purvis, M., & Grainger, A. (Eds.). (2005). *Exploring sustainable development: Geographical perspectives*. Routledge.

Reed, M. S., Fraser, E. D. G., & Dougill, A. J. (2006). An adaptive learning process for developing and applying sustainability indicators with local communities. *Ecological Economics*, *59*(4), 406–418. doi:10.1016/ j.ecolecon.2005.11.008.

Robidoux, M., Gorcik, B., Hughes, S., Sameh, R., & Steinfels, D. (2011, March). Spatial Representations of Emergency Food Assistance in the Little Village and Pilsen Communities. Retrieved from http:// gis.depaul.edu/shwang/cgis/Win1011_EC_FA.pdf.

Roseland, M., & Connelly, S. (2005). *Toward sustainable communities: resources for citizens and their governments*. Gabriola Island, BC: New Society Publishers.

Sampson, R. J., Morenoff, J. D., & Gannon-Rowley, T. (2002).Assessing "Neighborhood Effects": Social Processes and New Directions in Research. *Annual Review of Sociology*, *28*, 443–478.

Sheppard, S. R. J. (2005). Landscape visualisation and climate change: the potential for influencing perceptions and behaviour. *Environmental Science & Policy*, *8*(6), 637–654. doi:10.1016/j.envsci.2005.08.002.

Sieber, R. E. (2000). GIS Implementation in Grassroots. *URISA Journal*, *12*(1), 15–29.

Solomon, S. (Ed.). (2007). *Climate change 2007-the physical science basis: Working group I contribution to the fourth assessment report of the IPCC* (Vol. 4). Cambridge University Press.

Solow, R. M. (1986). On the Intergenerational Allocation of Natural Resources. *Scandinavian Journal of Economics*, *88*(1), 141–49.

Stoll, M., Burton, G., Noble, M., & Sprovkin, J. (2009, March). Access to Child Care in Cook County. Retrieved from http://gis.depaul.edu/ shwang/cgis/Win0809_ILAC.pdf.

Stutsman, C., Beer, K., & Kulack, E. (2010, November). Spatial Representation of Humboldt Park Community & Nutritional Assets. Retrieved from http://gis.depaul.edu/shwang/cgis/Aut1011_PRCC.pdf.

The White House. (2014, March 19). FACT SHEET: The President's Climate
    Data Initiative: Empowering America's Communities to Prepare for the
    Effects of Climate Change. Retrieved April 7, 2014, from
    http://www.whitehouse.gov/the-press-office/2014/03/19/fact-sheet-
    president-s-climate-data-initiative-empowering-america-s-comm.
United Nations. (1992). Agenda 21: UN Conference on Environment &
    Development.
United Nations. (2007). *Indicators of sustainable development: guidelines and
    methodologies* (3rd ed.). New York: United Nations.
Valentin, A., & Spangenberg, J. H. (2000). A guide to community
    sustainability indicators. *Environmental Impact Assessment Review*, *20*(3),
    381–392. doi:10.1016/S0195-9255(00)00049-4.
Weiss, J., & Rygh, L. (2007, November). Chicagoland Bicycle Federation.
    Retrieved from http://gis.depaul.edu/shwang/cgis/Aut0708_CBF.pdf.
Whitehead, M. (2006). *Spaces of sustainability: geographical perspectives on
    the sustainable society*. London; New York: Routledge.
Wilbanks, T. J. (1994). "Sustainable Development" in Geographic
    Perspective. *Annals of the Association of American Geographers*, *84*(4),
    541–556. doi:10.1111/j.1467-8306.1994.tb01876.x.
Williamson, I. P., Rajabifard, A., & Feeney, M.-E.F. (2004). *Developing
    Spatial Data Infrastructures: From Concept to Reality*. CRC Press.

Submitted on April 10th, 2014

Chapter 3

SPATIO-TEMPORAL VISUALIZATION AND ANALYSIS TECHNIQUES IN GIS

Song Gao[*]

Department of Geography, University of
California, Santa Barbara, CA, US

ABSTRACT

The spatio-temporal visualization and analysis techniques play important roles in geographic information systems and knowledge discovery. In this research, we introduce three spatio-temporal analytical techniques including spatio-temporal visualization, space-time kernel density estimation, and spatio-temporal autocorrelation-analysis for exploring human mobility and urban structure patterns. These spatio-temporal analytics can help to answer questions like: Where are the spatio-temporal hotspots of human activities? How to explore spatio-temporal patterns in three-dimension GIS? Experiments are conducted using a large scale of phone-call detailed records in urban space.

Expeditions on the spatio-temporal functionality and techniques contribute to the GIScience community for the future development of Space-Time GIS; and more broadly, it has potential to be applied in other disciplines, e.g., environmental, urban and social sciences.

---

[*] Corresponding author: Song Gao. E-mail: sgao@geog.ucsb.edu.

1. INTRODUCTION

Temporal geographic information systems or Space-Time GIS (STGIS) were designed to process, manage, and analyze spatio-temporal data (Yuan, 1996). In past decades, several spatio-temporal conceptual frameworks such as space-time path and prism for exploring individual activities (Hägerstrand, 1970; Miller, 1991; Yu and Shaw, 2008), the integration of GIS in space-time representations (Couclelis, 1999), and key spatio-temporal data models such as snapshot models (Armstrong, 1988), event-based models (Peuquet and Duan, 1995) and object-oriented data models (Worboys, 1992) have been widely studied and developed. Goodchild (2013) recently examined seven examples of distinct STGIS data types (i.e., tracking, temporal sequences of snapshots, temporal sequences of polygon coverages, cellular automata, agent-based-models, events and transaction, and multidimensional data) and related scientific questions.

Despite that humans have keen ability to discover patterns hidden in small-scale data; they may find it difficult for large-scale data that often vary over both space and time. Researchers have made great effort on spatial data mining and spatio-temporal visual analytics to raise the cognitive ceilings which often prevent the interpretation of large spatio-temporal datasets (Guo et al., 2006; Shaw, Yu, and Bombom, 2008; Andrienko et al., 2010).

In the Mobile Age, with the widespread use of location-awareness devices, it is possible to collect large-scale location-awareness datasets, such as mobile phone call data, GPS-enabled taxi trajectories, and social media data, to sense complex human movements and human-environment interactions. It would be of great significance to explore and understand how cities function in short-term temporal scales compared with traditional long-term strategic planning in the new era of Big Data (Batty, 2013).

For example, although the human movements and activities may vary over time across different regions, the observed activity hotspots and information flow might exhibit a pattern of spatial dependence. Also, ignoring the temporal dimension would not be sufficient to discover underlying urban dynamics.

For instance, urban governors might hope to monitor human movements by observing the neighboring regions in previous time periods. In such space-time integration contexts, the spatio-temporal analytics should help to answer questions such as:

- Where are the spatio-temporal hotspots of human activities?
- Do human/vehicle movement flows exhibit different spatio-temporal patterns in contrast to overall trips?
- How do these patterns relate to the population distribution and urban land-use structure?
- How to conduct the spatio-temporal autocorrelation analysis?
- What is the impact of spatio-temporal granularity and uncertainty?

To cope with these research questions and problems, spatio-temporal data mining techniques and workflows need to be studied. However, mining big geo-data and discovering knowledge of spatial-temporal relations, patterns and trends about the real world process are not trivial. Issues on spatio-temporal data organization, computation and integration with visual representation and human cognition still challenge researchers to make great efforts with interdisciplinary knowledge. To this end, this paper aims at proposing a spatio-temporal data processing and analytical framework which can be applied not only in exploring dynamic mobility and intra-urban flow patterns, but also in other human and social science research from the emerging big geospatial datasets and computer techniques.

This paper is structured as follows: In Section 2, we will briefly discuss some related work and propose a spatio-temporal analytical framework which includes spatio-temporal visualization (STV), space-time kernel density estimation (STKDE), and spatio-temporal autocorrelation-analysis (STAA) for exploring human mobility and urban dynamic patterns. The methodology, technical implementation of these analytics will be presented in detail. Then we apply the framework to analyze amounts of geo-referenced mobile phone call records in a city to reveal the spatio-temporal patterns hidden in such big geo-data and further, to understand the complex urban dynamics.

The data processing, experiments, main findings and discussions are presented in Section 3 and 4. We conclude the paper with summarization and directions for further research in Section 5.

2. SPATIO-TEMPORAL ANALYTICAL FRAMEWORK

Modelling human mobility patterns and understanding dynamic urban structures based on a large amount of GPS sensors, mobile devices, persons, vehicles, and street networks have become a hot topic in many fields such as urban planning, transportation, GIScience and computer science (Jiang and

Claramunt, 2004; Ratti et al., 2006; González et al., 2008; Kang et al., 2012a, 2012b; Liu et al., 2012; Yuan et al., 2012; Gao et al., 2013b, 2013c; Shen et al., 2013). In general, the mining and analyzing processes of such spatio-temporal data require combined qualitative-quantitative approaches which involve data extraction and analytics, statistical inference and geovisualization. We present a spatio-temporal analytical framework (Figure 1) which combines STV, STKDE and STAA for understanding spatial-temporal patterns (both individual and aggregated) hidden in the Big Geo-Data. Each of them has different characteristics and data-format requirements. In the processing, the raw data were converted into different data structures for various analytical purposes. In the following part, we will discuss the roles of different spatio-temporal analytics for the presented research.

2.1. Spatio-Temporal Visualization Techniques for Trajectory and Flow

By utilizing the power of human vision, previous studies have demonstrated the effectiveness of geovisualization in spatial data exploration and knowledge discovery (MacEachren and Kraak, 2001; Kwan, 2004; Guo et al. 2005; Andrienko et al., 2008).
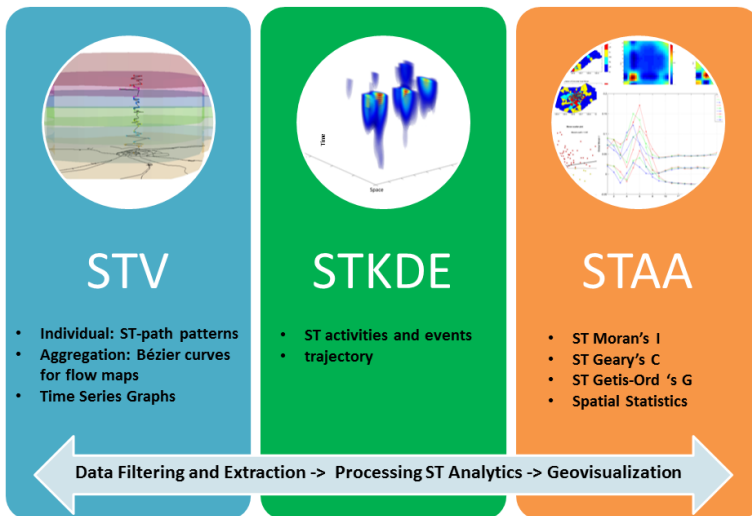
Figure 1. A spatio-temporal analytical framework for identifying human mobility patterns and urban dynamics.

The understanding of urban spatial structures can benefit the studies of visualizing individual space-time behaviors (Kwan, 2000; Chai, 2013). We can use both *individual-based visualization* and *aggregation-based visualization* to explore dynamic patterns in urban studies. However, the representation of dynamic human activities and movements over both space and time is one of the major challenges in geocomputation and geovisualization. Hägerstrand's time-geography conceptual framework provides an excellent integrated representation of human movements in space and time (Hägerstrand, 1970).

But the space-time cube idea was not applied so widely until the development of GIS-based implementations and analytical discussions about space-time relationships, interactions and uncertainties (Miller, 2005; Shaw, Yu, and Bombom, 2008; Chen et al., 2011; Nakaya, 2013) moved forward, as well as the opportunity to explore potential human activities in both physical and virtual spaces (Yu and Shaw, 2008).

For the individual-based movement representation, a *space-time path* (3D polyline) was created to connect time-ordered sequence of locations of one person in a 3D-GIS environment which consists of a two-dimensional horizontal geographic plane and one vertical dimension of time (Figure 2).
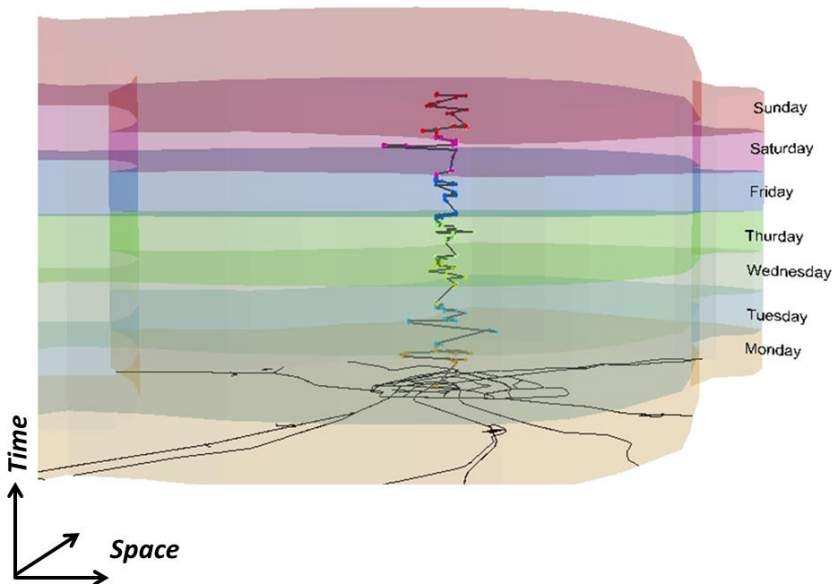
Figure 2. Space-time path of an individual's movement in a week.

It can be used for visual exploration of continuous spatial and temporal movement patterns. Several analytical models and measurements have been developed by Miller (2005) such as space-time prism, composite path-prisms, stations, bundling and intersections to further analyze the complex spatio-temporal relationships among human activities and interactions under special space-time constraints. But when numerous of trajectories were collected in the datasets, it was hard to visualize and interpret.

Different approaches for generalization and aggregation of massive move-ment data have been introduced such as *traffic-oriented view* and *trajectory-oriented view* (Andrienko and Andrienko, 2008)*.*

In the urban context, the aggregation of massive human movement trajectories by origins and destinations (OD) can be utilized to understand the dynamic OD-flow patterns among traffic analysis zones (TAZs) or other poly-gonal divisions of region in different temporal scales. Traditional flow mapping is used for representing the amount and the direction (with arrow symbol) of *from-to* movements of human or things among regions in a 2D space, such as migration and goods trade (Tobler, 1987).

Some graph layout optimization algorithms and aggregation strategies have been suggested to minimize the edge crossings between flow symbols (Phan et al., 2005; Andrienko and Andrienko, 2011). Here we introduce another approach of using vertical Bézier curves in 3D-GIS environment for interactive visual exploration of information or movement flows between places. The main advantages of such an approach lie in the integration of 3D visualization techniques which support interactions between 3D geometry objects and OD-flow values in multiple time snapshots or in a continuous animation.

A Bézier curve is defined by a set of control points P_0 through P_n, where n represents called its order (n = 1 for linear, n = 2 for quadratic which is used in our work, etc.). Bézier curves have been widely used in computer graphics and geometry designs (Farin, 1996). We develop an algorithm to approximate the quadratic Bézier curves.

As shown in Figure 3, the first point P_0 and the last point P_2 are used to represent the centroids of two regions (i.e., the origin and the destination of each flow) and the intermediate control points are interpolated by the standard Bézier functions. We then project a flow between regions in the 3D-GIS environment. We write a Python script to generate all Bézier curve controlling points based on the OD-flow matrix table and link them in Esri's ArcScene software for further interactive exploration of information flow or physical movement flow patterns.
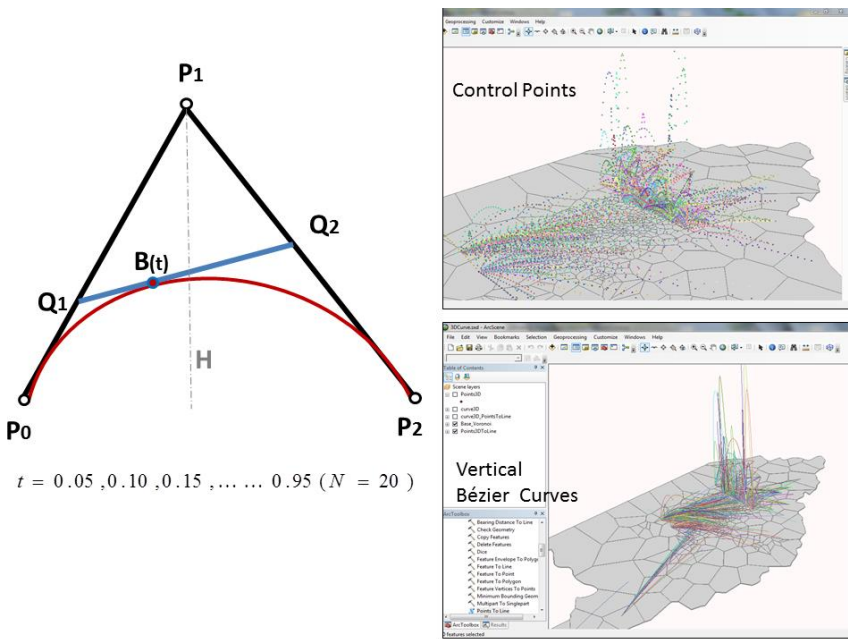
Figure 3. Drawing and visualizing vertical Bézier curves in 3D-GIS environment (ArcScene).

2.2. Space-Time Kernel Density Estimation

As discussed above, the temporal information of movements in geographic space is important to detect the spatio-temporal trends of underlying human mobility. But with the increasing number of aggregated human/vehicle trajectories in urban space, the space-time path representation model will be hard to interpret because of the overlapping and cluttering issues. To solve this problem, an extension of kernel density estimation (KDE) (Silverman, 1986) was suggested. The KDE has been widely used in spatial analysis to characterize a smooth density surface that shows the geographic clustering of point or line features in 2D space. In order to incorporate the time information, the space-time kernel density estimation (STKDE) can be taken as a generalization approach of the 2D-space KDE into the 3D space-time cube which can support the exploration of spatio-temporal patterns, clusters and changes. Such STKDE techniques have been used in several studies, such as crime clustering analysis (Brunsdon et al., 2007; Nakaya and Yano, 2010), trajectory data mining (Demšar and Virrantaus, 2010), publication citation analysis (Gao et

al., 2013a), and dengue fever pattern discovery (Delmelle et al., 2014). The STKDE value of each voxel (volumetric pixel) in the three-dimensional space-time cube is estimated as:

$$D(x, y, t) = \frac{1}{nh_s^2 h_t} \sum_i K_s(\frac{x - x_i}{h_s}, \frac{y - y_i}{h_s}) K_t(\frac{t - t_i}{h_t})$$

(1)

where $D(x, y, t)$ is the density estimation of each voxel based on the data in neighboring volumetric pixels; n is the number of point events, and h_s and h_t are the spatial and temporal neighboring bandwidths. Each point in the neighboring pixels is weighted based on the proximity in both space and time to the voxel using kernel functions (K_s and K_t). In this study, the Epanechnikov kernel is used for multivariate probability density estimation within the bandwidths (Epanechnikov, 1969).

Similar to the 2D spatial KDE, larger bandwidths may result in smooth surface while smaller bandwidths may result in the lack of trending patterns, so we need to calibrate both spatial and temporal bandwidths of STKDE based on the experiments with actual datasets.

The results of STKDE are volume data, i.e., 3D-grids. Direct visualization of such STKDE would require four-dimensional space because of their volumetric data structure consisting of 2D geographic space, time and another one for the density estimation scalar. Such volume visualization is not very common in GIS but very popular in geophysics, geology, medical science, and in computer graphics (Kaufman, 1990). The three main approaches for volume visualization were discussed by Demšar and Virrantaus (2010): (1) direct volume rendering by assigning color and transparency to voxels; (2) isosurface that is the equivalent of isoline connecting points of equal value on a two-dimensional map; and (3) volume slicing by planes. We apply the volume slicing approach with color schema and transparency to the voxels regarding the consistency of KDE visualization in GIS.

2.3. Spatio-Temporal Autocorrelation Analysis

Analyzing spatio-temporal autocorrelation structures of human activities would be helpful to understand the urban dynamic patterns in space and time simultaneously. In statistics, autocorrelation can be taken as the correlation of a variable with a lagged specification of itself (Box et al., 2008).

The temporal autocorrelation can be defined as the correlation of the same variable X between values at different time s and t.

$$R(s,t) = \frac{E[(X_t - \mu)(X_s - \mu)]}{\sigma^2} \tag{2}$$

while E is the expected value operator, μ is the mean of the observation values and σ^2 is the variance. The temporal autocorrelation can be used to explore the time-series autocorrelation patterns.

With regard to the spatial dependence, spatial autocorrelation (association) statistics have been used to analyze the degree of dependency among observations in a geographic space (Cliff and Ord, 1973). These measurements can be divided into two categories: global indices and local indices. Classic global indices of spatial autocorrelation include Moran's I (1950), Geary's C (1954), and Getis-Ord's General G (1992), while local indices of spatial association (LISA) can be established by transforming the global indices into corresponding local measurements based on different measures of similarity (Anselin, 1995). All of these spatial autocorrelation statistics require a spatial weights matrix that reflects the intensity of the geographic relationship between observations and their neighbors, e.g., the distance-to-neighbor matrix or the binary matrix in which the element value is 0 or 1 determined by whether there is a shared boundary between the observation location and neighbors. As suggested by Hardisty and Klippel (2010), adding the temporal neighbors into the weights matrix would be one approach to extend the traditional spatial autocorrelation measurements.

Here, we present three extended global measures of spatio-temporal association regarding the spatial version of Moran's I, Geary's C, and Getis-Ord's General G:

$$I_{st} = \frac{\sum_{i=1}^{N} \sum_{j=1}^{N} w_{ij} [z_i(t) - \bar{z_t}][z_j(t+\tau) - \bar{z_{t+\tau}}]}{\sigma_t \sigma_{t+\tau} \sum_{i=1}^{N} \sum_{j=1}^{N} w_{ij}} \tag{3}$$

$$C_{st} = \frac{\sum_{i=1}^{N} \sum_{j=1}^{N} w_{ij} [z_i(t) - z_j(t+\tau)]^2}{2\sigma_t \sigma_{t+\tau} \sum_{i=1}^{N} \sum_{j=1}^{N} w_{ij}} \tag{4}$$

$$G_{st} = \frac{\displaystyle\sum_{i=1}^{N}\sum_{j=1}^{N} w_{ij} z_i(t) z_j(t+\tau)}{\displaystyle\sum_{i=1}^{N}\sum_{j=1}^{N} z_i(t) z_j(t+\tau)}$$

(5)

where I_{st}, C_{st}, and G_{st} can be taken as different formats of space-time cross-correlation (or cross-product) models (Getis, 1991); Z is the target variable of interest; i and j are indices of total N spatial units; w_{ij} is an element of the k-order-neighbor spatial weighted matrix (1st, 2nd, ⋯⋯, kth); $\bar{z_t}$ and $\bar{z_{t+\tau}}$ are the means of variable Z within a time lag, while σ_t and $\sigma_{t+\tau}$ are the variances. The local measures of spatio-temporal autocorrelation can be derived by decomposing a global measure into particular spatial neighboring units.

In the experiment section, we will evaluate how different spatial and temporal neighbors (lags) affect the results of three spatio-temporal autocorrelation measures for the mobile phone call activities in a city.

3. DATA PROCESSING

In this research, the dataset contains a week of about 74, 000, 000 anonymized mobile phone call detail records (CDR) in a large city from a Chinese telecommunication operating company. The CDR data lists the information of caller, receiver, mobile base stations, date, time, duration et al. (Table 1).

As shown in Figure 4, every time when a user (caller/receiver) made a call, he/she was geo-referenced to a corresponding mobile base station that has a unique longitude/latitude position. The coverage area of each mobile base station can be expressed as a Voronoi polygon for call activity analysis and termed as a "cell".

In this Voronoi partition, all phone calls within a given polygon are closer to the corresponding mobile base station than any other station.

Generally, urban central regions have a higher density of mobile cells (the coverage area of each cell is smaller) than the outer suburb regions.

Different data subsets have been extracted and processed for various research purposes such as human mobility modelling (Kang et al., 2012b),

travel behaviour studies (Yuan et al., 2012), population estimation (Kang et al., 2012a), and urban community structure analysis (Gao et al., 2013b).

Table 1. Data format of mobile phone call detail records

Caller	Receiver	Date	Start Time	End Time	Duration (seconds)	Base Station	Long	Lat
Serve Nub1	oppNub1	2007-07-23	09:25:10	09:28:20	190	A	127.495	50.243
Serve Nub1	oppNub2	2007-07-23	12:15:32	12:15:52	20	B	127.502	50.241
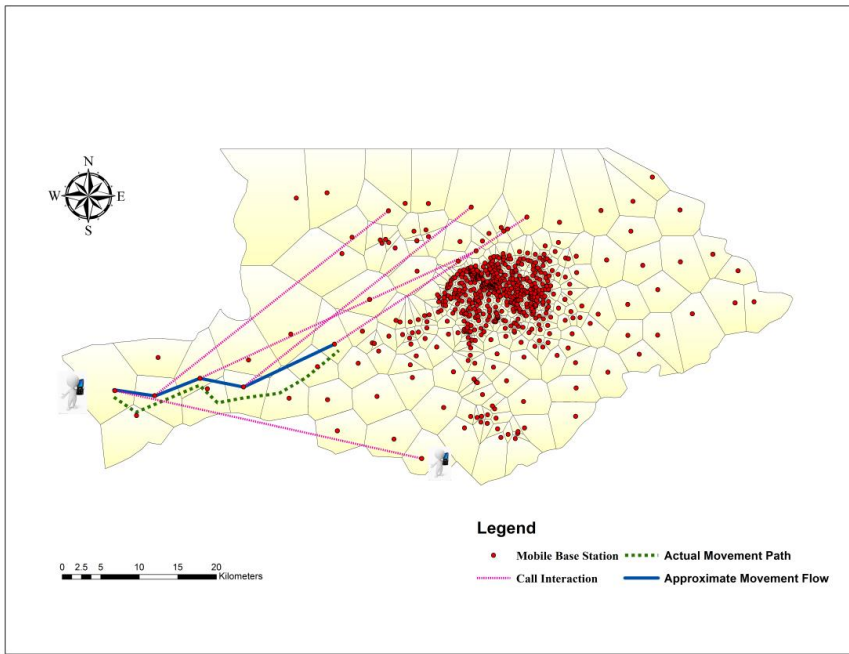
Figure 4. Spatial distribution of mobile base stations and an illustration of phone call interactions among cells.

In this work, on one hand, for individual spatio-temporal mobility pattern analysis, the corresponding approximate movement trajectories of each mobile subscriber were created by connecting his/her a series of geo-referenced call records in space and time.

On the other hand, for urban dynamic structure analysis, phone call activities and phone users' physical movement flows were aggregated based on the Voronoi polygons.

More detailed spatio-temporal analysis and results will be presented in the following section.

4. EXPERIMENTS

4.1. Individual Spatial-Temporal Movement Patterns

In urban studies, the understanding of human movement patterns over time is very important in transportation planning and city management. Figure 5 illustrates the 3D STV of a person's mobile tracking trajectories in space over one-week. Each color represents a single mobile subscriber. Different shapes of 3D polylines reveal different space-time behaviors for specified users. For instance, the regular patterns at fixed locations (e.g. home and job places) with respect to the daily/weekly cycles can be indicated by the length of vertical segments of the space-time paths (Figure 5a). In addition, irregular movement patterns have been also found for certain type of individuals (Figure 5b). One might guess that the user is a delivery employee or working for related professions. The STV technique can help to simultaneously visualize the mobile trajectory patterns in space and time with an intuitive manner but may need the statistical analysis to extract more meaningful personal places of interests (POIs). Figure 6a displays the spatial distribution of a mobile user's call-activity movement in a week. It tells that this person has a higher probability (Cell A: 0.31, Cell B: 0.22; Cell C: 0. 14) to frequently visit a few places, while the visiting probability of most cells is less than 0.05). The interpretation of the time series graphs of these frequently visited places by the user offers the possibility to identify the personal POIs. As shown in Figure 6b, the user often made phone-calls at Cell A and Cell B during 19:00~24:00 throughout the whole week.

One can infer that his/her home might locate nearby or inside the boundary of the two cells. Also, the temporal signature of Cell C may indicate a working place since the user present there only during office hours (9:00~18:00) on weekdays and not on weekends. However, the detailed information about personal characterized POIs may need more investigation on daily-activity trips of the mobile subscribers or the study of geographical contexts.

In order to identify the spatio-temporal hot-spots of individual phone call locations, we calculated the space-time kernel density estimation (STKDE) of each user's call activities. Figure 7a shows an individual's mobile phone call activities over a week in a space-time cube. The STKDE of this user's call activities was calculated in a spatial resolution of 500 meters and a temporal resolution of 100 minutes. The different combinations of spatio-temporal bandwidths result in various visual representations.

a   b
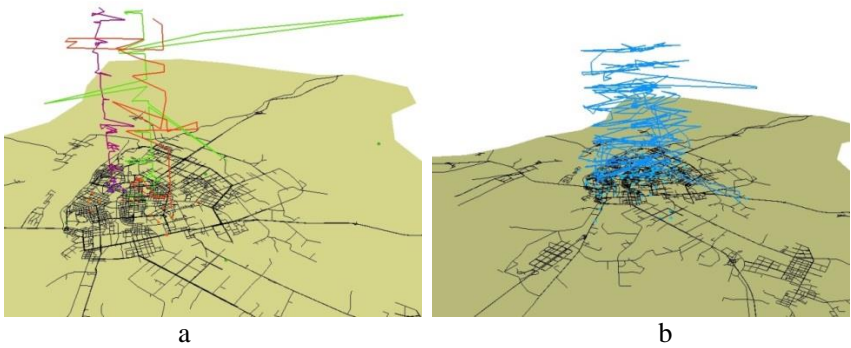
Figure 5. Space-time visualization of mobile phone users' trajectories: (a) regular movement patterns of three individuals; (b) irregular movement pattern of an individual.

a
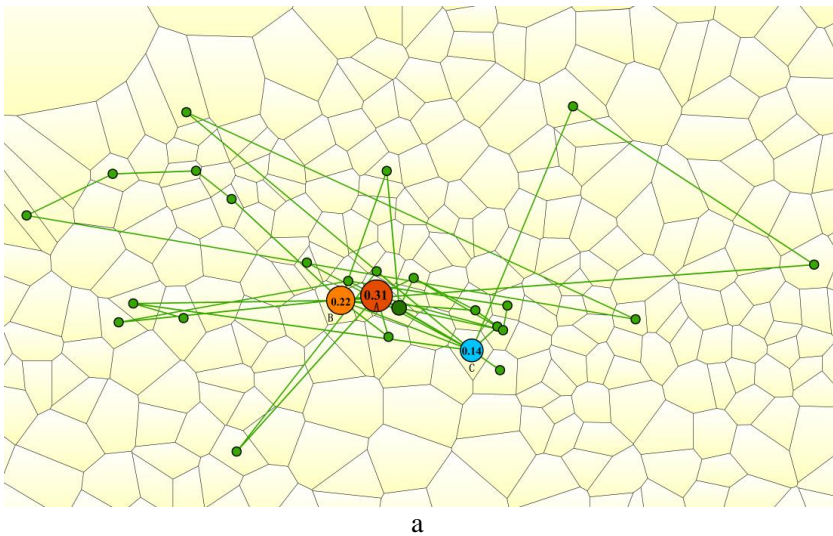
Figure 6. (Continued).

b
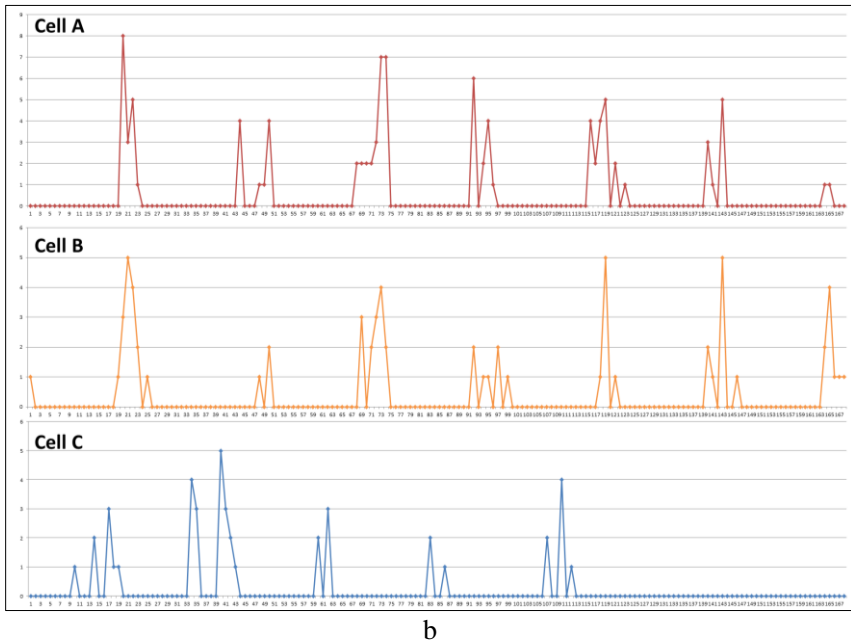
Figure 6. Spatial distribution and temporal signatures of individual frequent visited mobile cells: (a) Spatial display of cell visiting probability for a user (the larger circle represents higher probability); (b) The time series graphs show temporal signatures (visiting frequency) of the user's frequent visited places (mobile cells) over a week.

a

b
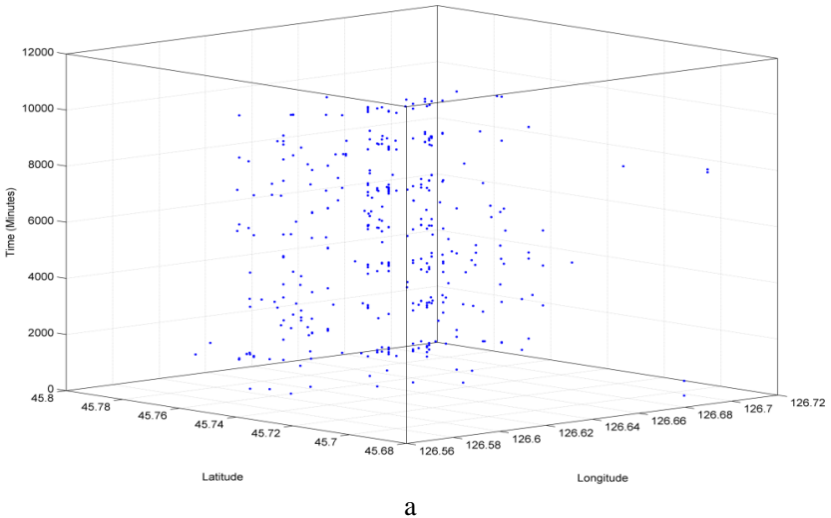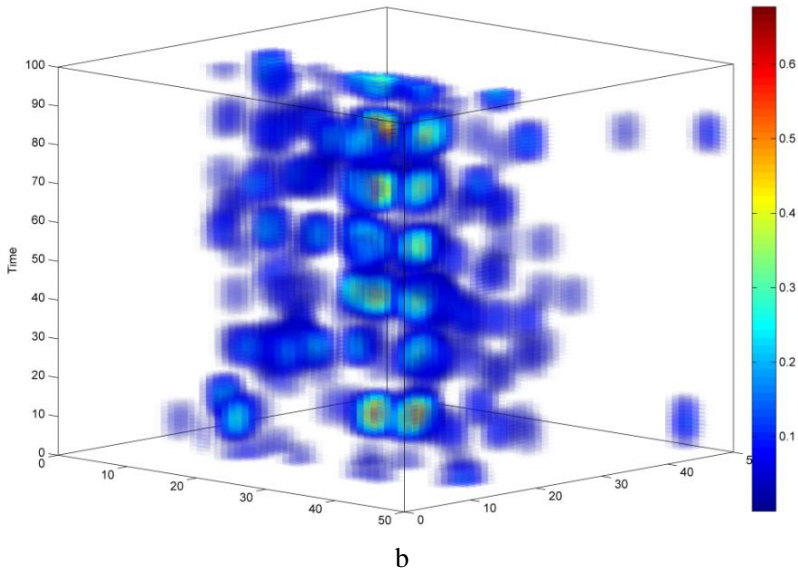
Figure 7. Visualizing georeferenced phone call activities and space-time density: (a) phone call events in space-time cube; (b) STKDE results for a specified mobile user in a week.

The selection of bandwidths needs several rounds of calibration by adjusting both spatial and temporal bandwidths to find an optimization which can help to uncover hidden patterns. We used twice the spatial resolution (1km) as the spatial bandwidth for both horizontal dimensions and 500 minutes as the temporal bandwidth for the vertical dimension.

The resulting density volume of 50*50*100 voxels for a user's call activities is visualized in Figure 7b.

One may find that this user is more likely to make calls in certain fixed locations (red and orange voxels) across time. This example shows that it is much easier to visually identify the spatio-temporal hot-spot patterns of call activities by using the STKDE approach.

4.2. Aggregated Phone-Call Interaction Patterns

One of the prominent characteristics of phone call data lies in its indication of human communications and spatial interactions among different places. The aggregated phone call interactions among mobile cells in different

time represent the dynamic intra-urban communication landscape which cannot be captured using other traditional activity survey data. As shown in Figure 8, the vertical Bézier curves were created to represent the hourly phone-call flow across cells. The height of the arcs represents the relative volume of phone calls. The tall and narrow arcs show strong call communication within a nearby intra-urban space; while some long distance curves across non-adjacent cells indicate strong call interactions among these spatially separated regions.
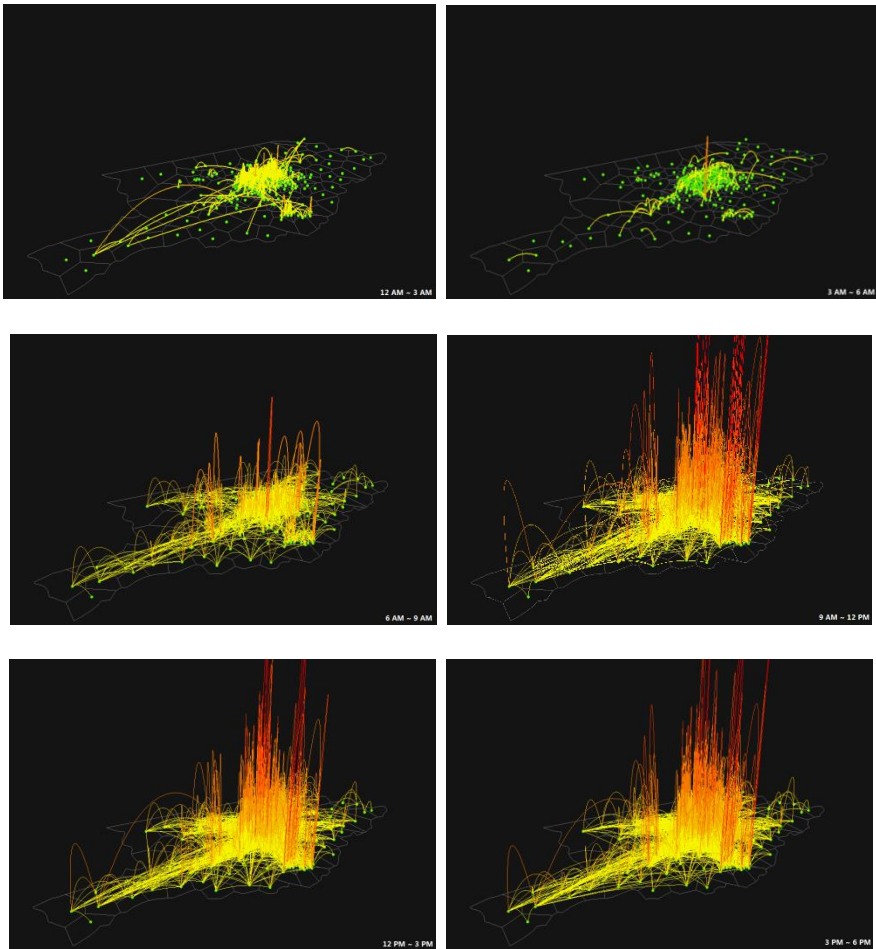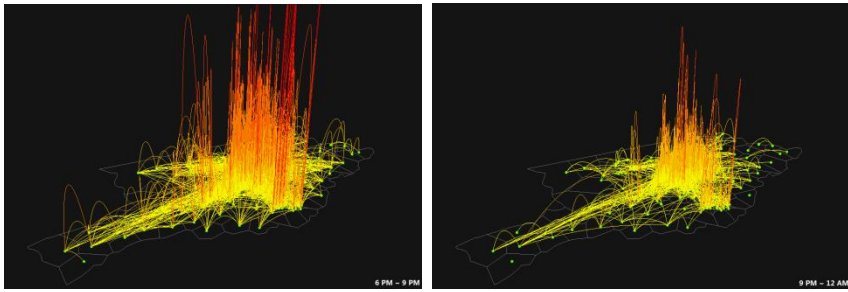
Figure 8. Vertical Bézier curve 3D visualization of hourly phone-call flow patterns across cells in a day. (Green dots are locations of mobile base stations; each arc represents an OD flow linking two mobile cells).

Such information flow patterns are strongly related daily human activity rhythms and working-social connections, as well as geographical contexts including urban land-use types and spatial distributions of home-job locations (Ratti et al., 2006; Gao et al., 2013b).

In order to understand the dynamic "source-sink" structures of information landscape (Liu et al., 2012), we calculated the phone call net-balance-flow for each mobile cell by subtracting the outgoing call volume from the incoming call volume in each hour. Figure 9 shows the time-series plot of phone-call net flow among all cells. Each line represents the net flow pattern for a specific Voronoi mobile coverage area. In Figure 10, it is clear to see dynamic spatial distributions of the "source" areas (red color) which have more outgoing phone calls and the "sink" areas (blue color) which have more incoming phone calls in different hours. The yellow cells mean that the net-balance call flow in that hour is zero. One can interactively interpret the call flow patterns in the 3D-GIS environment or sense the dynamic urban phone-call landscape under the animation mode.

4.3. The Spatio-Temporal Autocorrelation Patterns of Phone Calls

The study of spatio-temporal autocorrelation structure of mobile phone calls in urban space can help to understand the citizens' mobile communication patterns and urban structures. In order to investigate how the spatial autocorrelation structure changes throughout the day in this city, the phone-call volume was aggregated into the Voronoi cells by hour at first.

Then, the Moran's I local indicator of spatial association (LISA) (Anselin, 1995) was calculated for each cell in every three hours (See Figure 11). The value of Moran's I has been standardized to lie in [-1, 1]. If the index is larger than 0, the cell shows positive spatial autocorrelation with its neighbors; while it indicates the negative spatial autocorrelation of phone call patterns if the index is smaller than 0. The closer the value is approaching to 1 (or -1), the stronger the positive (or negative) spatial autocorrelation is. Examining the spatial structure of LISA in different time periods, we can clearly see that the spatial autocorrelation patterns of phone calls across all cells are very dynamic and heterogeneous.

The central region (small cells) shows more diverse patterns than the outer suburb areas, where most spatially adjacent cells show similar values in the whole day.

It might reflect the mixture land-use types of urban central areas and human's convergence and divergence in this place with various phone call behaviors in different time periods.

To identify a more stable autocorrelation structure, we apply the spatial statistic test of running 10000 simulations of randomized permutations of neighboring cells to find the local significant spatial autocorrelation patterns (Anselin, 1995).
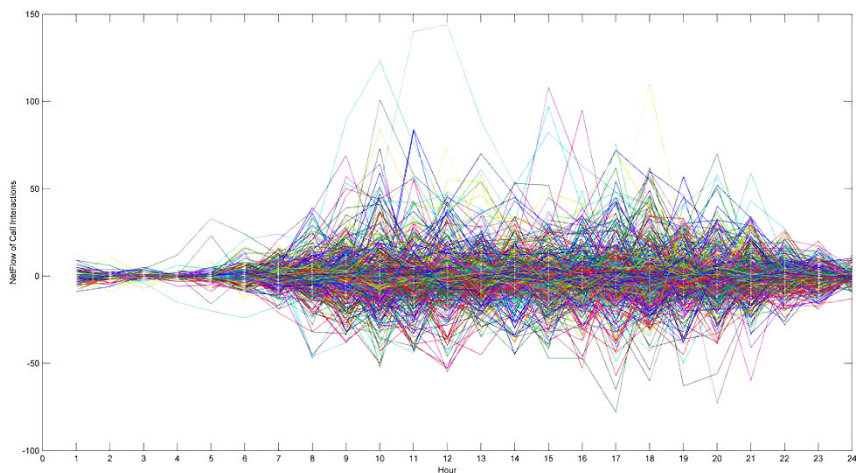
Figure 9. Time-series plot of phone-call net flow among all mobile cells (each line represents a different mobile cell).

As shown in Figure 12, we generated both Moran's scatter plot and spatial distribution of the labelled mobile cells with IDs to visually and interactively identify the statistically significant local association cells (with a 0.05 significance level).
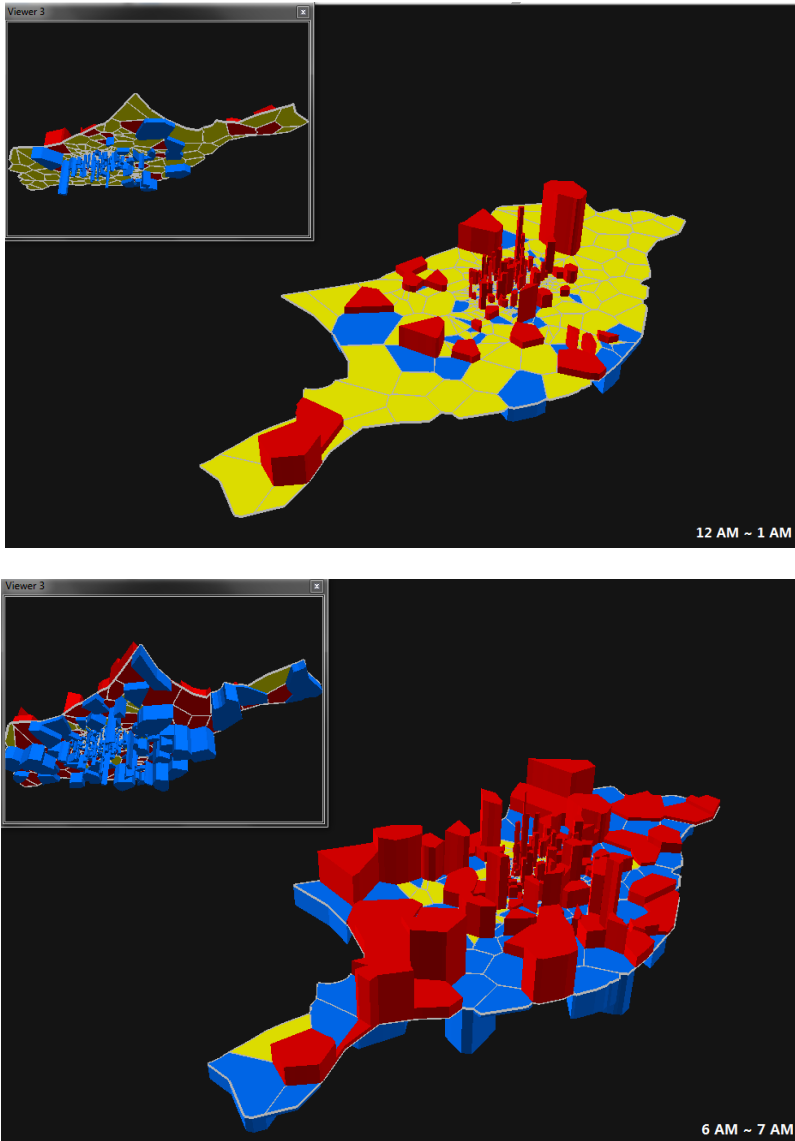
Figure 10. (Continued).
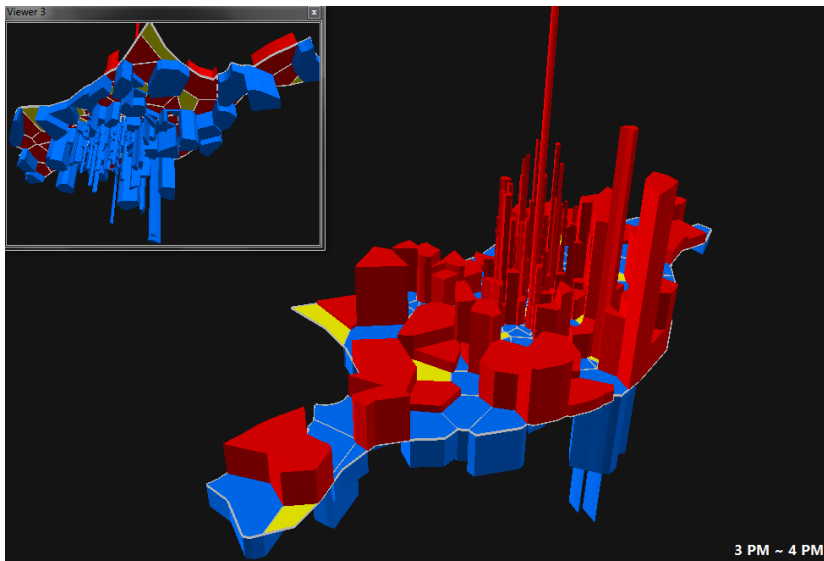
Figure 10. Visualizing the dynamic phone-call "source" areas (red), "sink" areas (blue) and "zero-balance" areas (yellow) in 3D-GIS environment.

By comparing the phone call volume of each cell with its 1st-order adjacent neighbors, there are four types of associations identified: (1) HH: observations in both the target cell and neighbors are high; (2) HL: high call volume in the target cell with low volume in neighbors; (3) LH: low call volume in the target cell with high volume in neighbors; (4) LL: the call volume in both the target cell and neighbors are low. Figure 12a illustrates the results of significant Moran's I LISA in the period 3AM~6AM.
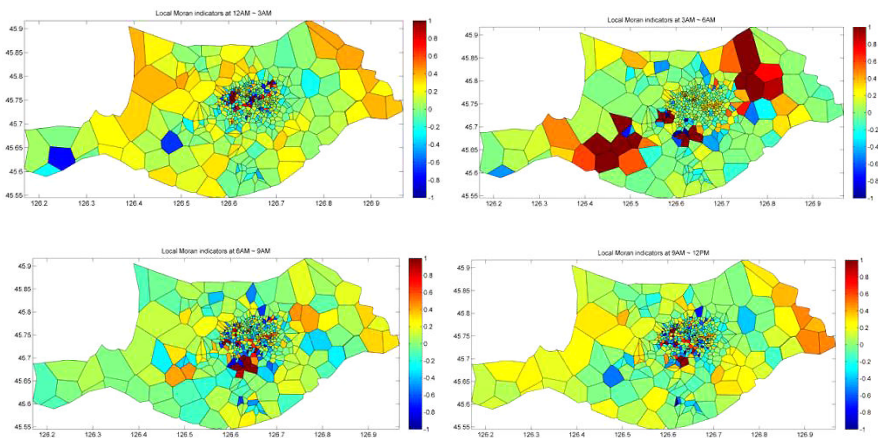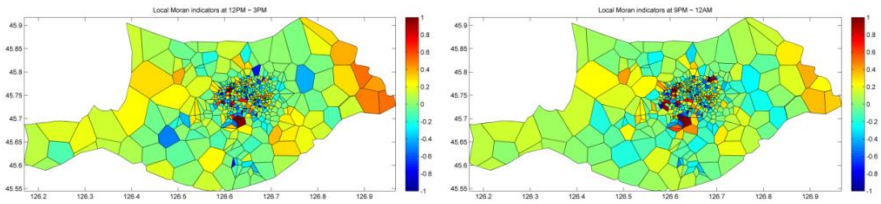
Figure 11. Local Moran's indicators of spatial autocorrelation (LISA) analysis on phone calls in different time periods of a day (using the 1st-order-neighbor spatial weighted matrix).

There are continuous significant LL spatial associations in the urban central region and HH association structure in the southwest and northeast suburb regions which contain large residential housing referring to the Google Earth imagery[1] in this city. But such spatial autocorrelation structure changes over time, for instance, the central area tends to have mixture patterns of all HH, HL, LH, LL association types in the period 9AM~12PM (See Figure 12b).

The spatial weighted matrix plays an important role in spatial autocorrelation analysis (Getis and Aldstadt, 2010). As shown in Figure 13, a larger-order of spatial adjacency tends to have larger number of neighbors.

Another important factor for identifying spatio-temporal autocorrelation structure is time granularity (e.g., half an hour, per hour, two hours and others). It inspired us to examine how the different combinations of spatial weights and temporal neighbors affect the STAA results.

Using the methodology introduced in Section 2.3, we implement the global Moran's I like statistic of STAA with different spatial lags and time lags for hourly phone-call patterns across all cells. Examining the results reveals two key findings (See Figure 14a). First, the strength of global Moran's I like spatio-temporal autocorrelation measure (I_{st}) for hourly phone calls is temporally dynamic and there is a positive-association peak between 6 AM~7AM. Second, the I_{st} measure is more sensitive to the spatial order than the temporal neighbors. A higher-order of spatial weights generally results in higher strength of spatio-temporal autocorrelation structure.

---

[1] The imagery with labels is not shown here as required by the data provider.
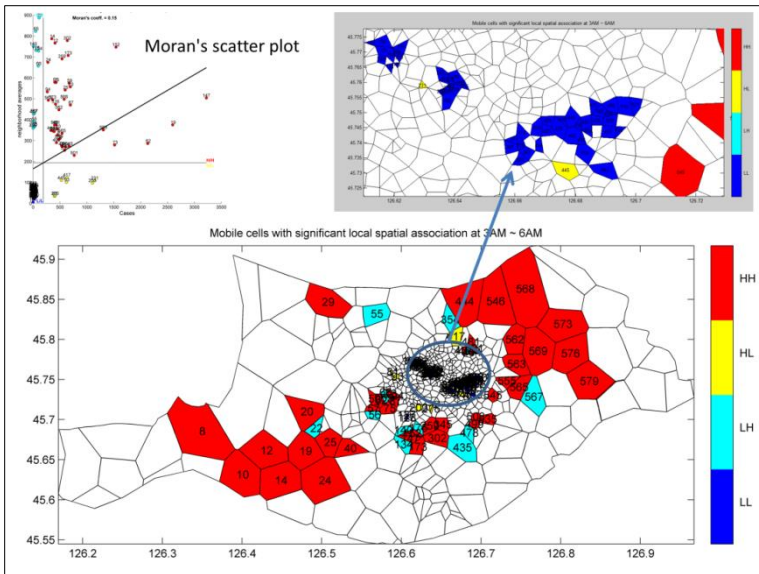
a
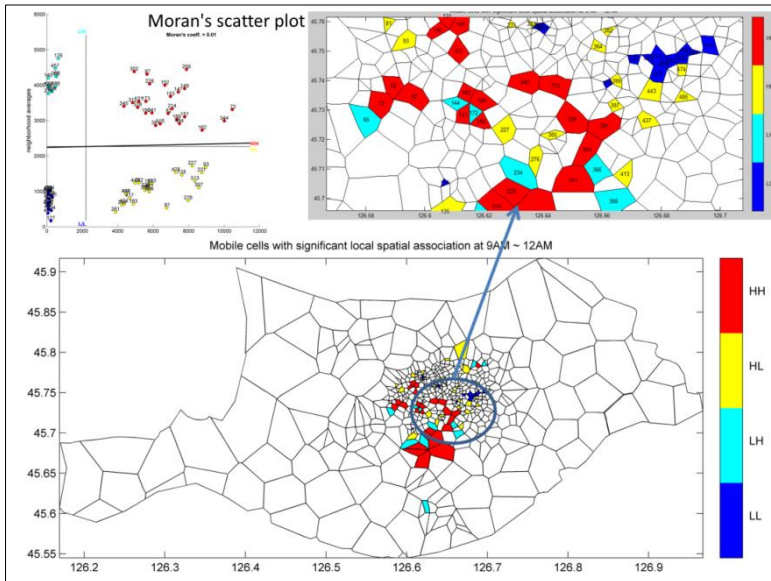
b

HH: High-High; HL:High-Low; LH: Low-High; LL: Low-Low: (a) period 3AM~6 AM; (b) period 9AM~12PM.

Figure 12. Moran's scatter plot and spatial display of mobile cells with statistically significant local associations.
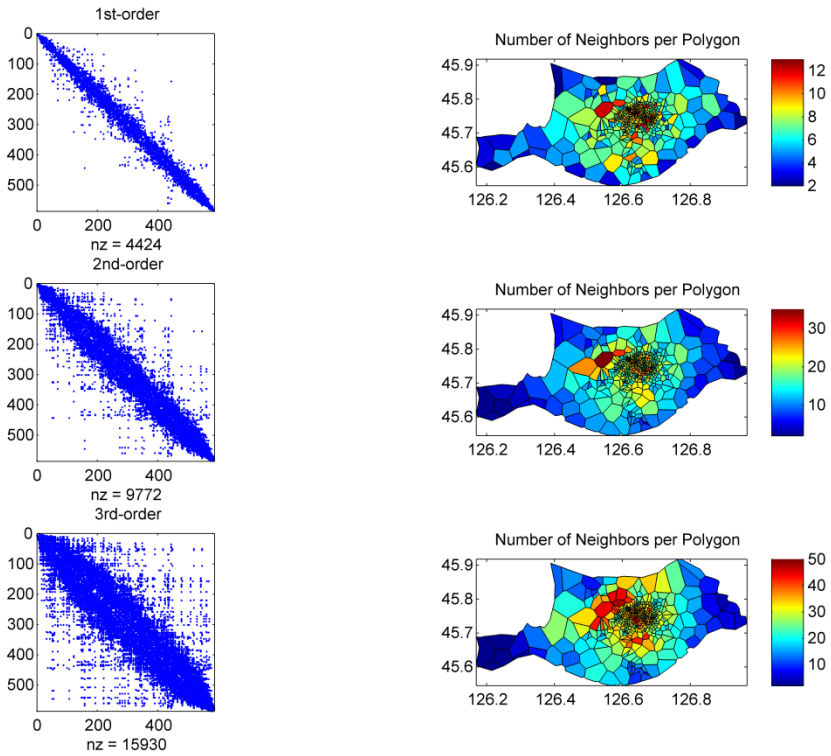
Figure 13. The 1st, 2nd and 3rd-order of spatial adjacency matrix (a dot means the weight between the two cells is 1; otherwise is 0) and the corresponding distributions of neighbors for each mobile cell.

In addition, we implement the global Geary's C like STAA measure (C_{st}) and Getis-Ord's G like STAA measure (G_{st}) to identify the spatio-temporal autocorrelation of hourly phone-call patterns in different hours. Note that the C_{st} statistic indicates a positive autocorrelation structure when the value lie in (0~1); while it is a negative autocorrelation when the value lie in (1~2).

It is found that the hourly autocorrelation trends of C_{st} measures are more similar to the I_{st} measures (Figure 14b). But using the G_{st} measure didn't reveal the temporal dynamics of autocorrelation strength in our datasets. The G_{st} statistic is also sensitive to the spatial-order of weighted matrix (Figure 14c).

a

b

c
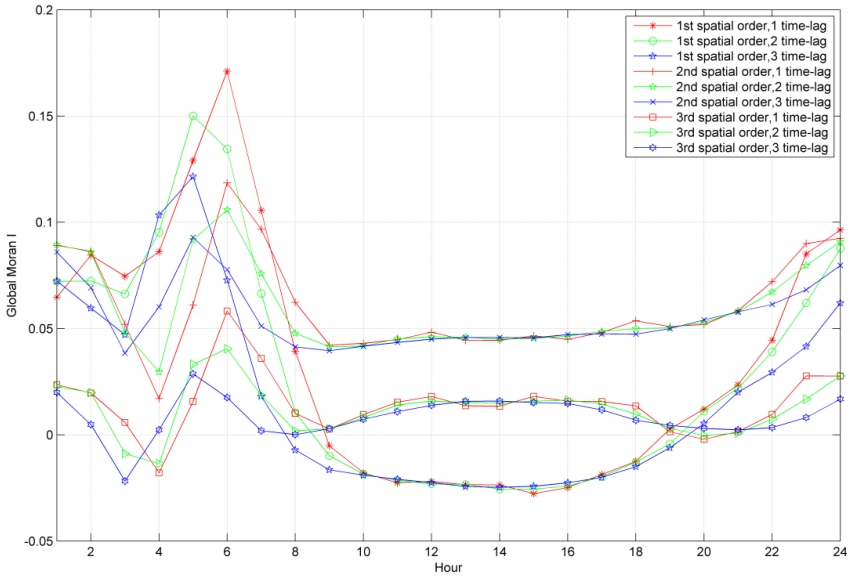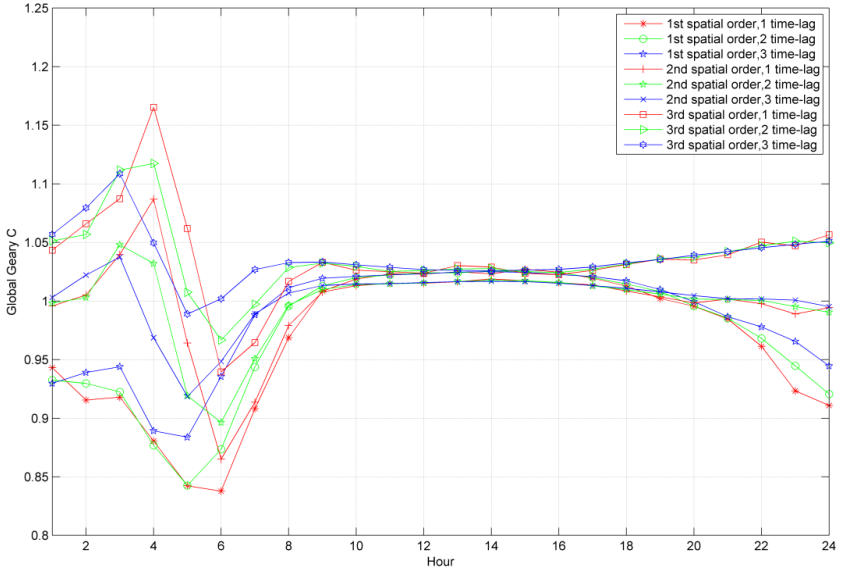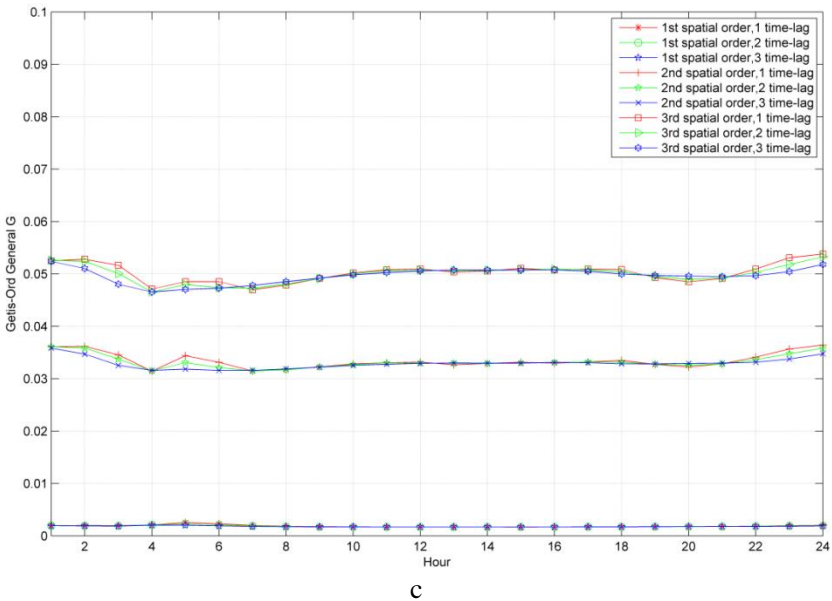
Figure 14. Three global measures of spatio-temporal association with different combinations of spatial weights (spatial orders) and temporal neighbors (1 time-lag: 1 hour; 2 time-lag: 2 hours; 3 time-lag: 3 hours) for hourly phone-call patterns: (a) I_{st}; (b) C_{st}; and (c) G_{st} measures.

CONCLUSION AND FUTURE WORK

In this paper, we introduce a spatio-temporal analytical framework for exploring human mobility patterns and urban dynamics with the help of GIS. The integration of spatial-temporal visualization, space-time density estimation and spatio-temporal autocorrelation analysis can not only help to represent spatio-temporal data visually and interactively but also offer quantitative analytics to identify the spatio-temporal patterns (such as spatio-temporal hotspots) in the mobile phone data. Our experiments have demonstrated that different spatio-temporal techniques have their potential advantages but also limitations. For instance, space-time path model is good for visual exploration or overview of individual regular (or irregular) movement patterns but might not be suitable for massive trajectories because of overlapping and cluttering problems in the space-time cube. The study also demonstrates that the user's "home" and "working places" can be inferred based on statistical information

of visited mobile cells with the characteristics of personal temporal signatures on these places. In addition, we implement the STKDE to analyze the continuous spatio-temporal density structure for the georeferenced phone call activities and this technique can facilitate the identification of spatio-temporal patterns. Furthermore, to understand the phone-call spatial interaction structure, we introduce a novel 3D flow visualization approach of generating vertical Bézier curves in the 3D-GIS environment which also support interactive analysis of spatial information and thematic attributes.

Moreover, we have investigated different statistical measures *(I_{st}, C_{st} and G_{st})* which extended the classic spatial association indices for the spatio-temporal autocorrelation analysis.

The spatial order of weighted matrix was found to have more significant effects than the temporal neighbors on influencing the autocorrelation strength of hourly phone-call volume across the whole study area.

The spatio-temporal analytical framework introduced in this paper can be also applied in other spatio-temporal datasets (e.g., infectious diseases, crimes, and GPS tracks) for facilitating knowledge discovery and decision support in urban informatics and social sciences.

REFERENCES

Armstrong, M. P. (1988). Temporality in spatial databases. In: *Proceedings: GIS/LIS.* 88 (2), 880-889.

Andrienko, G. and Andrienko, N. (2008). Spatio-temporal aggregation for visual analysis of movements. In: *Visual Analytics Science and Technology*, 2008. VAST'08. IEEE Symposium on (pp. 51-58). IEEE.

Adrienko, N. and Adrienko, G. (2011). Spatial generalization and aggregation of massive movement data. *IEEE Transactions on Visualization and Computer Graphics*, 17(2), 205-219.

Andrienko, G., Andrienko, N., Demsar, U., Dransch, D., Dykes, J., Fabrikant, S. I., Jern, M., Kraak, MJ., Schumann, H., and Tominski, C. (2010). Space, time and visual analytics. *International Journal of Geographical Information Science*, 24(10), 1577-1600.

Andrienko, G., Andrienko, N., Dykes, J., Fabrikant, S., and Wachowicz, M. (2008). Geovisualization of dynamics, movement and change: key issues and developing approaches in visualization research. *Information Visualization*, 7(3 4), 173-180.

Anselin, L. (1995). Local indicators of spatial association—LISA. *Geographical analysis*, 27(2), 93-115.

Batty, M. (2013). Big data, smart cities and city planning. *Dialogues in Human Geography*, 3(3), 274-279.

Box, G. E., Jenkins, G. M. and Reinsel, G. C. (2008). *Time series analysis: forecasting and control*. John Wiley and Sons.

Brunsdon, C., Corcoran, J. and Higgs, G. (2007). Visualising space and time in crime patterns: A comparison of methods. *Computers, Environment and Urban Systems*, 31(1), 52-75.

Chai, Y. (2013). Space–Time Behavior Research in China: Recent Development and Future Prospect. *Annals of the Association of American Geographers*, 103(5), 1093-1099.

Chen, J., Shaw, S. L., Yu, H., Lu, F., Chai, Y., and Jia, Q. (2011). Exploratory data analysis of activity diary data: a space–time GIS approach. *Journal of Transport* Geography, 19(3), 394-404.

Cliff, A. D. and Ord, J. K. (1973). *Spatial autocorrelation* (Vol. 5). London: Pion.

Couclelis, H. (1999). Space, time, geography. In: *Geographical Information Systems: principles, techniques, management, and applications*. (Second Edition), eds. Paul Longley, Michael Goodchild, David Maguire, and David Rhind. New York: Wiley, vol. 1, 29-38.

Delmelle, E., Dony, C., Casas, I., Jia, M. and Tang, W. (2014). Visualizing the impact of space-time uncertainties on dengue fever patterns. *International Journal of Geographical Information Science*, DOI:10.1080/13658816. 2013.871285.

Demšar, U. and Virrantaus, K. (2010). Space–time density of trajectories: exploring spatio-temporal patterns in movement data. *International Journal of Geographical Information Science*, 24(10), 1527-1542.

Epanechnikov, V. A. (1969). Non-parametric estimation of a multivariate probability density. *Theory of Probability and Its Applications*, 14(1), 153-158.

Farin, G. E. (1996). *Curves and Surfaces for Computer-Aided Geometric Design: A Practical Code*. Academic Press, Inc.

Gao, S., Hu, Y., Janowicz, K., and McKenzie, G. (2013a). A spatiotemporal scientometrics framework for exploring the citation impact of publications and scientists. In: *Proceedings of the 21st ACM SIGSPATIAL International Conference on Advances in Geographic Information Systems* (pp. 204-213). ACM.

Gao, S., Liu, Y., Wang, Y., and Ma, X. (2013b). Discovering spatial inter-action communities from mobile phone data. *Transactions in GIS*, 17(3), 46 3-481.

Gao, S., Wang, Y., Gao, Y., and Liu, Y. (2013c). Understanding urban traffic-flow characteristics: a rethinking of betweenness centrality. *Environment and Planning B: Planning and Design*, 40(1), 135-153.

Getis, A. (1991). Spatial interaction and spatial autocorrelation: a cross-product approach. *Environment and Planning A*, 23(9), 1269-1277.

Getis, A. and Ord, J. K. (1992). The analysis of spatial association by use of distance statistics. *Geographical analysis*, 24(3), 189-206.

Getis, A. and Aldstadt, J. (2010). Constructing the spatial weights matrix using a local statistic. In: *Perspectives on Spatial Data Analysis* (pp. 147-163). Springer Berlin Heidelberg.

González, M. C., Hidalgo, C. A. and Barabasi, A. L. (2008). Understanding individual human mobility patterns. *Nature*, 453(7196), 779-782.

Goodchild, M. F. (2013). Prospects for a Space–Time GIS. *Annals of the Association of American Geographers*, 103(5): 1072–1077.

Guo, D., Chen, J., MacEachren, A. M., and Liao, K. (2006). A visualization system for space-time and multivariate patterns (vis-stamp). *Visualization and Computer Graphics, IEEE Transactions on*, 12(6), 1461-1474.

Guo, D., Gahegan, M., MacEachren, A. M., and Zhou, B. (2005). Multivariate analysis and geovisualization with an integrated geographic knowledge discovery approach. *Cartography and Geographic Information Science*, 32(2), 113-132.

Hägerstrand, T. (1970). What about people in regional science?. *Papers in regional science*, 24(1), 7-24.

Hardisty, F. and Klippel, A. (2010). Analysing spatio-temporal autocorrelation with LISTA-Viz. *International Journal of Geographical Information Science*, 24(10), 1515-1526.

Kang, C., Liu, Y., Ma, X., and Wu, L. (2012a). Towards estimating urban population distributions from mobile call data. *Journal of Urban Techno-logy*, 19(4), 3-21.

Kang, C., Ma, X., Tong, D., and Liu, Y. (2012b). Intra-urban human mobility patterns: An urban morphology perspective. *Physica A: Statistical Mechanics and its Applications*, 391(4), 1702-1717.

Kaufman, A. (1990). Volume visualization. *The Visual Computer*, 6(1), 1-1.

Kwan, M. P. (2000). Interactive geovisualization of activity-travel patterns using three-dimensional geographical information systems: a methodolo-

gical exploration with a large data set. *Transportation Research Part C: Emerging Technologies*, 8(1), 185-203.

Kwan, M. P. (2004). GIS Methods in Time-Geographic Research: Geocomputation and Geovisualization of Human Activity Patterns. *Geografiska Annaler: Series B, Human Geography*, 86(4), 267-280.

Liu, Y., Wang, F., Xiao, Y., and Gao, S. (2012). Urban land uses and traffic 'source-sink areas': Evidence from GPS-enabled taxi data in Shanghai. *Landscape and Urban Planning*, 106(1), 73-87.

Jiang, B. and Claramunt, C. (2004). Topological analysis of urban street networks. *Environment and Planning B*, 31(1), 151-162.

MacEachren, A. M. and Kraak, M. J. (2001). Research challenges in geovisualization. *Cartography and Geographic Information Science*, 28(1), 3-12.

Miller, H. J. (1991). Modelling accessibility using space-time prism concepts within geographical information systems. *International Journal of Geographical Information System*, 5(3), 287-301.

Miller, H. J. (2005). A measurement theory for time geography. *Geographical analysis*, 37(1), 17-45.

Moran, P. A. (1950). Notes on continuous stochastic phenomena. *Biometrika*, 37(1-2), 17-23.

Nakaya, T. and Yano, K. (2010). Visualising Crime Clusters in a Space-time Cube: An Exploratory Data-analysis Approach Using Space-time Kernel Density Estimation and Scan Statistics. *Transactions in GIS*, 14(3), 223-239.

Nakaya, T. (2013). Analytical Data Transformations in Space–Time Region: Three Stories of Space–Time Cube. *Annals of the Association of American Geographers*, 103(5), 1093-1099.

Peuquet, D. J. and Duan, N. (1995). An event-based spatiotemporal data model (ESTDM) for temporal analysis of geographical data. *International journal of geographical information systems*, 9(1), 7-24.

Phan, D., Xiao, L., Yeh, R., and Hanrahan, P. (2005). Flow map layout. *IEEE Symposium In Information Visualization* (INFOVIS) (pp. 219-224).

Ratti, C., Williams, S., Frenchman, D., and Pulselli, R. M. (2006). Mobile landscapes: using location data from cell phones for urban analysis. *Environment and Planning B Planning and Design*, 33(5), 727.

Shaw, S. L., Yu, H. and Bombom, L. S. (2008). A space-time GIS approach to exploring large individual-based spatiotemporal datasets. *Transactions in GIS*, 12(4), 425-441.

Shen, Y., Kwan, M. P. and Chai, Y. (2013). Investigating commuting flexibility with GPS data and 3D geovisualization: a case study of Beijing, China. *Journal of Transport Geography*, 32, 1-11.

Silverman, B. W. (1986). *Density estimation for statistics and data analysis* (Vol. 26). CRC press.

Tobler, W. R. (1987). Experiments in migration mapping by computer. *The American Cartographer*, 14(2), 155-163.

Worboys, M. F. (1992). A model for spatio-temporal information. In: *Proceedings of the 5th International Symposium on Spatial Data Handling*, 2: 602-611.

Yuan, M. (1996). Temporal GIS and spatio-temporal modeling. In: *Proceedings of Third International Conference Workshop on Integrating GIS and Environment Modeling*, Santa Fe, NM.

Yuan, Y., Raubal, M. and Liu, Y. (2012). *Correlating mobile phone usage and travel behavior–A case study of Harbin, China*. Computers, Environment and Urban Systems, 36(2), 118-130.

Yu, H. and Shaw, S. L. (2008). Exploring potential human activities in physical and virtual spaces: a spatio-temporal GIS approach. *International Journal of Geographical Information Science*, 22(4), 409-430.

Chapter 4

GIS APPLICATIONS IN MODERN CROP PROTECTION

Martin Scheiber[1,],*
Benno Kleinhenz[1] and Manfred Roehrig[2,†]
[1]ZEPP - Central Institute for Decision Support Systems
in Crop Protection, Bad Kreuznach, Germany
[2]ISIP - Information System for Integrated Plant
Production, Bad Kreuznach, Germany

ABSTRACT

Crop Protection is besides agricultural engineering, plant breeding and fertilization an indispensable part of modern agriculture. Still, even though not substitutable, there is a downside. The use of pesticides and therefore the application of chemicals into the environment bears substantial risks for both nature as well as human beings. Geographical Information Systems (GIS) can help making crop protection more

---

[*] Dipl. Geogr. Martin Scheiber is working as research associate in the field of Geographical Information Systems (GIS) and Dr. agr. Benno Kleinhenz as chief executive officer at ZEPP - Central Institute for Decision Support Systems in Crop Protection Ruedesheimer Str. 60-68, 55545 Bad Kreuznach, Germany, scheiber@zepp.info / kleinhenz@zepp.info.

[†] Dr. agr. Manfred Roehrig is working as chief executive officer at ISIP - Information System for Integrated Plant Production Ruedesheimer Str. 60-68, 55545 Bad Kreuznach, Germany, roehrig@isip.de.

sustainable. This chapter describes two possible examples of how GIS is used by the Central Institute for Decision Support Systems (DSS) in Crop Protection (German acronym ZEPP) to support farmers in Germany with their pesticide applications.

The first example describes a DSS that creates machine readable application maps using a web based GIS application. Application maps offer the possibility to automate the pesticide spraying process. The maps created by the DSS include legal buffer zones to water bodies and protected terrestrial structures, e.g. hedges, where spraying of pesticides is prohibited. Provided that a tractor with Global Navigation Satellite System (GNSS) and a pesticide sprayer with section control is available, an automated application is possible. Once the sprayer moves into an area of the field that is a buffer zone, the respective section is switched of automatically. The DSS helps farmers to comply with legal rules and to prevent the contamination of the environment.

The second example describes how GIS is used in pest forecast systems. With the help of GIS it is possible to obtain results with higher accuracy for disease and pest simulation models. Pest forecast systems developed by ZEPP use GIS to interpolate geographical factors like temperature and relative humidity such getting meteorological data for every km^2 in Germany. The interpolated data and the parameter precipitation, taken by radar measured precipitation data are used as input for the simulation models. The output of these models is presented as spatial risk maps in which areas of maximum risk of the disease outbreak, infection pressure or pest appearances are displayed. The modern presentation methods of GIS lead to an easy interpretation and further-more promote the use of the system by farmers.

INTRODUCTION

Agriculture is the targeted production of plant or animal products. It serves primarily for food production and therefore is of highest importance to human society. Agriculture nowadays has reached a very high level of techno-logy and efficiency. This is necessary, because in a world with an ever growing number of inhabitants and an equally growing demand for quantity as well as quality of agricultural products a big emphasis has to be put on getting the most out of what is available. This is especially important since the amount of arable land stays the same or is even declining because of climate change and other issues (Oerke et al. 1999).

Unfortunately but as well inevitably, the development of useful plants and their intensive cultivation have triggered an evolution of pathogens like plant diseases and pest attacks.

Several times such pathogens have had an deep impact on human development. One example is the outbreak of late blight in Ireland between 1845 and 1849. Four years of bad to no harvest in potatoes caused the death of 500.000 Irishmen due to famine and triggered the emigration of 1,6 Million more to the US.

Crop protection tries to fight such pest attacks to assure yield amounts stay on the necessary level. Besides agricultural engineering, plant breeding and fertilization it has become an indispensable part of modern agriculture.

Experts guess, that without any type of intelligent crop protection, agricultural yields would on average be around 50 % lower. The fact that we have not seen hunger crisis in the western world since many years is due to a highly efficient agriculture that includes crop protection measures.

Still, even though not substitutable, there is a downside to crop protection. The use of pesticides and therefore the application of chemicals into the environment bears substantial risks for both nature as well as human beings.

Spraying helps to avoid plant diseases and pest attacks but the number of treatments is often not optimal adjusted to the appearance of noxious organisms. Achieving the optimal efficiency is difficult. This often leads to negative economic and environmental impacts for farmers and the environment.

To minimize the negative effects of crop protection, several preconditions have to be met. On the one hand there have to be strong regulations in place on how, when and where to use pesticides or how, when and where not to use them. Additionally Decision Support Systems (DSS) have to be set in place to allow smarter decisions e.g. when and where to use pesticides.

In Germany forecasting models and advice by the government are used in the planning of spraying, taking economic and ecological aspects in account. The prediction of the occurrence and the prevention of plant diseases and pest attacks is an important component of integrated pest management.

Since location plays a crucial role in agriculture GIS-Systems can play an important role here. They can support sustainable crop protection by helping to get better answers to questions like:

- Where should be applied which amount of pesticide to achieve optimal results and to comply with legal regulations?

- When is the optimal date for certain crop protection measures in a specific location?

The mission of the ZEPP is to develop, collect and examine existing forecasting and simulation models for important agricultural and horticultural pests and diseases and to adapt these models for practical use.

GIS is an integral part of these models. In the following two examples for how GIS is used in DSS shall be shown.

1. CREATING MACHINE READABLE APPLICATION MAPS FOR CROP PROTECTION

Expectations towards the use of pesticides in Germany are high. This is necessary to sustain public acceptance of modern agriculture. Farmers need an efficient data management because complying with rules and requirements regarding planning, application and documentation of pesticide measures causes a high level of information density.

To prevent deposition of pesticides into water bodies as well as other damage to the environment several laws about legal buffer zones to rivers, etc. apply. The instructions coming with each pesticide explain the product specific buffer zones. Certain pesticides require e.g. to keep a distance of 20 meters to water bodies if the field slopes more than 2%. Besides that, legal buffer zones depend as well on the application technique. The drift reduction class of spray nozzles is the important point here. Additional there are specific laws in each German state that oblige buffer zones to water bodies and if a district does not have an adequate amount of small landscape features (e.g. hedges) buffer zones to such structures apply, too.

Because of these factors and the necessary documentation proper crop protection is challenging for farmers who want to achieve an optimal and correct implementation. Considering changing agricultural machines, drivers and work regions for agricultural service supply agencies these challenges are even bigger (Scheiber and Kleinhenz 2013b). In agricultural day-to-day reality the planning and implementation of crop protection measures as well as the compliance with laws, rules and any sort of documentation are mostly due to the responsibility of the operator who is conducting the action. Much of this work is still done manually and without the support of information technology which results in high workloads as well as an increased error-proneness.

GIS systems can help to automate and therefore optimize the processes mentioned above.

One option is to automate the spraying process and the protection of adjacent natural and aquatic ecosystems by using GIS-created application maps, that include legal buffer zones, where spraying is prohibited. These maps can then be aplied to sprayer terminals.

ZEPP and ISIP have, in cooperation with different project partners[1], developed an internet-based DSS that creates such application maps (Scheiber et al. 2012, Scheiber and Kleinhenz 2013a-d). Figure 1 describes the underlying concept:

The DSS consists of six steps, in which data from the farmer as well as public information and geodata are integrated (Figure 2). Each step will be described in detail in the following:

Step 1: GNSS Survey of Field Geometries, Water Bodies and Terrestric Structures

The process starts with the mapping of field geometries and sensitive landscape areas adjacent to the field. Geodata about water bodies and terrestric structures like hedges or skirts of the forest are necessary to be able to calculate the required buffer zones.

A technical procedure how to conduct such surveys has been developed. A GNSS-RTK based approach is promoted, which reaches an accuracy of up to just a few centimeters. The procedure allows the farmer to map the applicable landscape elements during a tractor ride using an off-set method. It has been developed in cooperation with German supervising authorities to promote that data recorded this way are officially accepted.
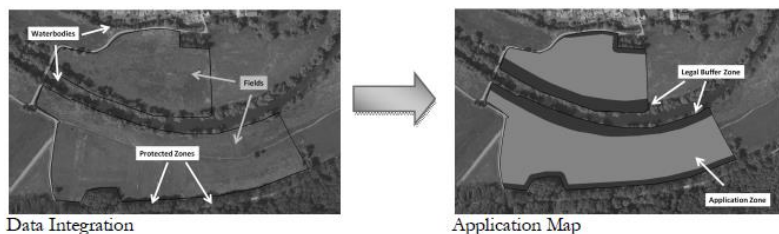
Figure 1. Concept of creating application maps.
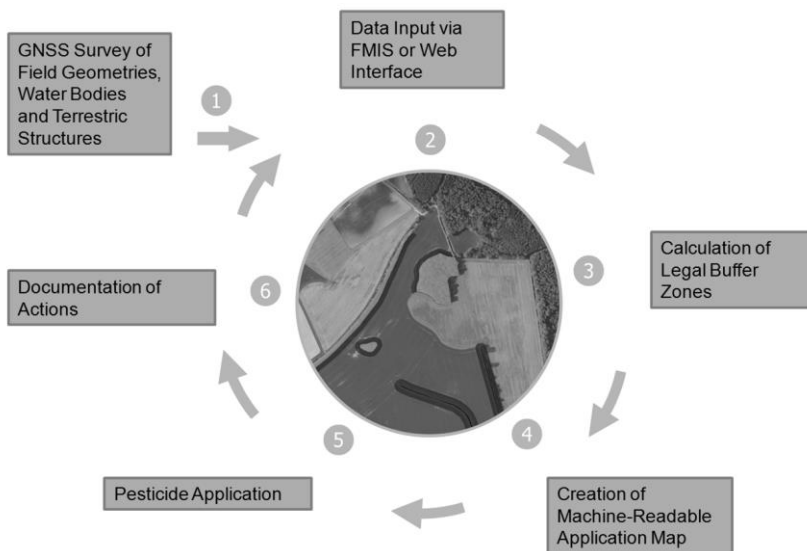
Figure 2. Decision Support System.

Step 2: Data Input Via Farm Management Information System (FMIS) or Web Interface

To allow field specific advice, data from the farmer are necessary. This includes information about cultivated crop, geographic coordinates of the field (e.g. from Step 1) or spray nozzle used (drift reduction class). Data input can either be done using a direct connection to a FMIS system (e.g. Landdata Eurosoft or HELM Software) or via a web interface on www.isip.de. Figure 3 shows an example for a web interface.

Step 3: Calculation of Buffer-Zones Based on Legal Regulations

In a third step zones inside the field are being identified, in which pesticide application is not allowed under the conditions of the specific pesticide application. The output is a machine readable application map. The following factors are included in the process:

- Pesticide specific buffer zones to water bodies or other landscape structures deserving protection based on information from the pestici-

de database of the German Federal Office of Consumer Protection and Food Safety (Bundesamt für Verbraucherschutz und Lebensmittel-sicherheit 2013)

- Buffer zones that arise from the slope of a field (e.g. >2%)
- Buffer zones that arise from spray nozzles used (drift reduction class)
- Buffer zones to water bodies depending on which German state the field is in
- Buffer zones to terrestric structures deserving protection based on the index of small landscape features by the the Julius Kühn-Institut (JKI), Federal Research Centre for Cultivated Plants

The calculation of the buffer zones is carried out by an online-GIS-application. Within the scope of a complex geoprocessing service information and geodata from the sources mentioned above are intersected to identify zones in the field where pesticide spraying is prohibited. The result is a map that defines application zones and legal buffer zones (Figure 1). The farmer has the possibility to edit this map.

Figure 3. Example for a web interface.

Step 4: Creation of the Machine-Readable Application Map

The application map is provided using the non-proprietary ISO-XML format (ISO 11783-10 2009) which can be applied to terminals of different manufacturers. The file format ISO-XML is becoming more and more established in agricultural engineering.

Figure 4 shows examples for crop protection tasks on terminals of John Deere and the Competence Center ISOBUS e.V. (CCI).

Figure 4. Application Tasks on a Terminal of John Deere and CCI.

Step 5: Application

Provided that a tractor with GNSS and a pesticide sprayer with section control is available, an automated application is possible. Once the sprayer moves into an area of the field that is a buffer zone, the respective section is switched of automatically (Figure 5).

Step 6: Documentation

Modern terminals are able to record data about pesticide applications. This considerably facilitates the documentation process. The protocol file can be used as justification towards public authorities or purchasers. The compliance with legal buffer zones can be proven. Furthermore the information generated can be used for consecutive treatments.

In summary using the DSS brings several benefits for farmers:

- Oberservance of legal buffer zones
- Facilitation of a proper pesticide application
- Cost optimization due to automated section control
- Environmentally sound and sustainable use of pesticides
- Automated documentation

2. USE OF GEOGRAPHIC INFORMATION SYSTEMS IN PEST FORECAST SYSTEMS[2]

As described in the introduction, the main mission of ZEPP is to develop, collect and examine existing forecasting and simulation models for important agricultural and horticultural pests and diseases and to adapt these models for practical use. More than 40 weather-based forecasting models for pests and diseases have been successfully developed within the last years.

The occurrence of diseases/pests and periods of high-intensity attacks can be calculated with high accuracy. The forecast models are based on different concepts.

---

[2] The information in this subchapter is based on Racca P. et al. 2011.

Figure 5. Crop Protection Measure.

These range from simple temperature sum models to complex population matrices with integrated rate based algorithms to calculate growth, reproduction and distribution of noxious organisms.

DSS are employed for the

- estimation of disease/pest risk
- estimation of the necessity for pesticide treatments
- forecast of the optimal timing for field assessments
- forecast of the optimal timing for pesticide treatments
- recommendation of appropriate pesticides

Results of DSS are distributed to the farmers via warning services, using different transmission media (bulletins, letters, faxes and telephone answering machines) and via the internet platform www.isip.de (Information System for Integrated Plant Production) (Röhrig and Sander, 2004). The predictions are suitable for integrated as well as organic farming.

Meteorological data as well as assessed field data are needed as input for DSSs. With these input data the decision support systems calculate an output result, e.g. the date of the first appearance of a pest.

The meteorological data in Germany are provided on the one hand by the German meteorological service, on the other hand some federal states in Germany built up their own meteorological networks.

At the moment data of 148 stations of the German meteorological service and 417 stations owned by the Governmental Crop Protection Services (GCPS) of federal states are available. In sum these are data of 565 stations which can be used to run decision support systems.

However, in some agricultural areas, the distance between meteorological stations (MS) exceeds 60 km.

Forecast models did not give satisfactory results for fields separated by such large distances to MSs (Zeuner, 2007). With the help of Geographic Information Systems (GIS) a plot-specific classification of temperature and relative humidity has been developed using complex statistical interpolation methods described by Zeuner (2007). The method, however, cannot be applied to the parameter precipitation.

Especially in the case of frequent spatially and temporally limited rainfall (so-called convective rainfall event), the interpolation for precipitation does not give plausible results (Zeuner and Kleinhenz, 2007, 2008, 2009).

To overcome this restriction, precipitation data is not interpolated but obtained from radar measurements with a high spatial resolution.

Using these spatial input parameters for the currently available disease forecast models leads to accurate forecasting for areas in-between two or more distant MSs. With the use of GIS, daily spatial risk maps for diseases and pests can be created in which the spatial and the temporal process of first appearance and regional development are documented (Figure 6). These risk maps lead to improved control and a reduction in pesticide use.
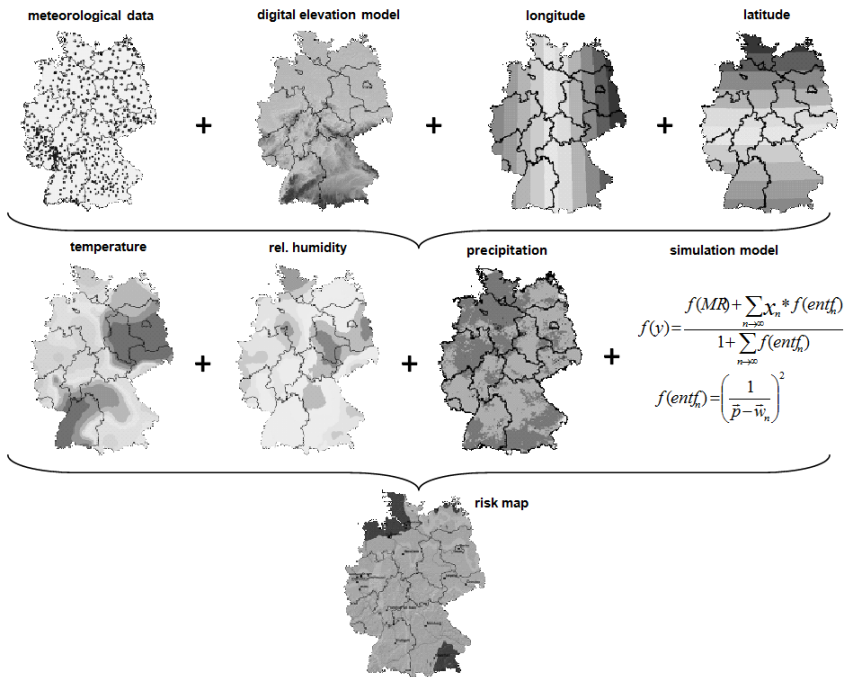
Figure 6. Scheme of process to calculate risk maps using GIS.

2.1. Storage

In order to store the results of interpolation, a grid was laid out over Germany. At present, the GCPS use about 565 MSs to represent an agri- cultural area of aprox. 200.000 km^2, or an average of one MS per 350 km^2. With the new GIS method, grid cells have a size of 1 km^2 and, after inter- polation, are represented by virtual MSs (Liebig and Mummenthey, 2002).

2.2. Spatial Data of Temperature and Relative Humidity

For the interpolation of temperature and relative humidity the multiple regression method was chosen because it gave the best results by the shortest calculation time of all tested interpolation methods. The first calculations with the four interpolation methods (Inverse Distance Weighted, Spline, Kriging and Multiple Regression) showed that deterministic interpolation methods were not suitable. The general purpose of multiple regressions (the term was first used by Pearson, 1908) is to learn more about the relationship between several independent or predictor variables and a dependent or criterion variable. MR is an interpolation method that allows simultaneous testing and modelling of multiple independent variables (Cohen, et al., 2003).

Parameters that have an influence on temperature and relative humidity, e.g. elevation, slope, aspect, can therefore be tested simultaneously. MR uses matrix multiplication and only variables with a defined minimum influence that will be included into the model. The result of MR is a formula (x = const + A1*const1 + A2*const2+ A3*const3+…+ Ax*const) which allows a calculation of a parameter set for each grid cell from which independent variables are known (Zeuner, 2007).

To validate the results of the interpolation, 13 MSs were ignored in the interpolation process. After interpolation, the deviation between calculated values and measured data of these stations were compared. The study was conducted from January to August in the years 2003 to 2006. For all stations, MR gave results with highest accuracy (Table 1). In all cases, the coefficient of determination (CoD) ranged between 96 and 99% for temperature and 92 and 96% for relative humidity, respectively. For the 13 MSs, the mean deviation for temperature was less than 0.1°C and for relative humidity less than 0.6% as calculated with MR. The absolute maximum and minimum for temperature was less than 4.7°C and for relative humidity less than 32.6%. The data also were tested for significance between calculated and measured

data using a t-test. The test indicated that for all stations the differences between the calculated and measured values were random. The MR method gave plausible results, so it was chosen to interpolate the meteorological data to be used as input for the forecasting models.

2.3. Spatial Precipitation Data

16 radar stations are run by the German meteorological service to record precipitation all over Germany. These stations do not measure the amount of precipitation at ground level but the signal reflected from the rain drops in the atmosphere. These measurements at first only allowed calculation of an unspecific 'precipitation intensity', a shortcoming. With the system RADOLAN intensity is now calibrated online with data from a comprehensive network of ombrometers, using complex mathematic algorithms. As a result the amount of precipitation can be provided in a spatial resolution of 1 km² (Bartels, 2006). These calibrated amounts of precipitation based on radar measured rainfall intensities are referred to as "radar data" in the following. The validation of precipitation data took place in intensely used agricultural areas, joining the radar grid with stations of the meteorological network. In this way, it was possible to relate each station to a grid cell.

The radar derived precipitation at the station's grid cell and the actually measured data formed the basis for the statistical verification. Since rain events differ throughout the year, two representative months (May and August 2007) were selected to analyse uniform rainfalls in spring as well as convective rainfall events in summer. This resulted in a validation dataset of 1488 hours for each MS.

Table 1. Validation of data on temperature and relative humidity; deviation between calculated values and measured data with MR

year	temperature [°C]				relative humidity [%]			
	2003	2004	2005	2006	2003	2004	2005	2006
CoD	96%	96%	99%	98%	94%	96%	95%	92%
mean dev.	0.0	0.0	0.0	0.1	0.3	0.1	0.1	-0.6
maximum	4.4	4.1	4.3	4.7	19.6	32.6	21.6	21.2
minimum	-3.8	-4.5	-4.5	-4.1	-18.9	-21.9	-22.8	-22.8
t-test	n.s.	n.s.	n.s.	n.s.	n.s.	n.s.	n.s.	n.s.

n = 92160 hours, n.s. = not significant.

Depending on the region, the number of MSs ranged from 9 to 29. In addition, the influence of the distance between radar station and MSs was analysed.

Furthermore, a leaf wetness simulation model used by ZEPP (Racca, 2001, unpublished) was run on data from both methods of precipitation measurement and the results were compared.

The parameters for the amount of precipitation, number of hours with precipitation and calculated leaf wetness showed high correlations between radar values and measured data. The maximum of the hourly deviation of the amount of precipitation was 0.06 mm. In hours with rainfall the deviation was slightly higher (0.36 mm). No correlation could be detected for the distance between radar stations and MSs.

For hourly rainfall pattern, a correlation of 91.4% between stations and validation areas was measured. The best correlations were obtained for the leaf wetness model for which values > 99.9% were achieved.

The results clearly show that the use of radar data as an input parameter in disease forecast models is valid. By adding data of temperature and relative humidity with high spatial resolution, an optimal basis for plot-specific forecasts has been established.

Moreover, this system allows the exact detection of local convective rainfall events, which at the moment often remain undetected using individual MSs. Significant improvements of the spatial forecasting by plant disease simulation models can be expected from the use of radar data.

2.4. Introducing Spatial Risk Maps into Practice (www.isip.de)

ISIP, the Information System for Integrated Plant production www.isip.de, is a Germany-wide online decision support system. It has been initiated in 2001 by the German Crop Protection Services as a common portal, thus achieving synergies by pooling existing information.

Target groups are farmers as well as advisors.

Since information transfer is the primary task of extension services, the system is intended to make this work more efficient by using modern information technology. Therefore a bi-directional data flow between the services and the farmers was developed. By combining general with specific data, recommendations can be refined from regional to individual.

The information is primarily distributed via HTML pages, thus a browser is necessary to use the system (Röhrig and Sander, 2004).

In 2010 a new way of presenting results of prognosis models for plant pests and diseases has been implemented. Using interpolated meteorological data in a high spatial resolution as input parameters, so-called 'risk maps' are drawn (Figure 7). These maps have several advantages compared to results representing point information based on single MSs:

- Risk maps are more suitable to identify hot spots and ease the inter-pretation of the model's results.
- The user does not have to choose a specific MS, which might even not be valid for his plant production site.
- The maps are produced conform to the OGC standards, thus can be used in other systems.

In addition to the GIS functionalities of zooming and panning, it is possible to scroll through the maps of the last ten days. This gives an excellent overview of the temporal development of the pest or disease risk.

The system is supplemented by a spatial three-day weather forecast offered by the German Meteorological Service.

Figure 7. Risk map of the German Federal State of Lower Saxony for Potato Late blight in September 2013. Shown are the infection pressures in five classes (very low [Sehr niedrig] to very high [Sehr hoch]) and the respective spraying intervals in days.

It is expected that this further supports the decision and management processes of the farmer.

In a summary it can be concluded that pest forecast systems need plausible and complete meteorological data as main input. In Germany meteorological data are mainly provided by the German meteorological service. Additionally several German states built up their own meteorological networks.

However by using meteorological data of MSs a good prognosis is only reached in the scope of a MS. That is the reason why the ZEPP developed a new technology based on GIS. With the help of GIS it is possible to obtain results with higher accuracy for disease and pest simulation models.

The influence of geographical factors on temperature and relative humidity were interpolated with GIS methods getting meteorological data for every km^2 in Germany. The parameter precipitation was taken by radar measured precipitation data and the results of all measured meteorological data were used as input for the simulation models.

The output of these models is presented as spatial risk maps in which areas of maximum risk of the disease outbreak, infection pressure or pest appearances are displayed.

The modern presentation methods of GIS lead to an easy interpretation and will furthermore promote the use of the system by farmers.

CONCLUSION

The two examples mentioned above show that the use of GIS can support crop protection measures in different ways and make them more sustainable.

GIS helps in planning pesticide applications, answering the question if pesticide spraying in a specific location is appropriate at all, because the weather conditions have been favorable for a certain plant disease or pest. Thus the pesticide application can be optimized under economic and ecologic aspects. GIS helps as well in the actual spraying process by assuring that zones like water bodies that deserve protection are automatically taken into account. GIS-created application maps automate the spraying process.

When a protected zone is entered the sprayer automatically stops the pesticide application. Water bodies or hedges are not contaminated with chemicals.

REFERENCES

Bartels, H. (2006). Projekt RADOLAN - Routineverfahren zur Online-Aneichung der Radarniederschlagsdaten mit Hilfe von automatischen Bodenniederschlagsstationen (Ombrometer). <http://www.dwd.de/RADOLAN>, Offenbach.

Bundesamt für Verbraucherschutz und Lebensmittelsicherheit (Ed.) (2013). *Pflanzenschutzmittel-Verzeichnis 2013*, Teil 1–7. Braunschweig, Saphir Verlag, 61. Aufl.

Cohen, J., Cohen, P., West, S., Aiken, L. (2003). Applied multiple regression/correlation analysis for the behavioural sciences, *Lawrence Erlbaum*, 0805822232.

Gisi, U. (2012): Pflanzenschutz – alternativlos: Beiträge der Wissenschaft. 58. *Deutsche Pflanzenschutztagung*, 58. Braunschweig.

ISO 11783-10:2009 (2009). *Tractors and machinery for agriculture and forestry – Serial control and communications data network – Part 10*: Task controller and management information system data interchange.

Liebig, W., Mummenthey, R. D. (2002). *ArcGIS-ArcView(c)*, Halmstad. Norden.

Oerke, E-C., Dehne, H-W., Schönbeck, F., and Weber, A. (1999): Crop Production and Crop Protection. *Estimated losses in major food and cash crops.* Amsterdam.

Racca, P., Kleinhenz, B., Zeuner, T., Keil, B., Tschöpe, B., Jung, J. (2011). Decision Support Systems in Agriculture: Administration of Weather Data, Use of Geographic Information Systems (GIS) and Validation Methods in Crop Protection Warning Service. In: Chiang, Jao (Ed.): *Efficient Decision Support Systems: Practice and Challenges-From Current to Future/ Book 1,* 331-354.

Röhrig, M., Sander, R. (2004). ISIP - online plant protection information in Germany. In: *Online Agrometeorological Applications with Decision Support on the Farm Level*. Cost Action 718: Meteorological Applications for Agriculture, I. Thysen, A. Hočevar, eds., 41-47. Dina publication.

Scheiber, M., Kleinhenz, B., Röhrig, M., Zeuner, T. (2012): iGreen Entscheidungsunterstützung: Applikationsassistent Pflanzenschutz. In: *58. Deutsche Pflanzenschutztagung,* 275 and 473. Braunschweig.

Scheiber, M., Kleinhenz, B., Röhrig, M. (2013). Pesticide Application Manager (PAM) – Decision Support in Crop Protection based on Terrain-, Machine-, Business-, and Public Data (Poster). In: *EFITA/WCCA/CIGR* 2013, 1209-1213.

Scheiber, M., Kleinhenz, B. (2013a). Abstand halten auf die einfache Art. In: *RBZ* 7/2013, 23-24.

Scheiber, M., Kleinhenz, B. (2013b). Creating machine-readable application maps using GIS and geodata. In: *Landtechnik / Agricultural Engineering*, 68(4), 273-277.

Scheiber, M., Kleinhenz, B. (2013c). GIS in der Präzisionslandwirtschaft, In: *arcAKTUELL* 3/2013, 24-25.

Scheiber, M., Kleinhenz, B. (2013d). iGreen Entscheidungsunterstützung: Applikationsassistent Pflanzenschutz. In: *GetreideMagazin* 3/2013, 32-36.

Zeuner, T. (2007). Landwirtschaftliche Schaderregerprognose mit Hilfe von Geographischen Informationssytemen. *Dissertation*, Johannes Gutenberg Universität, Mainz.

Zeuner, T., Kleinhenz, B. (2007). Use of geographic information systems in warning services for late blight. *OEPP/EPPO* (37), 327-334.

Zeuner, T., Kleinhenz, B. (2008). Optimierte Schaderregerprognose durch die Nutzung von Geographischen Informationssystemen (GIS). 56. Deutsche Pflanzenschutztagung in Kiel 22.-25. September 2008. Pflanzen-produktion in Wandel - Wandel im Pflanzenschutz?, *J. Kühn-Institut,* P.-T. Deutsche, eds., Julius Kühn-Institut, Kiel, 266.

Zeuner, T., Kleinhenz, B. (2009). Verbesserte Schaderregerprognosen durch GIS Flächengenaue Modelle durch Nutzung von Geographischen Informationssystemen. *Kartoffelbau*, 4, 108-110.

Chapter 5

GIS APPLICATIONS IN PRACTICE: EXPLORING SPATIAL DYNAMIC OF TRANSPORT ACTIVITIES

*Tiebei Li (Terry)**

Urban Research Program, Griffith University, Australia

ABSTRACT

The spatial pattern of urban transport activities has become a focus of recent academic enquiry and planning policy concerns. This is largely driven by the rapid urban growth and increased transport pressure in major international cities and the demand for improved transport infrastructure and services. This article focuses on the application of Geographical Information Systems (GIS) techniques in exploring geographic patterns of major urban transport activities at both urban and regional scales. The first part in this article develops GIS methods to analyse geographical pattern of commuting transport at a regional level. The methodology uses multiple spatial O-D transport data at regional geographical units and applies disaggregated spatial techniques to identify spatial patterns of commuting distance and traffic flow and the changes in these patterns over time. The second part of the article demonstrates the application of GIS techniques in exploring tempo-

---

* PhD in Geography (University of Queensland, Australia); Address: 170 Kessels road, Nathan, QLD 4111, Australia; Research: Urban Geography, Transport Geography; Profession: Mid-career research fellow, lecturer

spatial patterns of public bicycle trips in urban areas. A GIS technique called flow map is developed to explore tempo-spatial patterns of public bicycle under different calendar event and climatic conditions. The paper demonstrates how the results from the GIS techniques may form part of an evidence base for the transport planner with the potential to inform future development to enhance the efficiency, and how the application of GIS techniques will enhance the planner's toolbox whilst responding the transport planning issues.

1. INTRODUCTION:
TRANSPORT ANALYSIS AT DIFFERENT SCALES

In transport studies, transport-related activities and processes can be analysed across a whole range of scales. This may include regional, local and individual levels. The scale of transport study and analysis is closely related to the transport phenomenon under investigation and the questions being posed about it. In general, the transport structure can be broken down into regional, local and micro levels.

Regional Level

The system-wide transport analysis can be applied to the regional or national level. At this level, regional researchers and strategic planners account for the general transport interactions of people in large regions across space, for example, national migration, freight movement, and inter-state flow and interactions. Regional transport analysis is fundamental in many strategic transport planning and policy issues (Miller, 1998). The major outputs of analysis at this level include the regional economic interactions and population migration, the transport infrastructure, the processes between industries and interregional trade, and transport systems.

Since the 1950s and 1960s, various geographers and economists have developed a suite of analytical approaches. They are typically used to model structural relationships and spatial interactions between the regional economies as well as regional mobility of population. Some research methods are based on the macro-economic theory. Examples are regional economic-base analysis (Tiebout, 1962) and multi-regional input-output analysis (Leontief, 1986). These are able to resolve a degree of regional interactions

and relationships between the regional economies. Gravity-based model (Lowry, 1964) is one of the most widely-used methods at a regional level for the analysis of the regional economic interactions and transport. Gravity-based models explicitly model and predict the spatial interactions in a region's (or a nation's) economy. Regional planning uses spatial interaction analysis to forecast trends in migration, employment and capital flows. The spatial division of regional spatial interaction typically uses economic regions to reflect regional economic and transport performance.

Metropolitan Level

Research at the metropolitan-level scale focuses on the transport processes of smaller spatial units (e.g. traffic zones). At this intermediate level, the processes focus on the actions of main elements of the urban transport systems, such as, the interactions and behaviours of the institutes or the local residential/economic communities of a region. The problems under investigation at this level include transport activities to various functional destinations such as travel to work, school, shops and recreational activities. The transport problems typically focus on the geography of transport zones, inter-zonal transportation, transport patterns and associated energy consumption (Dodson et al., 2007) and performance of transport networks including road and public transport systems. In addition, congestion is also a common question at city level around the world and solution must be sought to alleviate these problems.

Essentially the transport interactions at metropolitan level have an inherent spatial component comprising area of transport zones (e.g. origin zone and a destination zone), and interactions and movements between transport zones. Developing an understanding of the basic relationship of the transport interactions, and its variation according to the type of activities, and transport mode are central to the search for solutions to the problem. Geographical Information Systems (GISs) have a potentially large role to play in the analysis and visualization of transport data permitting more in-depth studies to be undertaken. Especially its ability to integrate multiple data sources such as census statistics, road networks and their associated capacities permits more advanced measures of movement between traffic zones to be incorporated.

Theories and research methods have been developed at this level since about the 1960s. The transport analysis based on the micro-economic theory or

location theory (Alonso, 1964) have been widely used to analyse the transport demand and route choice between trip origin and destinations at metropolitan areas (for example, choosing a path with lowest travel cost or shortest distance). The GIS analysis at this level typically focuses on the inter-zonal interactions. For example, spatial interaction models specify an overall governing relationship for flow between locations. The powerful visualization and data manipulation capabilities of GIS permit transport data to be visually explored to uncover spatial patterns and trends. GIS techniques that are capable of tracking changes in the spatial dimension of transport behaviour can help identify the ever varying nature of travel demand.

Individual Level

The aggregate analytical approaches are not recommended for analysing the more complex transport processes at the very disaggregate level. This is because the greater diversity of behaviours that exist at the lower levels of observation need a variety of social behavioural theories to explain, rather than using a simple spatial interaction formulation. At the micro-level scale, research typically focuses on the fundamental units of human behaviour (an individual, a household). This includes individual social/behavioural geography, travel patterns and location and route decision choices and trip chain (activity) patterns. Micro-level analysis became a major area of transport geography because there was a greater variety of human behaviours and an increased level of spatial variability in the urban transport systems.

The micro-level modelling perspective represents the activity-based analysis at the highest possible level of disaggregation. It studies the emergence of complex patterns from behaviour and the interactions at the individual level — e.g. the location choice for an individual person. Such a description of an individual's behaviour is often referred to as microeconomic theory and discrete choice theory (McFadden, 1978). The actors in micro-level analysis can be an individual or a household. The research methods for transport activity at the micro-level are based on the theories and concepts of behavioural geography (Golledge and Stimson, 1997). For example, micro-simulation or agent based modelling, are used to simulate the transport choice and processes at the level of the individual actors. Time geography (Hagerstrand, 1970)approach describes how an individual's travel behaviour and route choice vary according to the trip purpose, time, and the location attributes of the neighbourhoods (Kwan, 1998). In comparison to spatial

aggregate analysis, these local approaches have shown potential in explaining the social and economic behaviour at the individual level. Hence, they can provide a detailed pattern of urban transport at the most disaggregated level. Nevertheless, micro-level analyses are not suggested for modelling spatial variations for a large geographical area. This is because of the considerable modelling complexity and demands for micro-scale data.

The geography of urban transport in essence consists of the study of people's location of activities coupled with the route and distance travelled between those activities. The application of GIS to study the spatial dynamics of commuting has been applied in a variety of instances. Discussions on how to properly use GIS-based methods are relatively sparse in transport studies. This article focuses on the application of GIS techniques in exploring geographic patterns of major urban transport activities at various scales. Although not all GIS techniques presented in this article are new, they demonstrate how those GIS techniques can be tailored for transport studies at different level of scales to better address scale specific transport questions. The purpose of doing that is to contribute to the discussion and theory of linking GIS with a wide range of transport research and applications. The first part in this article develops GIS methods to analyse geographical pattern of commuting transport at a regional level. The methodology uses multiple spatial O-D transport data at regional geographical units and applies disaggregated spatial techniques to identify spatial patterns of commuting distance and traffic flow and the changes in these patterns over time. The second part of the article demonstrates the application of GIS techniques in exploring tempo-spatial patterns of public bicycle trips in urban areas. A GIS technique called flow map is developed that explores tempo-spatial patterns of public bicycle under different calendar event and climatic conditions. The paper demonstrates how the results from the GIS techniques may form part of an evidence base for the transport planners with the potential to inform future development to enhance uptake of this new urban transport mode, and how the application of GIS techniques will enhance the planner's toolbox whilst responding the transport planning issues.

2. GIS FOR REGIONAL TRANSPORT ANALYSIS

Investigate transport dynamic for a large region is important giving increasing challenge for regional transport, some key transport issues are associated with low access to transport, lengthy travel distance and increased

transport energy cost. Such transport issues have received increasing attention in transport studies for a large regions. For instance, in popular journey to work studies, developing an understanding of the broad relationship between a worker's residence to their locale of work and commuting behaviours in a given region, its variation over space and time and how this differs according to industry sector and travel mode are central to the search for solutions to transport problems.

2.1. The Need for GIS

GIS techniques that are capable of tracking changes in the spatial dimension of regional mobility can help identify the ever varying nature of transport demand. The geographical dimension of journey to work activities has received significant attention over time (see for example Mogridge, 1979; O'Connor, 1978, 1980; Gipps et al., 1997; Horner and Murray, 2003; O'Kelly et al., 2005; Titheridge and Hall, 2006; Sakanishi, 2006; Sultana and Weber, 2007; Mees et al., 2008). The application of GIS to study the spatial dynamics of commuting has been applied in a variety of instances. An early work provided by Mogridge (1979) who used the Euclidean distance analysis between traffic zones to investigate journey to work lengths in London. This is followed by Wachs et al., (1993) who utilized GIS-based techniques to track changes in wokers' home and work locations in California. Other GIS applications include Christopher et al., (1995) spatially explored the direction of travels for 9 counties in Chicago. Results indicated minor change in directional biases over the 20 year study period despite significant regional growth and urban decentralisation. The more recent GIS operations was given by Vandersmissen et al., (2003) to analyse changes in worker travel time and distance for Québec City using disaggregate household travel survey data. Horner (2007) investigated urban form and transport change in Tallahasse, Florida using both global and local measures of transport change and relationship between land use and transport patterns. At a regional level, many of these studies have also used higher levels of aggregation in census and travel survey data.

This section demonstrates a series of GIS applications that it is possible to model regional transport patterns, even at a disaggregate scale. Their capacity to assess detailed transport flows and the use of transport networks, and manipulate the aggregate transport data into a meaningful geo-visualization. In this section, the journey to work datasets were used to conduct GIS analysis of

transport dynamics at a regional level. Two JTW datasets for South East Queensland (SEQ) region were obtained from the Australian Census for 1996 and 2006. Specifically, the compiled JTW matrices for 1996 and 2006 for the SEQ region contained 300 origin zones and 300 destination zones (using suburbs) covering geographic region of Brisbane, Gold Coast and Sunshine Coast. There are three types of information contained in the JTW data: GIS coverages for both the origin and destination zones for all trips, and the JTW (origin-destination) matrix. The JTW matrix simply comprises one column and one row, specifically a destination code and an origin code and the total number of people travelling between each origin and destination.

2.2. Modelling Travel Distance

Firstly, the travel distance of JTW was modelled using disaggregated GIS network analysis. One spatial issue of aggregated transport analysis is the geographical unit of transport zones (suburb) are relatively large (especially suburbs for regional areas), the measure of JTW distance between the centroid of each suburb was not appropriate to represent the multiple route choices for all commuters within the suburb. Therefore, we randomly generated 10 points within each suburb and each point was used as the single departing location and arrival location of the travel. The use of this method permits more advanced measures of movement of commuters on the road between multiple home locations and workplaces. Then the point-to-point based travel distances were summarized within the suburb to give an average suburb-suburb travel distance. The suburb-suburb commuting distance was then multiplied by the number of commuting trips between each origin-destination pair (provided by JTW data), and the total travel distance for all commuting trips for every single surburb (including all destinations) was calculated. Then the average commuting distance for each suburb was obtained based on the total number of commuters in a suburb. In order to identify variations in peoples' commuting behaviour for local areas, the commuting distance is calculated based on suburb of residence (trip origins). The Queensland road network data was applied to calculate the network travel distance between origin and destination.

Next, the same GIS modelling procedure was applied to the 2006 JTW data in order to compare the change in commuting pattern over time. However, a major difficulty in the analysis of changes in transport is the changes in travel zones of JTW data over census years. As such, this has raised a crucial

analytical issue of how these independent zonal structures can be spatially integrated into a single, consistent set of geographical units. To overcome this problem, an area interpolation technique was applied to transform the spatial data from the zones supplied by the ABS to a new set of spatial units which are consistent between 1996 and 2006. We used 2006 suburbs as the new destination zones (consistent to the origin zones) and applied an areal weighted proportioning method to transform the spatial data. The data estimation for the new destination zones was based on the degree of spatial overlap with known data for the previous destination zones. Although the concept of the technique is fundamental, it proved challenging as the areal calculation for the large spatial matrix data was computationally intensive.

Finally, the results of the average commuting distance across suburbs for year 1996 and year 2006 are provided in Figure 3 (a) and (b). This shows that the commuting distance tends to be shorter among workers who live closer to central city areas (e.g. Brisbane metropolitan area, Gold Coast and Toowoomba City), whilst longer commutes (mainly cross-suburban travel) tend to be for workers in the middle and outer suburbs. Therefore, the regional trend is that the travel distance increases as residences are separated further from the city centre. The further one's home is from a city centre, the longer one's commute tends to be.

The result also reveals the local difference in average commuting distance between 1996 and 2006. In general, there was minor change in average JTW distance between 1996 (15.75 km) and 2006 (15.95 km). There were an increased number of commuters travelling shorter distances to work (less than 10 km) by 2006, but the distance of travel for commuters in the middle range (e.g. 10 to 30 km) slightly increased. The number of commuters with very long commutes (30 km or more) remained stable between 1996 and 2006. By comparing Figure 3 (a) and (b), the map shows that over time a decrease in average commute distance occurred at the Sunshine Coast (far north to Brisbane), Brisbane's west, and the Gold Coast suburbs. The possible reasons include fast urban growth and employment relocation, which have introduced increasing numbers of employment opportunities into these areas. People living in these areas tend to find work locally, travelling relatively shorter distances. In addition, areas with an increased commuting distance were observed at some outer-urban and regional areas. Tentatively, the increase in long commuting could be driven by economic restructuring, and new residents in emerging peri-urban locations who are often reliant on employment well outside their local area, perhaps explaining increasing general commute distances.
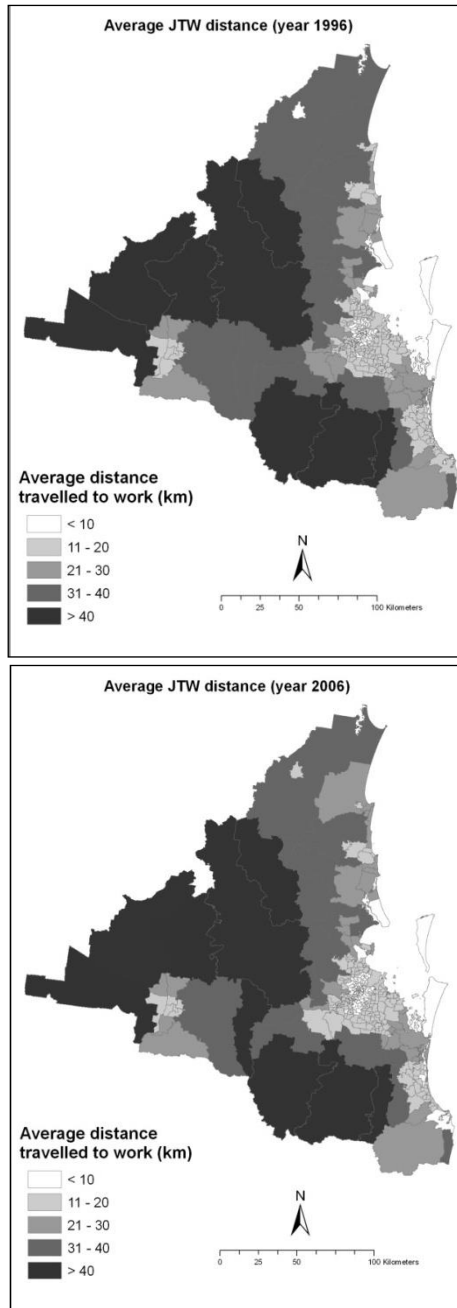
Figure 1. GIS mapping of travel distance for year 1996 and year 2006.

2.3. Modelling Traffic Flow

In this section, the GIS-based network modelling was used to model the distribution of traffic flows over the road networks.

First, we calculated the shortest route for commuting travel between each origin and destination, assigning all trips to the shortest routes possible. All shortest paths carrying traffic flows were then overlapped with suburb boundaries, and total commuting flows were summed for each individual suburb based on the total number of commuters passing through, originating, and ending in that suburb.

Next, because the spatial unit for suburbs is too coarse to represent the spatial distribution of the commuting flows, we transformed the total number of commuting flows from suburbs to 1km by 1km grid cells across the study area. A *binary dasymetric mapping* method (Langford and Fisher, 1996) was applied to spatially disaggregate the data. The binary dasymetric method assumes that the number of travellers is uniformly distributed inside some part of a suburb (in this case, the grid cells that intersect with the road networks) and the remaining parts of the zone (non-road areas) necessarily have a zero commuting flow value.

The maps of spatially disaggregated commuter flows for year 1996 and 2006 are illustrated by Figure 6 (a) and (b). At the regional level, the highest commuting flows are concentrated in the central Brisbane area, extending north and south through the transport networks. The 1996 data showed the commuting flow stretching to the southern areas; and this tendency was found to be more significant in 2006. The increased commuting flow across the north-south corridor may have been caused by rapid urban expansion and new population settlements, especially in the southern suburbs of Brisbane, which generated increased commuting trips towards Brisbane. A similar pattern of commuting development was also found in the Gold Coast City area, where commutes spread considerably towards the north and south areas of the city along the coast.

A comparison between travel flows between 1996 and 2006 demonstrated that the central Brisbane area has experienced the highest growth in commuting flows. This was not only driven by an increase in inbound commuters but also the increased cross-suburban traffic that passes through the central Brisbane area. The most significant growth in commuting was found along the transport corridor between Brisbane and Gold Coast. The major growth areas along this corridor involves some spatial clustering effect indicating that in addition to increased commuting interactions towards

Brisbane, some increased internal commuting has also developed in these areas. The change in commuting flows in the Brisbane's west was not significant.
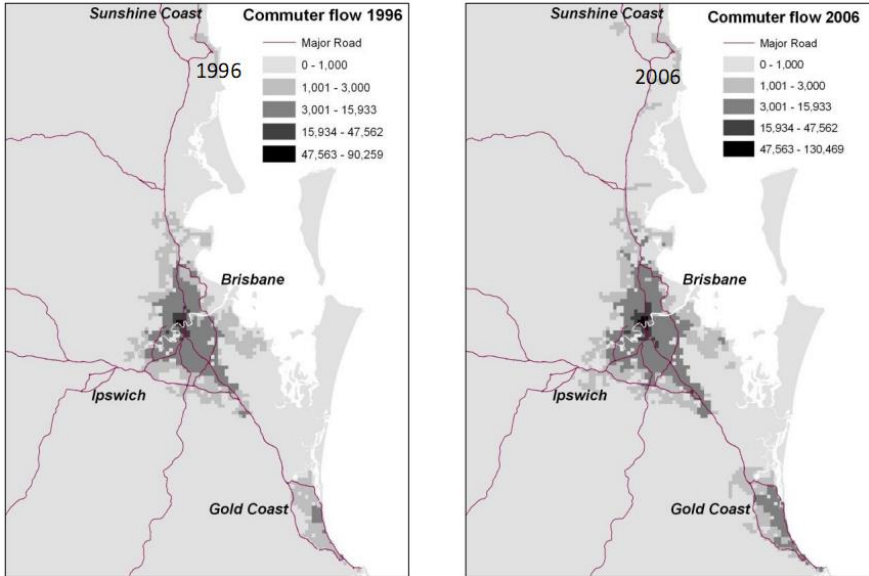
Figure 2. The distribution of travel flows for year 1996 and year 2006 (by 1k by 1k grid cells).

3. GIS FOR LOCAL TRANSPORT ANALYSIS

In the last section, we demonstrated a range of GIS techniques applied to model and explore the spatial dynamics of urban transport activities over a large region. In this section, we focus on the GIS analysis of spatial dynamics of transport activities at local scale using disaggregated Brisbane City Cycle travel data. In different to the motorized transport (e.g. private cars), the non-motorized transport such as walking and cycling appear to be route flexible and more sensitive to the external conditions (such as wether and temperature). Therefore, the transport patterns are considered more complex and dynamic over space and time. A more spatial-temporal dedicated technique is needed to capture the temporal-spatial dynamics.

3.1. The Need for GIS

Technological improvements introduced in third generation public bicycle systems permit continuous monitoring of traffic flows of public bikes (Shaheen et al. 2010). As such, operators of public bicycle systems are able to gain access to real-time usage data of their networks. Collected via mobile devices or other ICT-based measures, this information can then improve our understanding of individual traveller's behaviour, offer real-time travel information, and also present personalised location-based services. Moreover, fine-grained data on the status of shared bicycles also enables an empirical measurement of the impacts of proposed system improvements or policy changes (e.g. fare restructuring) as well as the results of force majeure on the system (e.g. flooding).

A number of studies have utilised stock or usage data to explore spatial and temporal patterns. For example, examining Barcelona's shared bicycling system 'Bicing', Froehlich, Neumann and Oliver (2009) investigated user behaviour across stations in relation to location, neighbourhood, and time of day. Still in the European context, Borgnat et al. (2009) predicted the number of bikes hired per hour in Lyon's community bicycle program to describe the daily and weekly patterns. The prediction method involved several explanatory factors such as the number of subscribed users, the time of the week, the occurrence of holidays or strikes, and weather parameters. However, methods to identify and visualise spatio-temporal patterns (i.e. location and times when frequency of bike use is particularly high) based on flow or trip data have not been adequately examined in past studies, particularly, within the Australian context. There is, therefore, an imperative need to better understand the location, time and reasons for these individual uses to inform strategies to ensure a more successful public bicycle implementation.

The Brisbane's CityCycle dataset was used to conduct GIS analysis of transport dynamics on urban areas. The CityCycle data contains trip level information in the form of an origin-destination matrix. There are total of 150 CityCycle stations distributed in the Brisbane CBD and its immediate surrounding suburbs. The rows represent origin stations and the columns destination stations along with individual counts of transitions. Analysis of this type of dataset in raw form is not generally viable given that it consists of a large matrix of numbers with no geographic information included. This is particularly the case in multivariate situations where the difference in origin-destination matrices conditional on other variables (for example, hour of day) is of interest. The argument for the role of exploratory spatial data analysis has

been made convincingly elsewhere (see for example, Haining et al. 1998; Anselin 1999) and would be strong in our case with the CityCycle dataset, where no simple descriptive statistic can be easily defined that captures the complex dynamics of an origin-destination matrix.

3.2. Using Flow Mapping

The flow map is a well-established cartographic technique. It can assist in our understanding of these matrices by mapping transitions between spatial units. Here, lines depicting the transitions between spatial units are typically appended with arrows to indicate flow direction and the width of the line is used to indicate the volume of flow. While the flow map can be used to develop an understanding of origin-destination matrices, it does not readily allow the incorporation of other variables such as weather and calendar events as a component of the visual output. In such circumstances, the analysis of bivariate spatial data can be analysed using a technique termed the comap in which plots with overlapping subsets of data are selected using non-spatial variables. These plots of raw data can be used to give a sense of how spatial relationships change conditional on one or more external variables (for example, how bicycle trips vary spatially according to how windy it was at the time the particular trips were made).

Flow mapping, a visual analytical tool to depict spatial interaction and movement, has a long history dating back to 1869 where Charles Minard first used the technique to depict Napoleon's army's advancement towards Moscow (Minard 1869). The development of computerised flow mapping tools, however, only commenced in the late 1980s with Waldo Tobler's flow mapper program. This program was designed to visualise discrete node-to-node movements (Glennon & Goodchild 2005). Since then, a number of significant efforts, particularly in computer science, have been made to develop more advanced tools to visualise flow information in various standalone applications (see for example, Phan et al. 2005; Guo 2009; Boyandin et al. 2010; Boyandin et al. 2011).

The flow map, on its own, only conveys pertinent information of an origin-destination matrix where the objective of the investigation is to study the matrix in isolation. In circumstances where there is a need to investigate the extent to which the origin-destination matrix changes as a function of other variables (for example, under certain weather conditions), another technique

must then be employed. In this section, the flow map technique was embedded into another spatial exploratory data analysis technique called the comap.

The comap (Brunsdon 2001) and its older, more generic cousin, the coplot (Cleveland 1994), provide an effective means of visualising multivariate data in order to assist with uncovering previously hidden patterns embedded within complex data. The basic idea is that a bivariate subset of raw data is selected based upon some condition (for example, a defined range of rainfall or a categorical variable such as weekend or weekday). This data is then plotted either in raw form in a scatter plot panel or a mapped kernel density surface. The comap and coplot embrace the small multiple principle (Tufte 1991) by using multiple panes of similar and typically overlapping regions, in order to illustrate how gradual changes can be observed as a function of external variables.

Embedding the flow map into the comap to form a combined technique that represents a straightforward extension of the two techniques which allows multivariate exploration of origin-destination data which otherwise would not be readily possible.

3.3. CityCycle Flow Dynamics

We examine the spatial flows of City Cycle over a 24-hour period and the effect of specific calendar events (i.e. weekdays, weekends, public and school holidays) on the trip patterns. The flow maps of CityCycle between Brisbane's inner suburbs are displayed by Figure 3. The number of trips between suburbs represented using a variable line thickness, where the width of the line is proportional to the total flow volumes. Origin-destination pairs generating less than 200 trips in total were not mapped in order to preserve graphical clarity and highlight the main suburb-to-suburb interactions. The choropleth classification of suburbs represents the within-suburb flows (i.e. where the bicycle release and return are in the same suburb), with the darker colour representing the higher number of internal trips.

As Figure 3 shows, a high proportion of trips taking place over relatively short distances, along with a high degree of interaction between adjacent suburbs. The number of trips appears to be higher (but not concentrated) between the Brisbane Central Business District (CBD) and the immediate surrounding suburbs, whilst the trips between suburban locations are lower. In regards to self-containment, a number of suburbs exhibit relatively high levels of within suburb trips.
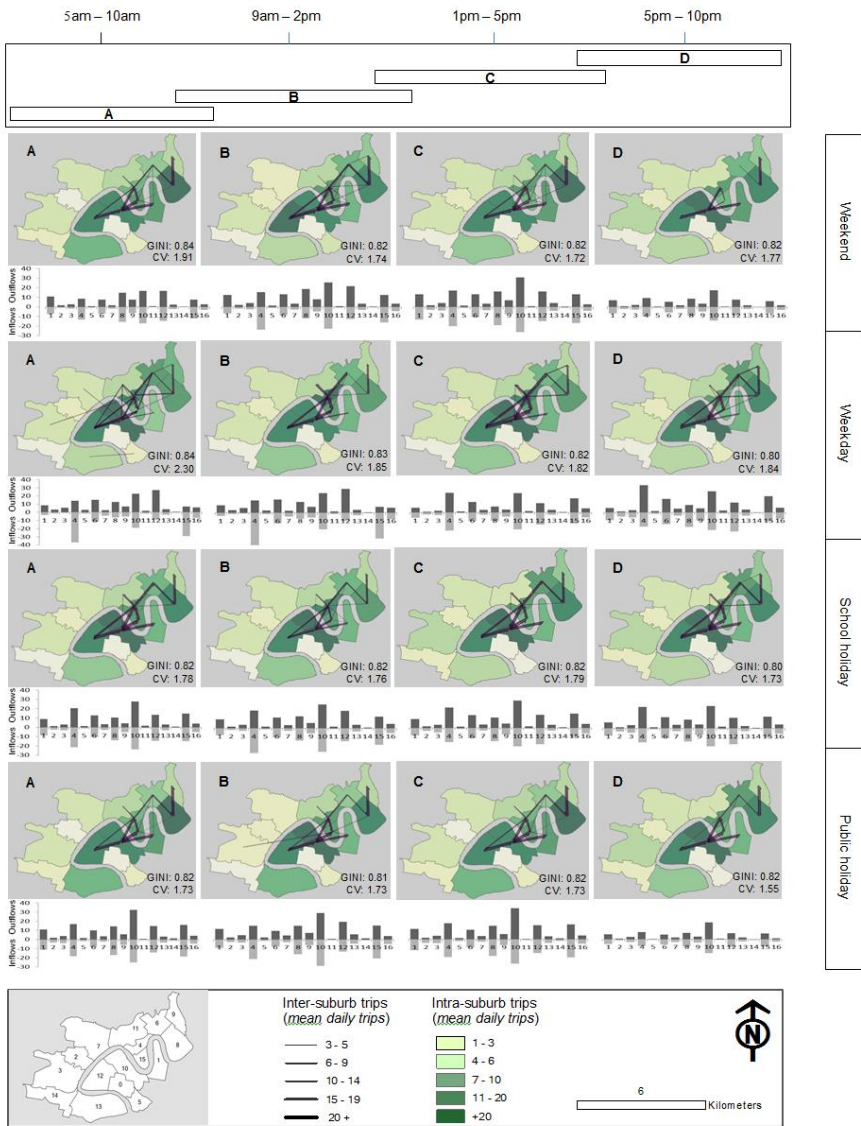
Figure 3. Flow map for public bicycle trips (by hour of day and for specific calendar events).

These results are expected given that each has high concentrations of urban amenities that include parks and river-side bike paths, and public transport links. Results also highlight that early morning trips (between 5am

and 10am) are more spatially dispersed. Later on in the morning and early afternoon (from between 10am and 2pm), trips tend to be more concentrated and spatially focussed around the CBD and the immediate surrounding suburbs. This spatial flow pattern continues until around 5pm where after (from 5pm to 10pm) trips begin to spread further into the suburbs but appear less dispersed than during the morning peak hours. There is also evidence that there are a relatively high proportion of self-contained trips that remain relatively constant across the 24-hour period at some suburbs.

The effects of specific calendar events (i.e. weekdays, weekends, public and school holidays) and hour on trip patterns simultaneously using an array of flow maps. A number of specific observations can be made. First, CBD-based trips taking place during weekends, especially between the hours of 9am to 5pm are shown to be markedly less concentrated that those occurring during workdays. Trips taking place during the evening (i.e. after 5pm) show a significant reduction in weekdays that is not as marked during weekends. The effect of public holidays on the spatio-temporal patterns is very similar to weekend patterns. Trips occurring during school holidays differ very little from regular weekdays apart from a small reduction in the number of trips taking place between the suburbs and the CBD during peak hours.

4. DISCUSSIONS

Understanding the spatial patterns of transport activities have always gain increase in importance. As GIS techniques become more established in this area, they will enhance the analysis of transport data that seek to derive deeper understanding of the transport pattern and underlying spatial structure and dynamics. The development and application GIS-based techniques will supplement the planners' toolbox. When the techniques presented in this paper are well developed into deployable solutions their added value to the urban and transport analysis can be fully evaluated. At this point, it would then be possible to better respond to the transport questions to inform the future development timely and geo-targeted policy; that could potentially enhance planning efficiency.

The first part of this chapter has investigated the JTW dynamics in a large region based on spatial analysis of JTW data with a focus on geographic patterns of travel distance and travel flows. The use of JTW datasets is far from straightforward because of complexity of the data and changes in geography of traffic zones over time. Therefore, we utilised advanced GIS

techniques to spatial analysis with JTW data and present JTW data with different form better serving transport analysis. Firstly, we employed an area interpolation technique to transform two data sets (1996 and 2006 JTW matrices) into consistent geographical units that independent of the two original and inconsistent zonal structures. This method provides new opportunities to examine spatial and temporal changes in urban transport patterns. Secondly, we applied a GIS-based network analysis to compute the average travel distance between the origin-destination traffic zones. The method accounts for all possible routes between randomly generated points in order to give more advanced measures of effects of multiple residential locations, workplace and road choices on the resulting travel distance. The GIS network modelling is also used to model the distribution of traffic flows through road networks. The procedure calculated the number of trips travelling on every road (network link) to estimate a traffic map. The map is used to analyse the distribution of traffic flow over time and congestions. The result is spatially disaggregated at 1km by l km grid cells, making them suitable to inform the transport analysis and policy making at local level (e.g. traffic noise, carbon emission and energy consumption at street block level). Both these GIS techniques are found to be very useful tools to model the spatial dynamics of commuting from the complex JTW datasets.

The second part of the chapter has shown that at a disaggregated scale, a flow mapping technique was used to explore spatio-temporal dynamics of public bicycle. In most of the previous research into public bicycle data capturing, the stock data has been the predominant source of data to study their underlying dynamics. In this study, we have highlighted the utility of flow or trip-level data that offers new opportunities for research to examine the spatio-temporal dynamics of public bicycle. Developing an understanding of the complex spatio-temporal dynamics of public bicycle at a local scale is critical to compiling evidence base with the capacity to ensure the system is configured in a manner that meets the needs of the public bicycle users. The data necessary to establish such an evidence base often exists in the form of disaggregate trip-level records. The challenge now for transport planners and researchers is to draw upon existing data, and where necessary, develop new tools and techniques to examine these data in a manner that has the potential to improve the operation of public bicycle systems. This paper has attempted to progress research in this area through the development of a visual analytic, the flow map, to explore new insights into the association of bicycle trip patterns. Gaining a better understanding of these underlying dynamics is a first step to establishing a fully automated monitoring tool with the capacity to identify

expected movements of bicycles around the system, given certain temporal and environmental circumstances. The analysis presented here has extended our knowledge of public bicycle dynamics through adopting a GIS approach to examine disaggregate-level relationships between bicycle trips and their complex relationships with hour and calendar events. Whilst findings reported in this paper are important for transport planners, conducting such research could in turn lead to operational benefits for public bicycle including the way in which bicycles are distributed across the system on weekends and weekdays to ensure that supply and demand are met in the most optimal manner possible.

CONCLUSION REMARKS

Understanding urban transport pattern using spatial analysis will increase in importance. Two sets of GIS-based techniques were presented in this chapter each demonstrates how useful recognized GIS applications in practice to better understand questions on transport activities from the large regions to the smaller metropolitan areas. As GIS techniques and applications become more established, they will enhance the transport planning that seeks to derive a deeper understanding of the spatial structure and dynamics of transport systems under various conditions.

The development, application and validation of the spatial disaggregation techniques will supplement the planners' toolbox. When the GIS techniques presented in this chapter are well-developed into deployable solutions, their added value to the transport planning and research can be fully evaluated. At this point, it would then be possible to better respond to the transport questions to inform the future development of timely and geo-targeted policy; that could potentially enhance the deployment of public investment and enhancing the efficiency and reducing the costs.

REFERENCES

Alonso, W. A. (1964). Location and land use: Toward a general theory of land rent. Harvard University Press, Cambridge.

Borgnat, P., Abry, P., Flandrin, P., et al. (2009). Studying Lyon''s Velo'V: A Statistical Cyclic Model. In: European Conference on Complex Systems, Warwick University (UK), 21- 25 September.

Boyandin, I., Bertini, E., Lalanne, D. (2010). Using flow maps to explore migrations over time. *Proceedings of Geospatial Visual Analytics Workshop in conjunction with The 13th AGILE International Conference on Geographic Information Science*, vol. 2, no. 3. https://diuf.unifr.ch/main/diva/sites/diuf.unifr.ch.main.diva/files/jflowmap-geova10.pdf

Boyandin, I., Bertini, E., Bak, P., Lalanne, D. (2011). Flowstrates: An Approach for Visual Exploration of Temporal Origin-Destination Data. *Computer Graphics Forum*, vol. 30, no. 3, pp. 971-980.

Brandenburg, C., Matzarakis, A., & Arnberger, A. (2007). Weather and cycling—a first approach to the effects of weather conditions on cycling. *Meteorological applications*, vol.14, no. 1, pp. 61-67.

Brunsdon, C. (2001). The comap: exploring spatial pattern via conditional distributions. *Computers, environment and urban systems*, vol. 25, no.1, pp. 53-68.

Christopher, E., Matthew, R., Siim S. (1995). Changes in the directions of urban travel for the Chicago area 1970 to 1990. *Transportation Research Record*, vol. 1477, pp. 48-57.

Cleveland, W.S. (1994). Coplots, nonparametric regression, and conditionally parametric fits. *Lecture Notes-Monograph Series*, pp. 21-36.

Gipps, P., Brotchie, J, Hensher, D, Newton, P., O'Connor, K. (1997). 'Journey to Work: Employment and the Changing Structure of Australian Cities' Research Monograph 3, Australian Housing and Urban Research Institute, Melbourne.

Glennon, A., and Goodchild, M. (2005). A GIS Flow Data Model. Flow White Paper. Accessed 14 August 2013, http://dynamicgeography.ou.edu/flow/..

Golledge, R., and R, Stimson. (1997). Spatial Behaviour: A geographic perspective. Guilford Press, New York.

Guo, D. (2009). Flow mapping and multivariate visualization of large spatial interaction data. Visualization and Computer Graphics, *IEEE Transactions*, vol. 15, no. 6, pp. 1041-1048.

Hagerstrand, T. (1970). What about people in regional science? *People of the Regional Science Association*, vol. 24, pp. 7–21.

Horner, M.W., and Murray, A.T. (2003). 'A multi-objective approach to improving regional jobs-housing balance', *Regional Studies*, vol. 37, no. 2, pp. 135 -146;

Horner, M.W. (2004). 'Spatial dimensions of urban commuting: A review of major issues and their implications for future geographical research', *The Professional Geographer*, vol. 56, no. 2, pp. 160-73.

Horner M.W. (2007). 'A multi-scale analysis of urban form and commuting change in a small metropolitan area (1990-2000)', *Annals of Regional Science*, vol. 41, pp. 315 – 332.

Langford, M., and Fisher, P F. (1996). 'Modelling sensitivity to accuracy in classification imagery: A study of areal interpolation by dasymetric mapping', *Professional Geographer*, vol. 48, no. 3, pp. 299–309.

Leontief, W. (1986). Input–Output Economics. Oxford University Press, New York.

McFadden, D. (1974). Conditional logit analysis of qualitative choice behaviour. In Frontiers in Econometrics, P. Zarembka, eds., Academic Press, New York.

Mees, P.G., O'Connell, K., Stone, J. (2008). 'Travel to Work in Australian Capital Cities, 1976-2006', *Urban Policy and Research*, vol. 26, no. 3, pp. 363 - 378.

Miller, J.R. (1998). Spatial aggregation and regional economic forecasting. *The Annals of Regional Science*, vol. 32, pp. 253–266.

Minard, C.J. (1869). Carte figurative des pertes successives en home de l'Armée Fançaise dans la campagne de Russie 1812-1813. Paris: Réginer et Dourdet.

Mogridge, M.H. (1979). 'Changing spatial patterns in the journey-to-work: A comparison of the 1966 and 1971 census data in London', *Urban Studies*, vol. 16, pp. 179 -190.

O'Connor, K. (1992). 'Economic activity in Australian cities: national and local trends and policy', Urban Futures, Special Issue vol. 5, pp. 86–95.

O'Kelly, M.E., and Lee, W. (2005). 'Disaggregate journey-to-work data: Implications for excess commuting and jobs housing balance'. *Environment and Planning A*, vol. 37, pp. 2233-2252.

Phan, D., Xiao, L., Yeh, R., Hanrahan, P. (2005). Flow map layout. *Information Visualization, 2005. INFOVIS 2005. IEEE Symposium,* 219-224. IEEE.

Kwan, M.-P. (1998). Space-time and integral measures of individual accessibility: a comparative analysis using a point-based framework. Geographical Analysis, vol. 30, no. 3, pp. 191–216.

Sakanishi, A. (2006). 'Commuting patterns in the Osaka metropolitan area: A GIS-based analysis of commuter rail passengers', *RURDS* vol. 18, no. 1, pp. 41 - 59.

Shaheen, S., Guzman, S., Zhang, H. (2010). Bikesharing in Europe, the Americas, and Asia: Past, Present and Future. *Transportation Research Record,* vol. 2143, pp. 159-167.

Sultana, S., and Weber, J. (2007). 'Journey-to-work patterns in the age of sprawl: Evidence from two midsize southern metropolitan areas', *The Professional Geographer*, vol. 59, no. 2, pp. 193-208.

Tiebout, C. M. (1962). The Community Economic Base Study, Committee for Economic Development, New York.

Titheridge, H., and Hall, P. (2006). 'Changing travel to work patterns in South East England', Journal of Transport Geography, vol. 14, pp. 60 – 75.

Tufte, E.R. (1991). Envisioning information. *Optometry & Vision Science*, vol. 68, no. 4, pp. 322-324.

Vandersmissen, M.H, Villeneuve, P & Theriault, M. (2003). 'Analyzing changes in urban form and commuting time', *The Professional Geographer*, vol. 55, no. 4, pp. 446 – 463.

Wachs, M, Taylor, B.D, Levine, N., Ong, P. (1993). 'The changing commute: A case study of the jobs-housing relationship over time', *Urban Studies*, vol. 30, no. 10, pp. 1711-1729.

Chapter 6

ESTABLISHING MEGALITH TRANSPORT ROUTES USING GEOGRAPHICAL INFORMATION SYSTEM

*Graham Brodie[1] and Leslie C. Hazell[2]**

[1]Melbourne School of Land and Environment, Melbourne University, Dookie, Victoria, Australia
[2]FILAS, La Trobe University, Melbourne Victoria, Australia

Limited evidence has led to considerable debate about land routes and methods to move megaliths chosen for sculpture by prehistoric societies. The current research is investigating the question using Geographic Information System (GIS) to determine likely land pathways to transport megaliths over 100 kilometres in Mesoamerica by Preclassic Olmec society. Access was restricted and the terrain included floodplains, seasonal rivers and extensive swamps. Analyses were derived from digitised survey maps using slope gradient tools initially from ARCVIEW 3.2 and finally ARC10. Although compatibility issues arose with this combination as we describe, tools of both versions provided a starting point between stones' source from which to then define a pathway across the challenging terrain.

---

* Corresponding author: phone: +61 3 5767 2353, Email: leshazell@activ8.net.au. Postal Address: 105 Lewis Road Tatong, Victoria, Australia 3673.

INTRODUCTION

The study by archaeologists of large stone or megalith transportation by prehistoric societies is often restricted by limited physical evidence. The known evidence will frequently show the stones were retrieved over long distances, across difficult and variable terrain. These considerations influence the transportation methods that could have been employed, the routes used and the time needed to complete these tasks. Most transportation efforts are affected by seasonal restrictions and manpower availability.

These considerations impose the need to manage, collate and analyse extensive spatial data sets to establish starting points for the archaeological investigation. Further analysis may then be possible using other methodologies and information sources. These analyses would include replication experiments, ethnographic observations and environmental data linked by mathematical models. All megalith transportation efforts are constrained by slope gradient limitations, which define viable movement of stones. Analysis of environmental factors using Geographic Information Systems (GIS), incorporating human physiology capability and slope gradient analysis as a constraint allows viable transportation routes to be identified. This paper describes how we established a database, applied the GIS analysis, while identifying its limitations and compatibility concerns between early analysis and those that followed.

The study of megalith transport in ancient societies provides an insight into various elements of these societies such as the necessary economies to support this activity and the relationship between the sculpture and political or hierarchical status of individuals within the society.

Replication experiments are often limited to specific examples (Cyphers, 2006, Richards and Whitby, 1997) and so require a methodology that can be used to synthesize relevant factors. Establishing how the transportation was done and where, is often the subject of considerable debate hence the use of slope gradient analysis to define both method and routes is important.

In theory massive weights can be moved by manpower alone; however in reality these loads are limited by the hauling teams' ability to co-ordinate their power. Richards' experiment (Richards & Whitby, 1997) suggested in theory 200 persons were needed for a 40 tonne stone to be moved uphill on a gradient of 1 in 20. In practice 130 people were used, while only 60 were needed for downhill hauling or control (Richards and Whitby, 1997).

The experiment described by Richards & Whitby, (1997) concluded that progress of approximately 1 km per day on level ground can be expected.

These data, together with ethnographic sources (ArchaeoNews, 2004, Harmon, 2005, Mladjov and Mladjov, 1999, Van Tilburg, 1995) and other sources (Royal Engineers, 1960, Royal Engineers, 1952) were used in conjunction with GIS slope analysis during this study. The following section describes the GIS research methodology associated with the megalith transport research. Analyses are detailed and conclusions outline its application to Olmec megalith transport and issues arising from this approach using GIS.

OLMEC COLOSSAL HEADS AND THEIR MEGALITH TRANSPORT

The Olmec are often referred to as the "Mother Culture" a title that is debated. This society held a sphere of influence some 200 kilometres long and 80 kilometres wide (125 x 50 miles) known as the "heartland", At its centre during a period between 1200-900BC known as the Preclassic was the San Lorenzo (SL) Plateau, the political hub of the period. Situated some 60 kilometres (38 miles) from the Gulf of Mexico, the SL Plateau is a partly man made ridge around 1200 metres long and rising some 45 metres above the extensive floodplains and swamplands, characteristic of the Rio Coatzacoalcos Basin. Its position and elevation make the plateau a dominant feature over this area, underwritten by the agriculturally productive floodplains that supported the general population and its hierarchy comprising artisans and rulers.
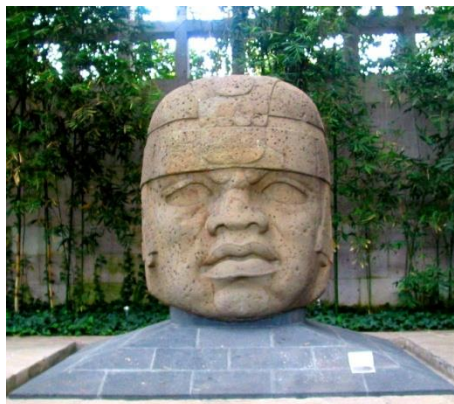
Photo Leslie C. Hazell.

San Lorenzo Head 1; Xalapa Museum of Anthropology.

Of the eighteen known Colossal Heads attributed to the Olmec, ten heads were found on the San Lorenzo Plateau and these weigh between six tonnes and 25 tonnes. They vary in height between one and a half metres to nearly three metres. Their circumference varies from just over three metres up to nearly six metres (Clewlow, et al., 1967). Their source is accepted as being from or near Cerro Cintepec in the foothills of the Tuxtla Mountains (Williams and Heizer, 1965). The straight line distance is around 80 kilometres or 50 miles with swamps, flood plains and many rivers that must be crossed.

At least one head is believed to have been a reused altar stone (Porter, 1989). The heads are noteworthy for their broad noses, short faced styles and having a flat backed form. The latter observation may be a clue to the method of transport as striations are visible, and such marks could be caused by direct contact with the ground, conversely these may be created by sculptors (Clewlow, et al., 1967).

A study using and testing various parameters essential for viable transport concluded that water routes would not be viable due to environmental, watercraft and crew capability limitations (Hazell, 2013, Hazell, 2011). These uncertainties indicate the difficulties of conflicting evidence and the need for robust data analysis of transport routes and methods. Many other smaller stones were moved and used in other sculptures, but the size and mass of the Heads makes their retrieval over such a distance and challenging terrain logistically complex. The GIS analyses, as shown in the various figures, indicated viable corridors that would avoid most river crossings, swamps and adverse gradients. Further analysis suggested that land transport was viable by using a direct contact dragging process as soil bearing capacity of dominant soils was adequate even in the vicinity of floodplains (Hazell, 2011). The known technology of the Olmec indicated their willingness and capacity to construct causeways to overcome problems associated with the floodplains (Cyphers, 1997).

MEGALITHIC TRANSPORT BY LAND

While slope analyses formed an important part of the investigation, identifying viable land routes had to include the avoidance of wide or fast flowing rivers, flood plains and swamps. Gradient is a major constraint when hauling megaliths uphill or while maintaining control during descents, as ethnographic records and replication experiments clearly describe (Dillon, 2004, Heyerdahl, 1958, Richards and Whitby, 1997). Arguably, significant

labour sources influence transport pathways, so the location and size of villages may have also contributed to route choice. Some routes *appear* possible but seasonal variations change their viability.

Floodplains, swamps and river positions could all change over millennia. Using GIS, allowed us to establish a viable database of terrain features that included signs of a feature's past position, as in the example of ox bow lakes or lagoons. So it is possible to interpret past landscape features and take these into account during the analysis process.

This investigation was a theoretical exercise using GIS technology as an analytical and management research tool. It was limited as later comments will highlight.

In modern times, hauling large stones over long distances would be a mechanised process. Therefore our expectations of what was possible, in terms of capability, time frames and commitment, could be vastly different from those of prehistoric societies. With a limited archaeological record, our database and GIS software, allows interpretative analyses and comparative testing of potential scenarios to provide testable outcomes on the question of land transport routes.

ESTABLISHING THE DATABASE

1:250000 and 1:50000 survey maps were sourced to establish the database comprising themes of contours, rivers, swamps, soil types and vegetation (Figure 1). This data was combined with historical observations and contemporary archaeological surveys of land features where possible. Nevertheless these sources would not portray or indicate prehistoric terrain conditions, while hydrology dynamics would change the position of swamps and oxbow lakes on the floodplains. Such positional changes could not be expected to materially affect analytical outcomes, as pathways would shift marginally within the same area to suit these changes.

The management advantages of GIS database are well known (Longley et al. 2001) but its application to the Olmec research should be explained. The regional nature of the stone transport in Mesoamerica posed particular elements for which GIS tools were well suited. Nevertheless considerable scanning of hard copy maps and data processing was needed to form a comprehensive geo-database. In the early stages of this process it was evident that the resolution would determine interpretation quality required to generate a usable terrain model. This necessity became a compromise between

practicalities of managing file sizes and the need for reasonably accurate data. Larger files allowed clear image processing, however file handling was limited by available hardware (Figure 2).

Our study began by developing a geographical surface model of the region using ArcView 3.2 software and its accompanying 3-D Analyst tool (Figure 3). This model allowed us to geo-spatially analyse slopes in an extensive landscape and identify potential transport corridors without the need for extensive individual pathway calculations. The surface model was developed using current topographical maps of the area. Without ground-truthing, our interpretation and digitising is subject to the tolerances and accuracy of the source survey maps. Error when using a Digital Elevation Model (DEM) and the associated slope tools in the GIS was expected during this assemblage process (Hageman and Bennett, 2000). The digitising process itself was understood to be another potential source for errors, which arise from interpretation. This was a problem that was noted by others as are strategies to minimize the problem (Bolstad, et al., 1990, Morad, et al., 1996).
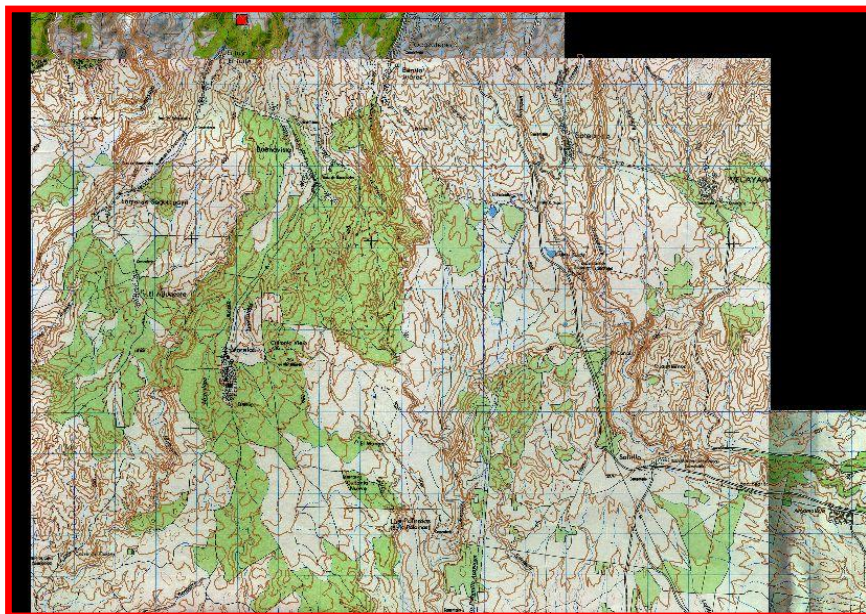
Figure 1. Preliminary digitising using INEGI survey map 1:50000 (L. C. Hazell).
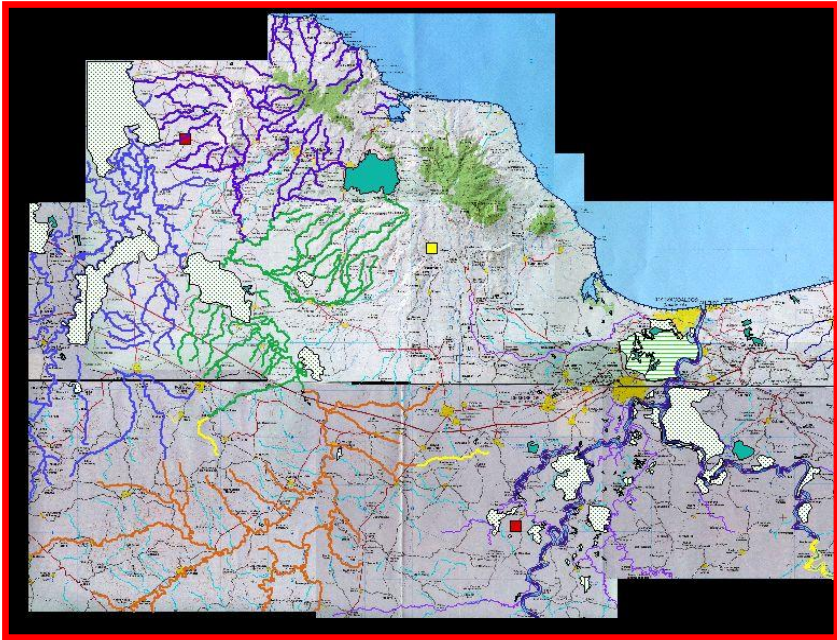
Figure 2. GIS matrixof the region after INEGI survey map 1:250000 (L.C. Hazell).
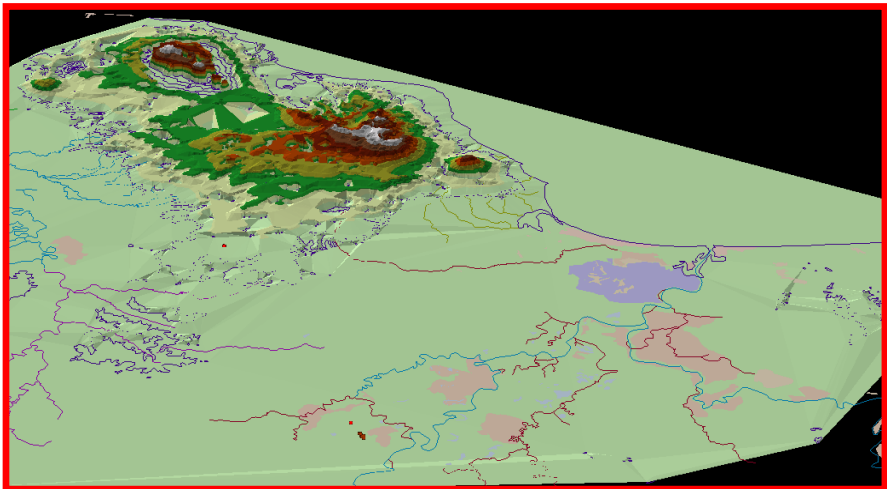
Figure 3. 3D terrain scene using ARC10 Scene (L.C. Hazell).

In the background the Tuxtla Mountains can be seen whilethe San Lorenzo Plateau is in the centre foreground.

The initial digitising procedure was undertaken using a HP 5100c flatbed scanner with a default scan speed for high quality scans. Resolution was set at a 150 dots per inch (DPI). Even with the larger scale of the survey maps, each map required at least four and sometimes six A4 scanned sheets that needed to be geo-located and joined in the GIS software. This also became a potential source of accumulative errors.

In an attempt to overcome these potential errors, digital photography was used on the original survey maps. The camera used in this process was a Digital SLR Nikon D1X with a 28-70mm 2.8 lens. The picture quality setting for this process was the RAW format with a resolution of 300dpi. The photographs were taken outside in a shaded area with natural light and a distance of 1 to 1.5m between the map and the camera. Generally, shutter speed was 100th of a second, but the aperture was varied between f18 and f11 with a focal length between 42 and 31 mm, which when translated into 35 mm film equivalents, was between 63 mm and 46 mm. The advantage of speed and efficiency that was anticipated by this procedure was negated by a lack of map clarity and consequent limitations on interpretation of the final photographic images. This was in spite of enhancement using Adobe Photoshop 7 filters and image adjustments to the image sharpness, brightness and contrast.

With these disappointing results we returned to the initial process of joining A4 scanned images, see also (Hazell and Brodie, 2012).

To keep within a practical research time frame we adopted a multi-layered approach by capturing thematic layers from scanned 1:250,000 survey maps. In later analysis, maps with a scale of 1:50,000 were used to provide greater detail in specific areas of interest. All maps were scanned and enhanced using Adobe Photoshop 7 to improve legibility and associated accuracy during final digitisation. Nevertheless our interpretation of specific features such as contour position and value imposed limitations on final accuracy. Points on contour lines were inserted at changes in direction and intermediate points were included as frequently as possible to minimize error (Douglas and Peucker, 1973). The individual maps were joined into a matrix, as shown in Figure 3, from which an initial analysis could be undertaken. The contour data was then used to create a surface model of the landscape as a Triangular Irregular Network (TIN) that was formed from our digitised contour data (Figure 4).
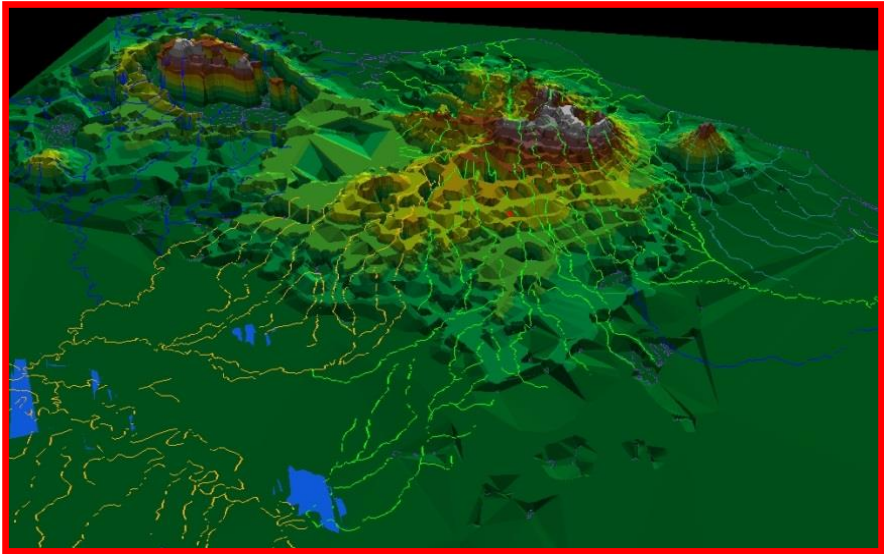
Figure 4. 3D scene of same area using Arcview 3.2 (L.C. Hazell).

In the background errors noted in the text due to contour crossovers in digitising can be seen. These did not affect analyses.

The slope gradient and 3D model tools produced analyses and representations with visible errors formed through contour crossing or incorrect digitising. This occurred with the earlier version of Arcview 3.2; however, when digitising contours using ARCMap 10, it was necessary to zoom in or deactivate the Snapping tool to avoid crossing contours or incorrect joining of different elevation contours. The same technique applies when editing vertices. This problem occurred only when contours were close to together.

In spite of this problem, only a small percentage of the final map area was affected and usually these contour crossings only occurred when contours were very close together indicating a steep gradient. This would automatically exclude these parts of the resulting terrain surface from consideration as a transport route because of the excessive gradients involved. Attempting to control a twenty tonne stone on steep downward slopes would have been impractical as replication and historical observation illustrated (Dillon, 2004, Heyerdahl, 1958, Richards and Whitby, 1997). In any case the analyses identified safer, more practical options that were nearby (Figure 5).
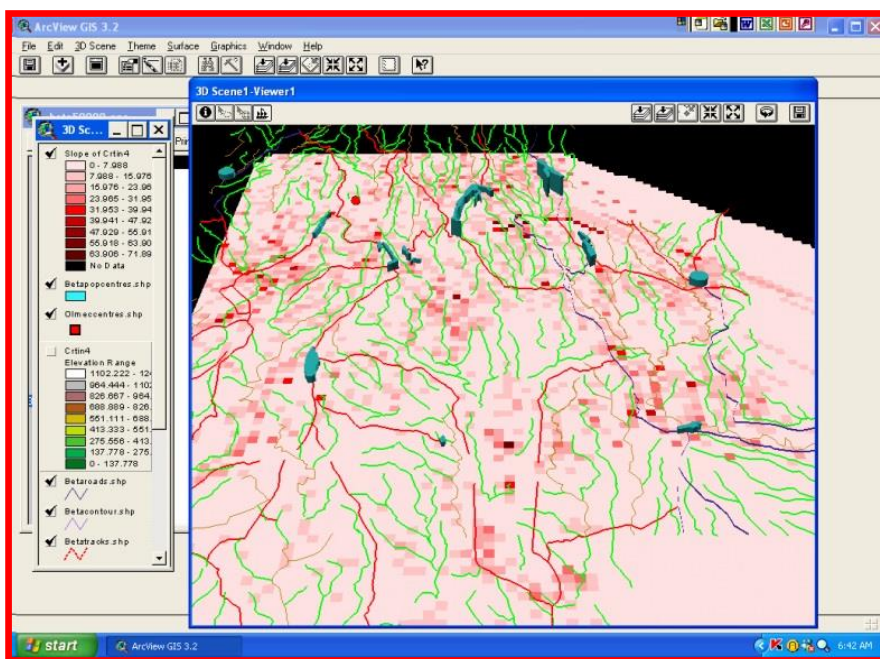
Figure 5. Detail of Slope Gradient analysis using Arcview 3.2 (L.C. Hazell).

The darker pixels indicated the steeper gradients and generally these are gradients which modern roads or tracks follow.

The analysis could have been undertaken empirically by simply reading the contours on the map or trace likely routes that showed minimal grades and then marking these on photocopied survey maps. But this would have necessitated either assessing contour spacing visually or measuring and calculating the grade along a multitude of potential pathways. The study area exhibits complex landforms, reflecting their volcanic origins. Using the slope gradient tool in ArcView ensured consistent analyses. This is particularly valuable when working with large areas and small-scale maps. Slope is defined by pixel size. Adobe Photoshop pixel counts and grid value tools determined the ground area that each pixel represented on our maps. Therefore a linear distance of: ±40 m on 1:250000 scale maps; ±16 m at 1:50000 and ±4 m for 1:16000 per pixel applied in our maps.

To manually sample slope grades at these scales would require analysis of each change of contour value across a potential pathway. The total fall from the source to the floodplain is some 400m in vertical height with contour

intervals between 10 m and 20 m. Analysis of this area and gradient range would require between 50 and 260 individual measurements for each potential path even if this was confined to a width of only 500 metres. Therefore, the slope gradient tool is more efficient in research hours and provides acceptable accuracy for route options that can be used with other data such as soil types, vegetation and hydrology to corroborate likely pathways (Figure 6).
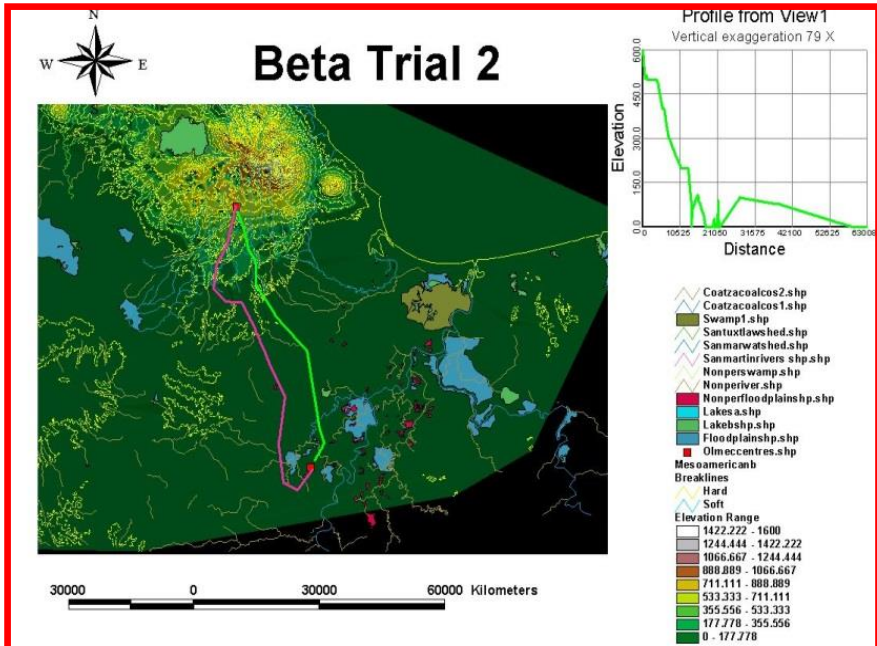
Figure 6. Route corridor options using Arcview 3.2 (L.C. Hazell).

LIMITATIONS ASSOCIATED WITH GIS APPLICATION TO THIS RESEARCH

A major limitation in this study was the process of data acquisition. Digitising such extensive landscapes is always a challenging undertaking. Without access to large scale remote sensing technologies, this study relied on the digitisation and interpretation of topographical land survey maps. Errors in interpretation of contour lines do occur and may have influenced the gradient analysis; however the points of shallowest gradient in the landscape correspond to those parts of the digitised map which are easiest to interpret

accurately. Additionally, correlation between the route corridors identified by this method, show similar pathways to modern roads in the general area. Therefore the choice of potential transport paths, based on gradient analyses has validity. The benefits of GIS slope gradient and thematic database analyses are emphasised when linked to other research methodologies including: soil bearing capacity; friction coefficient studies; and other technology such as High Resolution Satellite image analysis. However we also noted some limitations while using GIS with this research:

- Care must be taken when using data from ARCView3.2 files and its coordinate systems with in ArcScene 10. The need to ground truth data is highlighted by this problem.
- ArcView 3.2 Slope gradient tool outcomes were easier to interpret than those derived from ArcView 10.

CONCLUSION

The pathways identified in these analyses are not final solutions to the megalith transport problem; however a research project of this type and scale required a manageable protocol from which further research, including field surveys, could be established. The purpose of this paper was to highlight the value and options of using GIS software for doing this. We have noted some limitations in its use but we have also demonstrated how this technology contributed to this research. It is proposed further studies of Olmec land transport be undertaken on the basis of this work. Research is also proposed that will include megalith transport in Neolithic Britain, to retrieve the Bluestones used in Stonehenge and standing stones on the Orkney Islands. Utilising other GIS attributes, research will be extended to human energetic aspects of megalith use. This focus will include constructing various funerary enclosures at Nan Modal on Pohnpei and Palauan terraces in the Oceania region.

ACKNOWLEDGMENTS

REFERENCES

ArchaeoNews. (2004). Megalithic tradition is preserved in Indonesia, *Stone Pages*, 5th June 2004 ed.

Bolstad, P. V., Gessler, P. & Lillesand, T. M. (1990). Positional uncertainty in digitized map data, *International Journal of Geographical Information Systems*, *4*, 399-412.

Clewlow, C. W., Cowan, R. A., O' Connell, J. F. & Benemann, C. (1967). Colossal Heads of the Olmec Culture, Department of Anthropology, University of California, Berkeley.

Cyphers, A. (1997). Olmec Architecture at San Lorenzo, in: Stark, B.L., Arnold 111, P.J. (Eds.), Olmec to Aztec, University of Arizona Press, Tucson, 96 - 114.

Cyphers, A. (2006). Re: Olmec stone transport, in: leshazell@cnl.com.au (Ed.), Melbourne Australia.

Dillon, P. (2004). Indonesia : *Megalithic Arts Struggle on*.

Douglas, D. H. & Peucker, T. K. (1973). Algorithms for the reduction of the number of points required to represent a digitized line or its caricature, *The Canadian Cartographer*, *10*, 112-122.

Hageman, J. B. & Bennett, D. A. (2000). Construction of Digital Elevation Models for Archaeological Applications, in: Westcott, K.L., Brandon, J.R. (Eds.), *Practical Applications of GIS for Archaeologists*, Taylor & Francis, London UK, 113-127.

Harmon, D. b. P. (2005). Qala Yampu project: *Tiwanaku Experimental Archaeology*.

Hazell, L. C. (2013). An Analysis of Log Raft Open Water Performance and Crew Capability to move Megaliths Pre-classic Olmec used for Colossal Head Sculptures, *Journal of Maritime Archaeology*, *8*.

Hazell, L.C., Brodie, G., (2012). Applying GIS tools to define prehistoric megalith transport route corridors:Olmec megalith transport routes: a case study, *Journal of Archaeological Science*, 1-5.

Hazell, L. C. (2011). An Investigation of Olmec water and land megalith transport methods and route options, School of Historical and European

Studies: Archaeology, La Trobe University, Bundoora, Vic. Australia, p. 319.

Heyerdahl, T. (1958). Aku-Aku, George Allen & Unwin Ltd., London, England.

Mladjov, R. V. & Mladjov, I. R. (1999). *This Side up, Discovering Archaeology*, 90-93.

Morad, M., Chalmers, A. I. & O'Regan, P. R. (1996). The role of root-mean-square error in the geo-transformation of images in GIS, *International Journal of Geographical Information Systems*, *10*, 347-353.

Porter, J. B. (1989). Olmec colossal heads as recarved thrones, *Res*, *17*, 22-29.

Richards, J. & Whitby, M. (1997). The Engineering of Stonehenge, in: Cunliffe, B.R., C. (eds.) (Ed.), *Science and Stonehenge*, Oxford University Press, Oxford.

Royal Engineers. (1960). Royal Engineers Supplementary Pocket Book No. 5A, War Office, London.

Royal Engineers. (1952). Royal Engineers Supplementary Pocket Book No. 5D, The War Office

Van Tilburg, J. A. (1995). Moving the Moai: Transporting the Megaliths of Easter Island, *Archaeology*, *47*, 34-43.

Williams, H. & Heizer, R. F. (1965). Sources of Stones used in Prehistoric Mesoamerican Sites, University of California Archaeological Research Facility.

Chapter 7

GEOINFORMATION SYSTEMS FOR STUDYING SEISMICITY AND IMPACT CRATERING USING REMOTE SENSING DATA

A. V. Mikheeva[1], An. G. Marchuk[2] and P. G. Dyadkov[3]

[1]ICM&MG SB RAS; IPGG SB RAS; HCI NSU.
[2]ICM&MG SB RAS; NSU
[3]IPGG SB RAS; NSU

ICM&MG SB RAS - Institute of Computational Mathematics and
Mathematical Geophysics SB RAS;
IPGG SB RAS - Trofimuk Institute of Petroleum Geology and Geophysics
SB RAS;
SB RAS - Siberian Branch RAS of the Russian Academy of Sciences
HCI NSU - Higher College of information theory NSU;
NSU – Novosibirsk State University, Russia

ABSTRACT

This chapter presents a tool for studying natural disasters, such as
seismic and impact events, using real data from Catalogs of earthquakes
(EC) and Earth's impact structures (EISC) [1]. It is ENDDB [2] (the

Earth's Natural Disasters DataBase), a new version of a geoinformation system (GIS). The algorithms implemented in ENDDB allow visualizing a selected part of a current catalog in a pseudo-3D background map. With its mathematical support, the ENDDB system can plot frequency dependences of magnitudes or sizes (crater diameters) of events from various samples, as well as other distributions of integrated parameters in time and space, or their relationships with one another.

The expert earthquake database (EEDB). There existed an earlier GIS version, an EEDB system [3], which had a wide range of seismological applications. It was gradual transition from a conventional GIS (originally created by the authors) to a high-tech expert system updated by including successively various mathematical methods for earthquake data processing, new parameters of seismic regime, and advanced representation tools. The realized algorithms [4] allow the user to compute and visualize maps and diagrams of seismicity parameters (slope of magnitude-recurrence curves, seismic quiescence, earthquake density, etc.), to reveal clustering of events, and remove aftershocks. Modifications and versions of GIS-EEDB for different geodynamic regions [5] are illustrated in the chapter with case studies of seismic anomalies.

Visualization and analysis of EISC data. Applying the EEDB system software to EISC data [1] (in the new GIS system, called Earth's Impact Structures Catalog (EISC) [6]) allows gaining insights into spatial patterns of impact structures. In addition, the shapes of craters are constrained using a shaded relief model based on NASA data arrays of SRTM (Shuttle Radar Topography Mission) and ASTER GDEM (Global Digital Elevation Model), and the technology of digital mapping. Thus typical elements of impact craters morphology have been systematized and can be used as indicators of the crater origin [7].

Gravity data and new applications of GIS ENDDB. The reliability of geomorphically expressed diagnostic indicators of crater shapes was checked against geophysical features revealed by gravity data, namely, the presence of tail-shaped negative gravity anomalies produced by large impact craters. By mapping gravity anomalies, using our shaded relief model and "Global marine gravity" data (V18.1), we can verify the gravity patterns associated with impact cratering and check their validity as tracers of bolid trajectories. Gravity data also have seismological implications and can be used to identify seismic blocks, lineaments, and other structures detectable with GIS ENDDB mathematical tools and thus to analyze the spatial patterns of seismicity.

INTRODUCTION

An. G. Marchuk

In the late 1980-s, a custom system with GISelements for simulating tsunami waves was designed at the Institute of Computational Mathematics and Mathematical Geophysics (formerly the Computing Center) in Novosibirsk. The system allowed setting an elliptic model source of the tsunami and then calculating the arrival times of tsunami waves at all grid nodes of the modeling domain using two built-in programs, as well as estimating the height and velocity wave components in subregions selected from a large offshore and coastal area. The digital geographic map had a complex structure, with the coastline and sea depth contours presented in a vector format and the land topography and bathymetry displayed by different colors on the computer screen. The system was first demonstrated in 1989 during the International Tsunami Symposium [8]; its description was reported at the All-Union Tsunami Workshop in 1990 [9] and at the XX IUGG General Assembly in 1991 [10], and in *Computing Technologies* [11]. Concurrently, a lot of work was initiated by A. Mikheeva in 1990 to develop an independent GIS for visualizing the Earthquake and Tsunami Database on a map and to collect information for the Database [12].

In 1994 the systems were combined into an expert system (Expert Tsunami Database, ETDB) for visualizing earthquake and tsunami catalogs with the possibility of modeling different scenarios of tsunami generation and propagation from model sources [13]. A modification of ETDB [14] was recommended as a prototype for regional Tsunami Databases at the Fifteenth Session of the International Coordination Group of UNESCO for the Tsunami Warning System in the Pacific [15]. At the same time, Anna Mikheeva and Petr Dyadkov began to develop a parallel version of an expert system (Figure 1) for seismicity studies in the Baikal region (Expert Earthquake Database, EEDB), at the Trofimuk Institute of Petroleum Geology and Geophysics (Novosibirsk). It was gradual transition from a usual GIS and DB to a high-tech expert system updated by including successively various mathematical methods for earthquake data processing, new seismicity parameters, and advanced representation tools.

The term "expert" in the name of these systems reflects one of its basic features: providing the user with necessary information and advanced techniques for specific research tasks.

Later subprograms were designed for seismic and tsunami data processing in various samples from databases in ETDB, in addition to updated Digital Mapping [16]. Visualization of digital mapping was implemented in several projections (geographical, orthographical, etc.). The system required geographical and geophysical data, which either were unavailable to the developers or did not exist in the digital format. To provide the system tools with such data, an interactive system was developed for digitizing bathymetric and other paper maps [17-18]. Specifically, the same approach was used to create vector data of seismogenic faults in some areas of the Russian Far East and a new detailed bathymetry grid for areas around the Kamchatka Peninsula and the Kuriles [19-20].

The following versions of geographic information systems created using the above achievements of the authors appeared in the 2000s and covered new subject areas of geology and geophysics. The ETDB, EEDB, and ENDDB systems all share the same structure and represent a set of interacting software units: a relevant database subsystem (tsunami, earthquake, or impact structure databases), a geographic subsystem, and a subsystem for data analysis, joined in the user interface part. The first unit in the prototype systems we developed before ENDDB and applied to tsunami research [14, 21, 22] contained an earthquake and tsunami database, while in its latest modification ENDDB was a database of earthquakes and impact structures.

The **user interface part** of the systems have changed significantly, from graphical shell functioning in the MS-DOS environment (Figure 1), with *Turbo-Pascal* tools, limited by the resolution of the EGA and VGA graphic adapters, to the up-to-date *Windows* standards of menus and dialogs (Figure 2), produced by means of the MFC-library. The environment formed by this library defines the skeleton of the application to be developed and provides the developer with standard tools of creating a multi-window interface. The first prototype (WinETDB-project) of the Windows-95 user interface was created by Denis Ivaykin, Alexander Lyskovskiy, and Ekaterina Chernykh, students of the Higher College for Information Theory at Novosibirsk University, who also converted the geographical subsystem into the Visual C++ codes [22, 23].

Recently A. Mikheeva has adapted the development environment and all subsystems of ENDDB to a 64-bit platform, and made a new version of the package for *Windows* 7 and 8. The same work was carried out for the environment of supported applications designed specially to complement the resources of ENDDB. The codes of the main program and its supported applications were translated to the standards of the latest *Visual Studio* and *Firefox* versions. One such application, a new converter of seismological

formats for 64-bit computing has been written with assistance of Magomedrasul Magomed-Kasumov, engineer of the Dagestan Branch of RAS Geophysical Surveys.

This chapter gives a review of a tool for studying natural disasters, such as earthquakes and impact events, using real data from catalogs of earthquakes (EC) and Earth's impact structures (EISC) [1]. It is a new version of a geoinformation system (GIS), the ENDDB (the Earth's Natural Disasters DataBase [2]), which combines two earlier systems: GIS EEDB [3, 24] and EISC [6]. These two prototypes are described in more detail in Parts 2 and 3 of the chapter. The methods implemented in ENDDB allow visualizing selected parts of a current catalog on a pseudo-3D background map. With its mathematical support, the ENDDB system can plot frequency dependences of magnitudes or sizes (crater diameters) of events from various samples, as well as other distributions of integrated parameters in time and space, or their relationships with one another.
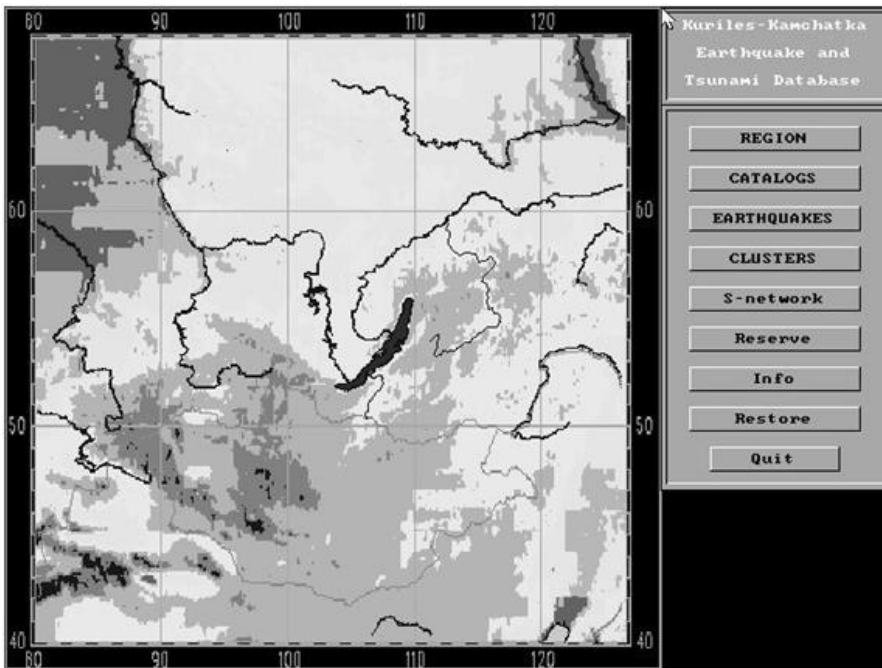
Figure 1. The main window of the EEDB, DOS platform.
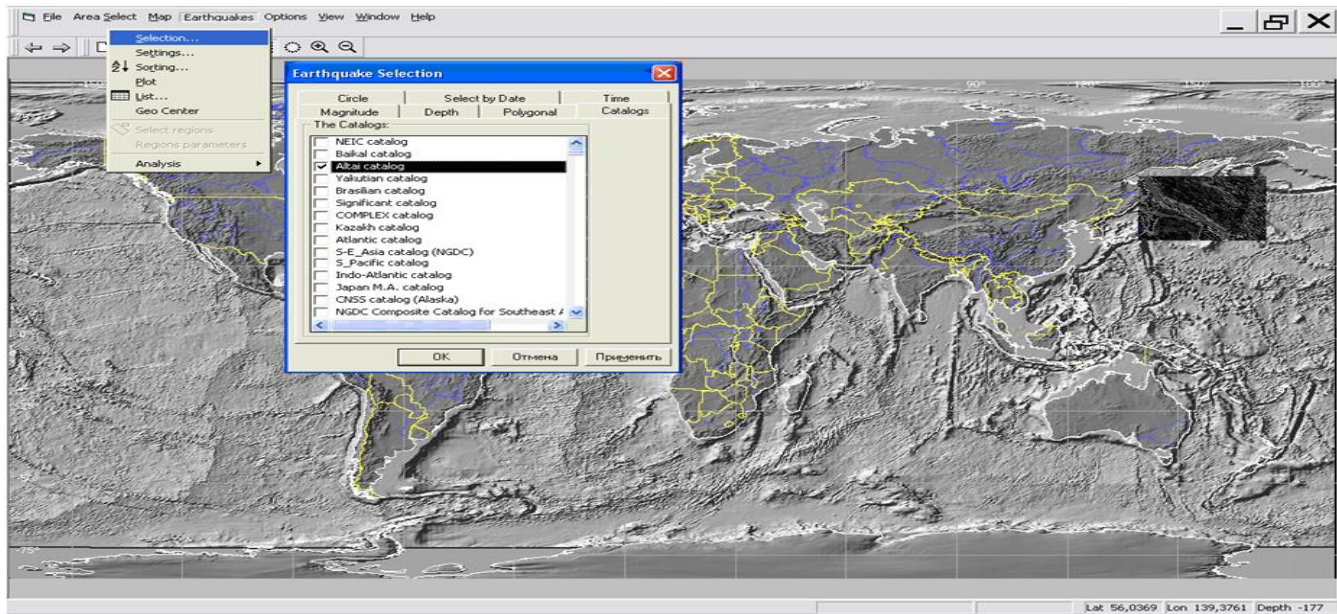
Figure 2. The main window of ENDDB, Win 64 platform. The original World map for the primary region choice. The option of the earthquake catalog listing is open.
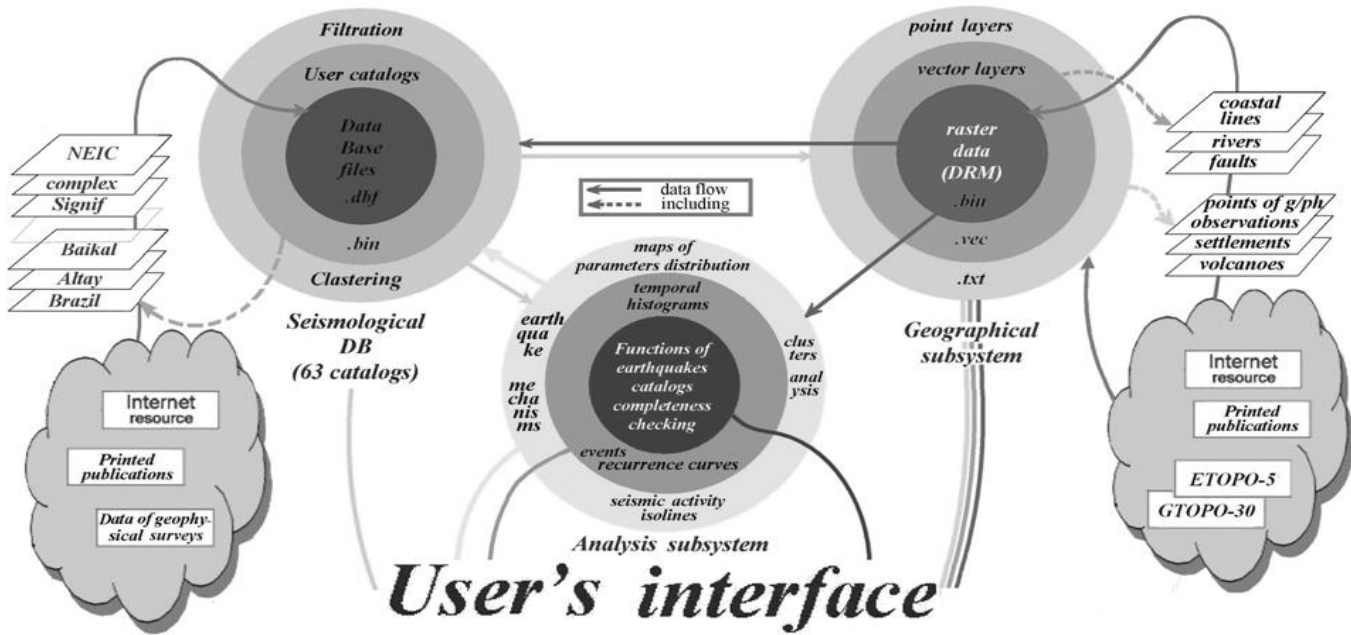
Figure 3. The flow chart of the GIS-EEDB software.
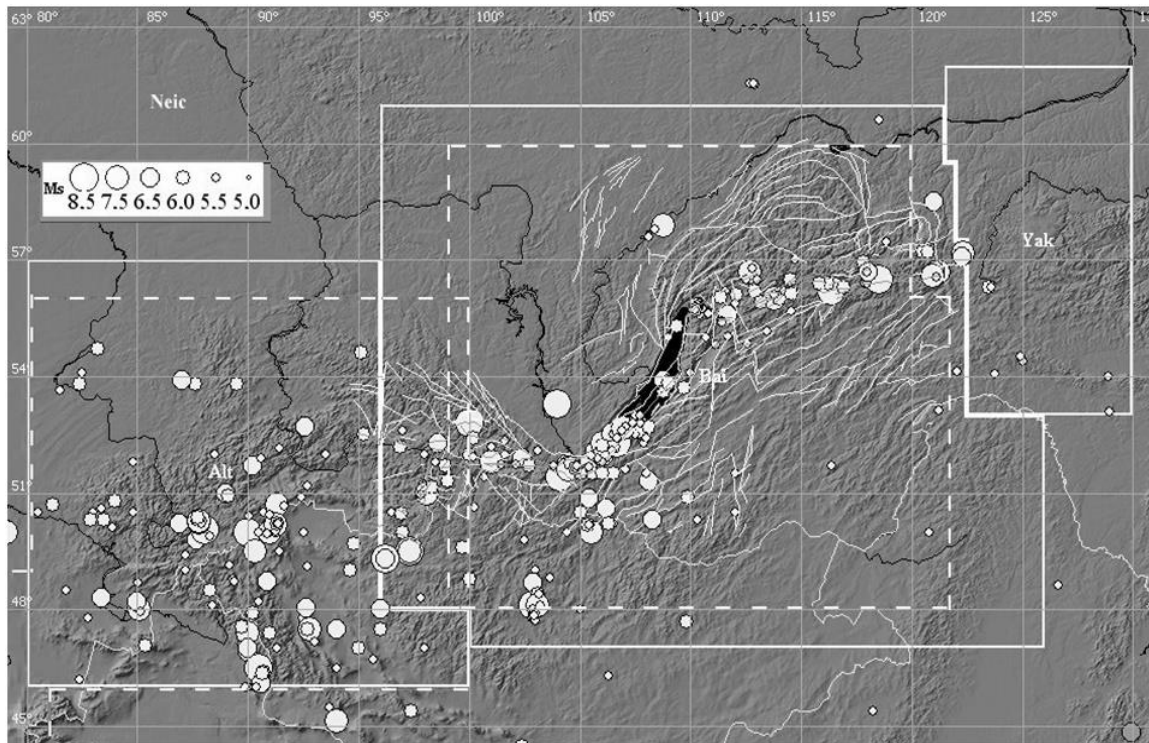
Figure 4. Regional zoning according to the completeness of earthquake catalogs. Geographical layers on the elevation map: earthquakes (Ms ≥ 5), country boundaries, rivers, and different fracture zones. Dashed line shows the GS RAS region boundaries according to [25, 26].

The **geographic subsystem** of ENDDB, which is an extension of the previous geographic shell [22], comprises the following components:

- primary geographic data;
- set of algorithms and processing software modules;
- map visualization software;
- tools for forming and implementing spatial queries.

Methods of digital mapping and GIS technology have made it possible to create a system for selecting and visualizing geophysical data on a cartographic base, which serves as a tablet (in our case, in the rectangular projection for plotting data of catalogs and other related data). Description of the methods is given below (Part 1).

The main problem in cartographic modeling of the Earth's surface topography is to choose the simplest and most appropriate way of populating the Geographic Database. Mapping in our system is performed using a grid digital elevation model. The initial region choice is made from an overview World map stored in the memory, in a rectangular projection. Once the elevation map, the shoreline contours, and the default geographic layers appear in the window, the region can be selected using the inverse frame (Figure 2).

Currently, the total volume of the auto-generated and author's program code (2/3 created by Anna Mikheeva) of GIS-ENDDB is about 23 MB and consists of ~ 240 classes.

The program product GIS-ENDDB can be installed on any computer from the original media based on Win32 and 64-bit platforms (including Windows 95, 98, 2000, 2003, 2007, 2010 NT/XP, and Windows 7 & 8) and requires approximately 4 GB of memory on a hard disk.

PART 1. THE EXPERT EARTHQUAKE DATABASE (EEDB)

P. G. Dyadkov, A. V. Mikheeva and An. G. Marchuk

The EEDB interactive computing system [3] was developed by the authors for seismic and geodynamic applications and can be considered as an automated workstation for users engaged in seismic and geodynamic research of different geographic areas on different scales. The EEDB flow chart [24]

(Figure 3) represents a set of interacting program units: a seismological database, a geographical subsystem, and a subsystem for data analysis.

The seismological DB lying at the base of the system contains 63 catalogs of historical and instrumental earthquakes, among which both the catalogs from known agencies and geophysical surveys, and the authors' own catalogs representing incorporated and filtered data collected from various sources. The reasons for using several catalogs are as follows. First, this allows dealing with both global- and local-scale (world and regional catalogs, respectively) earthquake data. Second, by comparing different geographically overlapping catalogs in terms of completeness, with the use of the EEDB methods (earthquake frequency histograms and plotted time series of magnitudes), one can divide the map into zones ("*regions*") and select the respective preferable catalogs (Figure 4).

We most often use global catalogs (e.g., NEIC, 1973 to present, and SIGN, -2000 to 1993, of the American Geophysical Survey, USGS) and regional catalogs, such as the Baikal catalog (BAIK in sequel, in which 87% of data belong to the Baikal Branch of Geophysical Survey (GS) SB RAS, available at http://www.seis-bykl.ru) and the Altai catalog (Altay-Sayan Branch of GS SB RAS). The overlapping boundaries of catalog completenesses we revealed for the case of the BAIK catalog are even wider than those indicated by the authors of the GS catalogs (Figure 4) [25, 26].

Year	Month	Day	Hour	Min	Sec	Latitude	Longitude	Depth	Ms	Kl	Book	Length
1964	10	17	20	50	12,0	52,28	106,50	0	4,5	11,5	11	4,85
1964	12	11	7	30	41,0	52,37	106,30	0	4,5	12,0	11	4,85
1965	5	6	2	33	10,0	52,55	107,00	0	3,9	11,0	11	2,61
1965	5	29	15	42	59,0	54,72	109,28	0	4,0	11,0	11	2,92
1965	6	23	15	1	22,0	53,38	107,82	0	3,9	11,0	11	2,61
1965	7	17	15	6	58,0	51,07	109,73	0	3,9	11,0	11	2,61
1965	7	17	19	37	22,0	53,32	108,38	0	3,9	11,0	11	2,61
1965	8	25	11	45	11,0	51,81	105,15	0	3,9	11,0	11	2,61
1965	11	14	15	47	43,0	52,73	106,61	0	4,0	11,0	11	2,92
1966	1	22	5	37	44,0	55,27	109,77	0	3,6	10,5	11	1,97
1966	4	3	6	13	39,0	54,00	108,62	0	4,0	12,0	11	2,92
1966	7	24	4	22	39,0	53,59	109,01	0	3,6	10,5	11	1,97
1966	8	30	6	10	31,0	51,76	104,61	20	5,5	14,0	11	13,35
1966	9	25	18	14	46,0	54,00	108,81	0	3,6	10,5	11	1,97
1966	10	31	15	40	45,0	52,66	107,21	0	4,0	11,0	11	2,92
1966	11	21	14	25	59,0	51,64	104,47	0	3,6	10,5	11	1,97
1966	11	27	20	16	4,0	52,85	107,03	0	3,9	11,0	8	2,61

Figure 5. Earthquake catalog format.

The format of the earthquakes contains fields with key source parameters: energy, magnitude, epicenter size (length), origin time, location (coordinates), and depth (Figure 5). The released seismic energy is the principal characteristic, which may be expressed either on the magnitude or on energy scales. Most catalogs worldwide (e.g., NEIC) use the magnitude scale based on body waves (*mb*) while Russian catalogs use the energy scale (e.g., that for

the Altai territory), with energy classes $K = lgE$ determined by T. Rautian's technique [27]. To bring all data to the universal scale, we convert energy classes to surface-wave magnitudes (Ms) using Richter's formula $K = 4.8+1.5 \cdot Ms$ (for the global catalogs) and its variants $K = 4.0+1.8 \cdot Ms$ for $K<14$ and $K=8+1.1 \cdot Ms$ for $K>=14$ (applied to regional catalogs, specifically, to events in West and East Siberia). Ms is recalculated from mb as $Ms = (mb - 2.4)/0.5556$, which is an empirical ratio, obtained from known magnitude pairs. The length of seismic rupture (L) is found as $lg\,L = aK + c$, where a and c are empirical constants [28].

The seismological unit also includes preprocessing of the initial catalog data to select a subset of earthquakes according to the inquiry parameters: choice of a current catalog, time range, space range, magnitudes, etc. Furthermore, the users can filter the selected earthquakes from aftershocks, with three independent algorithms. The first algorithm (tentatively named a *statistical* algorithm) is based on parameters responsible for the space-time difference between aftershocks and the main shock *(dT and dS)*, which have been obtained from the available aftershock statistics and depend on the main shock magnitude: $dT = (M_{s\ main} - 4) \cdot 162;\ dS = 3*L$.

The second (*elliptical*) algorithm (Figure 6), most frequently used to remove aftershocks, consists of several runs:

1) run 1: estimating the density of non-aftershock events (aftershocks are removed according to the statistically found parameters);
2) run 2: preliminary removal of aftershocks on a rectangular grid with the cell size proportional to the main shock magnitude;
3) plotting an aftershock ellipse isolating the aftershocks by the maximum-likelihood method or according to rms deviation from the sampling center.
4) subsequent runs: separating aftershocks level-by-level, in the elliptic metric.

At Steps 2 and 4, the time window (dT) of aftershock search increases proportionally to the ratio of the current number of aftershocks to the total number of events within rectangular or the elliptic areas [29].

Prozorov's method has been modified by A. Mikheeva as follows:

•   all located aftershock sequences are considered simultaneously in a single run,
•   the minimum size of the rectangular metric is set interactively,

- unlike the *classical* case (Figure 6 B, c) of calculating the elliptic metrics, it is suggested to create an ellipse of equal probability (Figure 6 B, a).

In the third method, called *interactive*, the space-time window values (*dS* and *dT)* are set up by the user. The results of the *elliptic* method are considered below in more detail (Figure 6).

In the *elliptical* method, which includes the described steps, the following parameters are set up: threshold signal/noise ratio $R_{s/n}$, minimum main shock magnitude, minimum aftershock magnitude, minimum size of the rectangular metric, etc. The *classical* way of finding the ellipse parameters [29] may be with or without weighting (Figures 6 B, *b* and *c*), which depends on the number of events that fall into the cell. Weighting makes sense if aftershock swarms are strongly scattered.

Experience has shown that, in some cases, our *modified* method of identifying aftershocks may be advantageous, in which ithe spatial pattern of aftershocks is constrained by an equal probability ellipse:

$$\varphi\,(x,y) = \frac{1}{1-\rho_{12}^2}\left(\frac{x2}{\sigma_1^2} - 2\rho_{12}^2\,\frac{xy}{\sigma_1\sigma_2} + \frac{y2}{\sigma_2^2}\right) = \text{const} = \lambda^2,$$

where $\lambda^2 \approx 2\cdot\left(1 - \frac{1}{9} + 3.29\cdot\frac{1}{3}\right)^3$ is approximation of the quintile distribution with two degrees of freedom at P = 0.9995; $\sigma_1^2 = DX$, $\sigma_2^2 = DY$ – are the variances of *x* and *y*, and ρ_{12} is the correlation coefficient between *x* and *y*. Thus estimated ellipse parameters for identifying aftershocks of the 09.16.2003 earthquake in the northern Baikal Rift Zone (BRZ) exceeded those obtained by the *classical* way in both number of selected events (263 and 246 respectively) and aftershock sequence length (3.9 and 1.6 times, respectively, - Figure 6 B, e). Another advantage of our *modified* method is that the results are almost independent of the $R_{s/n}$ threshold.

The *classical* and *modified* aftershock removal algorithms were compared in terms of efficiency by estimating the statistics of the resulting sets (Figure 6 B, f). The *classical* removal of aftershocks has shown significant deviation of the observed distribution from the theoretical Poissonian distribution [30] both before (Figure 6 B, f - 1), and after the procedure (Figure 6 B, f - 2), while the *modified* algorithm shows no deviation (Figure 6 B, f - 3).

The exponential Poisson distribution is given by:

$$f_T(\tau) = \lambda \exp(-\lambda\tau),$$

where $\tau = dT$ is the time between two subsequent earthquakes, λ is the flow rate of events in time, $\lambda = N/\tau_{av}$, where τ_{av} is the average recurrence time.

A

B
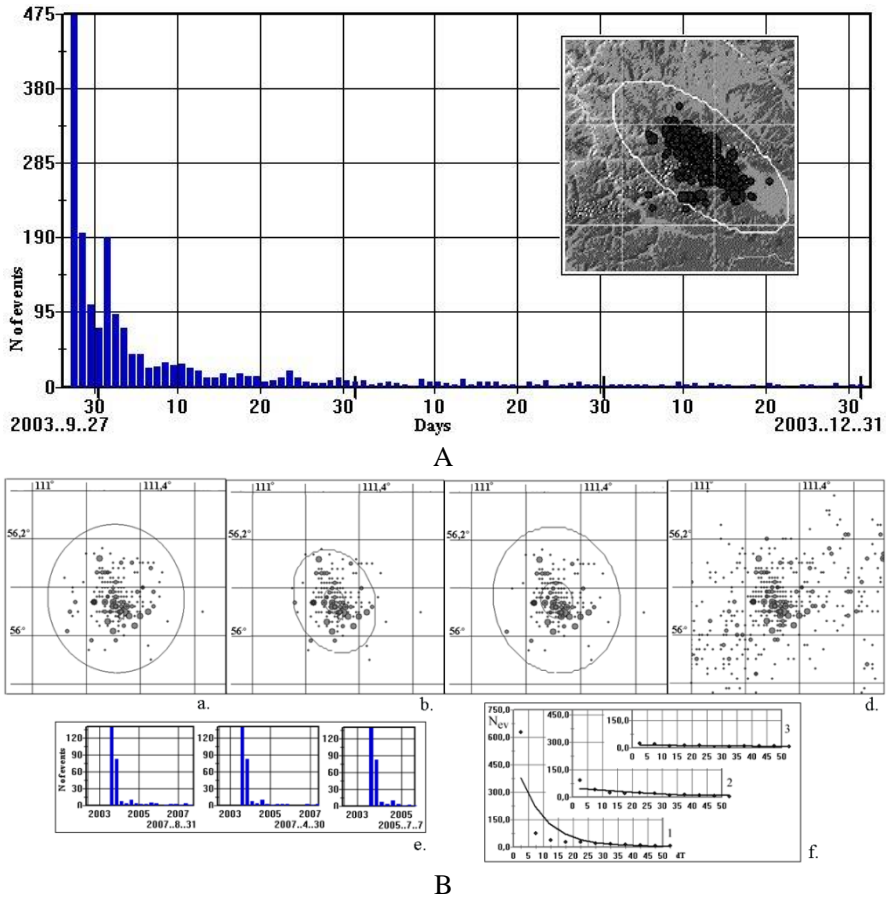
Figure 6. A – Histogram of the daily number of aftershocks of the 2003 Altai (Chuya) event. Shown on the right is a map view of the aftershocks. B – Options for calculating elliptic metrics to determine aftershocks, with an example of the $M = 5.8$ earthquake of 16.09.2003 in BRZ: a) confidence ellipse (equal probability), b) weight root-mean-square deviation [29], c) root-mean-square deviation, d) space distribution of events before removing aftershocks, e) time distribution of aftershocks identified by different ellipse metrics (a), (b) and (c), $R_{s/n} = 15$, f) deviation of the observed number of earthquakes ($M \geq 1.5$ since 1987) from theoretical Poisson's distribution before (1) and after (2, 3) removing aftershocks that followed the $M = 5.8$ event of 13.05.1989.

After the aftershock removal procedure, the sample contains many related events making up swarms. The swarms are removed in the same way as aftershocks, except for the magnitude relation between the main and subordinate events: in the case of swarms, the events following the one that triggered the swarm process may have any magnitude, either larger or smaller than the trigger event. Another point of difference is that the duration of the seismic process for swarm sequences is specified by the user interactively rather than being calculated (as in [29]) from the number of events as in the case of aftershocks, because the time distribution of events in a swarm is different from that in an aftershock sequences.

The geographic subsystem is an important part of any GIS, because proper visualization of geophysical data is a necessary prerequisite for correct interpretation. Methods of digital mapping and appropriate GIS-technologies allow developing a system for visualizing seismological data on the cartographic basis to meet the user's requirements for plotting earthquake catalogs, as well as the related information.

The GIS-EEDB subsystem of cartographical support uses *shaded-relief raster images* for creating digital geographic maps. The 3D-effect is provided by successive triangulations and by calculating the brightness of triangles.

First, the whole selected area is triangulated, with splitting each rectangular grid cell at least into two triangles (maximum 16 triangles). The number of triangles depends on the user-specified enlargement of the picture size relative to the original data array. The program computes the *brightness* of each *triangle* based on its orientation relative to the *light* source. In particular, if the original array and the created image are of the same size, the light plane is assumed to pass through the top left, top right and bottom left vertices of each cell. If the illumination direction is different, the cells are split in a different way as well. The parameters of illumination and the color scale are specified by the user, and various shades of brightness are then obtained therefrom.

The basic steps of the shading algorithm, designed by An. Marchuk, are as follows:

1) A surface is divided into a certain number of triangles calculated from the ratio of the desired picture size and the dimension of the array where the heights of all vertices with respect to a reference level are known for each triangle.
2) At each triangle, the vector product is found for vectors, parties to this triangle.

3) The resulting vector is normalized.
4) The brightness of the triangle is calculated according to the angle of the resulting normal vector to the light direction in the 3D scene. The light source is usually taken with parallel rays.
5) The computed brightness is used to obtain luminance gradation of the corresponding color determined by the above-sealevel elevation of the point and the user-specified color scale.
6) The 2D projection is drawn according to the parameters of the picture plane.

Similar algorithms known in the literature on 3D computer graphics are *Gouraud Rendering* (or *Gouraud shading*). To construct maps of different scales, from global to local maps, an appropriate data array with an optimum spatial resolution is automatically selected, with the quantity of triangular elements in each grid cell fitting the selected map scale [31]. Currently there are some global databanks representing the surface topography to different resolutions [32], such as the best known GTOPO-30 and SRTM-90 ones, with 30 and 3 arc-second resolutions, respectively. The GTOPO-30 and SRTM-90 databanks are open-file digital elevation models developed by the U.S. Geological Survey (USGS). The mapping program uses higher-resolution (90-m) SRTM-90 data at the local level, when zooming to specific areas of interest (in the territory of Russia). Then the vector and point layers, and explanatory texts, are superposed onto a raster image. The vector technology is applied to the level-by-level screen visualization of shorelines, rivers, national frontiers, fractures and faults of different geometries (thrust, reverse, strike-slip, normal, and oblique-slip faults). This technology aims at reducing the amount of saved data by storing the coordinates of linear objects as vectors. The thickness of lines in the image remains constant when objects are zoomed.

The point information is stored in simple text files and consists of such layers as geophysical observation points and locations of volcanoes and settlements, and can be easily populated with any other point data.

Full description of layers in the geographic database is given in Table 1. The system is open to adding vector, raster, and point digital geographic data, which can be converted into the system format.

Additional options developed for the geographical subsystem include:

a) different ways of visualizing (with or without animation) earthquakes in geographic maps and cross sections (Figure 8);

b) a mapping algorithm for creating a series of zonal maps at equal time intervals using linear interpolation of 2D Bessel function (1);
c) a program for seismic division for simultaneous analysis of several tectonic areas.

The mathematical method of linear interpolation (2D Bessel function) is:

$$Z(x, y) = ¼ (z_{00} + z_{10} + z_{01} + z_{11}) + ½ (u -½) (z_{10} - z_{00} + z_{11} - z_{01}) + \\ + ½ (v -½) (z_{01} - z_{00} + z_{11} - z_{10}) + (u -½) (v -½) (z_{11} - z_{10} - z_{01} + z_{00}) + \dots$$

$$(1)$$

where $\Delta x = \Delta y = h$ is a fixed increment and:

$$\begin{cases} z (x_0 + j\Delta x, \; y_0 + k\Delta y) = z_{jk} \; (j,k = 0, \pm 1, \pm 2, \dots) \\ u = \dfrac{x - x_0}{\Delta x}, v = \dfrac{y - y_0}{\Delta y} \end{cases}$$

The visualization technology of the zonal maps, which uses the 2D Bessel linear interpolation by (1), includes three stages:

1) Dividing the area into elementary cells;
2) Calculating the sought parameter for each cell;
3) Mapping this parameter (by linear interpolation) for successive time intervals before a large event.

See Figure 9 for the mapped damage parameter K_{avg} as an illustration to this technology.

The data analysis subsystem includes methods and algorithms [4] for GIS analysis of earthquake catalogs based on our research and on published results by experts in seismicity and geodynamics.

The first layer contains procedures of checking the completeness and quality of catalogs using the time series of earthquake number and magnitudes ($N(t)$ and $Ms(t)$, respectively) [33]. The next layer provides visual analysis of seismic parameters and consists of a graphical and a cartographical sublayers (Figure 3). The graphical methods apply to plots, histograms, and diagrams, including petal and azimuthal diagrams. They are, for example, histograms of released seismic energy averaged over a selected time interval (*lg* $E_{avg}(t)$, *joules*), magnitude vs. frequency relationship (linear-regression empirical histograms of the number of events of certain magnitudes), slope of recurrence

curve vs. time *b(t)*, etc. The empirical regression line of the magnitude-frequency function is obtained using the maximum-likelihood and least squares methods. The *b*-values can be also estimated using Utsu's formula [34], without calculating the *N(M)* function, to a better accuracy than with the least squares.

Table 1. Structure, format and content of the GIS EEDB geographic database and the relevant geographic layers

Data format	Folder	Layer names	Information content
Raster data (files *.bin)	Raster	Relief	Digital elevation model
Vector data (files *.vec)	Vector	Coast	Data on coastlines
		Rivers	Global network of rivers and lakes
		River details	Detailed local networks of rivers and lakes
		Country	National frontiers
		Republics	Frontiers of autonomous republics
		Administrative units	Administrative division
		Roads	Roadway network
		Railways	Railway network
		Plates	Plate boundaries
		Tectonic Zones	Seismic lineaments
		Faults	Fault zones
		Thrust	Thrust faults
		Normal	Normal faults
		Oblique-slip	Oblique-slip faults
		Reverse	Reverse faults
		Reverse-oblique	Reverse-oblique-slip faults
		Cities	Cities and towns
Point data (files *.txt)	Point	Earthquakes	Earthquake epicenters
		Volcanoes	Locations of volcanoes
		TideNet	Tsunami observation points
		SeismNet	Seismic observation points
		Mag points	Tectonomagnetic observation points
		Regions	Vertics of regions covered by different catalogs
		Mech points	Earthquake focal mechanisms
Computable data		Grid	Geographical network
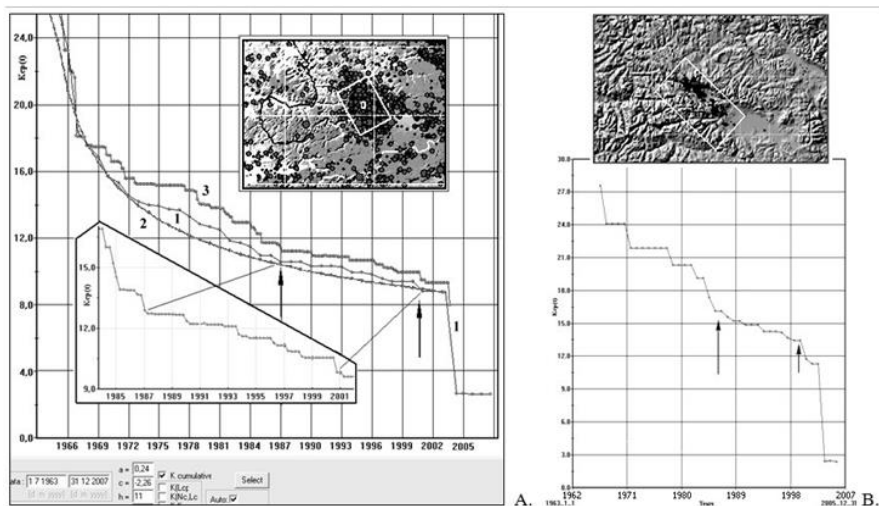
Figure 7. A – Time series of rupture density K_{avg} [35] for the Chuya earthquake area, $M_s \geq 2$: 1) real curve with $\Delta T = 1$ year, 2) theoretical curve of uniform fracture growth ($\Delta T = 1$ year), 3) real curve with $\Delta T = 1$ month shifted upward. Arrows show coincidence of curves 1 and 2. Box frames a fragment corresponding to the period between 1987 and 2000 when the real curve flattened out with $\Delta T = 3$ months. B – real curve of K_{avg} for the Chuya earthquake area, $M_s \geq 2.5$. The curves have become smoother since 1986 and fall abruptly since 2000.

The module for calculating the parameter of environment damage or seismic rupture density $K_{avg}(t)$ (Figure 7) was designed one of the latest among the graphic methods. The time series of this parameter provide an idea of seismic stability reflected in physical changes of the environment. The stability is understood as uniform increment of rupture length and number of earthquakes.

The cartographical methods imply contour line mapping, animation cartography (visualizing earthquakes as gradually fading flares spaced at time intervals proportional to real time) and constructing vertical cross sections and patterns of elevation and seismicity (Figure 8).

The built-in mapping subsystem unit can produce cartograms showing distribution of such seismicity parameters as total seismic energy, which is useful to highlight zones of quiescence preceding large earthquakes; distribution of the b parameter (slope of recurrence curve); maps of energy stability (K_{avg}) and its rms error σ; contour lines of seismic activity (A_{10}, A_{15}, where A is a long-term average number of earthquakes of certain energy: $K = 10, 15$) (as, for example, the K_{avg} map in Figure 9).
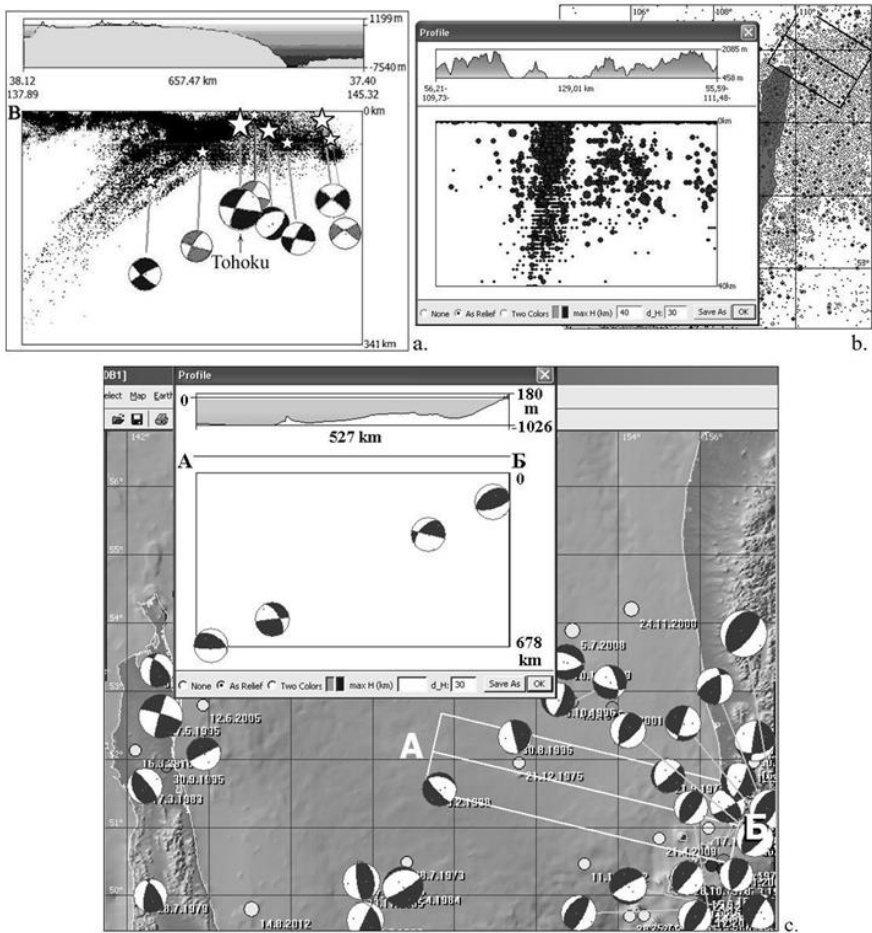
Figure 8. Vertical cross sections of topography and seismicity in Northeastern Japan, offshore area around the Tohoku earthquake (a), the North Baikal region (b), and area of the Pacific subduction zone (c).

Clustering of earthquakes (grouping according to their relations) is another method of spatial data analysis. The earthquake clusters are associated with natural localization of seismicity in zones of active faulting, e.g., along boundaries of plates or blocks. Clustering of earthquakes has implications for the pattern of seismicity, which then can be compared to locations of geological structures. To reveal earthquake clusters, the user has to specify the maximum space and time distance between events in all pairs (dT for time and dS for space) and the type (temporal or spatial) of clustering.
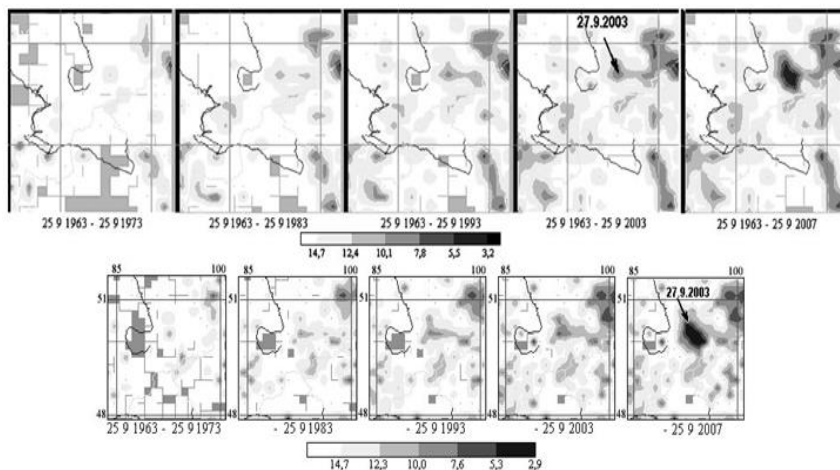
Figure 9. Spatial distribution of cumulative rupture density K_{avg} for Ms = 2.0-4.5 events in 1964 through 2007: Altai-Sayan area, lat. 46-52° N; long. 82-91.35° E (top panels), cell size 0.3×0.5º; area of Chuya earthquake of 27.09.2003 (bottom panel), cell size 0.2×0.3º. The maps present the data at every 10 years.

Cluster analysis programs allow plotting time series of the number of related events (with or without averaging), relationships of the number of events in clusters vs. total number of events, the conformity of the clustered events to the Poisson distribution $N(dt)$, etc., or constructing rose diagrams of cluster azimuths.

Detecting and analyzing clusters of related events shows the distribution of seismicity in space while comparing the seismicity patterns in different periods of time traces the history of the seismic process.

The EEDB system uses several methods to reveal earthquake clusters:

- introduction of space-time parameters dT and dS;
- Sobolev's method (calculating dT and dS automatically proceeding from the fractal space theory and physics of fracture) [36];
- estimating earthquake density using Morisita's index [37].

The clusters obtained by the first method are analyzed using jointly the geoinformation approach (methods of cartography) and elements of graphic analysis.

For example, changes in faulting activity can be detected from patterns of small shocks, in several steps:

1) Preliminary step: selecting a part of a catalog and filtering it from aftershocks and earthquake swarms (see above);

2) Main steps: detecting clusters using the relation parameters dT and dS. The values of the introduced parameters can be determined, for example, using dT or dS dependences of the number of earthquake pairs (two nearest successive events), and revealing intervals in which the number of pairs exceeds notably the exponential distribution (for dT) or earthquake number maxima (for dS) (Figure 10a);

3) Visualizing the azimuth patterns of segments that connect events nearest in time or space (clustered earthquake pairs). For the time analysis of the seismic process, the considered period is divided into intervals (years, months, etc.) to reveal clusters with anomalous orientations of the pairs. For example, the rose diagram for 1991 show the azimuths of clustered pairs in the Baikal rift to differ markedly from the usual pattern because 55% of the pairs have SE-NW directions unlike the N—S and SW—NE directions typical of the rift area (Figure 10b);

4) Checking whether the revealed clusters belong to aftershocks and swarms nearest in time, if they have similar primary azimuthal orientations (Figures 11a-c);

5) Checking whether the sample still contains overlooked aftershocks to make sure that the considered clusters are not the residuals of aftershock sequences (Figures 11d, 11e);

6) Zooming separate fragments of a territory in order to study the clusters of interest in more detail;

7) Additional quality checking of the cluster analysis results using a synthetic catalog created with real data points assigned to origin times the user specifies on random within a preset time range (an option realized in EEDB as well). The points in the synthetic catalog being invariable in space, the clusters hold their location but reduce considerably in number, which is implicit evidence for the validity of the previous interpretation made for the real data according to the mapping and plotting results.

Thus, clustering, along with other techniques, belongs to methods used to analyze spatial seismicity patterns and to reveal, stage by stage, real geological structures and processes. There are also programs for plotting diagrams of earthquake mechanisms, which have implications for crustal stress changes, and some other cartographical techniques (see below).
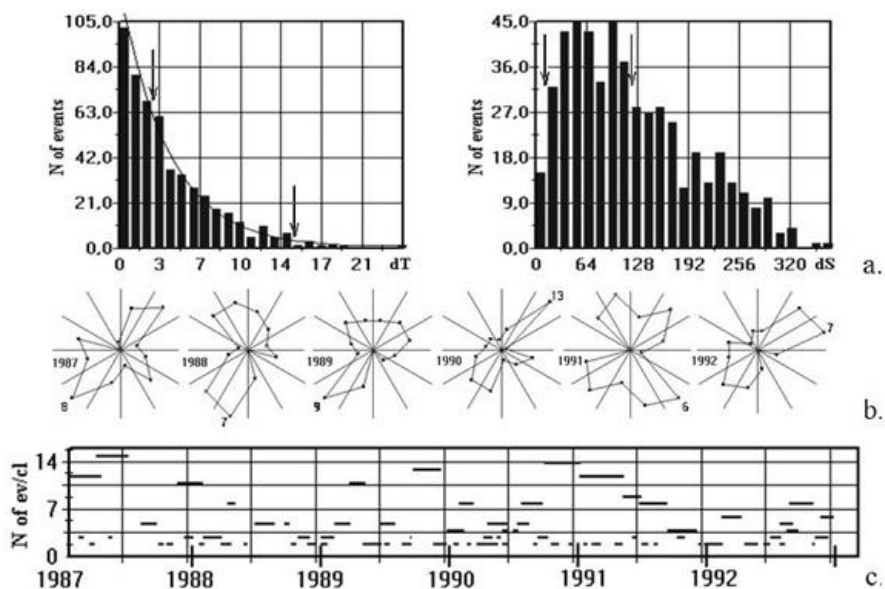
Figure 10. Cluster analysis of selected data from BAIK Catalog for 1987-1992: a) dT and dS dependences of the number of earthquake pairs, with marked intervals for further clustering; b) rose diagrams showing the space azimuth patterns of the clustered pairs (dT = 1-20, dS = 1-50). See prominent SE-NW orientations in 1991; c) the length of the revealed clusters and the number of earthquakes in them: the longest clusters of 1991 form a continuous sequence containing 12, 9, 8 and 4 event.
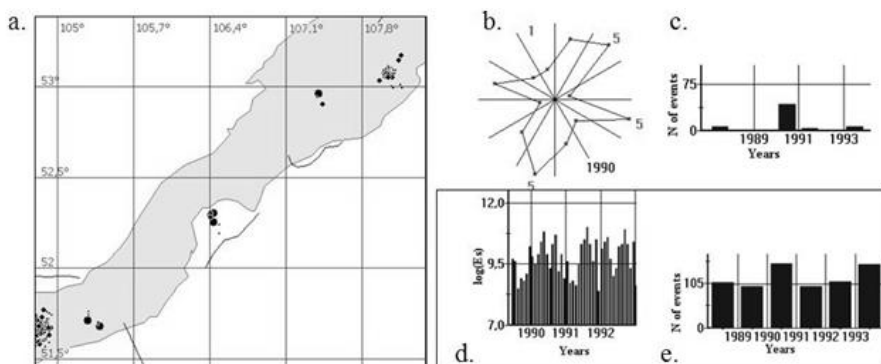
Figure 11. Aftershocks nearest in time: a) map of aftershock sequences and swarms detected by the program for 1987-1992; b) azimuths of aftershock pairs in 1990, when they markedly increased in number; c) number of events in aftershock sequences. Histograms describing the seismic process ($2 \le M \le 4$) in 1988-1992 after removal of aftershocks: d) total released energy per month and e) annual number of events.

The *b*-Value Method: Example Application of the Built-In Software for Data Analysis

Besides being a way to determine statistically significant magnitude range (the arrows in Figure 12 A, b), the magnitude-recurrence relationship $lg\ N = lg\ A_m - b\ (M_s - M_o)$ characterizes the seismic process, in terms of the seismic activity (A) normalized to a certain magnitude M_s (converted from the energy scale K) and the slope of the recurrence curve (b). Application of the algorithm for visualization of zonal maps can be illustrated with *b*-value cartograms.

Mapping *b* values may be problematic because the seismic process is irregular within elementary cells and, if there are few earthquakes in a cell, they may fail to represent the whole range of the magnitude-recurrence relationships used for estimating the *b* value. Furthermore, the estimation accuracy depends on the number of events in a sliding window, as well as on the statistical uniformity of the data sample, i.e. the window should cover a spatial area of the same geodynamic type and correspond to a time interval free from critical changes in seismic parameters [38]. That is why the method should be applied with great care, investigating whenever possible the distribution of seismicity in each cell and, checking whether the data sample is representative.

The *b* cartograms for the BRZ (Figure 12 A) have been generated on a dense grid (0.4×0.6º), at every 8 years. Such high resolution is possible due to the use of the complete BAIK catalog (which includes all $M \geq 1.5$ events) for the 1987-2003 interval and has an acceptable uncertainty: $\sigma = 0.08$ (see legend on the right in Figure 12 A, a).

The maps of isolines in Figure 12 A, *a* show a minor difference in average *b* values between the first and second time intervals, within one accuracy grade according to the color scale (0.90-1.05 and 1.05-1.20). The cartograms show the boundary of a considerably lower data density passing along 109ºE between the southwestern and northeastern BRZ.

Reliable definition of each value requires about 100 or more representative earthquakes of different energies [39]. We apply the concept of a confidence interval to obtain a statistically exact definition of a required data sample size and to allow for its influence on the accuracy of the estimated parameter.

In practical applications, rather exact confidence intervals for selective estimation (of $\bar{b}$ in this case) can be obtained based on the Moivre-Laplace theorem [40] used in the probability theory, according to which the 3% accuracy can be provided if the data sample has the size (n) given by:

$$|u|/(2\sqrt{n}) \leq 0.03 \tag{2}$$

Thus, if the confidence probability is 0.95 (an allowable statistical reliability of a conclusion), the quintile $|u|_{0.95} = u_{0.975}$ has the value 1.96. Based on (2), one can estimate the accuracy of the obtained values of $\bar{b}$. For this purpose, one can contour earthquake numbers inside the cells in EEDB, i.e., draw the sample size isolines (Figure 12 A, c). So, for the 0.4×0.6° averaging grid the error is 6-18% ($32 \leq n \leq 256$) in the axial BRZ area, but reaches 35% ($n = 8$) outside the lake. To improve the accuracy and keep the same cell resolution, the parameter can be calculated using an averaging window with double overlap. The error in thus obtained estimates reduces to 4-6% ($243 \leq n \leq 729$) over the whole BRZ area (dark gray) and even to 2 % ($n \geq 729$) at some sites (black)

An advantage of interpreting b cartograms is in implications for elastic energy buildup in the crust (stress sources): $\bar{b} = 1.8$ ($\gamma = 1$) if all potential elastic energy is released in an earthquake and $\bar{b} = 0.9$ ($\gamma = 0.5$) if the release is incomplete. Thus, the b value has bearing on relative amount of released elastic energy [41], and changes of the parameter in time correspond to changes in lithospheric stress and strain [42]. Proceeding from these assumptions, one may conclude that an increase in b observed, for example, in the central BRZ during the 1996-2003 interval records stress release in the area. The growth of average b values appears also in the time series (Figure 13).

Studying Spatial Seismicity Patterns with GIS EEDB

The use of GIS EEDB has revealed important features in the spatial patterns of seismicity at the junction of orogens and stable blocks with rigid lithospheric elements. In the case of Central Asia, for instance (Figure 14), earthquakes tend to the East Tien-Shan and its borders with the adjacent rigid tectonic units of Tarim and Dzungaria, both with low seismicity. The hypocenter pattern in the vertical cross section along the A-B profile likewise indicates a high seismic activity of the Tien-Shan against the nearly aseismic Tarim and Dzungaria areas. The earthquake origin depths in this part of Central Asia are within 30-40 km.

a

b
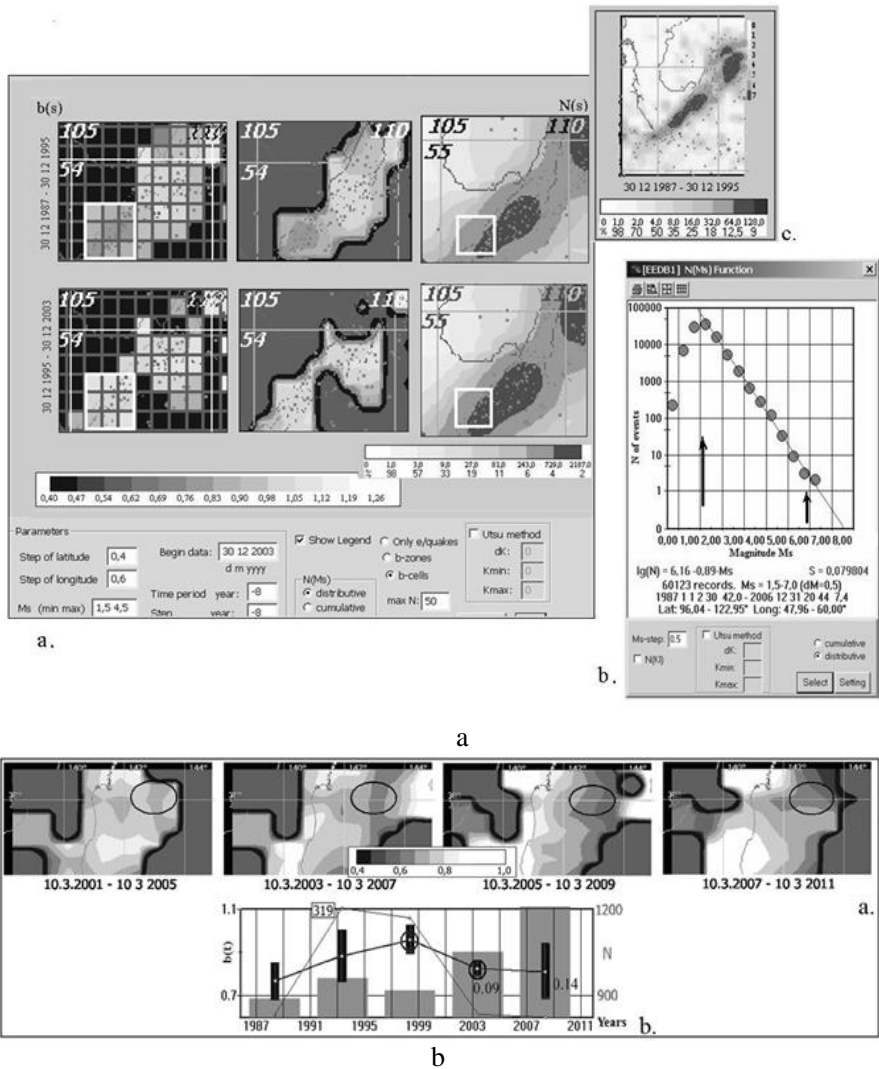
Figure 12. A − b variations in BRZ for 1.5 ≤ Ms ≤ 4.5 earthquakes from the Baikal catalog: a) spatial pattern of the b parameter (slope of the magnitude-recurrence relationship) as a grid of b(s) values, or b cells (on the left) and zonal maps or b zones (in the center) for the 0.4×0.6º grid with double overlap, and the respective maps of the number of earthquakes in the selected grid cells with double overlap (on the right). The color scale shows errors in b value; b) the magnitude-recurrence relationship within the 1987-2003 interval; c) a map of earthquakes number in cells without double overlap given for comparison and showing b errors exceeding 6% over the whole BRZ area.

B – *b* variations for earthquakes from the JMA catalog around Fukushima Prefecture (3.5≤*M*≤7, aftershocks are removed): a) spatial anomalies averaged over 4 years (grid size 0.4×0.6°, 3.5≤*M*≤7, rms error *σ* ≤ 0.3, aftershocks are removed, the oval marks the source area of the pending Tohoku earthquake); b) time series, averaged over 5 years. Vertical black bars are one-sigma error bars (*σ*), the oval marks points of *σ* < 0.09; gray boxes correspond to the number of events; black curve is the number ratio of small-to-large events.
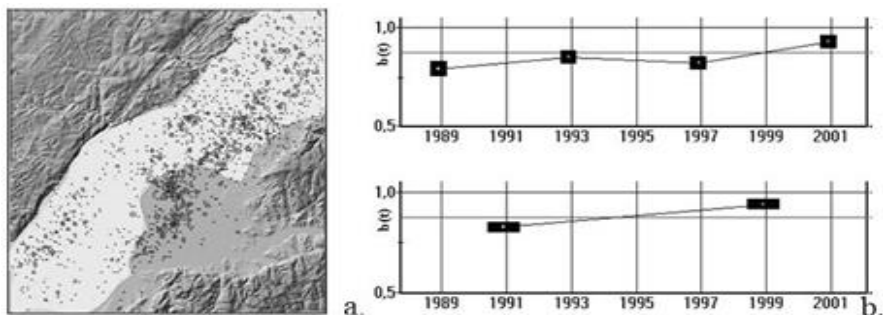
Figure 13. The BRZ area framed in Figure 12 A, *a* (a) and variations in *b* parameter at every 4 years (b, top panel) and every 8 years (b, bottom panel). Errors in *b* estimates are shown by segments and calculated by formula (2). The average *b* value increases from 0.75 to 0.9.
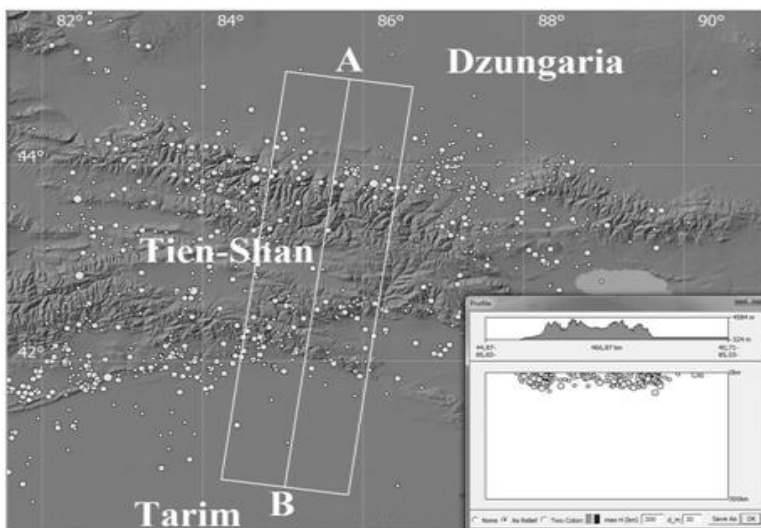
Figure 14. Seismicity in the East Tien-Shan and the adjacent Tarim and Dzungaria areas. Circles are M ≥ 3.5 earthquakes between 1980 and 2011. Inset shows hypocenters along the A-B cross-section, which obviously fall within the orogen.

In part 1 of this chapter, the EEDB system is considered as a GIS software (it was registered in *Rospatent* as GIS-EEDB program: No. 2011613755, 13.05.2011), which was developed to meet the demand for a geographical base applicable to study spatial patterns of seismicity and geodynamics, as systems of this kind were absent or inaccessible at the time when the research began.

The software's geographical environment consists of several basic modules considered above. The program shell is at the same time a control system for the seismological database, and the content and format of all included earthquake catalogs are presented correspondingly. This part of our research was registered in 2009 in the State Register of Databases as an *Expert Earthquakes Database*.

The geographical shell and the seismological DB are constantly being updated as new detailed geographical and earthquake data become available.

On the other hand, while it was developed, the GIS EEDB system has changed from an information system for geographical visualization of the earthquake database to a high-tech expert system. As a result, the GIS EEDB now represents a set of research techniques, in addition to the historical catalogs and the graphic shell of the Earth. The application of the GIS approach [38] to studies of seismicity and geodynamics is illustrated with examples of data analysis. The reported techniques of multistage analysis using the criterion of concentration, earthquake clustering, and the recurrence curve slope use the most complete, reliable, and comprehensive information the system can provide on seismicity and its dynamics. To synthesize and interpret this information (to make an expertise), the experience, intuition and knowledge of the researcher are required. An obvious advantage of the presented system consists in the possibility for its continuous updating with the advance in methods and technologies.

In conclusion, of Part 1, we note that the proposed version of the GIS-EEDB graphic shell, which develops the EEDB prototype first designed in FORTRAN and Pascal within the DOS operational system, has been written in Visual C++ and is maintained by *Windows* (NT, XP, Home, 7 and 8). It runs in a user-friendly interface, easily manageable even by inexperienced users, allowing them to review, visualize, and analyze data in a fast and effective way. The system has been successfully set into operation and has been in use for scientific purposes, being currently installed in a number of institutions, including IPGG (Novosibirsk) and Geophysical Surveys of the Russian Academy of Sciences. The software was used to study the seismicity of the Altai region [43, 44] and elsewhere, specifically, the areas of nucleation of large earthquakes.

Below we describe a modification of the GIS-EEDB high-tech expert system called *Fukushima-EEDB* and illustrate its use with examples for the seismicity of the Fukushima Prefecture area in Japan [5, 45].

PART 2. MODIFICATIONS AND VERSIONS OF EEDB FOR DIFFERENT GEODYNAMIC AREAS AND CASE STUDIES OF SEISMICITY ANOMALIES

A. V. Mikheeva

The EEDB subsystems are shown in the work flow chart of Figure 15.

It is appropriate to apply the EEDB potentialities to study seismic activity in the Fukushima Prefecture which was exposed to the Great East Japanese Earthquake of $M_w = 9.0$ of 11.03.2011, called also the 2011 off the Pacific Coast Tohoku-oki Earthquake by JMA, or shortly the Tohoku earthquake. We have limited the study to the area within 36-39°N, 138-146°E.

The adaptation and modification of the GIS-EEDB system to the local features of the area consists in.

1) Creating an optimal database using the regional earthquake data; adapting the instrumental programs for processing the regional data and converting it to the EEDB seismological subsystem format;
2) Developing a geographical system of regional EEDB version for qualitative visualization and analysis of seismic data from the region. Populating the EEDB geographical subsystem with detailed geographical data from the prefecture using ASTER GDEM (for the shaded relief model realized in EEDB) and the Natural Earth (for detailed cultural and physical layers in the vector and point formats);
3) Adapting the methods and algorithms to statistical processing of seismic data in terms of local geodynamics. Applying comprehensive geoinformation analysis to learn the common patterns and anomalies of seismicity in the region.

This preparatory work was carried out for the Fukushima Prefecture in the environment of supported applications to complement the resources of EEDB, and was followed by a preliminary seismicity analysis in the adapted Fukushima-EEDB system. At the same time, the development environment of

GIS EEDB was adapted to Windows 8, and its supported applications were translated to the standards of the *Firefox* versions and new versions of *Global Mapper* and *FireFox* utilities were employed.

For the seismological base, we chose the Japan JMA catalog as the most complete one to date. When making the choice, we compared several Japanese catalogs: JUNEC (Japan University Network Earthquake Catalog, 1985/07/01-1998/12/31), NIED (National Research Institute for Earth Science and Disaster Prevention Earthquake Catalog, 1979/07/01 - 2003/06/30) and JMA (Japan Meteorological Agency Earthquake Catalog, 1926/01/01 – 2013/05/31).
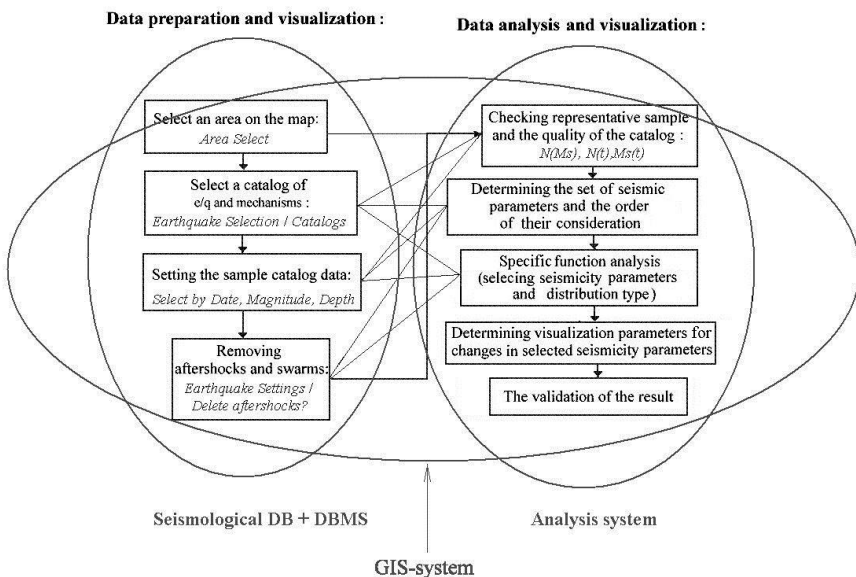
Figure 15. Work flow chart for seismicity research and the framework of the EEDB system.

Seismicity Pattern Visualized by Means of Fukushima-EEDB

Simple *visualization* in a map (with *sorting* by magnitude) and *selection* (by bolting small events) show some geologically active structures in the area adjacent to the Fukushima Prefecture. First, they are seismic lineaments and super-lineaments. The seismicity of the area was assumed to be a part of the trans-regional Japan-Sea lineament [46] (black boundaries in Figure 16), which extends from the Arctic Ocean to the Philippine Sea, including the

submerged Lomonosov Ridge, New Siberian Islands, Sakhalin Island, Hokkaido and the north-eastern part of Honshu Island. The Japan-Sea lineament, in turn, is an element of the Antarctic super-lineament being a planetary meridian seam [46]. In addition, the Fukushima map images local seismic structures within the linear trend of the largest events for the past decade (No. 1 in Figure 16); a response to these events 200 km to the south (No. 3 in Figure 16); an inner zone of weak volcanic activity in the form of a ring within the location of Aizu-Wakamatsu (No. 2 in Figure 16); a deep active zone (No. 4 in Figure 16); and a swarm (No. 5 in Figure 16) near the Pacific coast on the Ibaraki-Fukushima prefectural border (a sequence of shallow normal-slip earthquakes [47]), including the M_s=7.0 earthquake of April 11, 2011. This is an example visualization analysis of primary information on seismicity in a selected area, with the Fukushima-EEDB procedures (Figure 16).

The revealed linear pattern of great earthquakes ($M_s >= 7$), including the $M = 9.0$ Tohoku event, appears to be the most interesting result (No.1 in Figure 16; Figure 17a). In the map of Takashi NAKATA et al. [48], there are northeast- and north-striking tectonic elements in the area, which align with global structures. However, the orientations of some tectonic structures (stepwise displacement of an eroded anticlinal ridge, as well as a bend in the orientation of the Japan trench (Figure 17a) and faults along it, prompt the existence along 38°N of an ancient fault or another structure, which has shown up as a lineament with a high seismic potential through the past decade.
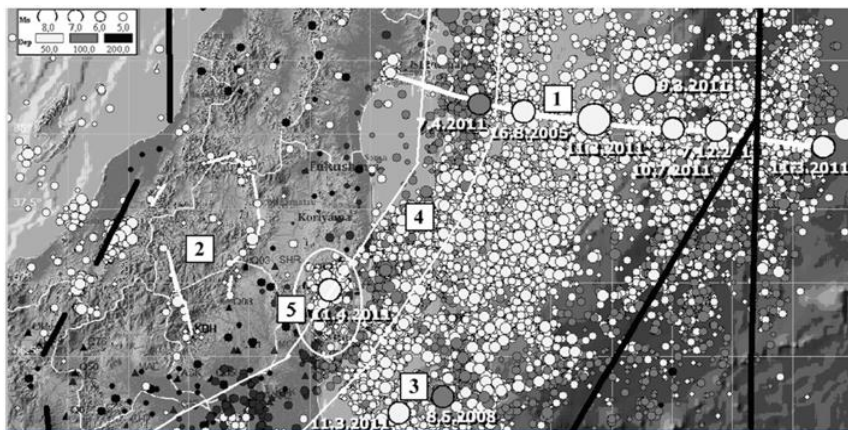
Figure 16. $M_s >= 3.5$ seismicity (13,742 events) near the Fukushima coast, since 2003.
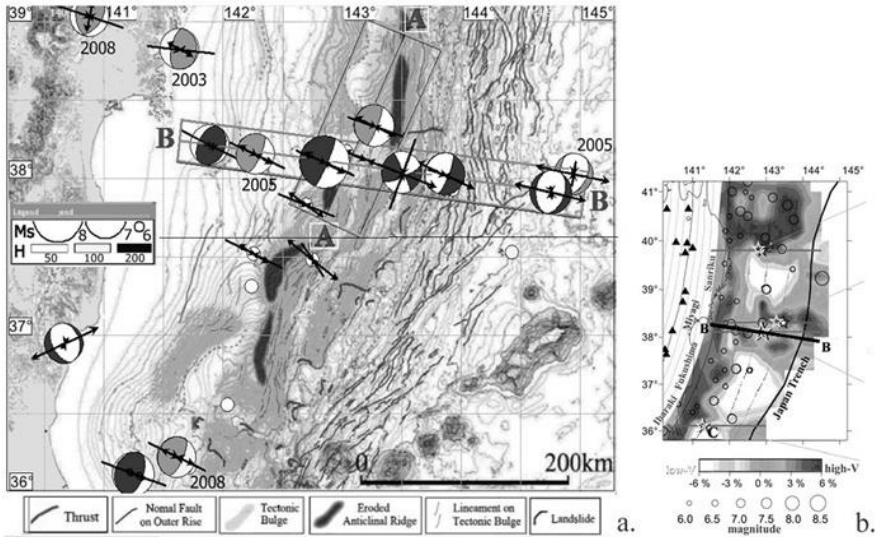
Figure 17. The rigid linear structure (BB): a) tectonic geomorphological map [48] (thin- and heavy-line circles show events before and after the Tohoku event, respectively); b) *P*-wave tomography image [50].

Incorporating this tectonic map as a *background map* into the GIS EEDB system and visualizing great earthquakes (in the mode of *drawing focal mechanisms*) (Figure 17), we can see that the events of this chain are localized in a gap between elongate tectonic uplifts and belong to seismotectonic segments of different slip geometries (reverse, strike-slip, and normal):

- first three earthquakes (left) in the chain, including the shallower foreshock of the Tohoku event located just to the north (Miyagi-oki event of 9.03.11) and the remote response in the southern part of the region, have compressive reverse-slip mechanisms;
- the event in the middle has a strike-slip mechanism;
- three events on the right have extensional normal-slip mechanisms.

Frequent changes in geodynamic regimes is characteristic of the plate boundary separating the North American, Eurasian, Pacific and Okhotsk plates [49] and corresponds to a change in directions of major tectonic strain in this region.

The *profile* AA (Figure 17a) striking along the main tectonic structures shows that the area between the Tohoku event and its foreshock was still weakly active after the event, though the center of the earthquake swarm had

shifted to the right of the main shock. This likewise suggests the presence of a rigid linear structure directed across the profile. The plate motion along this structure could trigger a cascade of destructive events at the plate edges.

P-wave high-velocity zones in the area provide more evidence for the existence of a rigid structure along 38° N [50, 51] (Figure 17b): "The high-*V* patches in the megathrust zone may result from subducted oceanic ridges, seamounts and other topographic highs on the seafloor of the Pacific plate that become asperities, where the subducting Pacific plate and the overriding continental plate are strongly coupled" [52]. Furthermore, "a landward extending oceanic fracture zone controlling the slab morphology change around 38°N" was assumed there proceeding from the lateral slip distribution of the Tohoku event [53] and other evidence [53, 54].

As shown by the profile BB (Figure 17a) running along 38°N and across the regional linear structure (Figure 8a), the great earthquake chain is conformal to the junction between the Pacific and continental plates. The compressive earthquake mechanisms correspond to the Pacific plate and its convergence with the continent, while the normal-slip mechanisms represent subduction-related extension. The largest event is located in the place where the oceanic slab bends down and the plate contact is at the shallowest depth.
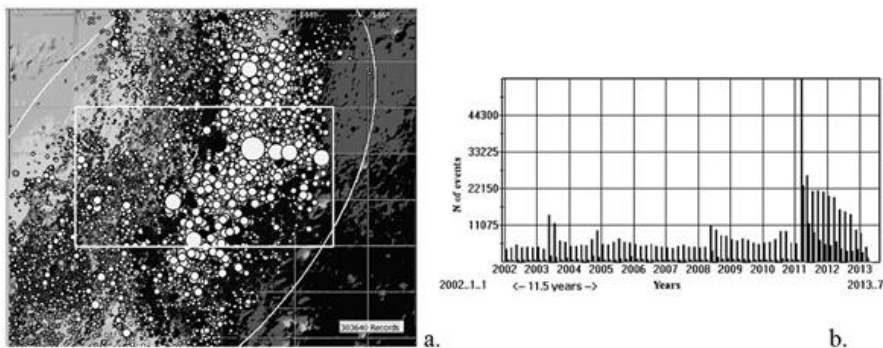
Figure 18. The aftershock process of the Tohoku event in space (a) and time (b), obtained using the elliptic algorithm based on Prozorov's method [29] (a). The box frames the study area. The curve (b) shows that the aftershock process is not over yet (blue and red bars correspond to the number of all and $M_s >= 2$ events, respectively).

Thus, we have considered an example of primary information analysis of seismicity by means of the GIS EEDB system using selection, sorting, and visualization. The visualization procedures include drawing focal mechanism solutions (beach-ball plots) in a map or in a cross section (with the vertical

projection of stereoplots in the latter case), using multi-layer coloring (in XOR mode) of asymmetrical quadrants calculated from parameters in catalogs of focal mechanisms; plotting focal mechanisms in the vector mode; selecting profiles and creating a relief profile and a cross section of seismicity in a selected visualization mode; loading whatever external raster map, as a background, into the EEDB environment; recognizing linear structures by a set of points distributed in space; etc. All the examples were shown using the functions from the first column of the flow chart (Figure 15), including the detection of aftershocks.

The functions of *detecting aftershocks* implemented in EEDB are a set of different methods (empirical, elliptic, and interactive) and various modifications of the elliptic method [3, 24]. The efficiency of different algorithms for detecting aftershocks was evaluated by estimating the statistics remaining after filtering and comparing it with random Poisson's exponential distribution. After removal of aftershocks by the elliptic method, only 14% of earthquakes have remained in the study area. We have estimated the number of aftershocks (using, also, the plot of Figure 18b) to be a few hundreds of thousands (303,640 shocks), and the aftershock process to continue, as the seismic background has not reached the average level observed before the event. Thus, we can draw an important conclusion that the greater part of earthquakes in this area belongs to triggered seismicity, rather than being independent; specifically, they are sequences of events induced by the Tohoku earthquake. Moreover, the spatial distribution of the Tohoku aftershocks (Figure 18a) has implications for the size of the active zone. Therefore, the territory adjacent to the Fukushima Prefecture can be considered a part of the nucleation area of the Tohoku event, which is suitable to retrospective search of indicators for earthquake prediction. Applying the procedure of removing earthquake swarms and aftershocks brings the seismicity parameters to the stationary baseline and thus significantly improves the quality of processing.

Studying Seismicity Parameters Using the Analysis Subsystem of Fukushima-EEDB

Investigation into seismicity anomalies can have different applications in seismic and geodynamic research. In this Part, we show how the analysis subsystem of Fukushima-EEDB is used for retrospective study of anomalies preceding a great earthquake, e.g., the Tohoku event. In addition to outlining

the nucleation area of the selected earthquake, it is important to estimate the quality of the selected catalog (Figure 15).

First, one can find out how the earthquake parameters recorded by the seismological network change in time by plotting data from the selected JMA catalog in EEDB:

1) The magnitude time series $M_s(t)$ shows (i) quality improvement of seismological networks in 1977 (for $M_s < 3$) and 1987 (for $M_s < 1.5$) evident in increased number of recorded earthquakes, 3 times on average in each year; and (ii) stabilization of the recording quality in the end of 1997 (for all magnitudes).

2) The $N(t)$ plot shows another step of improved recording (in 2002-2003), and an increased number of recorded events in the curve of a higher time resolution since mid-90s, followed by stabilization in recording quality.

3) The *Gutenberg-Richter $N(M_s)$ curve* (least squares method) shows a linear segment in the magnitude range $M = 3.5\text{-}6.5$ corresponding to the $K = 10\text{-}16$ interval of the energy scale (Utsu's [34] maximum likelihood thresholding methods).

Thus, we conclude that the catalog completeness is the best within the interval of 2002-2013 while the magnitudes from 3.5 to 6.5 are the best representative.

Seismic activity A [28] is the first characteristic of the seismic process explored by ***the cartographic method***, which implies calculation of contour lines for the average values of the parameter on a regular spatial grid. The resulting map of the parameter A_{15} shows the mean long-term trend of seismic activity normalized to $K = 15$ ($M_s \sim 5.5$), obtained from statistically uniform averaged seismicity data. The map (Figure 19) shows the peaks of the long-term seismic activity for the past 20 years in the area of Fukushima to follow the coastal line of the Fukushima Prefecture with a maximum near Hitachi City.

To visualize the spatial distribution of the ***parameter b,*** another cartographic method is used: mapping parameter changes at uniform time intervals. In the "fill" mode of contour line visualization, the program performs spatial interpolation using the 2D Bessel function (1). The map (Figure 12 B, a) shows a poorly pronounced zone of concentrated negative anomalies which originates in the epicentral area of the pending Tohoku event and strikes along 38°N in 2007 through 2011 before the main shock.

The average b value has become 0.15 lower for the past decade (from 0.95 to 0.8 according to Figure 12 B, b), with an error of $\varepsilon = 3.3\text{-}2.9\%$ according to formula (2). The stability of the estimate can be additionally checked by a standard deviation reaching 0.09-0.10 at the most significant points (Figure 12 B, b). A b decrease is known [42] to indicate deformation and self-organization in the crust with stress buildup in rigid structures, which may occur during nucleation of a large earthquake.
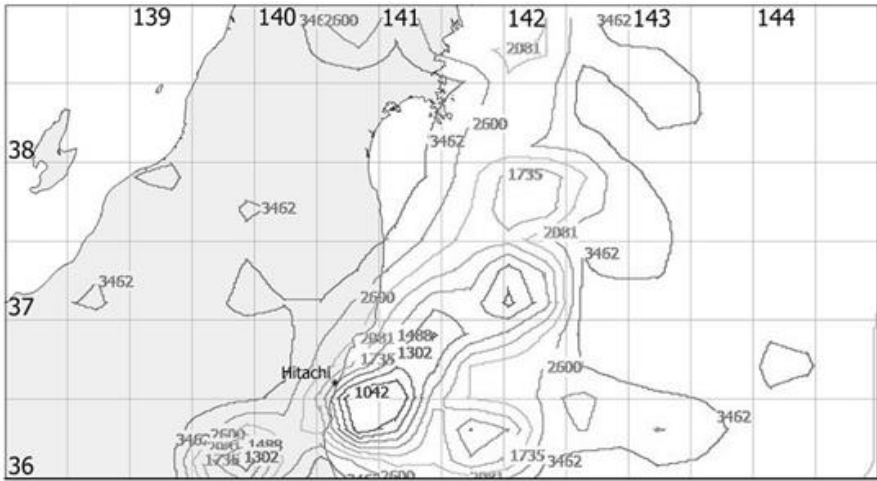
Figure 19. M_s=3.5-7 seismicity in 1994-2013; aftershocks are removed. The isolines (without coloring) show average frequencies of earthquake of a certain magnitude on a yearly scale.

Relative total energy released in earthquakes per unit time, normalized to the background value of mean seismic energy and presented as $log(E_{sum}/E_{norm})$, is another seismicity parameter we study.

This parameter, suggested by P.G. Dyadkov and Y.M. Kuznetsova [44], is advantageous due to its independence of the spatial seismicity pattern (taking into account the earthquake density in each cell is not required for the interpretation of results). The parameter highlights (Figure 20) the structure and dynamics of the quiescence zone formed two years before the Tohoku earthquake, since 2008-2009, north of the pending event. About a year before the main shock, quiescence in this zone gave way to weak foreshock activity, while another explicit quiescence zone appeared in 2010 west and south of the shock.
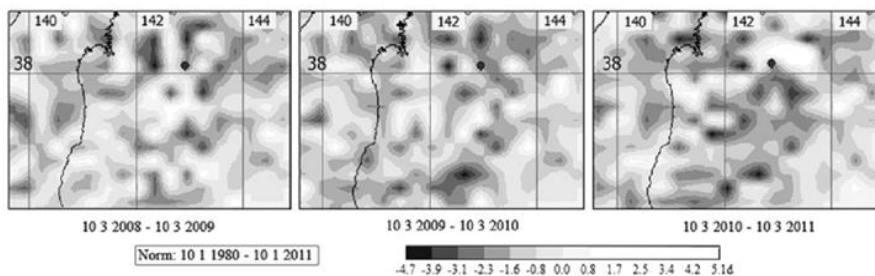
Figure 20. Relative seismic activity (white) and quiescence (gray) at one year intervals before the Tohoku event (grid size 0.2×0.3º, 3.5≤*M*≤6.5). Circle marks the pending Tohoku earthquake.

This indicates that the mechanism of a "seismic gap" has set into action. This effect was described in literature, including in Japanese publications [55], as a basic model predicting many large earthquakes. Moreover, the epicenter falls on the border of the quiescence zone, where the gradient between high and low relative total energy is the largest (rightmost map in Figure 20). This confirms our earlier idea [56] inferred from data of the Baikal rift zone that the largest earthquakes occur on the edge of negative seismicity anomalies at the points of maximum gradient of relative total energy. The gradient map clearly shows distinct positive anomalies between the pending Tohoku event and its foreshock, as well as in the area where the earthquake of April 11, 2011 was to occur on the Ibaraki-Fukushima coast (Figure 21b). The gradient calculation procedure we are using searches the maximum relative energy difference between the current and neighbor cells.
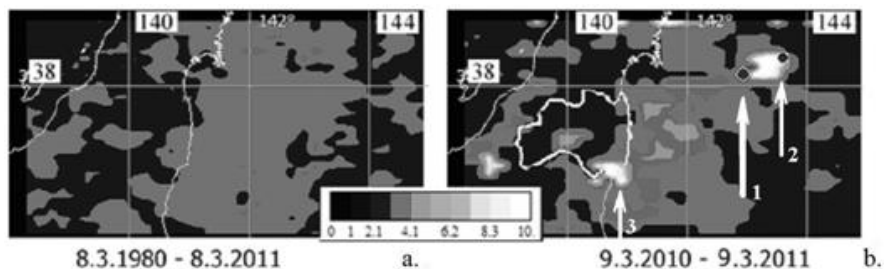
Figure 21. The map of relative energy gradients: a) for background seismicity; b) for seismic activity over a year prior to the Tohoku event (grid size 0.1×0.2º, 3.5≤*M*≤6.5; aftershocks are removed). Circles and white arrows mark the location of pending Tohoku earthquake (1), its Miyagi-oki foreshock (2), and an earthquake of 11.04.11 that occurred a month after Tohoku (3).

Density of seismogenic fractures or the concentration criterion K_{avr} is a perfectly physical parameter based on rock mechanics which describes the seismic process in terms of fracture of solids. The respective theory was developed by S. Zhurkov [57], and then A. Zavjalov proposed to use it for earthquake prediction and estimated the critical value of the fracture density parameter for the Kamchatka region [35]. P.G. Dyadkov proposed to use this parameter for characterizing seismicity in a different way [3], namely, to estimate the duration of seismic stability preceding a large event from flattening of the cumulative K_{avr} plot relative to the ideal curve of uniform fracture growth, as it was made for the Altai (Chuya) earthquake of 2003 (Figure 7).

In the case of the Tohoku earthquake, the K_{avr} curve also became flatter 6 years before the main shock, all over the nucleation area (Figure 22a). The mapped K_{avr} patterns (Figure 22b) reveals the BB structure (Figures 16 and 17), as well as expansion of fractures toward the area of the Tohoku-event and its foreshock.
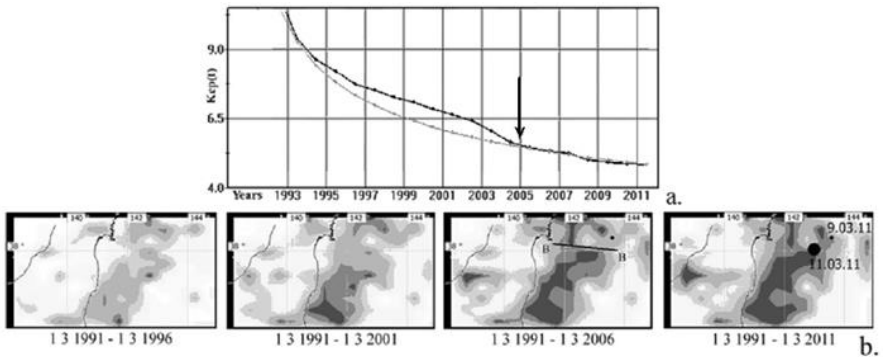
Figure 22. Variations of fracture density (K_{avr} parameter): in time (a) and in space (b). Black and gray colors in (a) show, respectively, real data and data corresponding to uniform fracture growth; in (b) the grid size is $0.3 \times 0.5°$, $3.5 \leq M_s \leq 9$, $H_{max} = 50$ km.

Thus, the application of the EEDB tools to seismicity studies in the area around the Fukushima Prefecture allows the following inferences:

1) There exists a rigid linear structure striking along 38°N orthogonal to the Japan Trench and other regional tectonic lineaments;

2) The hypothesis that the inward motion of this structure on 09.03.11 as a result of plate boundary slip could trigger a cascade of destructive events of 11.03.11 along its edge has been proven valid;

3) Inspection of the JMA catalog has shown that its completeness is the best within the interval of 2002-2013 and the earthquake magnitudes from 3.5 to 6.5 are the best representative;

4) The map of long-term seismic activity normalized to K = 15 (energy scale) shows the greatest activity in the the Japan offshore area for the past 20 years. It is next to the Fukushima Prefecture coast, with the maximum near Hitachi city.

5) The medium-term and long-term anomalies appeared before the Tohoku event in several seismicity parameters, including 1) weakly pronounced decrease in b for the past decade prior to the event; 2) flattening of the K_{avr} (fracture density) curve for the past 6 years; 3) formation of quiescence zones for the past 2 years; 4) prominent positive anomalies of relative energy gradient formed a year before the shock.

All these features may indicate seismic stabilization in the nucleation area preceding the Tohoku great earthquake.

PART 3. VISUALIZATION AND ANALYSIS OF EISC-DATA

A. V. Mikheeva

The catalog of the Earth's Impact structures, available at the website of ICM&MG [1, 6, 58] was created by Anna Mikheeva in 2005 based on different reference data: published evidence (papers, books), Abstract Journals, data deposited in VINITI (section "Geology and Geophysics"), as well as personal communications. As a result, the first Russian Internet catalog and a Complete Database of all observed, probable, potential, and even erroneously inferred structures of extraterrestrial origin have been compiled. There are fields with key parameters indicating the location of footprints left by an impact or an explosion of a cosmic body (CB) on the Earth's surface: event name (and/or geographical location, territory), continent or ocean code, underwater (*) and comet (') marks, the validity index according to 5-grade probability scale (from 0 to 4, Figure 23a), coordinates and geometrical size of the structures (latitude, longitude, diameter), age (or date) (Figure 23a), the relevant text and graphical information (as hyperlinks), and many other fields in the extended version (depth, number of objects, erosion rate, gravity and

magnetic anomalies, etc.). To date, the Earth's Impact Structure Catalog (EISC) has been one of the most complete published catalogs of this kind, with 2141 records. It is currently being used by many researchers and is open for updating. It is convenient to study the space patterns of impact structures and to analyze their parameters with an independent version of the control and visualization system (the EISC system). By applying the EEDB software to the EISC catalog, one can select a sample of impact structures from the original Catalog according to different parameters (diameter, validity, etc.) and working areas of different scales from global to local maps, and then obtain the related cartographic information, including the locations of impact craters (Figure 23b), geophysical and geological layers, etc. In addition to the map visualization, the system can list the catalog in the text format, plot different parameters, and show results of statistical data processing. The mathematical support and the software of the EISC system allow plotting frequency distributions of crater diameters (logarithmically proportional to impact energy) for events from various samples, as well as different distributions of integrated parameters with time, space, and with respect to one another. The curves shown in Figure 24 image log-log frequency distributions of craters of different diameters and rms deviation of the random distributions from the regression line (variance S). The curve in Figure 24a shows abrupt changes at $\lg D = 0.7$ ($D \sim 5$ km). When the curves for $D > 5$ km, 1 km $< D < 5$ km and $D < 1$ km are plotted separately, irregular distributions appear in two latter plots. It means that the data available for $D < 5$ km craters is incomplete, because the ancient surface structures may have been modified by erosion or sedimentation or, they may be poorly studied, as high-resolution surveys cover only a lesser part of the globe. The crater diameters are unevenly distributed in time (Figure 25), with age constraints missing for a half of events (50% of craters), which all are tentatively placed in the end of the time scale. The curves of Figure 26 show progressive growth in the number of discovered craters, the number of really discovered structures departing markedly from the exponential distribution $N \sim e^{2.83+0.12 \cdot t}$ predicted in the 1970s [60]. The updated time dependence of the number of real discoveries is rather nonlinear quadratic, obtained based on analysis of EISC catalogs:

$$N \sim 10 \cdot t^2 + 13 \cdot t - 11.$$

The published catalog has been used also to plot the size of craters against their age, which has implications for the relaxation time of impact structures. This plot is similar to the one published in [60] and [61] and is not shown here.

Another relationship, Depth (*Dep*) vs. Diameter (*D*), describing the crater geometry appears to be more interesting (Figure 27). The averaging line of all points independent of target rocks is described by the formula:

$$Dep = 66.25\ D^{0.738}.$$

The Complete Catalog of the Earth's Impact structures
by Anna Mikheeva, ICM&MG SB RAS.

Probability

246-proven	0
252-probable	1
1407-potential	2
223-questionable	3
13-discredited	4

ICM&MG

The related projects:
1. Catalogue of the Earth's impact structures (The dilated catalogue of 204 records)
2. "Tunguska Event"
3. "Expert Earthquakes Database (EEDB)" - system for the research into the seismic-geodynamic regime
4. "ENDDB-system (the Earth's Natural Disasters Database)" for analysis of the earthquakes and impact structure distribution (EEDB+EISC)

to russian version

to Map

LMA Map

NEWS:

Yama Korchazhikha structure (near the village of Bykovo, Lake Baikal)

Adirondack Impact
Agit Khangay
Airkumskaya
Akjayliau
Aldyubinsk
Albert prince

Name of structure	Terr	Prob	Lat	Long	Age (Ma)	Diam. (km)
Abaco Island (Little Harbor) * Bahamas	AC	3	26,33	-77		1,6
Abimily Australia	Au	2	-24,4	133,2		1,5
Absaroka Mts. USA	AN	2	44,2	-109,8		
Acores Azores	At	3	38,7	-27,2		
Acraman (Gawler, Ecremen) * Australia, South Aus	Au	0	-32,02	135,43	~590	90
Adh Dhuhaybah Jordan	As	2	31,5	35,7		0,75
Adirondack Impact * USA / Canada	AN	3	43,9	-74,4		200
Adrar Madet (sev.) Niger	Af	2	18,6276	10,3987	0.008	60
Afghanistan 1 Afganistan	As	2	35	65		16
Aflou (D'Aflow) * Algeria (Algiers)	Af	1	34	2,045	23 (<100)	5
Afrique du Nord	Af	2			-5000y (0.005)	
Afton USA	AN	2	32,1	-106,8		
Agatha Christie * Indian ocean, Kergelen Is.	IO	2	-50,7	77,7	0,045	14
Agheir Mauritania	Af	1	19,41	-11,5		1
Agit Khangay Mongolia,W	As	1	47,3	96,4	500	5,1
Agnak * Canada	AN	1	67,5	-108		0,17
Agto * Greenland	NO	2	67,94	-53,59		10
Aguila del Alfambra Spain	Eu	2	40,57	-0,82		7,5
Ahlshausen Germany	Eu	2	51,79	9,98		3,6
Ahmed (GKCF1) Egypt, Gilf Kebir	Af	2	23,242	27,4586		0,63
Ahuazotepec Mexico	AC	2	20	-98,1	2010.2.1	0,03
Ahvenlahti * Finland	Eu	2	63,33	29,675	3.1	1,7
Aimala Finland	Eu	2	61,26	24,2		2
Aimores Brazil	AS	2	-19,42	-41,05	1	8,5
Airkumskaya * Kazakhstan	As	2	48,8	64,7	Q3-Q4 (?)	150
Aix-Marseille France	Eu	2	43,5	5,4		43,4
Akchoky Kazakhstan	As	1	47,7	72,38	1	10
Akiyoshi Japan	As	2	34,2	131,2	350.0	28
Akjayliau * Kazakhstan	As	2	48	81,48		12
Akonvesi Finland	Eu	2	63,02	28,27		2,5
Aktyubinsk * Kazakhstan	As	2	50	55,3	~150	250
Akyumak Turkey	As	2	39,9	42,8		
Al Buyayrat Saudi Arabia	As	2	24,7	38,9		
Al Hashima Saudi Arabia	As	2	27,85	43,1		15
Al Madafi Saudi Arabia	As	1	28,67	37,18	< 360	6
Al Umchaimin (Tleachman) Iraq	As	1	32,68	39,42	50 (< 55,8)	3,2
Al'Amarah (=Umm al Binni lake) Iraq, S.	As	0	31,24	47,1	< 0.005 (-2300y, 2.4)	3,4
Ala-Kitka Finland	Eu	2	66,28	28,97		8
Alaape Sweden	Eu	2	67,7	19,2		10
Alamo Breccia * USA, Nevada	AN	0	37,6	-115,34	367 (382.1 + 3)	150
Albert prince Canada, Victoria Island, arctic archip.	AN	1	72,46	-113,8	130 - 350	25
Alberta /I (X-SAR 30) Canada, Alberta	AN	2	56,38	-115,44	<10	5,7
Alberta /J (X-SAR 31) Canada, Alberta	AN	2	56,42	-114,67	<25	3
Zhuan-Tobe (Juan-Tobe, Shuan Tobe) Kazakhstan	As	1	47,1	73,8		10
Zhoulu (Zhoulu) China	As	2	40,3	115,383	0.06	52
Zolotaya veshka * Russia, Moscow area	Eu	2	56,824	37,9	~0.01 (<0.02)	1,24
Zondo-Marianskaya * Pacific Oc., Sulu Sea	PO	2	8,5	120		5000
Zuider Zee * Netherlends	Eu	2	52,7	5,3		

* - underwater and coastal structures
' - comet impact structures
!, y - date or year of event
s, Ar, p - timing method of structure
? - uncertain data

per.N 0220711563 (ФГУП НТЦ "Информрегистр", 2005: per.свид.№10771 от 27.02.2007)
per.N DB10017 (ФАП СО РАН, 01.10.2010)
per.N 2011620195 (ФГУ ФИПС "Роспатент", 11.03.2011)

a.
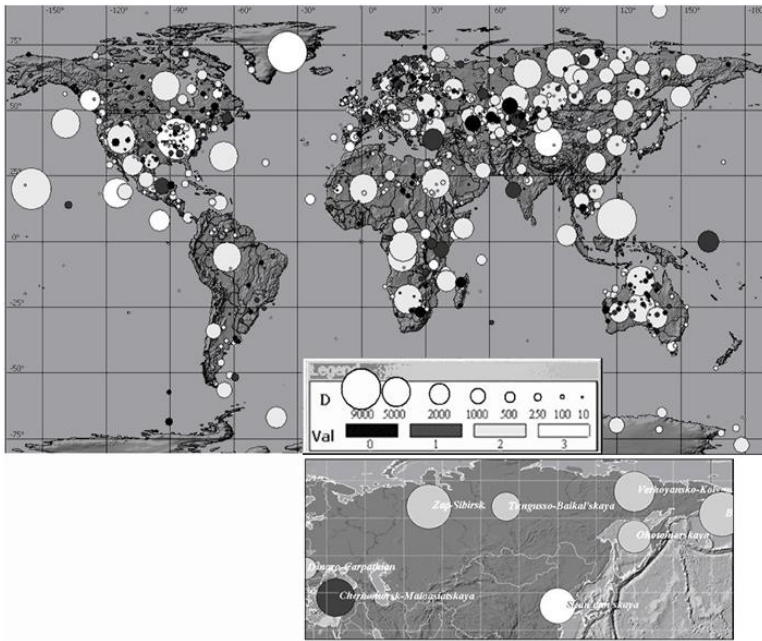
b.

Figure 23. Website views of ICM&MG site "The Complete Catalog of the Earth's Impact Structures" in the table and map forms: a) catalog format of impact events; b) an EISC GIS-system interactive map of catalogued events (http://labmpg.sscc.ru/impact/karta1.html) according to their sizes (crater diameter *D*) and validity (*Val*). The bottom panel is a map fragment with giant impact craters (*D*>1000 km) from [59].
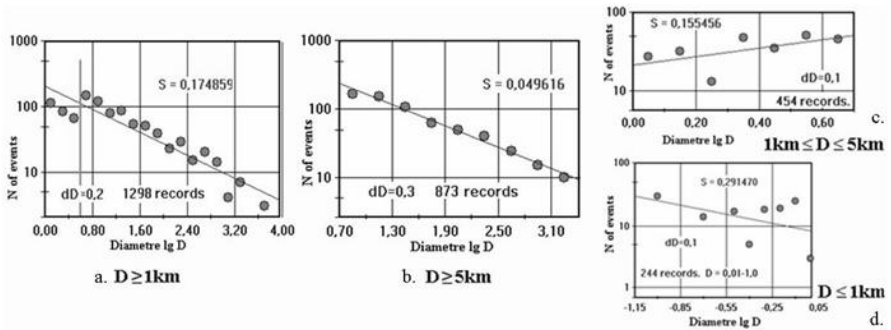
Figure 24. Recurrence of historic impact events, which left craters of different diameters: $D \geq 1km$ (a); $D \geq 5km$ (b); $1km \leq D \leq 5km$ (c) and $D \leq 1km$. Only 873 events with $D \geq 5km$ (b) show regular patterns.
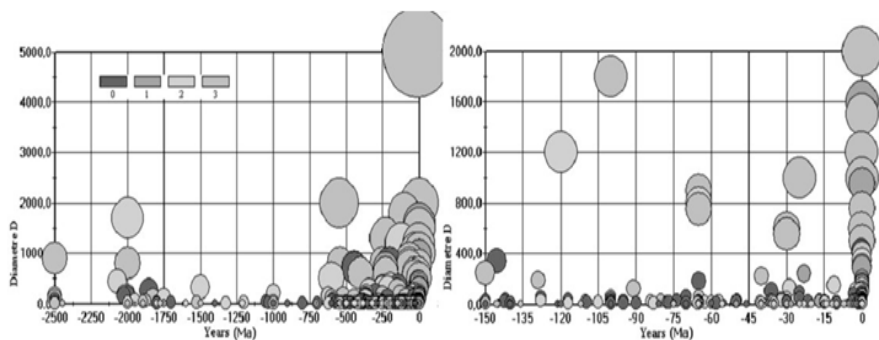
Figure 25. Time series of crater diameters (Ma). Color shows the reliability (validity) of structures.
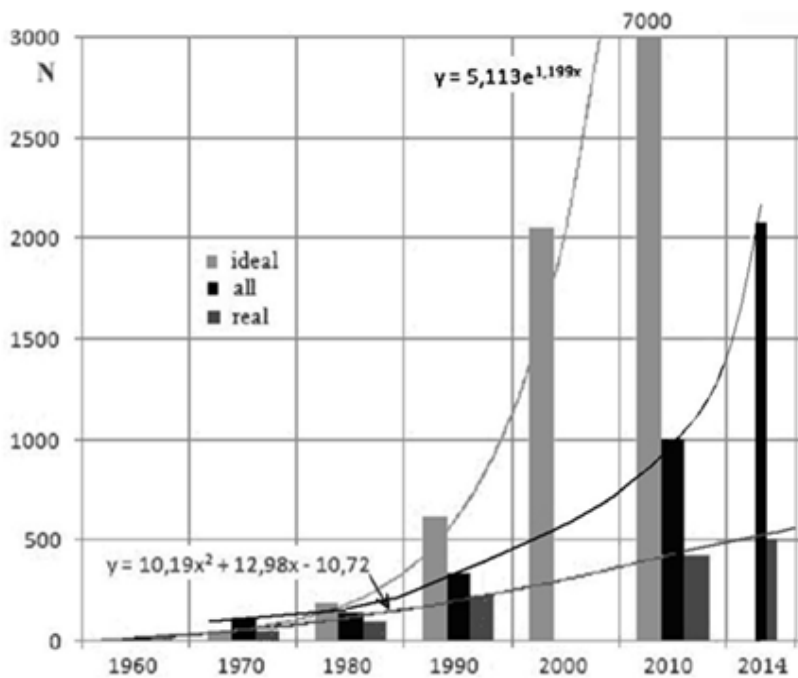
Figure 26. Progressive growth of the number of discovered craters: "ideal" is expected growth, "all" is the total of events in the EISC catalog, "real" refers to proven and probable craters (grades 0 and 1).
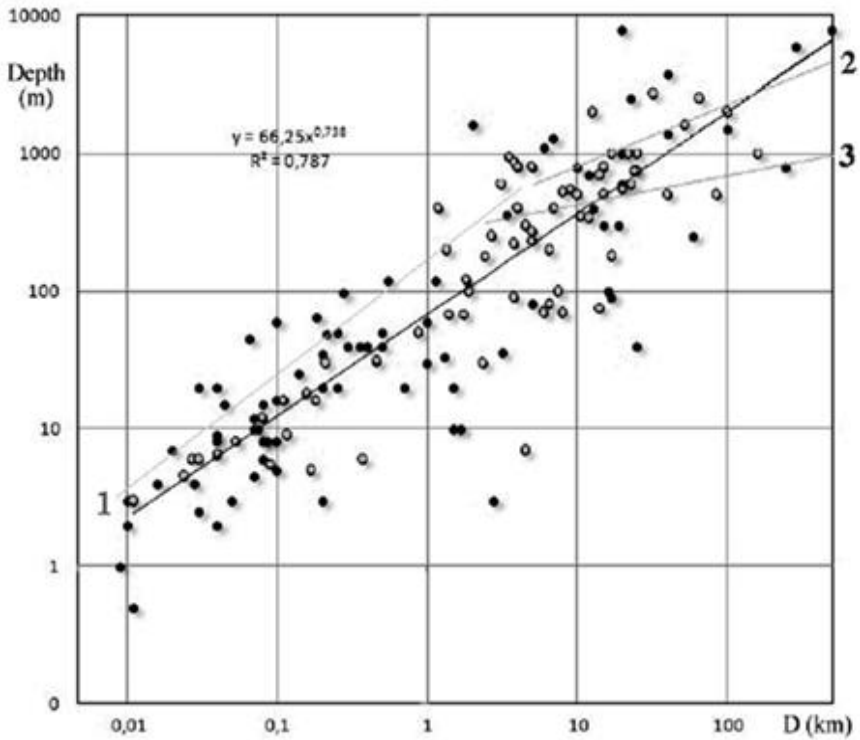
Figure 27. Geometry of impact craters. Lines 1-3 correspond to known depth-diameter relationships of craters for different target rocks [59]: 1) $Dep\sim159\cdot D^{0.829}$ for $D<3.8$ km in crystalline rocks and $D<1.2$ km in sediments; 2) $Dep\sim52\cdot D^{0.189}$ for $D>4$ km in crystalline rocks; 3) $Dep\sim204\cdot D^{0.27}$ for $D>2.5$ km in sediments. Dark color shows proven structures.

Information Technologies and Methods Used to Study the Shape of Craters

We study the geometry of craters using the shaded relief model and digital mapping. Typical morphological elements of impact structures have been systematized and can be used as diagnostic features [7, 62].

The basic hypothesis of the impact-explosive tectonics [63] is that meteorite craters on the Earth should be as frequent as on the Moon or on the Mars. To see how many large (D>>100 km) ring structures (RS) are there on the Earth, one can examine respective geological maps based on satellite imagery [64, 65] (Figure 28a). The use of processing algorithms for digital

elevation modeling [66] to find RS on the Earth's surface may be effective in the beginning of search for new craters, which are often difficult to detect in relief models.

However, these methods are insufficient to identify the origin of the detected RS. Discriminating the craters of potentially impact origin among many RS requires new diagnostic criteria associated with typical morphological elements revealed with advanced image processing technologies.
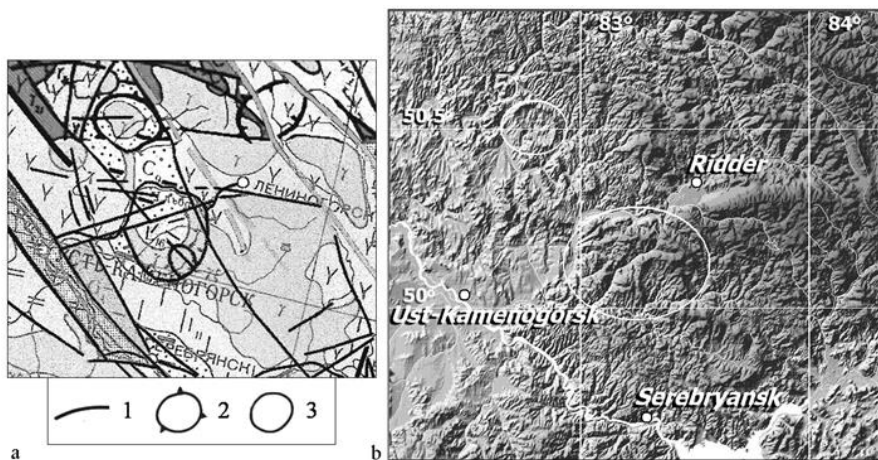
Figure 28. A fragment of a satellite map of the Ust'-Kamenogorsk area: a cosmogeological map [64] (a) and an EISC GIS map [6] (b). Symbols stand for: faults (1), arched structures (2), RS of uncertain or complex origin (3).

Cosmogenic ring structures (CRSs) can be successfully identified in tectonically stable areas (on Precambrian cratons and shields) [61] where they are well preserved due to the absence of magmatism and thick sediments. However, judging by geological evidence, almost all proven astroblemes in Russia described by V. Masaitis et al. [67] are buried under sediments or submerged, except for several craters (Logancha, Beyenchime-Salaatin) that partially remain on the surface and are detectable by morphological analysis of aerial photographs. Nevertheless, as real data have shown [1], the original cosmogenic terrain has been perfectly preserved in many areas of the Earth, for example, in Lake Balkhash surroundings, in Rudny Altai, Kola Peninsula, Mexico, Madagascar, and South Africa. Note that many impact craters have been identified on the Moon and other planets for the past century based exclusively on morphological criteria [68]. Thus, the morphological elements

of impact structures may be, in certain conditions, the basic diagnostic criteria of impact origin, superior over petrographic and mineralogical proofs.

In particular, our diagnostic methods based on the geometry of impact craters have allowed us to discover and add to the Catalog more than 40 potential astroblemes in Rudny Altai [1], as well as to better constrain the genesis of ten craters in Madagascar, Northern Italy, and Siberia. The impact craters identified only according to morphology are assigned validity grade 2 in the Catalog [1], which means "potential craters" in the five-grade (0 to 4) scale of I. Zotkin and V. Tsvetkov [69].

We study the morphology of impact structures by shaded relief modeling, using NASA data arrays of SRTM (Shuttle Radar Topography Mission) and ASTER GDEM (Global Digital Elevation Model) (Figure 29), with the digital mapping technology as described above.
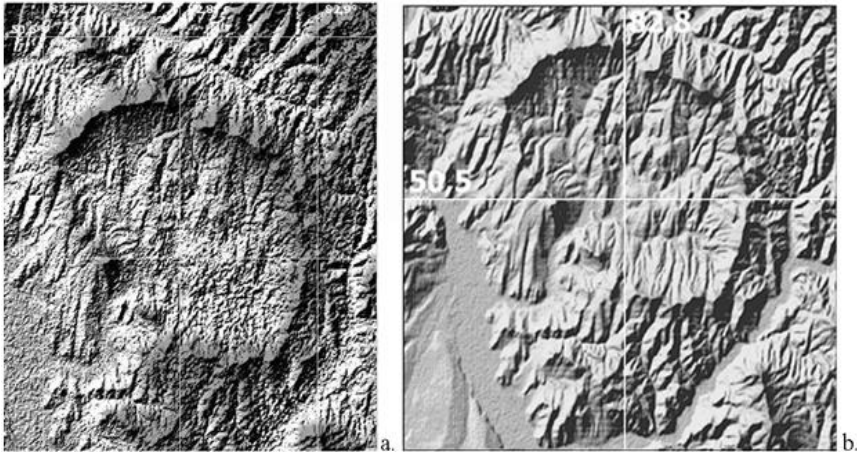
Figure 29. Figure 29. Probable astrobleme Volchikhinskaya: a) GIS-EISC shaded relief model (ASTER GDEM data), b) lower-resolution shaded relief model (SRTM data).

The new method of detecting impact craters consists in selecting optimum foreshortening of an image, or illumination parameters and shadow depth, to fill the gaps caused by modification of impact craters affected by erosion, deposition, tectonism or volcanism.

This image processing procedure allows detecting RS in a series of elevation models, as well as collecting evidence for standard elements diagnostic of CRSs. The procedure of CRSs identification includes several steps [61]:

1)   selecting typical morphological models for possible CRS of the region;
2)   selecting diagnostic criteria to prove extraterrestrial genesis of RS;
3)   comparing the RS in point with the proven cosmogenic structures;
4)   revealing contrasts of the discovered elements with the surrounding terrain.

To investigate the crater-related landforms, we use Google Earth satellite images in addition to the shaded relief model. In this study we refer only to the impact structures from EISC [1] that are in good conditions, with undisturbed craters located in tectonically stable areas (cratons or shields), with minimum of magmatism and sedimentary cover.

The approach was applied earlier to Rudny Altai, where the primary cosmogenic terrain has been perfectly preserved, and led to discovery of morphological elements of potential astroblemes (later confirmed in other regions as well), for example [62]: *raised rims*, *shadow* of *central cavity*, *"braces"* (called "*bank ridge*", "*central impact cone*", and "*stiffening ribs*", respectively, in [62]),and *mini-craters*.

Post-Impact Environmental Effects on the Crater Shape

Identification of CRSs may be problematic because post-impact environmental effects (e.g., erosion) can distort the proportions of the crater elements. However, according to evidence from many regions with preserved original cosmogenic terrain [1], erosion is less destructive for large craters (D > 1 km) than subsequent impact events or tectonic activity. For instance, the India-Eurasia collision, which has produced the great Himalayas–Tien-Shan– Altai–Sayan collisional system, can have "milled" many older astroblemes. Therefore, in identifying an impact crater one has to be aware of its possible modification by later tectonic movements (e.g., the case of Sudbury [1, 61]).

We [62] revealed such tectonic effects on the morphology of the potential *Madagascar* 1-5 impact structures discovered in 2006 by Matteo Chinellato (Tessera, Venetia, Italy). With the above method, we have identified both the main morphological elements and the post-impact tectonic evolution of Madagascar 1 [1] (D = 290 km) (Figures 30 a-c). Namely, we recognized the other half of the Madagascar-1 giant crater on the African plate [62] according to its typical morphological elements of a depression, raised rims (Figure 30a) and a central peak (Figure 30c), besides the elements of RS deciphering [70].
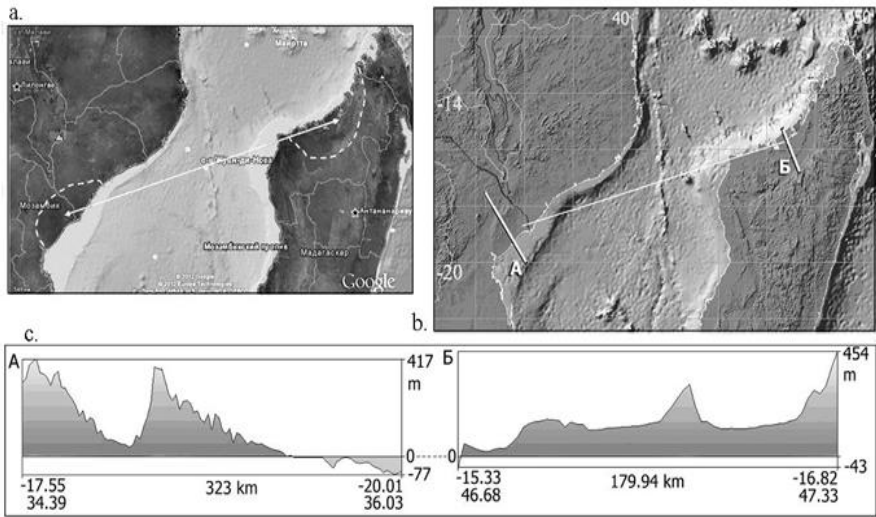
Figure 30. Contours of the Madagascar-1 crater ina Google Earth map [62] (a), a GIS-EISC digital elevation model(b), and in cross sections along profiles A and B (b) showing the entire crater ring (in GIS-EISC) (c).

Following the coastline contours (Figures 30: a-b) one can trace a probable location of the Africa-Madagascar junction (separated no earlier than 150 Ma). The fault line (underwater line in Figure 30b) breaking the RS in half is parallel to the major axis of the structure and, possibly, to the ballistic trajectory of a falling cosmic body (the direction of impact). The Madagascar half of the crater is shifted, likely due to velocity difference of the Madagascar terrane relative to the African plate. The seafloor motion direction is confirmed by the map of linear magnetic anomalies for the adjacent spreading zone [62, 71].

Thus, the new approach, with the updated morphological diagnostic criteria revealed by GIS technology and remote sensing, allows identifying impact craters even if they have been affected by active geological processes.

The potentialities of the EISC and EEDB GIS systems have been combined into a single version of GIS ENDDB, using gravimetric data uploaded into the GIS Database for both seismological and impact cratering applications.

PART 4. GRAVITY DATA AND NEW APPLICATIONS OF ENDDB

A. V. Mikheeva and An. G. Marchuk

The ENDDB system has acquired new applications as it processes satellite gravity and high-resolution topography survey remote sensing data. This allows verifying recently found diagnostic morphological elements of impact structures and revealing geomorphic patterns of seismic structures, using the respective EISC [1] and earthquake catalogs. With our complete global catalog EISC [1], one can identify typical persistent elements of impact structures, compare them, and estimate their diagnostic validity.

ENDDB System: Main Features and Geoinformation Technologies

The subject database of the ENDDB system is a combination of the EISC catalog and seismological data of more than 60 earthquake catalogs. Mathematical methods of catalog studies from GIS EEDB allow visualizing samples of the EISC catalog in a pseudo-3D background map according to the legend, or in the map scale.

ENDDB uses the NASA ASTER GDEM data arrays to obtain a high-resolution (1 arc-second) shaded relief model, as well as the digital mapping technology, which consists in shading surface points according to their brightness controlled by the illumination angle. A special technique has been developed to add fragments of ASTER GDEM open-file data into the ENDDB environment. This special operation is necessary because simple introducing of a single global file with high-resolution topographic data into ENDDB would be unfeasible (the system size of such file should be $1.62*10^{12}$ bytes). Incorporating the high-resolution data for an area of impact or seismic structures takes only a few minutes and consists in downloading the selected geographic area files from Internet (or Archive), converting their raw formats to ASCII by *Global Map*, with subsequent conversion of the ASCII file to the ENDDB format using a specially designed converter and the corresponding changes in the text file describing the external arrays. Besides these incorporated fragments, ENDDB stores elevation data of the same resolution as in EEDB (see above).

For modeling a shaded gravity anomaly with the ENDDB tools, *Global marine gravity* data (of models V16.1 and V18.1 [72]) are embedded into the system. These models, which are arrays of gravity pixel values, are of the same size (resolution), but V16.1 gives the maximum resolution only for the marine global map, while V18.1 includes also the land and can update data for coastal areas by interpolation. The resulting resolution of the V18.1 model becomes uneven only latitudinally because the original (Mercator) projection distorts the cells, and we transform it into a rectangular (i.e. transverse cylindrical conformal) projection. As a result, the resolution increases from the equator to the poles, being 30 arc-seconds per point on average, which is the same as in the more recent V21.1 model.

The gravity data sources for all these models are from the ERS-1 and Geosat/GM missions, as well as the recently published EGM-2008 global gravity model [72].

Identifying impact craters by ENDDB begins with selecting the optimum base colors of the image, the parameters of illumination and shadow depth [62] for shaded modeling on a regular grid. This procedure allows obtaining precise 3D images of the terrain and gravity patterns, and, moreover, furnishes data for recognizing standard morphological elements diagnostic of impact structures.

Typical Elements of Impact Craters Identified in GIS Digital Models

In addition to the elements reported in [7, 62], the EISC catalog [1] includes other new morphological elements typical of impact structures, which are expressed in the shaded elevation and gravity models and identified using the ENDDB visualization tools: *tail-shaped asymmetry, heart-shaped geometry of craters, and tail-shaped gravity lows*.

The tail-shaped crater asymmetry is an elongate topographic low accompanying the ring depression of the main crater (of a similar or even lesser expression) (Figure 31a-b).

This asymmetry was observed in eight reliably proven and four probable impact craters, as well as in seven potential and two questionable structures. To assess the diagnostic validity of this element, one has to take into account the astrobleme relaxation associated with the sedimentation rate and duration, besides the destructive effects of erosion, tectonism, volcanism, and later meteoritic activity [62]. For example, for the 455 Ma Lockne crater [1, 75],

preference is given to geologically expressed tail-shaped anomalies rather than to its topography because the impact-produced topographic lows have been filled with sediments, and the "tails" expressed in the modern surface topography (a lake contour) strike in a different direction.
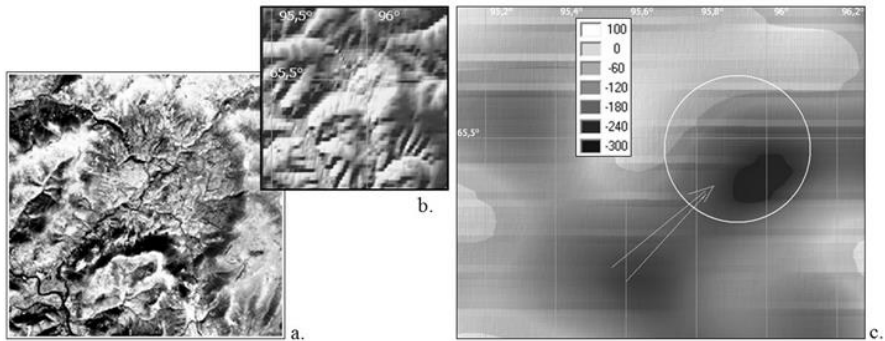
Figure 31. Tail-shaped asymmetry of the Logancha impact crater expressed in Google Earth satellite images (a), the ENDDB elevation model (b), and in the map of gravity anomalies accommodating the Logancha astrobleme obtained according to [72] (c). The scale shows gravity in mGal.

On the other hand, the probability of tail-shaped anomalies in an impact structure may depend on the kinematics of crater formation: the speed of the cosmic body (CB) and angle of its entry into the atmosphere. Particularly, for the Logancha crater [1] (Figure 31), the CB entry at a relatively low angle produced another morphological feature, a sort of *braces* on the frontal outer side, with gaps between them filled with recent sediments. More geomorphic evidence for the low-angle CB trajectory may come from its direction to a chain of minor craters or from the frontal part of the crater being prominent against the surrounding terrain, i.e. a shoe-shaped crater rim (e.g., in the Erofeev crater [1], Figure 32).

Some tails have a bending geometry (e.g., the Karikkoselkä, Möckeln, Korpinen, and Lasnamäe craters [1]). If they were produced by an energy (gravitational) influence of a cosmic body [73], the latter would appear to have "maneuvered" before falling. The same bends were observed also in the tail-shaped zones of craters imaged in gravity anomaly maps [73]. They may result either from the original gravity (density) heterogeneity of the target rocks, or from density decrease by explosion-induced brecciation [74]. The latter explanation is especially relevant to tails with prominent concentric anomalies inside [73]. The brecciation and fracture of rocks are caused by shock waves

from air-gas explosions associated with the CB motion through the atmosphere to the surface. However, the bending tail-shaped depressions rather suggest gradual destruction of the body on its way through the atmosphere, which forms a train of debris behind the body (the tail) thus elongating the impacted area of land.
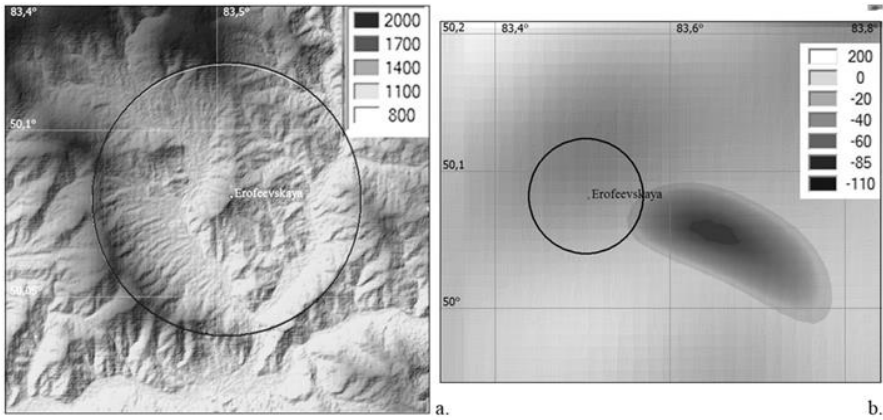
Figure 32. A shoe-shaped crater form and a tail-shaped gravity low of the Erofeev structure (D=10 km): a) the astrobleme relief according to ENDDB, b) gravity anomalies according to ENDDB. Note the resolution difference between the elevation and gravity data. The scale shows gravity in mGal.
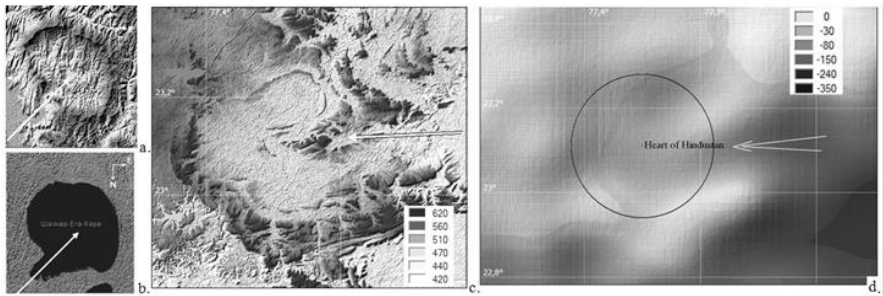
Figure 33. Tail-shaped relief anomalies and heart-like geometry of craters, according to ENDDB: a) Volchihinskaya probable structure, b) Chalkar-Yega-Kara yet questionable structure, c) Heart of Hindustan potential structure [1]. d) Gravity anomalies of Heart of Hindustan crater, according to [72]. The scale shows gravity in mGal.
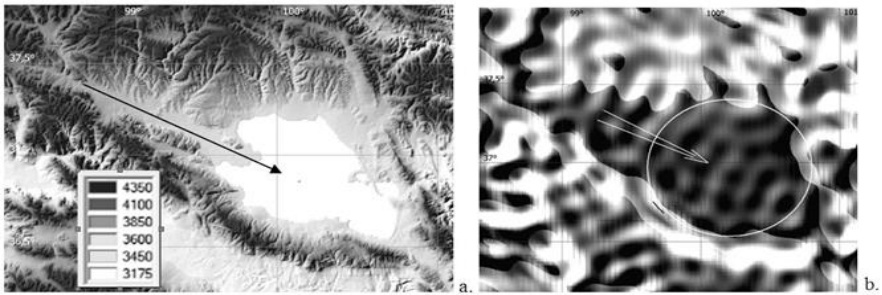
Figure 34. A heart-shaped crater of the Qinghai Lake probable structure (D=60 km) [1] according to ENDDB: a) relief according to ENDDB, b) tail-shaped gravity anomalies according to [72]. Dark color shows gravity lows.

A *heart-shaped geometry* is another morphological feature of craters, in addition to the tail-shaped asymmetry, likewise identified according to EISC [1]. This geometry is quite common to impact structures in the catalog (Figures 33, 34); some heart-shaped structures also have larger or smaller "tails" (e.g., the Lasnamäe crater [1]).
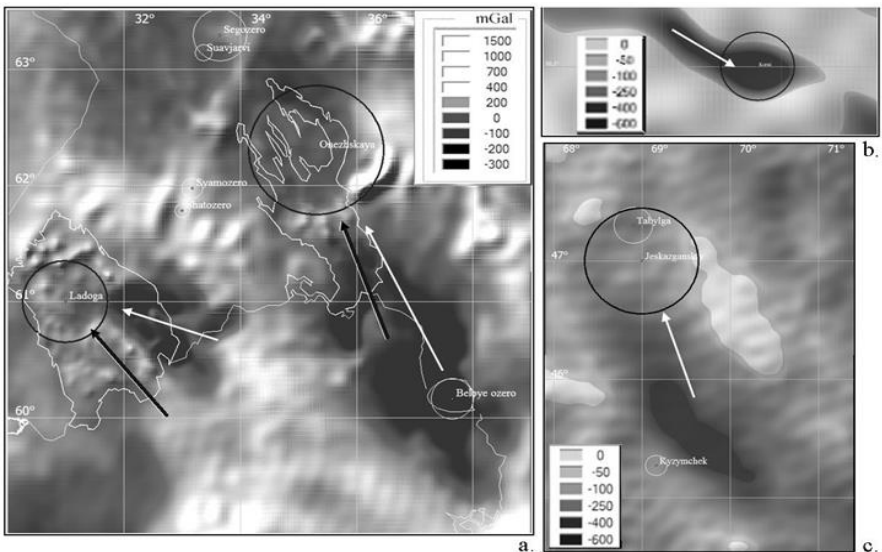
Figure 35. Tail-shaped gravity low according to ENDDB, accompanying potential astroblemes: a) Ladoga (D=80 km, 0.0385 Ma) and Onega (D=125 km, 0.0385 Ma), b) Kurai Basin (D=21,5 km, 34-200 Ma), c) Jeskazgan (D=100 km). Arrows in (a) show the direction of CB trajectory, determined from tail-shaped forms filled with water (black) and from gravity lows [72] (white). The scale shows gravity in mGal.

Earlier [62] we explained the formation of such crater landforms by superposition of three impact structures of different diameters with a common rim produced by an originally single falling body, which broke down but did not disperse into pieces. This asymmetry, even in the absence of a tail, is a reliable indicator of the CB trajectory (Figures 33, 34).

Both the 3D elevation model of ENDDB (Figures 31-34) and *Google Earth* 3D satellite images can highlight the morphological elements of impact structures at the optimum image foreshortening, or if the depressions are filled with water or thick vegetation (Figure 31a) [1].

Another diagnostic feature found in hundreds of craters from the EISC-catalog using ENDDB is associated with gravity: *tail-shaped gravity lows* [73] that accompany large astroblemes (Figures 31c; 32b; 33d; 34b). Assuming that the gravity lows and the tail-shaped asymmetry in craters are of the same origin, one may expect these features to appear in couple. Note, however, that such comparison is possible only for relatively large craters (D $\gg$ 15 km), the resolution of the available gravity data being much inferior to that of the elevation models (~ 30 sec per point in V 21.1 against 1 sec in ASTER GDEM). At the same time, the estimates of CB arrival direction from different morphological features may be ambiguous for individual structures [75].

For example, all three indicators we describe give similar azimuth estimates of ~ 300° in the case of the Qinghai structure (Figure 34) but show a 30-35° difference for the proven Wanapitei and Popigai craters [7, 73, and 75]. The variations in CB arrival azimuths estimated from tail-shaped asymmetry and gravity lows for the potential Ladoga and Onega structures (Figure 35) are 25° and 5°, respectively (the contours of the lakes are colored white and show a tail-shaped asymmetry).

We have checked the diagnostic value of tail-shaped negative gravity anomalies with craters in Russia using the Gravity maps 2010, scale 1:2500,000 and found this feature in **all** large craters produced by bodies for which we can assume a trajectory with a relatively low angle to the Earth's surface [73]. However, large proven structures (D > 15 km) are quite few in Russia (only 9), and it is important to check this pattern on a global scale. Indeed, the gravity imprints of CB trajectories show up in the new shaded model of "Global marine gravity" for hundreds of astroblemes (the data are available at the website [1]). Furthermore, gravity as part of the GIS-ENDDB system can be useful to prove the impact origin of many less certain structures (Figure 35), such as submerged or small island structures (where a small island is a part of a crater).
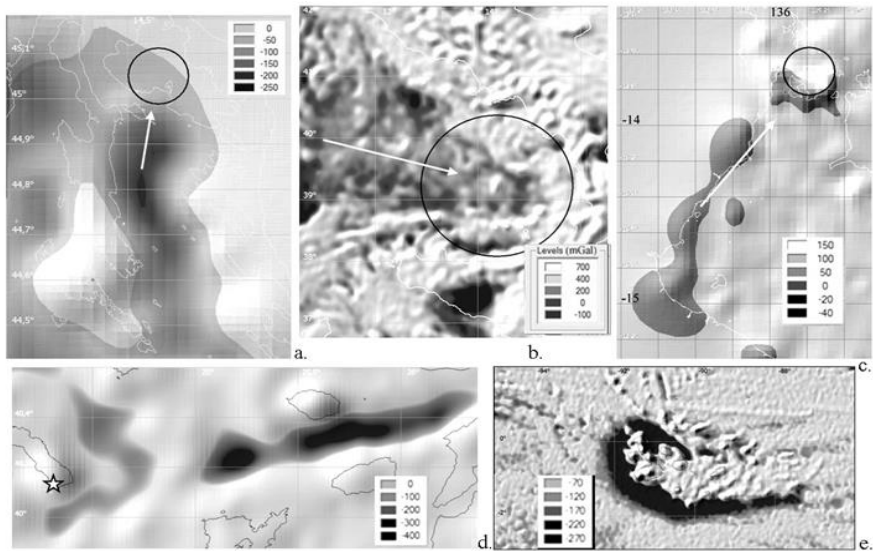
Figure 36. Tail-shaped gravity lows according to ENDDB that accompany potential underwater astroblemes: a) Krk (D=14 km, 40.4 Ma), b) Tyrrhenian Basin (D=200 km, 0.01 Ma), c) Bickerton Island (D=30 km), d) Athos (the observation point of 2003.07.21 is asterisked), e) Galapagos (D=14 km). Images (a) and (c) are obtained with V15.1; the other maps of this and previous figures are obtained with V18.1 [72]. The scale shows gravity in mGal.

Visual observation of submerged craters is difficult, and analysis of geophysical evidence in this case is simpler than the analysis of morphology. The surface gravity anomalies mimic the round shapes of well-preserved craters, which can be assigned to impact structures in the presence of a tail (Figure 36) even if no gravity data is available to reveal rootless anomalies. This assignment may be the first step in a complex study of submerged impact structures, when in addition to the standard geological and geophysical mapping methods there are such exotic ones as paleographical reconstructions of tsunami waves with location of the impact origin, or, for example, location of ring clouds and zones of oceanic heat flow anomalies [61].

Typical Structural Elements of Seismicity Identified in GIS Digital Models

The ENDDB (as well as its prototype GIS EEDB) software offers special methods for grouping related earthquakes: grouping earthquakes generated by

spatially proximal active faults, e.g., plate boundaries or seismic blocks (the groups can be revealed in the same way as detecting aftershocks, swarms, or clusters of earthquakes; spatial pattern recognition; migration of seismicity center, etc. [76]).
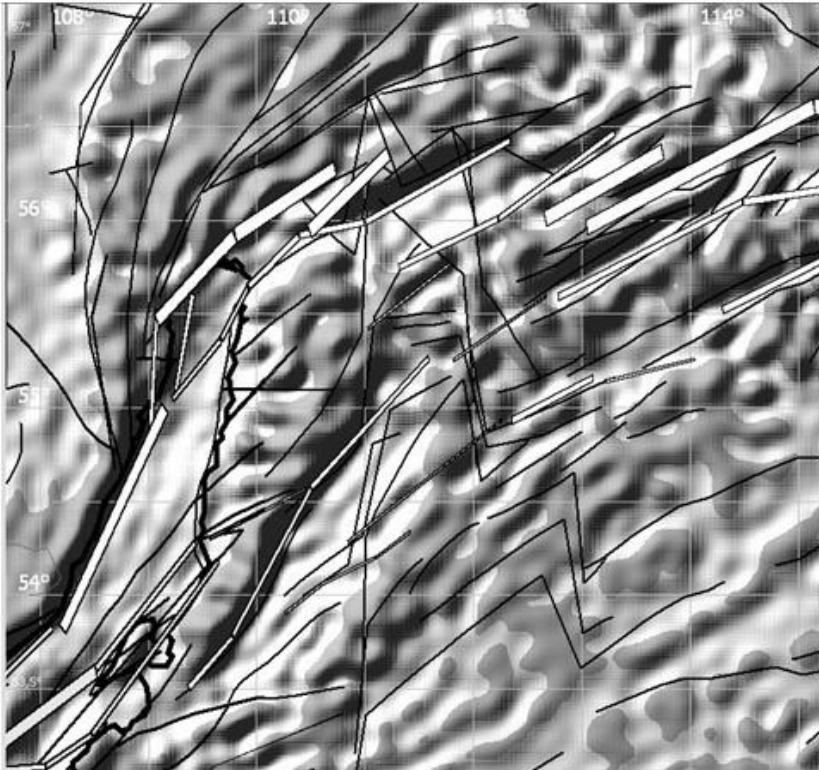
Figure 37. Gravity anomaly according to ENDDB along the boundaries of seismic blocks delineated by faults (black lines) and seismic lineaments (white bands according to [77]) in the northern Baikal Rift Zone. Dark color shows gravity highs or shadow.

For example, the algorithm for recognition of linear patterns (images) by a set of points distributed in space can identify some real straight and curved tectonic structures [78]. The algorithm implies setting up the maximum stepsize and deflection angle to find the next point in the chain of events on a seismic border. Thus, identified structures can be confirmed by geophysical data. Furthermore, the ENDDB geological-geophysical database contains layers of seismic lineaments, faults and trenches, which can indicate whether a

region under study consists of rigid (seismically inactive) or soft structures (Figure 37). Such comparison is necessary both to model a detailed crust structure by detecting seismic block boundaries or individual faults, and to study regional seismicity.

Another example shows how a gravity map can be used to detect the pattern of aseismic or weak seismic zones (Figures 38a), which have implications for interaction of rigid tectonic structures with orogens. This interaction was visualized using a special EEDB method suggested by P. Dyadkov for analyzing seismicity anomalies (activity and quiescence) proceeding from indicators of rigid zones (Figures 14, 38b-c).
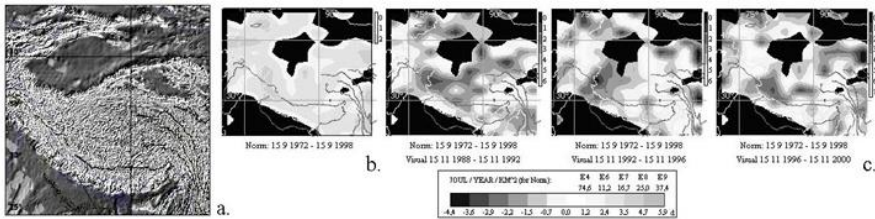
Figure 38. Spatial distribution of aseismic and weak seismic zones: a) gravity anomalies according to [72] and ENDDB tools (dark color shows gravity lows); b) distribution of average annual total energy for 1972-1998 taken as the norm; c) maps of aseismic areas (black) and zones of seismic quiescence (gray) in Central Asia, at every 4 years [24]. The maps were compiled using data of the combined earthquake catalog COMPLEX ($M \geq 4$, 1972-2000, 24-46º N; 70-102º E).

In conclusion, we illustrate the application of the method to the rigid structure previously identified (Figures 16-18, 22) by the seismicity analysis of Japan area along 38°N. The gravity map and vertical cross section AA show a prominent high in the epicenter of the pending Tohoku earthquake (Figure 39).

The examples of Figures 37, 39, as well as other evidence of relationship between the gravity and seismicity patterns [79], show that earthquakes are generally confined to prominent features of the gravity field. They are, for instance, regional and local gravity gradients at boundaries between blocks with different physical and structural properties, including active seismic boundaries. Note that regional features of the gravity field of a deep (most likely mantle) origin correspond to main structural elements of a zone bounded by seismic belts [79]. This determines the prospects of our future research.
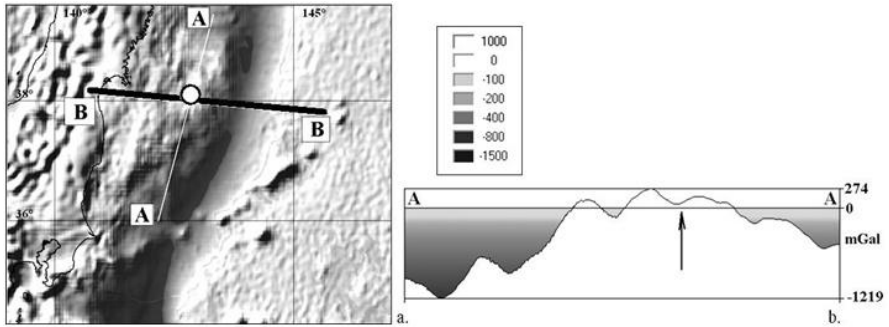
Figure 39. a) Gravity anomaly map of Tohoku earthquake area according to [72] and ENDDB tools. b) The vertical section AA of the gravity anomaly. White circle (a) and black arrow (b) show the Tohoku epicenter. The scale shows gravity in mGal.

CONCLUSION

The geoinformation system ENDDB (Earth's Natural Disasters Database) is an important tool to study natural disasters, such as earthquakes or impact events, using records of the respective catalogs. The GIS system has a user-friendly easy-to-run interface, detailed geographical databases for the whole Earth and its regions, and ample databases of seismological and impact structure parameters. With its mathematical support, ENDDB can plot frequency dependences of magnitudes or sizes (crater diameters) of events from various samples, as well as other distributions of integrated parameters in time and space, or with respect to one another. Necessity of using geological and geophysical parameters (gravity field, faults, etc.) for analysis of data from both EC and EISC (Catalogs of earthquakes and Earth's impact structures), has been a prerequisite for creating the combined system of ENDDB from its two prototypes, GIS EEDB (Expert earthquake database) and GIS EISC.

Introducing the gravity information into ENDDB expands largely its application; specifically, it has made possible detecting new morphological features characteristic of impact structures. It is especially important to find additional morphological indicators for the lack of absolutely reliable diagnostic features of extraterrestrial origin, even for the structures whose impact nature has been confirmed by rich shock-explosive evidence. This lack of certainty has given reason to the opponents of the impact genesis of ring structures to continue vigorous debates in the literature. Note that the asymmetry of different geomorphic characteristics of impact craters, and, in

particular, the tail-like shapes of related geological and geophysical fields or morphological anomalies (including the present-day topography), allows discriminating impact structures from ring structures of magmatic origin, to a large degree of confidence.

The use of gravity information is important for some seismological objectives as well, specifically, for identifying seismic blocks, lineaments, and other seismic-morphological structures revealed by means of GIS-ENDDB visualization and mathematical tools during analysis of the spatial patterns of seismicity.

An obvious advantage of the presented system consists in the possibility for its continuous updating with the advance in methods and technologies.

The authors are grateful to I.I. Kalinnikov (Institute of Physics of the Earth RAS, Moscow), K.K. Khazanovich–Wulff (Planetology Department of the Russian Geographical Society, St Petersburg) for useful discussions and ideas.

REFERENCES

[1]   Mikheeva, A.V. (2013). The Complete Catalog of the Earth's Impact Structures. *labmpg.sscc.ru/impact/index1.html*.
[2]   Mikheeva, A.V. On studying of natural disasters using the Earth's remote sensing materials; Proc. Latin American Remote Sensing Week (LARS 2013), October 23-25; Santiago de Chile, 2013.
[3]   Dyadkov, P.G.; Mikheeva, A.V. The EEDB – Expert Earthquake Database for Seismic Geodynamic Research. Bull. Novosibirsk Computing Center. Ser. Math. Model. in Geoph. 2010, vol. 13, pp. 15-30.
[4]   Mikheeva, A.V.; Djadkov, P.G. Methods of complex analysis used for learning the seismicity regularities and anomalies; Digital conference proceedings: 25th International cartographic conference of the ICA (Paris, 3-8 July 2011); Paris, 2011.
[5]   Mikheeva, A.V. Studying a spatial-temporal distribution of seismicity in the area around Fukushima Prefecture by GIS-EEDB program tools. Bull. Novosibirsk Computing Center. Ser. Numer. Anal. 2013, vol.16, pp. 65-79.
[6]   Mikheeva, A.V. General laws of spatial-temporal distribution of the Earth's impact structures. Bull. Novosibirsk Computing Center. Ser. Math. Model. in Geoph. 2010, vol. 13, pp. 127-140.

[7]   Khazanovitch-Wulff, K.K.; Mikheeva, A.V.; Kuznetsov, V.F. Structural elements of some astroblemes indicating directions of cosmic body trajectories. New Concepts in Global Tectonics Newspaper. 2013, vol. 1, no. 3 (September 2013), pp. 11-19.

[8]   Gusiakov, V.K.; Marchuk, An.G.; Titov, V.V. Application of new numerical methods for near-real time tsunami height prediction; Book of Abstracts: International Tsunami Meetings, July 31 - August 10, 1989; Computing Center, Novosibirsk, USSR, 1989.

[9]   Gusiakov, V.K.; Marchuk, An.G.; Titov, V.V. An interactive software package for numerical simulation of tsunami on a personal computer; Book of Abstracts: Marine Natural Disasters (tsunami and storm surge), 17-20 September 1990; Gorky: GPI, 1990.

[10] Gusiakov, V.K.; Marchuk, An.G.; Titov, V.V. Interactive software for near-real time tsunami modeling; Program and Abstracts: XX IUGG General Assembly, Vienna, 11-24 August 1991; IASPEI, Technical University, Gratz, Austria, 1991.

[11] Gusiakov, V.K.; Marchuk, An.G.; Titov, V.V. Interactive system of tsunami modeling on a personal computer; Vychislitelnye Tekhnologii; Novosibirsk: ICT SB RAS, 1992; Vol. 1, no. 3, pp. 189-195.

[12] Gusiakov, V.K.; Osipova (Mikheeva), A.V. The Earthquake and Tsunami Database of the Kuriles-Kamchatka region; Preprint No. 976; Novosibirsk: CC SB RAS, 1992; 20 p. (in Russian)

[13] Gusiakov, V.K.; Marchuk, An.G.; Osipova (Mikheeva), A.V. Expert tsunami database for the Kuriles-Kamchatka region. Bull. Novosibirsk Computing Center. Ser. Math. Model. in Geoph. 1994, vol.1, pp. 65-77.

[14] Gusiakov, V.K.; Marchuk, An.G.; Osipova (Mikheeva), A.V. Expert tsunami database for the Pacific region; Proc.: The International Emergency Management and Engineering Conference, April 18-21, 1994; J. Sulivan and S. Tufekci; Ed.; Hollywood Beach, Florida, USA, 1994; pp. 247-252

[15] Summary report; Fifteenth session of the international coordination group for the tsunami warning system in the Pacific (Papeete, Tahiti, French Polynesia, July 24-28, 1995); Paris: IOC/UNESCO, 1995; 50 p.

[16] Marchuk, An.G. Technique for digitizing bathymetry information using personal computer. Bull. Novosibirsk Computing Center. Ser. Math. Model. in Geoph. 1994, vol. 1, pp. 79-86.

[17] Marchuk, An.G. Technology for creating digital bathymetric information on PC; Vychislitelnye Tekhnologii, Special Issue *Computational Technologies-94* (Proc.: Conference on Numerical Methods for Wave

Hydrodynamics, Novosibirsk, ICT SB RAS, 2-4 October 1994); Novosibirsk: ICT SB RAS, 1995; Vol. 11.

[18] Marchuk, An.G. Interactive system for digitizing geographic and bathymetry information. Bull. Novosibirsk Computing Center. Ser. Math. Model. in Geoph. 1998, vol. 7, pp. 186-198 (in Russian).

[19] Marchuk, An.G. Technological support to create a bathymetric database for the modeling tsunami waves. Bull. Novosibirsk Computing Center. Ser. Math. Model. in Geoph. 1998, vol. 5, pp. 152-160 (in Russian).

[20] Marchuk, An.G. Providing detailed digital bathymetry data for tsunami modeling and warning; Proc.: NASA-FEMA-GWU Conference on the Applications of Remote Sensing and GIS for Disaster Prevention, January 19-21, 1999; Washington, DC, USA, 1999.

[21] Gusiakov, V.K.; Osipova, (Mikheeva), A.V.; Marchuk, An.G. Expert tsunami database for the Pacific: motivation, design and proof-of-concept demonstration region; Perspectives on Tsunami Hazard Reduction: Observation, Theory and Planning; G. Hebenstreit; Ed.; Dordrecht-Boston-London: Kluwer Academic Publishers, 1997; pp. 21-34.

[22] Gusiakov, V.K.; Ivaikin, D.V.; Marchuk, An.G. A simple Windows-based geographic mapping system for visualization and analysis of seismic and tsunami data; Proc.: NASA-FEMA-GWU Conference on the Application of Remote Sensing and GIS for Disaster Management (Washington, USA, January 19-21, 1999); Washington, DC, USA: George Washington University, 1999; CD-ROM; Track 4.

[23] Lyskovsky, A.V.; Marchuk, An.G.; Petrenko, V.E. Monitoring tracks of catastrophic events using global geophysical databases; Book of Abstracts: V Conference "Advanced Studies of Natural Phenomena". Krasnoyarsk, August 17 - 23, 1999.; Krasnoyarsk: ICM SB RAS, 1999; pp. 130-135.

[24] Mikheeva, A.V.; Dyadkov, P.G.; Marchuk, An.G. GIS-EEDB geoinformation system and methods for space-time analysis of seismological data. Geoinformatika. 2012, no 2, pp. 58-65.

[25] Emanov, A.F.; Filina, A.G.; Emanov, A.A.; Fateev, A.V.; Leskova, E.V. Altai and Sayan Mountains. Earthquakes of Northern Eurasia in 2000; Obninsk: GS RAS, 2006; pp. 127-136.

[26] Mel'nikova, V.I.; Gilyova, N.A.; Masal'skij, O.K.; Radziminovich, J.B. Pribaikalia and Transbaikalia. Earthquakes of Northern Eurasia in 2000; Obninsk: GS RAS, 2006; pp. 137-145.

[27] Rautian, T.G. Methods of Detailed Seismicity Analysis; Moscow: USSR Acad. of Sci., 1960 (in Russian).

[28] Riznichenko, J.V. The epicenter sizes of crustal earthquakes and seismic moment; Research into Physics of Earthquakes; Moscow: Nauka, 1976; pp. 9-27.

[29] Prozorov, A.G. A dynamic algorithm for separating aftershocks in the world catalog of earthquakes; Mathematical methods in seismology and geodynamics. Computing Seismology; Moscow: Nauka, 1986; Vol. 19, pp. 58-62.

[30] Ebel, J.E.; Kafka, A.L. A non-Poissonian element in the seismicity of the Northeastern United States. Bull. Seism. Soc. Amer. 2002, vol. 92, no. 5, pp. 2040-2046.

[31] Petrenko, V.E.; Marchuk, An.G. Estimation of the big cosmic bodies impact frequency and possibility of cosmogenic tsunamis; Proc.: Disaster and Emergency Management: International Challenges for the Next Decade. Proc. Intern. Emergency Management Society Conference-1998; Washington DC: The George Washington University, 1998; pp. 435-443.

[32] Smith, W.H.F.; Sandwell, D.T. Global seafloor topography from satellite altimetry and ship depth soundings. Science. 1997, vol. 26, no. 277.

[33] Gusyakov, V.K.; Osipova (Mikheeva), A.V. An automated catalog of earthquakes and tsunamis in the Kuriles-Kamchatka area; Vychislitelnye Tekhnologii; Novosibirsk: IVT SB RAS, 1992; Vol. 1, no. 3, pp. 197-204.

[34] Utsu, T. Aftershocks and earthquake statistics; J. Faculty of Science; Japan: Hokkaido University, 1970; Ser. 7, vol. 3, no. 4, pp. 197-266.

[35] Zavyalov, A.D. Medium-Term Earthquake Prediction: Principles, Methods, and Practice; Moscow: Nauka, 2006; 256 p. (in Russian).

[36] Sobolev, G.A.; Ponomapev, A.V. Physics and Precursors of Earthquakes; Moscow: Nauka, 2003 (in Russian).

[37] Arefiev, S.S. Seismic Source Study; Moscow: Akademkniga, 2003 (in Russian).

[38] Gitis, V.G.; Ermakov, B.V. Fundamentals of Existential Prediction in Geoinformatics; Moscow: Physmathlit, 2004; 256 p. (in Russian).

[39] Riznichenko, J.V. (Editor) Seismic Shaking Intensity Division of the USSR Territory; Moscow: Nauka, 1979 (in Russian).

[40] Tyurin, Yu.N.; Makarov, A.A. Statistical Data Analysis with PC; V.E. Figurnov; Ed.; Moscow: Infra-M, 2003; 544 p. (in Russian).

[41] Riznichenko, J.V. Problems of Seismology; Moscow: Nauka, 1985 (in Russian).

[42] Vostrikov, G.A. Correlation among the parameters of the magnitude-recurence relationship, seismic flow and seismic sources. Transactions GIN RAS, Moscow. 1994, vol. 482, pp. 1-19. (in Russian).

[43] Dyadkov, P.G.; Nazarov, L.A.; Nazarova, L.A.; Mikheeva, A.V.; Kuznetsova, J.M. Possible influence of the 2001 Northern Tibet and 2003 Hokkaido earthquakes on nucleation of the Altai earthquake. Fizicheskaya Mezomekhanika. 2006, vol. 9, no. 1, pp. 67-72.

[44] Dyadkov, P.G.; Kuznetsova, J.M. Seismicity anomalies prior to large Altai earthquakes. Fizicheskaya Mezomekhanika. 2008, vol. 11, no. 1, pp. 19-25.

[45] Mikheeva, A.V.; Vazhenin, A.P. Application of EEDB program tools on the example of studying seismicity of the area around Fukushima Prefecture; International Scientific–Practical Conference "Actual Issues of Seismic Science in the Prosperous Epoch of the Powerful State" (October 2, 2013, Ashgabat); Turkmenistan, 2013; pp. 39-41.

[46] Licht, F.R. Transit Line morphostructures in CCI geomorphologic space. Laws of the structure and evolution of the geosphere; Proceedings of 4th International Interdisciplinary Scientific Symposium; Khabarovsk, 1998; pp. 28-31.

[47] Imanishi, K.; Ando, R.; Kuwahara, Y. Unusual shallow normal-faulting earthquake sequence in compression northeast Japan activated after the 2011 off the Pacific coast of Tohoku earthquake. Geophys. Res. Lett. 2012, vol. 39, no. 9, L09306.

[48] Nakata, T.; Goto, H.; Watanabe, M.; Suzuki, Y.; Nishizawa, A.; Izumi, N.; Horiuchi, D. and Kido, Y. Active faults along the Japan Trench and source faults of large earthquakes; Proc.: International Symposium on Engineering Lessons Learned from the 2011 Great East Japan Earthquake; 2012; pp. 254–262.

[49] Imaev, V.S.; Imaeva, L.P.; Kozmin, B.M. Seismotectonic and other processes at northeastern Asia and Alaska plate boundaries. Tikhookeanskaya Geologiya. 1998, vol. 17, no 2, pp. 3-17.

[50] Zhao, D.; Huang, Z.; Umino, N.; Hasegawa, A. and Kanamori, H. Structural heterogeneity in the megathrust zone and mechanism of the 2011 Tohoku-oki earthquake (M_w 9.0). Geophys. Res. Lett. 2011, vol. 38, L17308.

[51] Zhao, D. Mechanism of the 2011 Tohoku-oki earthquake (M_w 9.0) sequence: Insight from seismic tomography; Proc.: G-COE Symp. 2012

"Achievement of G-COE Program for Earth and Planetary Dynamics and the Future Perspective", Japan, Sendai, September 25-28, 2012; A3-01.

[52] Kanamori, H. Rupture process of subduction-zone earthquakes. Ann. Rev. Earth Planet. Sci. 1986, vol. 14, pp. 293-322.

[53] Zhao, D.; Matsuzawa, T. & Hasegawa, A. Morphology of the subducting slab boundary in the northeastern Japan arc. *Phys. Earth Planet. Int.* 1997, vol. **102,** pp. 89–104.

[54] Maercklin, N.; Festa, G.; Colombelli, S.; Zollo, A. Twin ruptures grew to build up the giant 2011 Tohoku, Japan, earthquake. Scientific Reports. 2012, vol. 2: 709, October; DOI: 10.1038/srep00709.

[55] Kobayashi K. et al. Outer slope faulting associated with the western Kuril and Japan trenches. Geophys. J. Intern. 1998, vol. 134, no. 2, pp. 356-372.

[56] Djadkov, P.G.; Kuznetsova, J.M.; Mikheeva, A.V. Study of weak seismicity anomalies before strong earthquakes in southern areas of Siberia for medium-term forecast; Proc.: Asian Seismological Commission V General Assembly (Yerevan, Armenia, 18-21 October 2004); Yerevan, 2004; pp. 217-218.

[57] Zhurkov, S.N. Kinetic concept of strength. Doklady AN USSR. 1968, vol. 3, pp. 46-52.

[58] Alekseev, A.S.; Mikheeva, A.V.; Petrenko, V.E. Website "Catalogue of the Earth's impact structures"; Book of Abstracts: Conf. "Impact craters as indicators for planetary environmental evolution and astrobiology", Östersund (Sweden), June 8-14, 2006.

[59] Zejlik, B.S. The origin of arched and ring structures on the Earth and other planets (impact-explosive tectonics); M.: Geoinform, 1978; 58 p. (in Russian)

[60] Dabizha, A.I.; Zotkin, I.T.; Fedynskij, V.V. Distribution of meteoric craters on the Earth's surface; Meteoric Structures on the Surface of Planets; Moscow, Nauka, 1979; pp. 117-125 (in Russian).

[61] Alekseev, A. C.; Petrenko, V.E. Estimating the frequency of impact events on the Earth: possibility for their preliminary detection and change of trajectories; Report of SR, AS USSR; Novosibirsk, Computing Center, 1991; 128 p. (in Russian)

[62] Mikheeva, A.V.; Kusnetsov, V.F. On studying morphological features of impact craters using the Earth's remote sensing materials. Bull. Novosibirsk Computing Center. Ser. Num. Model. Atmosph. Ocean and Env. Studies. 2012, vol. 13, pp. 57-69.

[63]   Zeilik, B.S. Shock-explosive tectonics and a plate tectonic synopsis; Alma-Ata: Gylym, 1991; 120 p. (in Russian)

[64]   Bryukhanov, A.N. [et al.]. Satellite-derived Geological Map of the USSR, scale 1:2500000. 1984.

[65]   Petrov, O.V.; Morozov, A.F. (Editors), Satellite-derived Geological Map of Russia, scale 1:2500000; SPb.: FGUP "VSEGEI", 2011.

[66]   Marchuk, An.G.; Simonov, K.V.; Peretokin, S.A. Detection of possible impact structures at the bottom of the ocean by gravimetric and magnetometric data processing; Proc.: Protecting the Earth against Collisions with Asteroids and Comet Nuclei. International Conference "Asteroid-Comet Hazard-2009"; A. Finkelstein, W. Huebner, V. Shor; Eds.; SPb.: Nauka, 2010; pp. 206-210.

[67]   Masaitis, V.L. [et al.]. Geology of Impact Craters; Leningrad: Nedra, 1980; 230 p. (in Russian)

[68]   Wegener, A. The Origin of Lunar Craters; 1921.

[69]   Zotkin, I.T.; Tsvetkov, V.I. Search for meteorite craters on the Earth. Solar System Research. 1970, vol.1, no. 4, pp. 5-65 (in Russian).

[70]   Pronin, V.G.; Filippova, V.A. Deciphering satellite images for petroleum prediction in inaccessible terrains of Central Asia; Studies of Petroleum Provinces Using Satellite and Aerial Imagery; Leningrad: VSEGEI, 1989; pp. 13-19 (in Russian).

[71]   Rundquist D.V. (2006). Electronic Earth. *earth.jscc.ru/index_en.php*.

[72]   Sandwell, D.T.; Smith, W. H. F. Global marine gravity from retracked Geosat and ERS-1 altimetry: Ridge segmentation versus spreading rate. J. Geophys. Res. 2009, vol.114, B01411, doi: 10.1029/ 2008JB006008.

[73]   Mikheeva, A.V.; Khazanovitch-Wulff, K.K. The gravity trace of the falling cosmic bodies trajectories. Bull. Novosibirsk Computing Center. Ser. Math. Model. in Geoph. 2013, vol. 16, pp. 89-103.

[74]   Zeilik, B.S. The Tunguska comet, a hydrogen super-bomb and space-related problems of sustaining life on the Earth. Otechestvennaya Geologiya. 2011, no.3, pp. 116-120.

[75]   Mikheeva, A.V. Comparison of morphological and geophysical features of some impact craters. Ecological Bulletin of Scientific Centers of the Black Sea Economic Cooperation. 2013 (in Russian).

[76]   Mikheeva, A.V.; Dyadkov, P.G.; Marchuk, An.G. Methods for spatial earthquake grouping in seismic-geodynamic studies with the GIS-EEDB information system; Proc.: XI All-Russian Conference with International Participation "Environmental Monitoring Problems" (Kemerovo, 24-28 October 2011); Kemerovo, 2011; pp. 166-171.

[77] Ulomov, V.I. (Editor-in-Chief). (2000). Earthquake Source Zones of Northern Eurasia. Global Seismic Hazard Assessment Program (GSHAP). Region 7. *http://www.seismo.ethz.ch/static/gshap/neurasia/*.

[78] Dyadkov, P.G.; Mikheeva, A.V. Methods for detection of spatial grouping earthquakes infor seismogeodynamic study in areas of Central Asia; Proc.: Mathematical Methods for Pattern Recognition. 15th All-Russian Conference (Petrozavodsk, 11-17 September 2011); Moscow: MAKS Press, 2011; pp. 560-563.

[79] Ippolitov, O.M.; Nadežka, L.I.; Efremenko, M.A. Comments on the relation between elements in the transformed gravity field and earthquake locations in the VKM territory. Proc.: Lithospheric Structure, Properties, Dynamics, and Metallogeny of the East European Platform. 16th International. Conf.; Voronezh, 2010; Vol. 1, pp. 312-316.

Chapter 8

ROLE OF GEOGRAPHIC INFORMATION SYSTEM FOR WATER QUALITY EVALUATION

Deepesh Machiwal[1], and Madan Kumar Jha[2],†*

[1]Central Arid Zone Research Institute, Regional
Research Station, Bhuj, Gujarat, India
[2]AgFE Department, IIT Kharagpur,
Kharagpur, West Bengal, India

ABSTRACT

    Water quality evaluation is an overall process of evaluating physical, chemical and biological nature of water in relation to natural quality, human effects and intended uses particularly uses which may affect human health and the health of the ecosystem itself. Interpretation of enormous water quality data in a convenient manner for visual inspection is an important but often underestimated or omitted step in a water quality evaluation program. Recently, need of modern approaches and tools for interpreting water quality is emphasized for efficient water quality management. Geographic Information System (GIS), with an ability of capturing, storing, analyzing, manipulating, retrieving and displaying spatial data, has emerged as a powerful tool for decision-making in

---

* Corresponding author: Deepesh Machiwal. Central Arid Zone Research Institute, Regional Research Station, Bhuj – 370 105, Gujarat, India. E-mail: dmachiwal@rediffmail.com, tel.:+91-2832-271238, fax: +91-2832-271238.
† Madan Kumar Jha: AgFE Department, IIT Kharagpur, Kharagpur – 721 302, West Bengal, India. E-mail: madan@agfe.iitkgp.ernet.in.

several areas including environmental field. This chapter aims at highlighting the role of GIS in synthesising, compiling, presenting and interpreting chemical data of both surface and ground waters. Firstly, few relevant fundamental terms and process of water quality evaluation are defined and/or described. Thereafter, the chapter contains theoretical procedure for applying GIS to assess spatial change or variability in water quality by characterizing extent and patterns of contamination. In general, a water quality monitoring network consists of a group of point locations with known chemical attributes of water. GIS helps converting the point values into areal information through spatial interpolation.

Hence, an overview of spatial interpolation techniques is provided, together with the methodologies for employing geostatistical modelling (kriging) and inverse distance weighting techniques and for computing spatial statistics (mean, median, standard deviation and coefficient of variation). The major application of GIS in past groundwater studies has been for assessing groundwater vulnerability.

Therefore, the concept of groundwater vulnerability along with its historical perspective is described and different GIS-based overlay and index methods used for groundwater vulnerability assessment are summarized. Methodologies for applying different GIS methods in evaluating the groundwater vulnerability are illustrated through flowcharts.

The major tools for describing groundwater vulnerability in GIS framework include DRASTIC, modified DRASTIC, DRAMIC, GOD, AVI, SINTACS, EPIK, GLA, PI and COP.

Furthermore, the development of GIS-based water quality index for evaluating water quality is discussed. Finally, combined use of GIS and multivariate statistical analysis techniques in delineating water quality zones is discussed. It is concluded that GIS is a promising geospatial tool which offers efficient framework for sustainable management of freshwater resources.

1. INTRODUCTION

Water quality is governed by a set of complex factors and there is large choice of variables use to describe water quality status in quantitative terms.

Hence, it is difficult to provide a simple definition for water quality. Water quality of the aquatic environment is defined by (a) set of concentrations, speciation, and physical partitions of inorganic or organic substances, (b) composition and state of aquatic biota in the waterbody, and (c) description of temporal and spatial variations due to factors internal and external to the waterbody (Meybeck and Helmer, 1992).

Water quality is also defined as a consequence of natural physical and chemical state of water (surface or subsurface) as well as alterations caused by human activities (Fetter, 1994). The quality of water is a measure of its suitability as a water supply source for domestic and agricultural consumption as well as for irrigation, industrial and other purposes; the suitability of water is decided based on criteria for various uses and water quality standards. The definition of water quality is therefore not objective; rather it is socially defined depending on the desired use of water. Different water uses require different standards of water quality and water quality criteria define desirable characteristics and acceptable levels of constituents for water of various intended uses (Freeze and Cherry, 1979; Todd, 1980; McCutcheon et al., 1993; Fetter, 1994). To establish quality criteria, the measures of *physical*, *chemical*, and *biological* constituents must be specified, together with standard methods for comparing results of water quality analyses (Todd, 1980; McCutcheon et al., 1993). The pollution of the aquatic environment can be defined as introduction of substances or energy by man, directly or indirectly, which result in such deleterious effects as harm to living resources, hazards to human health, hindrance to aquatic activities including fishing, impairment of water quality with respect to its use in agricultural, industrial and often economic activities (Meybeck and Helmer, 1992), and reduction of amenities (GESAMP, 1988). The term *pollution* refers to changes caused by humans and their actions that result in water-quality conditions that negatively impact the integrity of the water for beneficial purposes, including natural ecosystem integrity (Johnson, 2009). Determining the extent of pollution is difficult, given the wide range of constituent measures that characterize water quality (e.g., dissolved and suspended solids, organics, bacteria, toxics, and metals).

Evaluation of water quality, assessment of spatial and temporal variations and its vulnerability mapping are among the important tasks in order to manage quality of the useful water resources.

There are many tools and techniques for evaluating the water quality and geographic information system is one of them, which is gaining a wide popularity nowadays because of several advantages of the technique.

Geographic Information System (GIS) has emerged as a powerful tool for capturing, storing, analyzing, manipulating, retrieving and displaying spatial data and using these data for decision making in several areas including engineering and environmental fields (e.g., Stafford, 1991; Goodchild et al., 1993; Burrough and McDonnell, 1998; Lo and Yeung, 2003). It allows for swift organization, quantification and interpretation of a large volume of spatial data with a computer accuracy and minimal risk of human errors.

GIS is an effective tool for analyzing spatial and temporal data of water quality (Burrough and McDonnell, 1998; Gurnell and Montgomery, 2000; Chang, 2002; Chen et al., 2004). Information on spatial and temporal variability/trends of water quality is very helpful in the decision-making process (Freeze and Cherry, 1979; Todd, 1980; Fetter, 1994). In addition, water quality mapping is essential for monitoring, pollution hazard assessment, modeling and environmental change detection (Goodchild et al., 1993; Skidmore et al., 1997; Chen et al., 2004; Jha et al., 2007). In a GIS framework, point estimates of water quality parameters can be spatially interpolated by spatial interpolation techniques such as kriging, inverse distance weighting, etc. to develop parameter concentration maps at different time scales or other related maps. GIS presents spatial information in the form of maps where different features are located by symbols, and is integrated with databases containing multiple attributes' data of the mapped features. A map helps providing knowledge of where and what things are, and how they are related. The GIS database containing spatial and point attributes can then be used to generate interactive reports and maps, which in-turn can support decision-making about the best design alternatives and their impacts. Furthermore, GIS-based maps serve as powerful communication medium in presenting information in such a way that the people involved in the planning and management of water quality can better understand and get more involved.

This chapter deals with various methods, i.e., statistical properties, vulnerability mapping, water quality indices, etc. for water quality evaluation using integration of the GIS technique. In all the methods, central role of GIS technique in water quality evaluation is highlighted.

2. POINT AND NON-POINT SOURCES OF POLLUTION

GIS plays a central role in water quality management practice and augments efforts to monitor water quality changes in surface waterbodies or aquifers, to calculate pollutant concentrations and loads to a surface waterbody or groundwater, and model water quality of aquatic systems (Johnson, 2009). Water quality protection and management require quantity of the waste-assimilative capacity of receiving waters to be known, which is determined using the concept of *'total mass daily loading'* (TMDL). A TMDL is assessed taking account of all sources of a pollutant, from both point and nonpoint sources, and the waste assimilative capacity of the receiving water body (USEPA, 1991).

Water quality evaluations require a broad range of environmental and administrative data and one of the major categories of data include pollutant sources. Pollution may result from point sources or non-point sources (diffuse sources). Point sources are clearly identified at a single or multiple locations such as wastewater flow in conduits from municipalities and industries. However, nonpoint sources are diffuse and may not be defined by certain point locations for pollution such as urban runoff, erosion from agricultural and deforested lands. In other words, non-point sources include everything else that is not a point source. Sometimes, it is difficult to distinguish between both the point and non-point sources of pollution because a diffuse source on a regional or local scale may result from a large number of individual point sources, such as automobile exhausts.

An important difference between a point and a diffuse source is that a point source is amenable to control through collection and treatment processes while a non-point source is difficult to control with engineered facilities, e.g. collection and treatment, because of diffuse character of this source.

A diffuse pollution source consisting of several point sources may also be controlled provided all point sources can exactly be identified. Most common point and non-point sources of pollution are listed in Table 1.

3. WATER QUALITY EVALUATION

Water quality evaluation is an overall process of evaluating physical, chemical and biological nature of water in relation to natural quality, human effects and intended uses particularly uses which may affect human health and the health of the aquatic system itself (Bartram and Ballance, 1996). Water quality evaluation includes the use of monitoring data to define the condition of water, to provide a basis for detecting trends and to provide information enabling the establishment of cause-effect relationships. Thus, important aspects of water quality assessment are: *interpretation* of water quality data, *reporting* of results, and *recommendations* for future actions. Three important components of water quality evaluation in a logical sequence are monitoring, followed by assessment, followed by management (Meybeck et al., 1992).

The process of water quality evaluation involves many complex operations, which are linked together forming a chain of about twelve links where every link is important as its failure will weaken the entire evaluation.

Elements of various water quality evaluation programmes may differ depending upon the objectives of the programme.

However, there are certain standard elements, which are common to almost all type of water quality evaluation programmes. A generalized structure of water quality evaluation programme consisting of twelve elements is shown in Figure 1.

Prior to designing a water quality evaluation programme, clear-cut objectives should be set on the basis of environmental conditions (pollution sources), water uses (present and future), and water legislation.

Once the programme objectives are set, monitoring design is determined based on review of existing water quality data, which is supported by preliminary survey. In next step, various monitoring operations are performed to collect water samples from selected sites in the field, and then, the collected samples are analysed in laboratory.

Table 1. Summary of point and non-point sources of pollution

Point Sources	Non-Point Sources
1. Municipal and industrial wastewater effluents	1. Return flow from irrigated agriculture and orchards
2. Runoff and leachate from solid-waste disposal sites	2. Runoff from crops, pasture, and rangelands
3. Runoff and drainage from animal feedlots	3. Runoff from logging operations, including logging roads and all-terrain vehicles
4. Runoff from industrial sites	4. Urban runoff from small communities and unsewered settlements
5. Storm sewer outfalls from urban centers	5. Drainage from failing septic tank systems
6. Combined sewer overflows and treatment plant bypasses	6. Wet and dry atmospheric fall-out or deposition over waterbodies (e.g., acid rain)
7. Mine drainage and runoff (also oil fields)	7. Flow from abandoned mines and mining roads
8. Discharges from storage tanks, chemical waste piles, and ships	8. Runoff and snowmelt from roads outside urban areas
9. Runoff from construction sites	9. Wetland drainage
10. Airport snowmelt and runoff from deicing operations	10. Mass outdoor recreation and gatherings
	11. Military training, manoeuvres, shooting ranges

After Johnson, 2009.

The last step, which is important but often underestimated or omitted in a program, is synthesis, compilation, presentation and interpretation of enormous chemical data in a convenient manner for visual inspection (Freeze and Cherry, 1979; Sara and Gibbons, 1991). On completion of the programme, recommendations should be communicated to relevant water authorities for water management, water pollution control, and eventually the adjustment or modification of monitoring activities.

4. TOOLS FOR WATER QUALITY ANALYSIS

Several conventional tools for the graphical analysis of water quality are described in standard textbooks on groundwater hydrology or hydrogeology (Freeze and Cherry, 1979; Karanth, 1987; Sara and Gibbons, 1991). Recently, the need for application of modern approaches and tools such as multivariate statistical techniques (e.g., principal component analysis, hierarchical cluster analysis, discriminant analysis and correspondence analysis), and remote sensing and GIS techniques have been emphasized for the efficient analysis of water quality (e.g., Jha et al., 2007; Steube et al., 2009). The state-of-the-art review of tools and techniques for the interpretation of water quality can be found in Machiwal and Jha (2010) wherein available tools and techniques (conventional as well as modern) for analyzing water quality are classified into four major groups: (i) graphical, (ii) statistical, (iii) remote sensing (RS), geographic information system (GIS) and geostatistical, and (iv) modelling techniques.

5. GIS-BASED ASSESSMENT OF WATER QUALITY VARIABILITY

Extensive literature search made by the authors of this chapter revealed that most studies dealing with GIS applications for evaluating water quality are focused on subsurface water compared to that on surface water.

This is most likely due to the relatively easy availability of large number of point groundwater samples through wells (hand pump, open well, tubewell, etc.).

However, sampling of surface waterbodies requires some mechanism (e.g., boat) to reach different points in the waterbody.
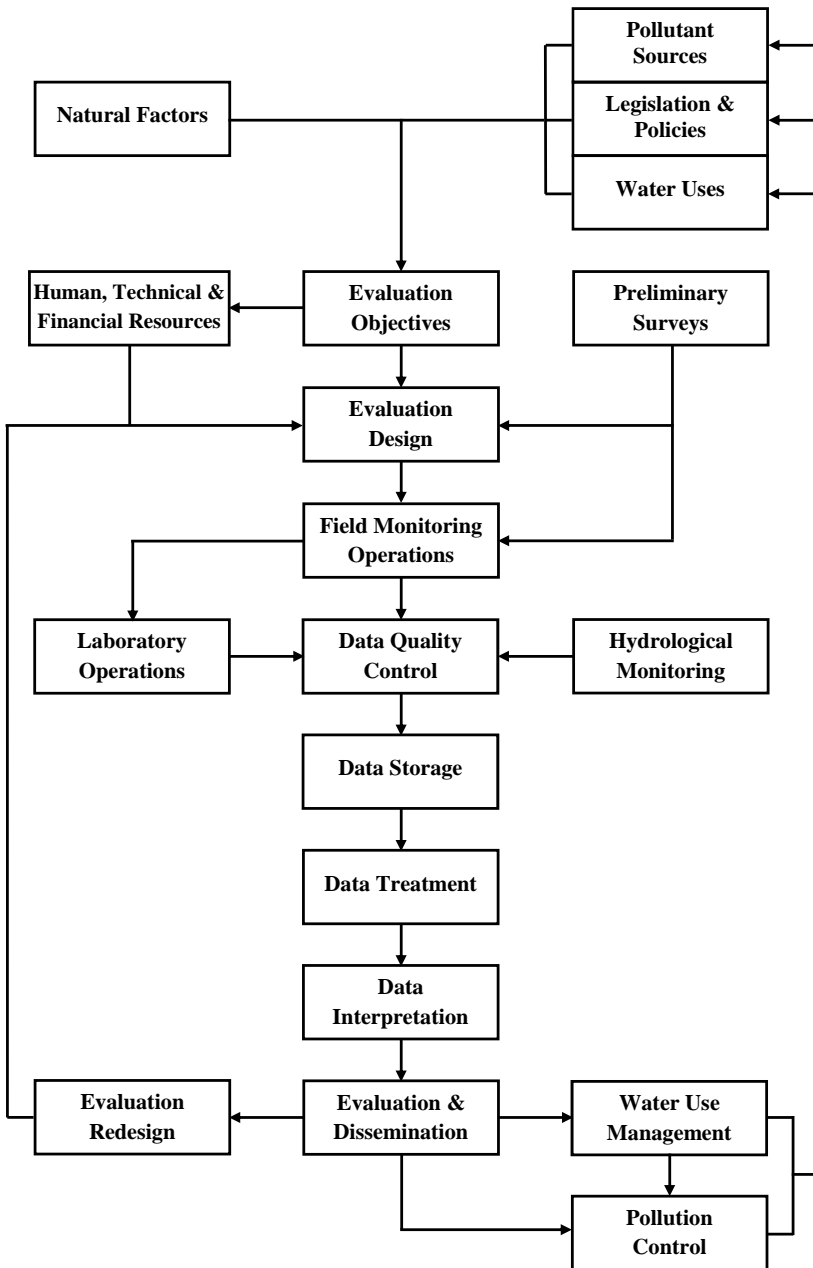
Modified from Meybeck and Helmer, 1992.

Figure 1. Generalized framework of water quality evaluation program showing standard aspects.

Another possible factor for the vast GIS application in groundwater quality studies is the significant variations in the water quality over a short distance within an aquifer. This is, in general, not the case of surface waterbody where water at point is free to move and mix with water at other points and this causes relatively less spatial variability especially in stagnant water of small ponds and reservoirs. Also, the water stored by the surface waterbodies is mostly the rainwater containing less concentration of the major ions as the water on surface has the least chances to come across different geological terrains comprising of certain minerals and other substances. On the other side, groundwater passing and moving through the subsurface formation meets different kind of salts, minerals, etc. which are easily dissolved with the flowing water. Thus, chances of increased concentration of the major ions and other metal contents are relatively higher for the groundwater as compared to surface water.

This, perhaps, may be one of the causes that groundwater quality studies cite large application of the GIS techniques.

Spatial and temporal variability of the water quality is one of main features of different types of surface and subsurface waterbodies. Water quality variations over space and time are largely determined by hydrodynamic characteristics of the waterbody. Water quality of a waterbody varies over a space in all three dimensions, which are further altered by flow direction, discharge and time (Meybeck and Helmer, 1992). Thus, one location measurements in a waterbody may not be appropriately represents the water quality of entire waterbody. Instead, one network or grid of sampling sites would be needed to present spatial variations of the water quality. Generally, one-dimensional samples are collected on a longitudinal profile in case of river and on a vertical profile in case of pond/reservoir/lake as illustrated in Figures 2 (a,b). Two-dimensional profile sampling is appropriate for observing plumes of pollution from a source and this is most-suitable for groundwater quality of aquifers (Figure 2c). Temporal variability of chemical water quality can be defined into five categories based on time scale as listed in Table 2.

5.1. Characterizing Extent and Patterns of Contamination

In water quality studies, activities begin with field data collection where it is a common practice to obtain the data from multiple locations and sources.

All the collected data need to be collated and converted into common format of the water quality database.

GIS provides excellent and powerful functions to capture and collate the water quality data. It is also seen that water quality studies involving repetitive, archival and historic use of the data requires the data be stored in a formal database that can be used for exploratory purposes. Water quality database to be utilized for GIS applications requires spatial coordinates, i.e. latitude and longitude (or x- and y- coordinates) to be attached with the data. The water quality data is further characterized by the depth at which the sample is taken (vertical z-coordinate).

Monitored data must also be characterized with regard to time t at which sample is taken. Thus, concentration (c) of any physical, chemical and biological parameter can be defined by the following function:

$$c = f(x, y, z, t) \tag{1}$$

In surface waterbodies such as rivers where discharge (Q) is a significant quantity, the flux determination and data interpretation also require knowledge of water discharge, and thus the concentration should also be a function of Q as shown below.

$$c = f(x, y, z, t, Q) \tag{2}$$

Firstly, the sampling locations based on their spatial coordinates are located within GIS environment. Then, spatial locations of the sampling points are attached with related attribute tables where different attributes of all individual sites/points are stored such as concentration of all major ions, calcium, magnesium, chloride, carbonate, etc. for one spatial point is stored.

Finally, the concentrations of a water quality parameter can be displayed over the entire space through spatial interpolation. There has been evolved a lot of spatial interpolation techniques over the time. An overview of the spatial interpolation techniques is provided in subsequent section.

5.2. Overview of Spatial Interpolation Techniques

In numerical analysis, spatial interpolation or multivariate interpolation is interpolation on multivariable functions. The spatial interpolation consists of interpolating the multivariable function, known at given points, to yield values at arbitrary points.
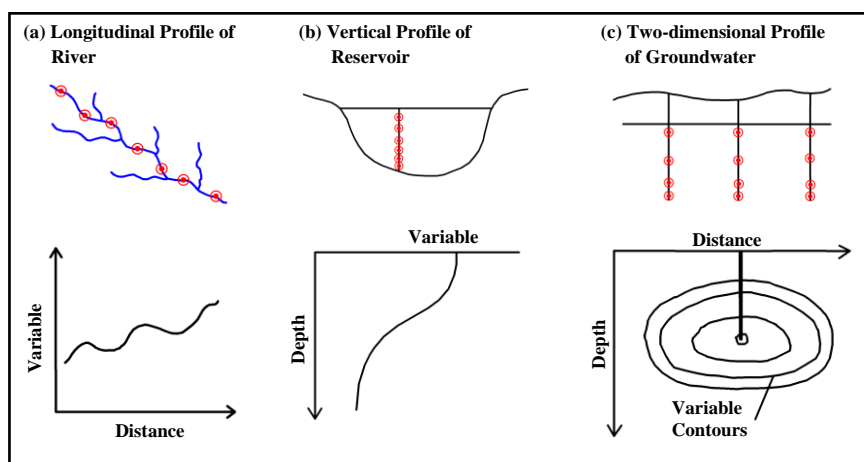
Modified from Meybeck and Helmer, 1992.

Figure 2. Sampling strategies for exploring spatial variations of water quality in (a) river, (b) reservoir and (c) groundwater aquifer.

Table 2. Scale of temporal water quality variability and causing factors

Scale of Temporal Variability	Causing Factor
Minute-to-minute to day-to-day variability	water mixing, fluctuations in inputs, etc., mostly linked to meteorological conditions and water body size (e.g. variations during river floods)
Dual variability (24-hour variations)	biological cycles, light/dark cycles etc. (e.g. $O2$, nutrients, pH), and to cycles in pollution inputs (e.g. domestic wastes).
Days-to-months variability	climatic factors (river regime, lake overturn, etc.) and to pollution sources (e.g. industrial wastewaters, run-off from agricultural land).
seasonal hydrological and biological cycles	mostly in connection with climatic factors
Year-to-year trends	human influences

After Bartram and Ballance, 1996.

Most hydrogeologic applications of spatial interpolation involve quantities that vary in space but the methods may also apply to quantities that vary in time (Kitanidis, 1999).

If function values are known on non-uniform grid, then available methods are nearest neighbor interpolation, natural neighbor, inverse distance weighting, kriging (one of the geostatistical techniques), and radial basis function (e.g., Gotway et al., 1996; Robinson and Metternicht, 2006; Namgial and Jha, 2009). Past studies dealing with GIS applications in water quality have mostly used geostatistical modeling and inverse distance weighting techniques for spatial interpolation. It is also revealed from the literature that geostatistical modeling tool was originally developed to deal with subsurface studies, and is widely-used for hydrogeologic studies.

5.2.1. Overview of Geostatistical Modeling Technique

Geostatistical modelling is a set of statistical estimation techniques involving quantities which vary in space (i.e., spatial variables). Geostatistical techniques for describing and interpolating spatially correlated data take advantage of the general observation that, on average, values closer together in space will be more similar than those farther from each other. The steps in applying these techniques include developing 'theoretical semi-variogram models' that describe the spatial variation between pairs of spatially or temporally related samples and then using these models to estimate sample parameters and their error variances at unknown locations. Although geostatistical modelling techniques were originally used in geological sciences (Journel and Huijbregts, 1978), they have also been frequently applied in hydrological, agricultural and ecological sciences to evaluate spatial dependence of surface/subsurface properties and ecological communities, or to interpolate these parameters (e.g., Goovaerts, 1999; Castrignanò et al., 2000; Mouser et al., 2005; Schaefer and Mayor, 2007). The process of applying GIS and geostatistical modelling techniques for developing a spatial distribution map of a water quality variable is illustrated in Figure 3.

(A) Spatial Estimation by Kriging Technique

In geostatistics, if $Z(x)$ represents any random function for concentration of any water quality variable measured at n locations in space $z(x_i)$, i = 1, 2, … n and if the water quality of the function Z has to be estimated at the point x_0, which has not been measured, the kriging estimate is defined as (Journel and Hujibregts, 1978; Kitanidis, 1997):

$$Z^*(x_0) = \sum_{i=1}^{n} \lambda_i \, z(x_i)$$

(3)

where, $z^*(x_0)$ = estimation of function $Z(x)$ at point x_0 and λ_i = weighting factors that minimize the variance of the estimation error (ordinary kriging weights).

Now two conditions are imposed to Equation (3), i.e., the unbiased condition and the condition of optimality. The unbiased condition means that the expected value of estimation error or the mean difference between the estimated $z^*(x_0)$ and the true (unknown) $Z(x_0)$ value of the concentration of water quality variable should be zero. The condition of optimality means the variance of the estimation error should be minimum.

The spatial structure defined by theoretical variogram, a kriging system of linear equations combining neighbouring information can be defined as

$$\sum_{j=1}^{n} \lambda_j C(x_i, x_j) - \mu = C(x_i, x_0) \quad , i = 1, 2, \ldots n \tag{4}$$

subjected to the constraint on weights:

$$\sum_{j=1}^{n} \lambda_j = 1 \tag{5}$$

where, μ = Lagrangian multiplier and $C(x_i, x_j)$ = value of covariance between two points x_i and x_j.

When we deal with an intrinsic case, i.e., working with variogram, the kriging Equation (4) and (5) are simply modified as follows (Marsily, 1986; Ahmed, 2006):

$$C(x_i, x_j) = C(0) - \gamma(x_i, x_j) \tag{6}$$

$$C(x_i, x_0) = C(0) - \gamma(x_i, x_0) \tag{7}$$

Eqnuations (6) and (7) hold good only when both the covariance and the variogram exist, i.e., variables are stationary.

(B) Geostatistical or Variogram Models

Experimental geostatistical or variogram model is the function of separation vector between two points i and j.
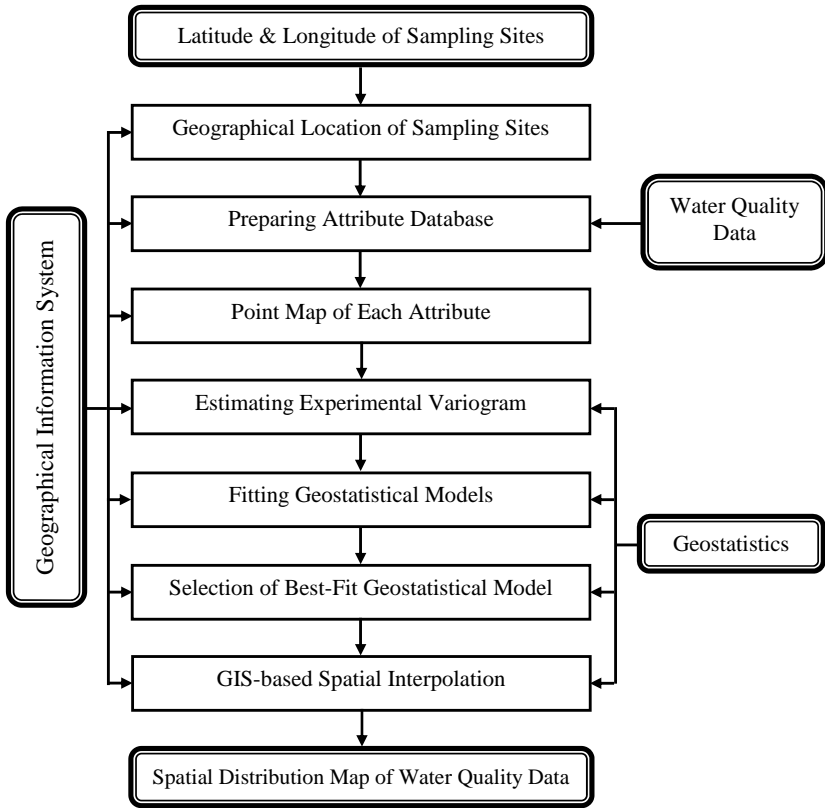
Figure 3. Flowchart showing step-by-step methodology for applying GIS and geostatistical techniques for generating maps of water quality data.

The values of separation vectors, e.g., h_1, h_2 etc. are decided first such that

$$h = |x_i - x_j| \tag{8}$$

Depending upon the value of h, the data are grouped into pairs and some function as defined below is averaged to obtain a variogram (γ_{ij}) (Goovaerts, 1997):

$$\gamma(h) = \frac{1}{2N_h} \sum_{i=1}^{N_h} \{z(x_i) - z(x_i + h)\}^2 \tag{9}$$

where, N_h = number of pairs for a given lag distance h.

A theoretical geostatistical or variogram model (Figure 4) can be defined essentially by 'sill' and 'range'. 'Sill' is the constant value on the y-axis around which a variogram stabilizes after a large distance and 'range' is the value at x-axis at which the variogram becomes constant or nearly constant. The sill value is usually very close to the variance of the variable (Matheron, 1965; Ahmed, 2006). In addition, the sudden apparent jump near the origin that occurs in some cases is known as 'nugget' effect. The shape of the variogram between origin and the point of stabilization is different for different variables, which entirely depends on its nature of variability (Matheron, 1965). In order to understand spatial structure, experimental water quality data are classified into lag distances with approximately the same number of data and semi-variogram values are calculated for each class (denoted by individual points shown in Figure 4) using geostatistics or GIS software packages such as MathWorks, GSLib, GSTAT, GeoPack, ILWIS, ArcGIS, IDRISI, etc.

(C) Fitting of Theoretical and Experimental Variograms

The experimental variogram calculated from the observed water quality data using Equation (9) is usually an erratic curve (Kitanidis, 1997, 1999).
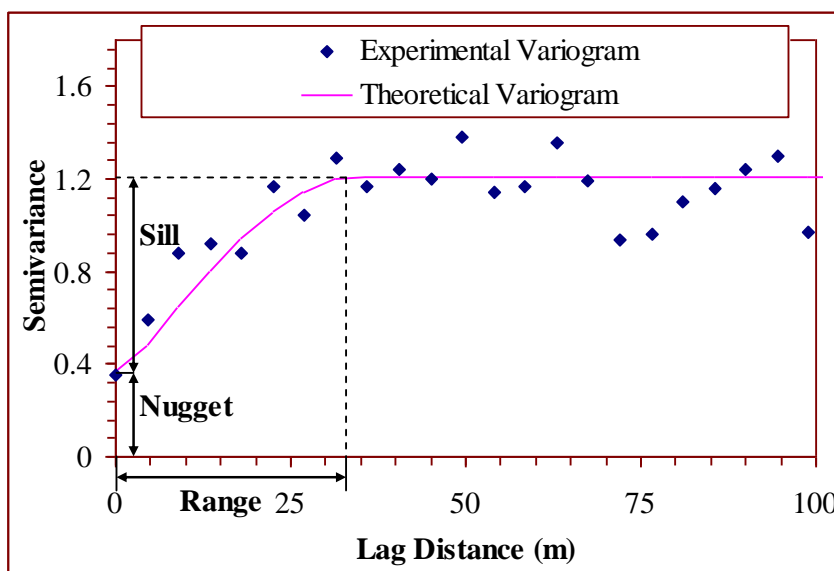
Figure 4. Fitting of the theoretical variogram to an experimental variogram.

It is not possible to use this experimental variogram in the estimation purpose due to its inconsistent nature. Therefore, the curve of the experimental variogram is approximated by another theoretical curve with a defined mathematical expression. This smooth curve fitted to the experimental variogram is known as 'theoretical variogram' as shown in Figure 4.

This fitting or modeling is performed in several ways mostly visual or using some form of difference between the two variograms but on a trial and error basis. Sometimes an automatic modeling is proposed but is not proved to be very useful. The commonly used variogram models are: spherical, circular, Gaussian, and exponential (Issaks and Srivastava, 1989; Kitanidis, 1997). The mathematical expressions for these theoretical variogram models are given below.

(i) Spherical Model:

$$\gamma(h) = C_0 + C\left(\frac{3h}{2a} - \frac{h^3}{2a^3}\right) \text{, for } 0 < h \le a \tag{10}$$

$$\gamma(h) = C_0 + C \text{, for } h > a \tag{11}$$

(ii) Circular Model:

$$\gamma(h) = C_0 + C\left[1 - \frac{2}{\pi} arc\,cos(h/a) + \frac{2h}{\pi a}\sqrt{1 - (h/a)^2}\right] \text{, for } 0 < h \le a \tag{12}$$

$$\gamma(h) = C_0 + C \text{, for } h > a \tag{13}$$

(iii) Gaussian Model:

$$\gamma(h) = C_0 + C\left[1 - e^{-(h/a)^2}\right] \tag{14}$$

(iv) Exponential Model:

$$\gamma(h) = C_0 + C\left(1 - e^{-h/a}\right)$$

(15)

where, $C_0 + C$ is the sill, a is the range, and h is the separation vector or lag distance.

(D) Selection of the Best-Fit Model

Once the fitting of experimental and theoretical variograms is over, the best-fit geostatistical model can be selected based on a set of goodness-of-fit criteria viz., mean error (ME), root mean squared error (RMSE), correlation coefficient (r), mean standard error (MSE), mean reduced error (MRE), reduced variance ($S_{R_e}^2$), and coefficient of determination (r^2). The details about these goodness-of-fit criteria can be found in Table 3.

5.2.2. Inverse Distance Weighting Technique

Inverse distance weighting (IDW) technique is one of the moving average methods for spatial interpolation. Moving average method performs a weighted averaging on point values and returns a spatial map as output based on a specified weight function and a limiting distance (Webster and Oliver, 2001). While applying the IDW technique for interpolating values of any water quality variable for an output point, the distances of all points (where the water quality parameter is known) towards the output point are calculated to determine weight factors for the points. The weight factors for the points are then calculated according to the specified weight function.

Two weight functions are available (Burrough and McDonnell, 1998): inverse distance and linear decrease. Weight for the inverse distance function is expressed below:

$$\text{Weight} = (1/d^n) - 1$$

(16)

where, $d = D/D_0$ = relative distance of a known water quality point to output point, D = Euclidean distance of known water quality point to output point, D_0 = limiting distance, and n = weight exponent.

The weights vary according to the relative distance of any known water quality point to output point and the weight exponent (Figure 5).

Thereafter, for each output pixel, value of particular water quality variable is calculated as the sum of the products of calculated weight values and point values divided by the sum of weights. That is,

$$WQ = \sum_{i=1}^{p}(w_i \times v_i)/\sum_{i=1}^{p} w_i$$

$$(17)$$

where, WQ = value of concerned water quality variable, w_i = weight value for the ith point, v_i = point value of the ith point, and p = total number of points within the limiting distance.

Table 3. Summary of the goodness-of-fit criteria

S. No.	Goodness-of-fit Criteria	Equation
1	Mean Error (ME)	$$ME = \frac{1}{n}\sum_{i=1}^{n}\left[z(x_i) - z*(x_i)\right]$$ Where, $z(x_i)$ and $z*(x_i)$ = observed and estimated values of variable z at the location x_i, and n = number of data points.
2	Root Mean Squared Error (RMSE)	$$RMSE = \sqrt{\frac{\sum_{i=1}^{n}\left[z(x_i) - z*(x_i)\right]^2}{n}}$$
3	Correlation Coefficient (r) (Rodgers and Nicewander, 1988)	$$r = \frac{n\sum_{i=1}^{n}\left[z(x_i)\cdot z*(x_i)\right] - \left[\sum_{i=1}^{n}z(x_i)\cdot\sum_{i=1}^{n}z*(x_i)\right]}{\left[\sqrt{n\left\{\sum_{i=1}^{n}\left[z(x_i)^2\right]\right\} - \{z(x_i)\}^2}\right]\cdot\left[\sqrt{n\left\{\sum_{i=1}^{n}\left[z*(x_i)^2\right]\right\} - \{z*(x_i)\}^2}\right]}$$
4	Mean Standard Error (MSE)	$$MSE = \frac{1}{n}\sigma_k(x_i)$$ Where, $\sigma_k(x_i)$ = estimation variance at the location x_i.
5	Mean Reduced Error (MRE) (Vauclin et al., 1983)	$$MRE = \frac{1}{n}\sum_{i=1}^{n}\left[z(x_i) - z*(x_i)\right]/\sigma_k(x_i)$$
6	Reduced Variance ($S_{R_e}^2$) (Vauclin et al., 1983)	$$S_{R_e}^2 = \frac{1}{n}\sum_{i=1}^{n}\left[\{z(x_i) - z*(x_i)\}/\sigma_k(x_i)\right]^2$$

S. No.	Goodness-of-fit Criteria	Equation
7	Coefficient of Determination (r^2) (Draper and Smith, 1998)	$r^2 = 1 - \dfrac{SSE}{(SSR + SSE)}$; Where, $$SSE = \sum_{i=1}^{n} \left[z(x_i) - z^*(x_i) \right]^2$$ and $SSR + SSE = \sum_{i=1}^{n} \left[z(x_i) - \overline{z}(x_i) \right]^2$ Where, $\overline{z}(x_i)$ = mean of $z(x_i)$.
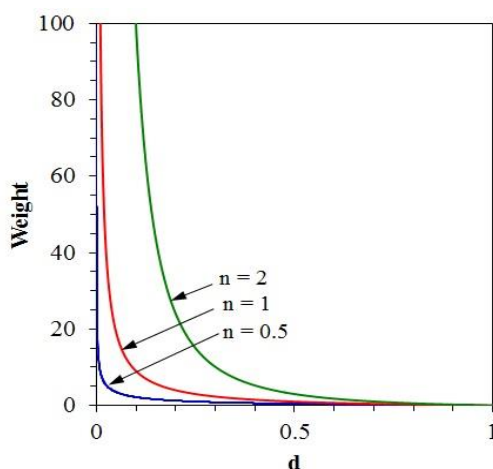
Figure 5. Inverse distance weights for relative distance of point to output point.

5.3. Statistical Measures in Spatial Context

Availability of multiple observations of water quality attributes both at spatial and temporal scales provides an opportunity for exploring spatial and temporal variations of the water quality in an area. Spatial statistics of the water quality database (mean, median, standard deviation, coefficient of variation, etc.) can be easily computed in GIS.

For example, if multi-year and multi-site water quality parameters are available for a given area. Then annual concentration maps for individual parameters and years can be prepared through spatial interpolation techniques (described earlier) in GIS framework. Subsequently, mean (C_{mean}) annual

concentration map for any of the water quality parameter can be created by using following equations (Machiwal et al., 2011):

$$C_{mean,i} = \frac{\sum_{n=1}^{N} C_{n,i}}{N}$$

(18)

where, $C_{mean,i}$ = mean annual concentration map of ith water quality parameter, $C_{n,i}$ = annual concentration map of the ith parameter in n^{th} year, and N = total number of years of data availability.

In order to compute the median, first rank the annual observations from the smallest ($C_{1}^{'}$) observation to the largest ($C_{N}^{'}$) observation and then use one of the following equations depending on the number of observations (N):

$$C_{median,i} = C_{(N+1)/2}^{'}, \text{ when N is odd}$$

(19)

$$C_{median,i} = \frac{1}{2}\left\{C_{(N/2)}^{'} + C_{(N/2)+1}^{'}\right\}, \text{ when N is even}$$

(20)

The spatial standard deviation map can be prepared from the following expression (Machiwal et al., 2011):

$$C_{sd,i} = \sqrt{\frac{\sum_{n=1}^{N}\left(C_{n,i} - C_{mean,i}\right)}{N-1}}$$

(21)

where, $C_{sd,i}$ = spatially-distributed standard deviation map of the ith parameter.

Thereafter, the coefficient of variation maps for different parameters can be developed using the following equation (Machiwal et al., 2011):

$$C_{cv,i}(\%) = \frac{C_{sd,i}}{C_{mean,i}} \times 100$$

(22)

Hydrologic variables with larger CV values are more variable than those with smaller values. Wilding (1985) suggested a classification scheme for

identifying the extent of variability for soil properties based on their CV values, where CV values of 0-15, 16-35 and >36 indicate little, moderate and high variability, respectively.

Typical ranges of CV values of salient soil properties are reported in the literature (Jury, 1986; Jury et al., 1987; Beven et al., 1993; Wollenhaupt et al., 1997).

6. GIS FRAMEWORK FOR GROUNDWATER VULNERABILITY MAPPING

6.1. Groundwater Vulnerability Concept

The groundwater vulnerability concept, evolved during end of the 1960s in France, aimed at creating awareness of groundwater contamination (Margat, 1968; Albinet and Margat, 1970). The vulnerability concept in hydrogeology began to be widely used in the 1980s (Haertle, 1983; Aller et al., 1987). It was defined as the possibility of percolation and diffusion of contaminants from the ground surface into the groundwater system.

Groundwater vulnerability deals only with the hydrogeological setting and does not include pollutant attenuation. Initially, the term 'vulnerability' was meant as relative susceptibility of aquifers to anthropogenic pollution without any formal definition. Later on, the concept began to mean different things to different people. Margat (1968) used the term 'vulnerability' to mean the degree of protection that the natural environment provides against the ingress of pollutants to groundwater. Thereafter, several definitions of vulnerability have been proposed. Foster (1987) defined aquifer pollution vulnerability as the intrinsic character of the strata separating the saturated aquifer from the immediately overlying land surface which determines its sensitivity to being adversely affected by a surface applied (anthropogenic) contaminated load. National Research Council (1993) defined groundwater 'vulnerability' to contamination as the tendency or likelihood for contaminants to reach a specified position in the groundwater system after introduction at some location above the uppermost aquifer. Vrba and Zaporocec (1994) defined 'vulnerability' as an intrinsic property of groundwater, depending on its susceptibility to natural and/or human impact. The groundwater vulnerability is a specific characteristic of the underlying groundwater system and cannot be practically measured in the field.

In general, the status of groundwater contamination is determined by the natural attenuation processes occurring within the zone between the pollution source and the aquifer. Mainly two natural factors, i.e. physical processes and chemical reactions occurring within the soil, unsaturated zone and saturated zone are responsible for alteration in physical states and chemical forms of contaminants, which ultimately leads to attenuation of contaminants. There may be a single or multiple chemical reactions to work with other processes resulting in a varying degree of attenuation.

These reactions depend on the specific soil and aquifer characteristics and particular geochemical properties of each contaminant. Thus, groundwater vulnerability is a function of geology and hydrogeology of the unsaturated and saturated zones and physico-chemical properties of the contaminants.

All factors affecting groundwater vulnerability may vary from one place to another. The groundwater vulnerability may be classified in two ways: intrinsic vulnerability and specific vulnerability. The term 'intrinsic vulnerability' refers to the vulnerability of groundwater to contaminants generated by anthropogenic or human activities taking into account the inherent geological, hydrological and hydrogeological characteristics of an area but being independent of the nature of the contaminants. On the other side, term 'specific vulnerability' is used to define the vulnerability of groundwater to particular contaminants or a group of contaminants taking into account the contaminant properties and their relationship with the various components of intrinsic vulnerability (Doerfliger et al., 1999; Gogu and Dassargues, 2000).

6.2. GIS-Based Methods to Evaluate Groundwater Vulnerability

Geographic Information System (GIS) technique has fundamentally changed our thoughts and ways to manage natural resources in general and water resources in particular (Jha et al., 2007).

GIS is designed to collect diverse spatial data to represent spatially variable phenomena by applying a series of overlay analysis of data layers that are in spatial register (Bonham-Carter, 1996). Vulnerability assessment is a basis for initiating protective measures for important groundwater resources and will normally be the first step in groundwater pollution assessment (Foster et al., 2002). The GIS technique is of great significance in assessing the pollution vulnerability of the aquifers over a large area.

Many approach such as process-based methods, statistical methods, and overlay and index methods have been developed to evaluate aquifer vulnerability (Tesoriero et al., 1998). Variability of land vulnerability to groundwater contamination leads to mapping of groundwater vulnerability (Piscopo, 2001). In the process-based methods, simulation models are used to estimate the movement of contaminant in groundwater.

The major drawback in using process-based methods is data shortage and computational difficulties (Barbash and Resek, 1996).

In statistical methods, statistical terms are used to determine relations between spatial variables and actual occurrence of pollutants in the groundwater.

Their major limitations include absence of sufficient water quality observations, data accuracy, and careful selection of spatial variables (Babiker et al., 2004). Overlay and index methods resulting in vulnerability indices mainly depend upon factors, which control the pollutant movement from the ground surface into the saturated zone. Their main advantage is that vulnerability assessments can be made at regional scale as some of the factors such as rainfall, soil type and groundwater depth are easily available over large areas, which makes them suitable to be used with geographic information system (Thapinta and Hudak, 2003).

In general, overlay and index methods and statistical methods are used for contamination assessments at map scales smaller than 1:50,000 (i.e., a large study area), while process-based simulation models are at larger map scales (i.e., a small study area) (Rao and Alley, 1993). Overlay and index methods and statistical methods are used to assess intrinsic vulnerability, while methods based on simulation models are used to assess specific vulnerability.

6.3. Groundwater Vulnerability Mapping by GIS-Driven Overlay and Index Methods

The most common approach to quantify aquifer vulnerability at present is the overlay and index method, whereby the protective effect of the overlying layers is expressed in a semi-quantitative way (Frind et al., 2006). Overlay and index methods efficiently determine groundwater vulnerability. These methods deal with overlaying and aggregation of multiple spatial maps and these spatial analyses of a group of maps can easily be performed in geographic information system.

Thus, the overlay and index methods are particularly suitable for use with geographic information systems (Tilahun and Merkel, 2010). An overlay and index method, being a multicriteria model, aggregates different hydrological/ hydrogeological factors that control the movement of pollutants from the ground surface to underlying aquifer.

A GIS-based overlay and index method combines factors controlling pollutant migration according to certain multi-criterion rule and computes resulting value of vulnerability index for different spatial locations.

A general methodology for applying groundwater vulnerability methods in GIS framework is shown in Figure 6.
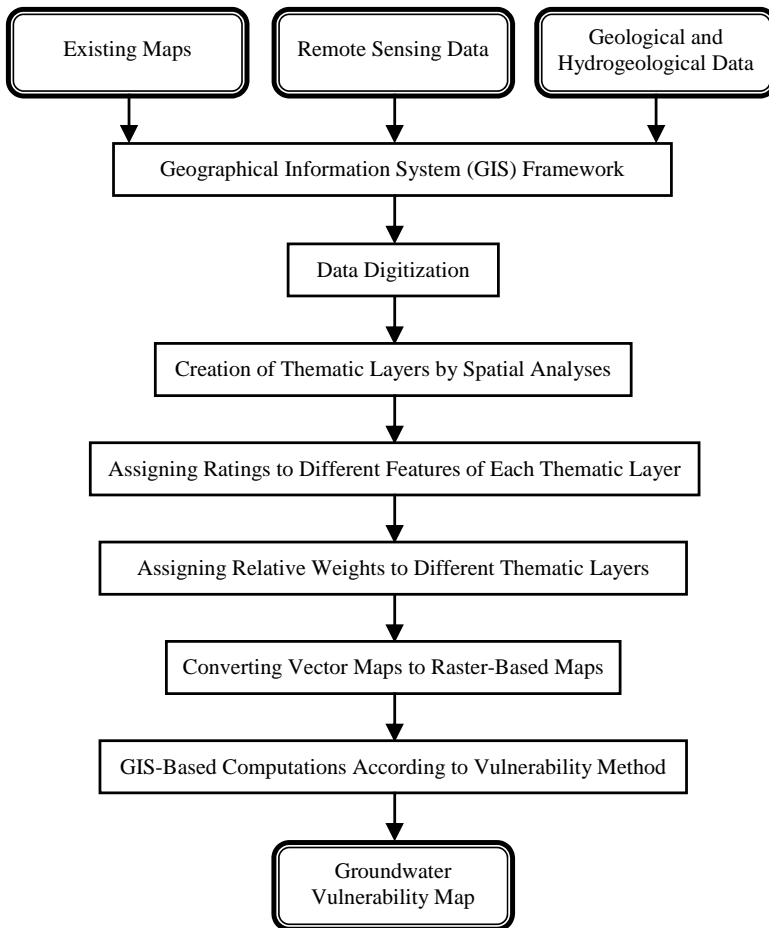
Figure 6. General GIS-based methodology for groundwater vulnerability study.

Before 1980s, there had been several attempts to formulate and establish a methodology to assess the vulnerability in order to present it in a map. However, the successful results could be obtained during the mid 1980s when two of the pioneer indices called DRASTIC (Aller et al., 1987) and GOD (Foster, 1987) were reported.

There are many kinds of vulnerability identified by different methods associated with a wide range of index values and labelled qualitatively. The categorization of vulnerability into different classes depends upon the index values and appropriate number of categories decided by a person.

The groundwater vulnerability assessment has rapidly developed over the past 20 years; many new tools and techniques are introduced for the groundwater vulnerability assessment along with specific applications being thoroughly analyzed and tested for different environments (Cramer and Vrba, 1987; Meinardi et al., 1995; Secunda et al., 1998; Lasserre et al., 1999; Al-Adamat et al., 2003; Lake et al., 2003; Rodriguez et al., 2003; Thapinta and Hudak, 2003; GEAM, 2005; Allen and Milenic, 2007; Zhou et al., 2010).

Moreover, many studies have used different scales and sources of information for the application of these techniques (Secunda et al., 1998; Foster et al., 2002; Civita and De Maio, 2004; Wang et al., 2007).

The widely-used models of index methods include DRASTIC (Aller et al., 1987), GOD (Foster, 1987), AVI rating system (Stempvoort et al., 1993), SINTACS (Gogu and Dassargues, 2000) and EPIK (Doerfliger et al., 1999).

Conventional methods, e.g., DRASTIC, GOD, AVI, SINTACS, etc. do not take into account the peculiar features of karstic (or carbonate) geological formations. Thus, to address pollution vulnerability assessment in karstic aquifers, few specific methods, e.g., EPIK (Doerfliger and Zwahlen, 1998; Doerfliger et al., 1999), PI (Goldscheider et al., 2000) and COP (Vias et al., 2006) have been developed. Available methods (conventional as well as non-conventional) for groundwater vulnerability mapping can be classified into two groups as shown in Table 4.

Three major limitations of overlay and index methods are: (i) defining groundwater vulnerability in qualitative terms, which is opposed by quantitative terms (Gogu et al., 2003; Frind et al., 2006; Popescu et al., 2008), (ii) finding it difficult to quantify exact amount of uncertainty involved in vulnerability assessments in order to handle inaccuracies incurred in analysis (Gogu and Dassargues, 2000), and (iii) strong homogeneous results observed over large areas in many parts of the world, which restricts for discrimination and delimitation of areas of different vulnerability to pollution.

These problems are addressed by the study reported by Massone et al. (2010), where different units with different categories of vulnerability in geological homogenous environments are discriminated.

Also, use of qualitative adjectives such as 'low' or 'moderate' is avoided because of their subjective meaning.

6.3.1. DRASTIC Method

DRASTIC is one of the most widely used standard groundwater vulnerability methods, which was developed by the United States Environmental Protection Agency (USEPA) as a method for assessing groundwater pollution potential (Aller et al., 1987). Seven most important mappable factors that control groundwater pollution were determined after a complete evaluation of many characteristics and the mappability of the data; the parameters are as follows:

Table 4. Conventional and modern methods for groundwater vulnerability mapping

S. No.	Method	Parameters	Source
Methods for Porous Aquifers			
1	DRASTIC and Pesticide DRASTIC	D – Depth to water R – (net) Recharge A – Aquifer media S – Soil media T – Topography (slope) I – Impact of vadose zone C – (hydraulic) Conductivity of the aquifer	Aller et al. (1987)
2	DRAMIC	D – Depth to water R – (net) Recharge A – Aquifer media M – Aquifer thickness I – Impact of vadose zone C – impact of Contaminant	Wang et al. (2007)
3	GOD	G – Groundwater occurrence including recharge O – Overlying lithology D – Depth to groundwater	Foster (1987)
4	AVI	c – Hydraulic resistance	Stempvoort et al. (1992)

S. No.	Method	Parameters	Source
Methods for Karstic (Carbonate) Aquifers			
5	SINTACS	S – Depth to groundwater I – Recharge action N – Attenuation potential of the vadose zone T – Attenuation potential of the soil A – Hydrogeologic characteristics of the aquifer C – Hydraulic conductivity S – Topographic slope	Civita (1994)
6	EPIK	E – development of Epikarst P – Protective cover I – Infiltration condition K – Karst network development	Doerfliger and Zwahlen (1995)
7	GLA	S – effective field capacity of the soil (rating for FCe in mm down to 1 m depth) W – percolation rate R – rock type T – thickness of soil and rock cover above the aquifer Q – bonus points for perched aquifer systems HP – bonus points for hydraulic pressure conditions (artesian conditions)	Hoelting et al. (1995)
8	PI	P – Protective cover I – Infiltration conditions	Goldscheider et al. (2000)
9	COP	C – flow Concentration O – Overlying layers P – Precipitation	Daly et al. (2002)

D – Depth to Water, R – (Net) Recharge, A – Aquifer Media, S – Soil Media, T – Topography (Slope), I – Impact of Vadose Zone, C – (Hydraulic) Conductivity of the Aquifer.

These seven parameters are briefly described in Table 5. The DRASTIC index model can be used to identify areas that are more vulnerable to contamination than others, or to give priorities to areas that need more groundwater quality monitoring. It is a vulnerability index model designed to calculate vulnerability scores (numerical values) for different locations by combining seven thematic layers/factors.

Before combining the factors, ratings and weights are assigned to the seven model parameters. The classes or features of each parameter represent the ranges, which are rated on the 1-10 scale based on their relative effect on

the groundwater vulnerability; a rating of 10 indicating a high pollution potential of the parameter.

Once the ratings are assigned to all classes of the parameters, the weights ranging from one to five reflecting their relative importance with respect to each other are assigned to seven parameters (Table 5).

The DRASTIC Index is then computed applying a weighted linear combination of all seven parameters by multiplying each parameter rating with its weight and adding together the resulting values according to the following equation (Aller et al., 1987):

$$DRASTIC_{Index} = D_R D_W + R_R R_W + A_R A_W + S_R S_W + T_R T_W + I_R I_W + C_R C_W \qquad (23)$$

where D, R, A, S, T, I, and C are the seven parameters expressed above and the subscripts R and W are the corresponding ratings and weights, respectively.

DRASTIC provides two weight classifications (Table 5), one for general conditions and the other one for conditions with intense agricultural activity. The latter, called the Pesticide DRASTIC index (DRASTIC-P), represents a specific vulnerability assessment approach. The DRASTIC-P method is the most suitable in agricultural areas mainly due to the greater weight given to the variables of soil and slope types (Massone et al., 2007).

In recent years, the originally developed DRASTIC method has been modified by using additional parameters or factors and/or by ignoring the existing unimportant parameters according to the local characteristics of the study area (Fritch et al., 2000; Al-Adamat et al., 2003; Lee, 2003; Thirumalaivasan et al., 2003; Babiker et al., 2005; Simsek et al., 2006; Guo et al., 2007; Wang et al., 2007; Umar et al., 2009; Martínez-Bastida et al., 2010; Awawdeh and Jaradat, 2010). This reflects flexibility of the DRASTIC model to modify according to need of the study. The well-established DRASTIC method has been applied in different parts of the world such as the United States (e.g., Rupert, 2001; Merchant, 1994; Loague and Corwin, 1998; Wade et al., 1998; Stark et al., 1999; Fritch et al., 2000), Canada (Murat et al., 2004), Europe (e.g. Stigter et al., 2006; Vias et al., 2005), South America (Tovar and Rodriguez, 2004; Herlinger and Viero, 2006), Australia (Piscopo, 2001), New Zealand (McLay et al., 2001), Asia (Al-Adamat et al., 2003; El-Naqa, 2004; Thirumalaivasan et al., 2003; Rahman, 2008; Kimand Hamm, 1999), and Africa (Lynch et al., 1997; Ibe et al., 2001).

Table 5. Description of DRASTIC and Pesticide DRASTIC parameters

Parameter	Description	Relative Weight	
		DRASTIC	DRASTIC-P
Depth to Water	Represents the depth from the ground surface to the water table, deeper water table levels imply lesser chance for contamination to occur.	5	5
Net Recharge	Represents the amount of water which penetrates the ground surface and reaches the water table, recharge water represents the vehicle for transporting pollutants.	4	4
Aquifer Media	Refers to the saturated zone material properties, which controls the pollutant attenuation processes.	3	3
Soil Media	Represents the uppermost weathered portion of the unsaturated zone and controls the amount of recharge that can infiltrate downward.	2	5
Topography	Refers to the slope of the land surface, it dictates whether the runoff will remain on the surface to allow contaminant percolation to the saturated zone.	1	3
Impact of Vadose Zone	Is defined as the unsaturated zone material, it controls the passage and attenuation of the contaminated material to the saturated zone.	5	4
Hydraulic Conductivity	Indicates the ability of the aquifer to transmit water, hence determines the rate of flow of contaminant material within the groundwater system.	3	2

After Aller et al., 1987.

The DRASTIC model is applicable in humid climates (Babiker et al., 2005; Piscopo, 2001; Kim and Hamm, 1999; and Osborn et al., 1998) as well as in semi-arid to arid climates (Werz and Hötzl, 2007; Al-Adamat et al., 2003; Secunda et al., 1998). In the original DRASTIC index model, semi-quantitative data layers were overlaid manually. However, the simple linear model of its combination factors expressing its vulnerability index shows the feasibility of employing the GIS for the computation of index (Fabbri and Napolitano, 1995).

For past 15-20 years, the GIS technique has been widely used in groundwater vulnerability mapping (Evans and Myers, 1990; Loague et al., 1996; Hrkal, 2001; Rupert, 2001; Lake et al., 2003; Massone et al., 2010; Yin, 2013; Edet, 2014). The major advantage of GIS-based mapping is the best combination of data layers and rapid change in the data parameters used in vulnerability classification. Integration of DRASTIC method with GIS involves following four steps (Massone et al., 2010).

(i) Preparation of thematic base maps (as a polygonal entity) for each parameter under consideration using GIS software packages. Subsequently, polygon map of each parameter is transformed into raster format using the spatial analysis functions of GIS. A suitable spatial cell resolution for spatial analysis can be chosen.

(ii) Procedure indicated by methodology are applied for the assignment of weights and values to each layer of information and the application of map algebra to obtain the aquifer vulnerability maps, called DRASTIC and DRASTIC-P vulnerability maps. Conveniently, the DRASTIC index values can be discretized into suitable number of classes indicating very low, low, moderate, high and very high vulnerability, since this is the number of classes that allows one to recognize both the "best" values and the worst ones as two alternatives (high and very high or low and very low); this is better than recognizing only three classes where there is only one possible option towards each end (low or high). This is favourable to decision-making related to the use of soil in land-use planning, in environmental impact evaluations, etc.

(iii) Reclassification of the DRASTIC vulnerability maps to obtain the DRASTICpriorities, which recognize five classes from priority 1 (lower values in the series) to priority 5 (higher values).

(iv) Combining the DRASTIC vulnerability map with the DRASTIC-priorities to generate an operational vulnerability index (OVI). For

this operation, both the vulnerability map and the DRASTIC-priorities are reclassified, assigning to each qualitative class a numerical value ranging from 1 (the lower class) to 5 (the higher one).

6.3.2. DRAMIC (Modified DRASTIC) Method

The DRASTIC method, originally developed for rural/agricultural lands, had some limitations and/or required modifications while applying in urban areas.

First, it was observed that the parameter C (hydraulic conductivity) of the DRASTIC method is closely related to the parameter A (aquifer media). Thus, impact of aquifer media has two-fold effect.

Second, topography of most cities in urban areas remains relatively flat (with negligible slope), and therefore, the parameter T (topography) can be ignored from DRASTIC method. Third, in urban areas, the ground surface is mostly covered by built-up structures, concrete, etc. and it is quite difficult to obtain comparable values of the parameter S (soil media). To overcome these problems, and to improve the predictability and applicability of the DRASTIC method, Wang et al. (2007) proposed DRAMIC method. The method is expressed in Equation (24), where parameters of DRAMIC method and their respective assigned weights are shown. Four parameters, i.e. D, R, A and I of the DRAMIC method are same as in DRASTIC method; parameter T is deleted and the parameters S and C are replaced with two new parameters, i.e. aquifer thickness (M) and impact of contaminant (C). DRAMIC index is described as (Wang et al., 2007):

$$\text{DRAMIC}_{\text{index}} = 5D_R + 3R_R + 4A_R + 2M_R + 5I_R + 1C_R \qquad (24)$$

where, D, R, A, and I are the same as in the DRASTIC method; M = aquifer thickness defined by media; C = parameter showing impact of contaminant; and R = rating. The computed DRAMIC index values can be used to delineate areas, which are more susceptible to groundwater contamination compared to other areas. The higher the value of DRAMIC index is, the greater the vulnerability to groundwater pollution. The hydrogeological significance, ranges and ratings for the four factors D, R, A, and I of the DRAMIC method are the same as in DRASTIC methods.

The ranges and ratings for the two new parameters of the DRAMIC method, e.g. aquifer thickness and contaminant characteristics are listed in Table 6.

6.3.3. GOD Scheme

GOD scheme is one of the earliest vulnerability index methods. GOD rating system is an empirical method for quick assessment of vulnerability incorporating three parameters: *G*roundwater occurrence including recharge, *O*verlying lithology, and *D*epth to groundwater (Foster, 1987). To each category of these parameters – namely the aquifer type (e.g. confined, semi-confined, unconfined), the lithology of the overlying aquitard or aquiclude (in case of a confined or semi-confined aquifer) or the aquifer unsaturated zone (in case of unconfined aquifer) and the depth to water – a rating value between 0 (not vulnerable) to 1 (highly vulnerable) is assigned. The vulnerability index is calculated using the following formula (Foster, 1987):

$$GOD_{index} = G_R \times O_R \times D_R \tag{25}$$

where, G = groundwater occurrence, O = overlying lithology (only in case of unconfined aquifer), and D = depth to groundwater, and subscript R indicates rating of the parameters. Schematic of the GOD system for assessing aquifer pollution vulnerability index is shown in Figure 7. The index values also ranges from 0 to 1 and gives the overall pollution vulnerability.

The vulnerability is classified into four classes according the index values as (i) low (GOD index<0.3), (ii) moderate (0.3<GOD index<0.5) and (iii) high (0.5<GOD index<0.7) and (iv) extreme (GOD index>0.7).

Table 6. Ranges and ratings for aquifer thickness and contaminant characteristics for DRAMIC method

Aquifer Thickness		Contaminant Characteristics	
Range (m)	Typical Rating	Characteristics	Rating
0-6	9	Stable, easy to infiltrate into aquifer	9
6-15	7	Stable, relatively easy to infiltrate	7
15-25	5	Stable, uneasy to infiltrate	5
25-32	4	Relatively stable, easy to infiltrate	5
32-40	3	Relatively stable, relatively easy to infiltrate	4
40-50	2	Relatively stable, uneasy to infiltrate	3
>50	1	Unstable, easy to infiltrate	3
		Unstable, relatively easy to infiltrate	2
		Unstable, uneasy to infiltrate	1

After Wang et al., 2007.

The method could not get wide popularity, although its performance has been assessed by applying it in GIS platform in some recent past studies (Debernardi et al., 2008; Polemio et al., 2009; Kazakis and Voudouris, 2011).

6.3.4. AVI Rating System

In this method, two physical parameters are considered: the thickness of every sedimentary unit above the uppermost, saturated aquifer surface (d) and the estimated hydraulic conductivity of each of these sedimentary layers (k).

Firstly, hydraulic resistance (c) is calculated by the following equation (Stempvoort et al., 1992):

$$c = \sum_{i=1}^{n} \frac{d_i}{k_i}$$

(26)

where, n = number of sedimentary units above the aquifer; d = thickness of each sedimentary unit above the uppermost aquifer, and k = estimated hydraulic conductivity of each sedimentary unit. The parameter c is defined as a theoretical factor used to describe the resistance of an aquitard to vertical flow (e.g. Kruseman and de Ridder, 1990).

The hydraulic resistance (c) has dimension of time, which indicates the approximate travel time for water to move by advection downward through the various porous media above the uppermost saturated aquifer surface. However, it should be noted that, in a strict sense, c is not a travel time for water or contaminants.

The calculated c or log(c) values can be used directly to generate iso-resistance map by using geostatistical techniques for spatial interpolation in GIS. The parameter c is related to a qualitative Aquifer Vulnerability Index (AVI) by a relationship, shown in Table 7.

The AVI rating system of aquifer vulnerability index, originally developed and applied in Canada (Stempvoort et al., 1992), has been demonstrated by a successful application in a GIS environment by Stempvoort et al. (1993).

6.3.5. SINTACS Method

The SINTACS method (Civita, 1994; Civita and De Maio, 2000), partially derived from DRASTIC, retains only the structure of DRASTIC. It evaluates the vertical groundwater vulnerability using the same seven parameters: *Soggiacenza* (depth to groundwater), *Infiltrazione* (recharge action), *Nonsaturo* (attenuation potential of the vadose zone), *Tipologia della*

copertura (attenuation potential of the soil), *Aquifero* (hydrogeologic characteristics of the aquifer), *Conducibilita* (hydraulic conductivity) and *Superficie topografica* (topographic slope). However, the SINTACS method is more flexible to ratings and weights of the parameters than DRASTIC method.

Table 7. Relationship between Aquifer Vulnerability Index (AVI) and hydraulic resistance

Hydraulic Resistance (c)	Log(c)	AVI
0-10 year	<1	Extremely High
10-100 year	1-2	High
100-1000 year	2-3	Moderate
1000-10000 year	3-4	Low
>10000 year	>4	Extremely Low

After Stempvoort et al., 1992.
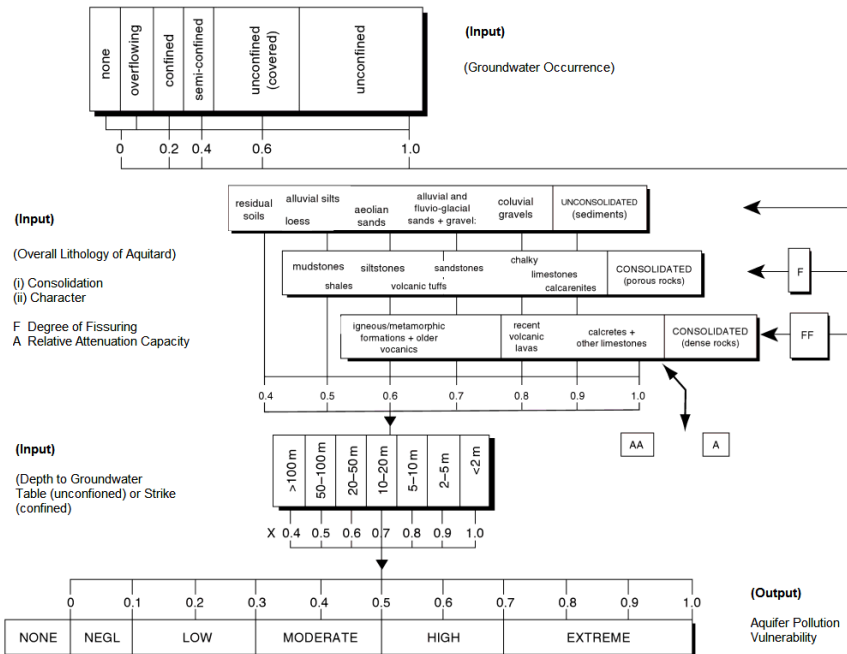
After Foster, 1987.

Figure 7. Schematic of GOD method for assessing aquifer pollution vulnerability.

The SINTACS method can easily be integrated with GIS where each parameter is first computed and mapped over a space in the form of raster map. Thereafter, each mapped parameter is classified into ratings (ranging from 1 to 10), which have an impact on potential pollution. Weight multipliers are then used for each parameter to balance and enhance their importance.

Then SINTACS vulnerability index (I_v), defined as weighted sum of the seven parameters, can be computed as (Civita, 1994):

$$I_v = \sum_{i=1}^{7}(P_i \times W_i)$$
(27)

where, P_i = rating of ith of seven parameters, and W_i = associated weight of ith parameter. The weight classes used by SINTACS depend on the hydrogeological features of each area.

6.3.6. EPIK Method

The EPIK method, through several evaluations, proved to be a suitable parametric weight and point tool to quantify the vulnerability of karstic (carbonate) aquifer zones.

Considering the karst aquifer's geological, geomorphological and hydrogeological characteristics, the four parameters influencing flow and transport in karst taken into account by the method are as follows (Doerfliger and Zwahlen, 1995; Doerfliger and Zwahlen, 1998; Doerfliger et al., 1999): *E*pikarst, *P*rotective cover, *I*nfiltration condition and *K*arst network development. Descriptive information about the attribute features for each of the four parameters may be found in Barrocu et al. (2007).

The parameters of the EPIK method constitute a protection index, F to be calculated for all parts of the catchments by weighted linear combination technique as follows:

$$Fp_i = aE_i + bP_i + cI_i + dK_i$$
(28)

where, $i = 1,..,n$ is the grid cell number; E_i, P_i, I_i, K_i = weights considered for the ith cell; a, b, c, d = attribute relative weights (constant for any attribute); Fp_i = i^{th} cell protection factor (pertaining to i^{th} cell). The lower the value of protection factor calculated for any i^{th} cell, the higher the vulnerability of the karst aquifer. The step-by-step methodology for applying the EPIK method is shown in Figure 8.

6.3.7. GLA Method

The GLA (*Geologisches Landesamt*) Method, first proposed by Hoelting et al. (1995), is based on a point count system similar to the DRASTIC method. The GLA method was further developed by Goldscheider (2000) into the PI-method within the framework of the European COST 620.
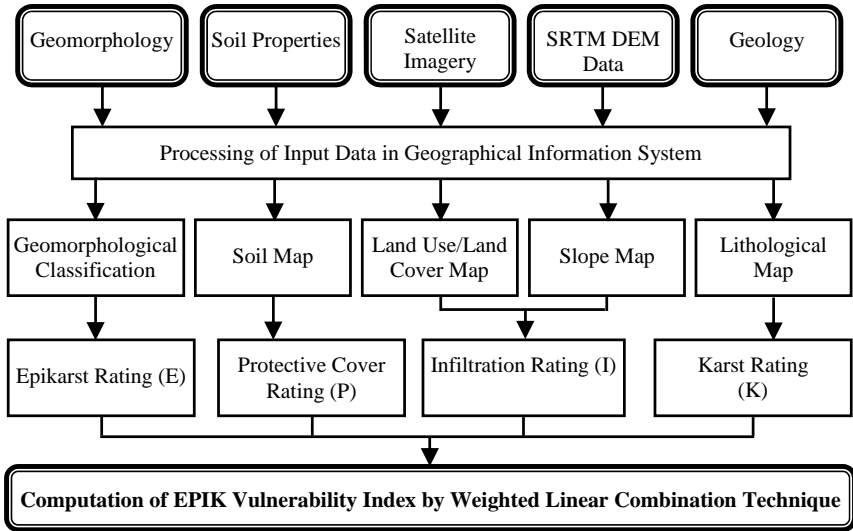
Figure 8. Flowchart showing step-by-step methodology for applying GIS-based EPIK method.

Unlike the DRASTIC, the GLA-method only takes the unsaturated zone into consideration. Attenuation processes in the saturated zone are not included in the vulnerability concept.

Perhaps, consideration of only unsaturated zone is the major reason that the method could not get wide popularity and applicability.

In this method, the degree of vulnerability is specified according to the protective effectiveness of the soil cover and the unsaturated zone. Six parameters considered for the assessment of the overall protective effectiveness are as follows (Hoelting et al., 1995):

Parameter 1: S- effective field capacity of the soil (rating for FCe in mm down to 1 m depth)
Parameter 2: W- percolation rate
Parameter 3: R- rock type
Parameter 4: T- thickness of soil and rock cover above the aquifer

Parameter 5: Q- bonus points for perched aquifer systems

Parameter 6: HP - bonus points for hydraulic pressure conditions (artesian conditions)

The protective effectiveness (PT) is calculated using the following expression (Hoelting et al., 1995):

$$PT = Pl + P2 + Q + HP$$
(29)

where, P1 = protective effectiveness of the soil cover; and P2 = protective effectiveness of the unsaturated zone (sediments or hard rocks)

Parameters P1 and P2 are defined as follows:

$$Pl = S \times W$$
(30)

$$P2 = W \times (R1 \times T1 + R2 \times T2 + \ldots + Rn \times Tn)$$
(31)

Based on the German mapping approach, the highest value assigned for factor W, is 1.75 for an annual groundwater recharge of less than 100 mm (Hoelting et al., 1995). A modified scale for the factor W was introduced which reflects the low amounts of groundwater recharge in many areas (Table 8).

6.3.8. PI Method

The PI method is used for mapping the intrinsic vulnerability of groundwater resources to pollution through a GIS-based approach (Goldscheider et al., 2000). This vulnerability method is applicable to all kind of aquifers, but provides special methodological tools for the karst aquifers. Conceptually, the method is based on an origin-pathway-target model. The land surface is taken as the origin for the contaminant, the water table in the aquifer is the target which is vulnerable to contamination, and the pathway includes all geologic layers in between. Aquifer vulnerability is assessed as the product of two factors: (i) protective cover (P) and (ii) infiltration conditions (I). The detailed assessment schemes for the two factors can be found in Goldscheider et al. (2000), Goldscheider (2004) and Zwahlen (2004).

PI method can be expressed as (Goldscheider et al., 2000):

$$p = P \times I$$
(32)

where, p = protection factor; P = parameter representing protective cover conditions; and I = parameter describing infiltration conditions. Vrba and Zaporozec (1994) proposed five classes of vulnerability (or protectiveness, p) ranging from 1 to 5: value of p = 1 indicates a very low degree of protection and an extreme vulnerability to contamination, whereas a p = 5 indicate a very high degree of protection and a very low vulnerability.

In the PI method, the parameter P describes the protective function of all subsurface layers that may be present between the ground surface and the groundwater table: the topsoil, the subsoil, the non-karst rock and the unsaturated zone of the karst rock.

Protectiveness is assessed on the basis of the effective field capacity (FC_e) of the soil, the grain size distribution (GSD) of the subsoil, the lithology, fissuring and karstification of the non-karst and karst rock, the thickness of all strata, the mean annual recharge and artesian pressure in the aquifer (Kouli et al., 2008). The parameter P is classified into five classes according to its value ranging from P=1 (extremely low degree of protection) to P=5 (very thick and protective overlying layers). A decadic (10 point) logarithmic scale is applied to make the parameter P one class higher and to show a ten times higher protectiveness (e.g. 10-m-layer thickness instead of 1 m). The parameter I, which is very critical for karst aquifers, describes the infiltration conditions. This parameter, in particular, given an idea about the degree to which the protective cover is bypassed due to lateral surface and subsurface flows that enter the karst aquifer at some another place. Values of the parameter vary from 0 (steep slopes with low permeability soil) to 1 (for horizontal and highly permeable soil). On steep slopes of low permeability, surface runoff will be diverted towards a sinking stream while on a horizontal plane of high permeability, diffuse recharge occurs by infiltration and subsequent percolation. In such a case, the protective cover will entirely be bypassed. For rest of the situations, intermediate values (0.2, 0.4, 0.6 and 0.8) of the I parameter are assigned depending on the soil properties controlling the predominant flow process, the vegetation and slope gradient, and the position of a given point inside or outside the catchment of a sinking stream.

In GIS application of the PI method, raster maps of the parameter P and I are to be considered, which may be generated through raster-based spatial analyses performed in GIS.

Finally, multiplication of P and I raster maps can be accomplished in GIS and resulted p factor map can be classified into suitable classes to identify high and low vulnerability areas.

Table 8. Modified values of the parameter W (percolation rate)

Groundwater Recharge (mm/year)	Percolation Rate (W)
>400	0.75
300-400	1
200-300	1.25
100-200	1.5
50-100	1.75
25-50	2
≤25	2.25

6.3.9. COP Method

The COP method of groundwater vulnerability assessment is mainly developed for the carbonate (karst) aquifers. This method provides assessment of intrinsic vulnerability of the aquifers based on three factors: flow **C**oncentration, **O**verlying layers and **P**recipitation.

According to European approach (Daly et al., 2002; Goldscheider and Popescu, 2004), the basic concept of this method is to assess the natural groundwater protection (O factor), which is determined by the properties of overlying soils and the unsaturated zone.

The method also aimed at estimating how the groundwater protection can be modified by the infiltration process (i.e., diffuse or concentrated) defined by C factor and the climatic conditions (e.g., precipitation) defined by P factor (Kouli et al., 2008).

Furthermore, the COP method establishes detailed guidelines, standard tables and formulae for vulnerability assessment and selects suitable variables, parameters and factors to be used according to the European Approach (Daly et al., 2002; Zwahlen, 2004).

The method can have wide acceptance in most countries of the world as the geoenvironmental data required by the method is easily available with some fieldwork but no extensive input from GIS is needed.

Moreover, the method is applicable in different climatic conditions and different types of carbonate aquifers, e.g. diffuse and conduit flow systems. These flexibilities associated with the COP method make the method more practical and useful for planners and decision makers framing and implementing suitable schemes of groundwater protection.

The COP method, comprising of the three factors to evaluate the intrinsic vulnerability of a groundwater resource, is expressed by the following formula (Daly et al., 2002):

$$\mathrm{COP_{index}} = C \times O \times P$$

(33)

Scores to all three factors are assigned according to their relative impact on the vulnerability of the karst aquifers. The numerical representations of the C, O and P factor values (or scores) are then multiplied to assess the vulnerability. In general, the final values of the COP index indicating the intrinsic vulnerability range from 0 to 15, which can be suitable classified into five vulnerability classes, i.e. very high, high, moderate, low and very low vulnerability (Vrba and Zaporozec, 1994).

The COP method is evaluated as the most effective in comparison to other methods such as DRASTIC, GOD, AVI, SINTACS, EPIK, and PI for assessing the prevailing vulnerability in the southern Spain (Longo et al., 2001; Brechenmacher, 2002; Vıas et al., 2005, 2006; Andreo et al., 2006) based on actual hydrogeological understanding of the aquifers.

7. GIS-BASED WATER QUALITY INDEX

Water Quality Index (WQI) technique is very useful for evaluating the water quality (Abassi, 1999; Adak et al., 2001; Pradhan et al., 2001), especially in resource-poor countries where cost is a major issue for water resources management. In one of the pioneer work, Horton (1965) developed general water quality indices by selecting and weighting several parameters. Although there are no hard and fast rules for constructing a water quality index, a WQI should be specific to a water use or a set of goals (Schultz, 2001). In general, two steps are required for developing a WQI. First, a set of parameters need to be selected that measure the important physical, chemical, and microbiological water characteristics. Of course, the selection of such parameters depends on the intended use of the water.

Once information about that set of parameters is available, a rule is needed to summarize all the information in a unique number, i.e., 'water quality index'. The usefulness of water quality indices has been demonstrated in water quality interpretation (e.g., Melloul and Collin, 1998; Soltan, 1999; Stigter et al., 2006; Babiker et al., 2007; Ramesh et al., 2010; Machiwal et al., 2011; Machiwal et al., 2013). Provencher and Lamontagne (1977) proposed one pioneering WQI, which is based on several parameters scored using the same transformations, generally but not always linear, and a final global score is

reached. In the past, a variety of water quality indices have been proposed by researchers worldwide (Table 9).

Geographic Information System (GIS) provides an efficient environment for the development of a WQI.

Table 9. Different water quality indices developed and used in the earlier studies

S. No.	Name of Index	Country	Parameters Used in Water Quality Index	Source
1	Groundwater Contamination Index	Finland	F, NO_3, UO_2, As, B, Ba, Cd, Cr, Ni, Pb, Rn, Se, pH, $KMnO_4$ consumption, SO_4, Cl, Ag, Al, Cu, Fe, Mn, Na and Zn	Backman et al. (1998)
		Slovakia	TDS, SO_4, Cl, F, NO_3, NH_4, Al, As, Ba, Cd, Cr, Cu, Fe, Hg, Mn, Pb, Sb, Se and Zn	
2	Groundwater Quality Index	Israel	Cl and NO_3	Melloul and Collin (1998)
3	Groundwater Quality Index	Egypt	NO_3, PO_3, Cl, TDS, BOD, Cd, Cr, Ni and Pb	Soltan (1999)
4	Surface Water and Groundwater Quality Index	Croatia	Temperature, mineralization, corrosion coefficient, DO, BOD, total N, protein N, total P and total coliform	Štambuk-Giljanović (1999)
5	Groundwater Quality Index and Groundwater Composition Index	Portugal	NO_3, SO_4, Cl and Ca	Stigter et al. (2006)
6	Surface Water Quality Index	Argentina	Temperature, hardness, DO, pH, EC, alkalinity, turbidity, NO_3, NO_2, NH_3, Cl and SO_4	Vignolo et al. (2006)
7	Malaysian Department of Environment – Surface Water Quality Index	Malaysia	DO, COD, BOD, TSS, NH_3-N and pH	Shuhaimi-Othman et al. (2007)
8	Groundwater Quality Index	Japan	Cl, Ca, Na, Mg, SO_4, TDS, NO_3	Babiker et al. (2007)
9	Surface Water Quality Index	Spain	pH, EC, TSS, NH_3, NO_2, NO_3, COD, BOD, DO, temperature and total P	Sánchez et al. (2007)

Table 9. (Continued)

S. No.	Name of Index	Country	Parameters Used in Water Quality Index	Source
10	Fuzzy Surface Water Quality Index	Brazil	Temperature, pH, DO, BOD, Coliforms, dissolved inorganic N, total P, total solids and turbidity	Lermontov et al. (2009)
11	Groundwater Quality Index	India	pH, EC, Na, Cl, SO_4, total alkalinity, total hardness, Ca, Mg, Fe, F, NO_3, NO_2, Mn, Zn, Cd, Cr, Pb, Cu, Ni, total coliform, salmonella	Ramesh et al. (2010)

In brief, the GIS-based WQI formulation process involves generation of representations for the spatial variability of originally scattered point measurements and the multiple transformations of water quality data into a corresponding index rating value related to water quality. The steps involved in the formulation of GIS-based WQI proposed Babiker et al. (2007) are described in the subsequent section.

7.1. Computing Normalized Difference Maps

In the first step, spatial maps (C) representing distribution of concentrations of the water quality parameters over the space are constructed for each parameter from the point sample values by spatial interpolation technique within GIS environment.

Thereafter, observed spatial concentrations (C_{obs}) of the water quality parameters are related to their maximum desirable limits (C_{mdl}) prescribed by the WHO (2006) on pixel-by-pixel basis using a GIS-based normalized difference index (ND_{index}) as follows (Babiker et al., 2007):

$$ND_{index} = \left(C_{obs} - C_{mdl}\right)/\left(C_{obs} + C_{mdl}\right)$$

(34)

Values of the resulted ND_{index} for each pixel range between -1 and 1.

7.2. Assigning Rank to Different Water Quality Variables

The ND_{index} maps are rated between 1 and 10 to generate a 'rank map'. The rank 1 indicates minimum impact on water quality, while the rank 10 indicates maximum impact. The minimum ND_{index} value (-1) is set equal to 1, the median value (0) is set equal to 5 and the maximum value (1) is set equal to 10. The following polynomial equation can be used to rank the contamination level (or ND_{index}) of every pixel between 1 and 10:

$$R = 0.5 \times (ND_{index})^2 + 4.5\,(ND_{index}) + 5$$

(35)

where R = rank value of every pixel corresponding to its ND_{index} value.

7.3. Developing Water Quality Index Map

Water Quality Index (WQI) is calculated as follows (Babiker et al., 2007):

$$WQI = 100 - \big[(R_1\,w_1 + R_2\,w_2 + \ldots + R_n\,w_n)/N\big]$$

(36)

where R = rate of the rank map (1–10), w = relative weight of the parameter which corresponds to the 'mean' rating value (R) of each rank map (1–10), and N = total number of parameters used in the suitability analysis.

The definition of WQI [Equation (35)] is similar to the weighted linear combination technique. The weight (w) assigned to each parameter indicates its relative importance to water quality and corresponds to the mean rating value of its 'rank map'. The total number of parameters (N) involved in the expression of WQI averages and limits the index values between 1 and 100.

The '100' in the first part of the formula is incorporated to directly project the WQI value such that high index values close to 100 reflect 'high water quality' and the index values far below 100 (close to 1) indicate 'low water quality'. The entire steps of developing a water quality index map are depicted in a flowchart shown in Figure 9.

8. GIS-COUPLED MULTIVARIATE STATISTICAL TECHNIQUES

Multivariate statistical analyses techniques such as principal component analysis (PCA) and cluster analysis (CA) are very useful for classifying aquifer groundwater quality according to the different pollution sources. It is observed that the results of the multivariate statistical analyses of water quality data can easily be combined with GIS in order to delineate the different groundwater quality zones.

Mapping of groundwater contamination is often complicated by infrequent and uneven distribution of sampling locations, analytical errors in sample analyses, and large spatial variation in observed contaminants over short distances due to complex hydrogeologic conditions.

Also, uncertainty may be associated with numerical modelling approach used to delineate groundwater contamination plumes due to inadequate knowledge about local hydrogeological conditions.
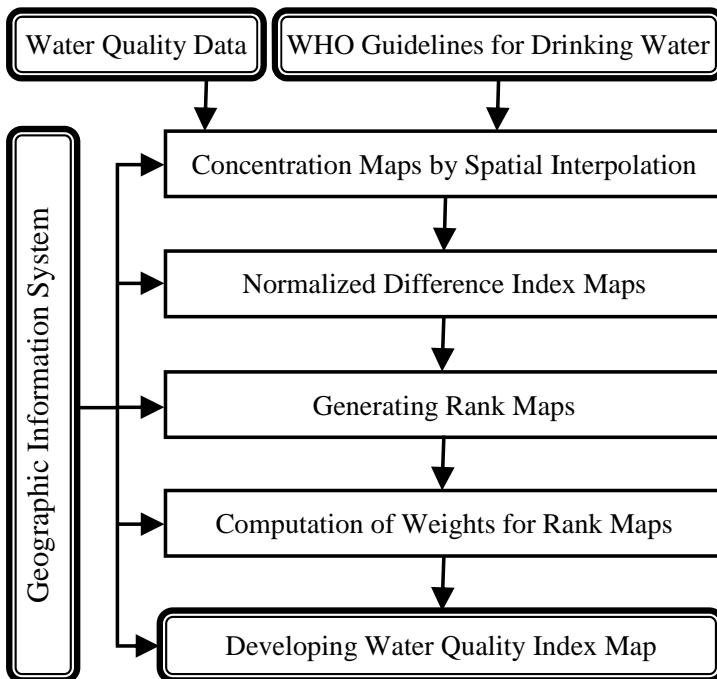
Figure 9. Flowchart depicting methodology for developing GIS-based water quality index maps.

Furthermore, managing and mapping extensive water quality datasets can be difficult due to the multiple locations, times, and analytes that may be present. An alternative to numerical modeling is to employ statistical analysis of groundwater quality data to infer zones of potential contamination.

Principal components analysis (PCA) is a multivariate statistical technique, which classifies/groups the water quality variables based on their correlations with each other. The major aim of applying PCA and CA is to consolidate a large number of observed water quality variables into a smaller number of factors that can be more readily interpreted. Thus, the multivariate statistical techniques reduce dimensionality of the data (Dillon and Goldstein, 1984). The PCA helps identifying underlying geologic and hydrogeologic processes for individual principal components or PCs (or factors) based on the water quality variables grouped under the PCs. The more PCs extracted, the greater is the cumulative amount of variation in the original water quality data. PC loadings show how the PCs characterize strong relationships (positive or negative) between groundwater quality variable and PC describing the variable. In order to determine the number of PCs to be retained, Kaiser Normalization Criterion (Kaiser, 1958) is used.

PCs, which best describe the variance of analyzed groundwater quality data (eigenvalue > 1) and can be reasonably interpreted (Harman, 1960), are accepted for further analysis.

The measure of how well the variance of a particular groundwater quality parameter is described by a particular set of factors is known as 'communality' (Jackson, 1991). Number of variables retained in principal components or communalities is obtained by squaring the elements in PC matrix and summing the total within each variable. Ideally, if a PCA is successful, number of PCs will be small, communalities are high (close to 1) and PCs will be readily interpretable in terms of particular sources or process (Dunteman, 1989). The PCA has previously been used to generate accurate maps of monitoring wells grouped by their water quality characteristics (Suk and Lee, 1999; Ceron et al., 2000; Güler et al., 2002).

Suk and Lee (1999) performed multivariate statistical analysis in combination with GIS to correlate contaminant data with groundwater quality parameters for the purpose of identifying contaminated aquifer zones.

Cluster analysis (CA) is another multivariate statistical analysis technique that results in data reduction and that can be used to group monitoring sites according to aquifer water quality behaviour (Suk and Lee, 1999). The CA is an unsupervised pattern recognition technique that uncovers intrinsic structure or underlying behaviour of a dataset without making a priori assumption about

the data, in order to classify the objects of the system into clusters based on their similarities (Otto, 1998). This method creates linkages between variables hierarchically in the configuration of a tree with different branches. Branches that have linkages closer to each other indicate a stronger relationship among variables or clusters of variables. Mathes and Rasmussen (2006) demonstrated the methodology for generating GIS maps of groundwater contamination using multivariate statistical analysis of water quality data. GIS is an important tool that is used to organize and manage large amounts of water quality information for use in decision support systems.

Nowadays, GIS has been started to be used routinely for displaying water quality data in map form but still use of statistical indicators of contaminant distributions are rarely seen. Presently, focus of GIS-coupled multivariate statistical analysis techniques has shifted from mapping of observed contaminant distribution to developing a map of contamination potential created using auxiliary water quality data.

Prior to applying multivariate statistical analysis, generally the observed water quality data, x_{ji} are standardized by z-scale transformation as given below:

$$z = \frac{x_{ji} - \overline{x}_j}{s_j}$$

(37)

where, x_{ji} = value of the jth water quality parameter measured at i^{th} site, $\overline{x}_j$ = mean (spatial) value of the jth parameter, and s_j = standard deviation of the jth parameter.

The analysis performed with standardized data is expected to be less influenced by small/large variance of the data. Furthermore, standardization of the data removes the influence of different measurement units of the data by making the data dimensionless.

CONCLUSION

Evaluation of water quality is necessary for managing water quality so as to ensure environmental sustainability. The important aspects of water quality evaluation are interpretation of water quality variables, reporting of results and recommendations for planners and decision makers. Logical sequence of any water quality evaluation programme consists of three key steps: *monitoring*,

evaluation and *management*. There are various tools and techniques available for water quality interpretation. However, selection of appropriate tools is very crucial for making the water quality evaluation to be effective.

Among the several tools used for water quality assessment, geographic information system (GIS) has been gaining a wide acceptance for past two decades among the researchers worldwide due to the capabilities of GIS such as handling, capturing, storing, analyzing and displaying large quantum of water quality data.

It is clear that with the advent of GIS technique, many conventional methods of water quality evaluation have been interfaced with GIS to enhance usefulness of the methods. The conventional methods coupled with GIS can be applied over relatively large areas. GIS-based spatial statistical analyses make it possible to explore spatial and temporal variations of the water quality. The point data of the water quality may accurately be converted to vector and raster formats through integration of geostatistical and GIS modeling techniques. Raster formats of the water quality data further enable spatial analyses to be performed under GIS platform for groundwater vulnerability mapping.

Among the various overlay and index methods for mapping groundwater vulnerability, DRASTIC, GOD, AVI, and SINTACS are mostly applied in many places of the world. Later on, few specific vulnerability methods applicable to karst (carbonate) aquifers were developed, e.g. EPIK, GLA, PI and COP.

Computation of water quality index is another way of evaluating the water quality where GIS technique plays a central role. With the aid of GIS, it is possible to locate areas having poor quality of the groundwater. The definition of WQI is flexible and many researchers have developed different types of water quality indices depending upon the data availability, aim of assessment, geologic condition, aquifer type, etc. Recently, GIS has also been associated with multivariate statistical analysis techniques, e.g., principal component analysis (PCA) and cluster analysis, etc.

Finally, GIS is considered as a modern powerful tool having large flexibility to be combined with conventional methods of water quality evaluation.

This new era tool has great potential to play a key role in water quality evaluation to ensure sustainable management of natural resources. In future, new areas for the assessment of water quality are to be explored wherein the application of GIS technique will further strengthen the interpretation of water

quality analyses ultimately leading towards more sustainable planning and utilization of the water resources.

REFERENCES

Abassi, S. A. (1999). Water quality indices: State-of-the art. *Journal of the Institution of Public Health Engineers*, 1: 13-24.

Adak, M. D. G., Purohit, K. M. and Datta, J. (2001). Assessment of drinking water quality of river Brahmani. *Indian Journal of Environmental Protection,* 8(3): 285-291.

Ahmed, S. (2006). Application of Geostatistics in Hydrosciences. In: M. Thangarajan (editor), *Groundwater Resource Evaluation, Augmentation, Contamination, Restoration, Modeling and Management*, Capital Publishing Company, New Delhi, India, pp. 78-111.

Al-Adamat, R. A. N., Foster, I. D. L. and Baban, S. M. J. (2003). Groundwater vulnérabilité and risk mapping for the Basaltic aquifer of the Azraq basin of Jordan using GIS, Remote sensing and DRASTIC. *Applied Geography,* 23: 303-324.

Albinet, M. and Margat, J. (1970). Cartographie de la vulnérabilité a la pollution des nappes d'eau souterraine, *Bull. BRGM 2me Series* 3(4).

Allen, A. and Milenic, D. (2007). Groundwater vulnerability assessment of the Cork Harbour area, SW Ireland. *Environmental Geology*, 53: 485-492.

Aller, L., Bennett, T., Lehr, J., and Petty, R. (1987) DRASTIC: a standardized system for evaluating ground water pollution potential using hydrogeologic settings. *Doc. EPA/600287035*, United States Environmental Protection Agency (USEPA), Washington, DC, 643 pp.

Andreo, B., Goldscheider, N., Vadillo, I., Vias, J., Neukum, C., Sinreich, M., Jimenez, P., Brechenmacher, J., Carrasco, F., Hötzl, H., and Perles, M. J. (2006). Karst groundwater protection: first application of a Pan-European approach to vulnerability, hazard and risk mapping in the Sierra de Libar (southern Spain). *Science of the Total Environment*, 357: 54-73.

Awawdeh, M. M. and Jaradat, R. A. (2010). Evaluation of aquifers vulnerability to contamination in the Yarmouk River basin, Jordan, based on DRASTIC method. *Arabian Journal of Geosciences*, 3: 273-282.

Babiker, I. S., Mohamed, A. A., Hiyama, T., and Kato, K. (2005). A GIS-based DRASTIC model for assessing aquifer vulnerability in Kakamigahara Heights, Gifu Prefecture, central Japan. *Science of the Total Environment,* 345: 127-140.

Babiker, I. S., Mohamed, A. A. M., Terao, H., Kato, K., and Ohta, K. (2004). Assessment of groundwater contamination by nitrate leaching from intensive vegetable cultivation using geographical information system. *Environment International*, 29(8): 1009-1017.

Babiker, I. S., Mohamed, M. M. A. and Hiyama, T. (2007). Assessing groundwater quality using GIS. *Water Resources Management*, 21: 699-715.

Backman, B., Bodiš, D., Lahermo, P., Rapant, S., and Tarvainen, T. (1998). Application of a groundwater contamination index in Finland and Slovakia. *Environmental Geology*, 36(1-2): 55-64.

Barbash, J. E. and Resek, E. A. (1996). *Pesticides in groundwater: distribution, trends, and governing factors.* Ann Arbor, Chelsea, MI.

Barrocu, G., Muzzu, M. and Uras, G. (2007). Hydrogeology and vulnerability map (Epik method) of the "Supramonte" karstic system, north-central Sardinia. *Environmental Geology*, 51(5): 701-706.

Bartram, J. and Ballance, R. (1996). *Water Quality Monitoring: A Practical Guide to the Design and Implementation of Freshwater Quality Studies and Monitoring Programmes.* The United Nations Environment Programme (UNEP) and the World Health Organization (WHO), 348 pp.

Beven, K. J., Henderson, D. E. and Reeves, A. D. (1993). Dispersion parameters for undisturbed partially saturated soil. *Journal of Hydrology*, 143: 19-43.

Bonham-Carter, G. F. (1996). Geographic information systems for geoscientists: modelling with GIS. *Computer Methods in the Geosciences*, Volume 13. Pergamon/Elsevier Science Publication, 98 p.

Burrough, P. A. and McDonnell, R. A. (1998). *Principles of Geographical Information Systems.* Oxford University Press, Oxford, UK, 333 pp.

Castrignanò, A., Giugliarini, L., Risaliti, R., and Martinelli, N. (2000). Study of spatial relationships among some soil physicochemical properties of a field in central Italy using multivariate geostatistics. *Geoderma*, 97: 39-60.

Ceron, J. C., Jimenez-Espinosa, R. and Pulido-Bosch, A. (2000). Numerical analysis of hydrogeochemical data: a case study. *Applied Geochemistry*, 15(7): 1053-1067.

Chang, K.-T. (2002). *Introduction to Geographic Information Systems*. Tata McGraw-Hill Publishing Company Ltd., New Delhi, India, 348 pp.

Chen, Y., Takara, K., Cluckie, I. D., and Smedt, F. H. D. (Editors) (2004). *GIS and Remote Sensing in Hydrology, Water Resources and Environment*. IAHS Publication No. 289, IAHS Press, Wallingford, 422 pp.

Civita, M., De Maio, M. (2004) Assessing and mapping groundwater vulnerability to contamination: the Italian "combined" approach. *Geofisica Internacional,* 43(4): 513-532.

Civita, M. (1994). Le carte della vulnerabilità degli acquiferi all'inquinamento: teoria e pratica [Contamination vulnerability mapping of the aquifer: theory and practice]. *Quaderni di Tecniche di Protezione Ambientale,* Pitagora Editrice.

Civita, M. and De Maio, M. (2000). Valutazione e cartografia automatica della vulnerabilità degli acquiferi all'inquinamento con il systema parametrico SINTACS R5 *[Evaluation and automatic cartography of aquifer vulnerability using the parametric system SINTACS R5].* Pitagora Editrice, Bologna.

Cramer, W. and Vrba, J. (1987). Vulnerability mapping. *Proceedings of the International Conference on Vulnerability of Soil and Groundwater to Pollutants.* Woordrijk aan Zee, The Netherlands, 30 March-3 April 1987, pp. 45-48.

Daly, D., Dassaargues, A., Drew, D., Dunne, S., Goldscheeider, N., Neale, S., Popescu, I. C., and Zwahlen, F. (2002). Main concepts of the European Approach for (karst) groundwater vulnerability assessment and mapping. *Hydrogeology Journal*, 10: 340-345.

Debernardi, L., De Luca, D. A. and Lasagna, M. (2008). Correlation between nitrate concentration in groundwater and parameters affecting aquifer intrinsic vulnerability. *Environmental Geology*, 55: 539-558.

Dillon, R. and Goldstein, M. (1984). *Multivariate Analyses: Methods and Applications*. Wiley, New York.

Doerfliger, N. and Zwahlen, F. (1995). EPIK: a new method for outlining of protection areas: a water vulnerability assessment in karst environment. In: *Proceedings of 5th International Symposium on karst waters and environmental impacts*, Antalya, Balkema, Rotterdam, pp. 117-123.

Doerfliger, N. and Zwahlen, F. (1998). *Groundwater Vulnerability Mapping in Karstic Regions (EPIK) – Application to Groundwater Protection Zones.* Swiss Agency for the Environment, Forests and Landscape (SAEFL), Bern.

Doerfliger, N., Jeannin, P. Y. and Zwahlen, F. (1999). Water vulnerability assessment in karst environments: a new method of defining protection areas using a multi-attribute approach and GIS tools (EPIK method). *Environmental Geology*, 39(2): 165-176.

Draper, N. R. and Smith, H. (1998). *Applied Regression Analysis*. Wiley-Interscience, New York, 407 pp.

Dunteman, G. H. (1989). *Principal Component Analysis*. Sage, Thousand Oaks, CA.

Edet, A. (2014). An aquifer vulnerability assessment of the Benin Formation aquifer, Calabar, southeastern Nigeria, using DRASTIC and GIS approach. *Environmental Earth Sciences*, 71(4): 1747-1765.

El-Naqa, A. (2004). Aquifer vulnerability assessment using DRASTIC index at Russeifa landfill, northeast Jordan. *Environmental Geology*, 47: 51-62.

Evans, B. M. and Myers, W. L. (1990). A GIS-based approach to evaluating regional groundwater pollution potential with DRASTIC. *Journal of Soil and Water Conservation,* 45(2): 242-245.

Fabbri, A. G. and Napolitano, P. (1995). The use of database management and geographical information systems for aquifer vulnerability analysis. *Contribution to the International Scientific Conference on the occasion of the 50th Anniversary of the founding of the Vysoka Skola Banska*, Ostrava, Czech Republic.

Fetter, C. W. (1994). *Applied Hydrogeology*. 4th edition, Prentice Hall, NJ, pp. 543-592.

Foster, S. S. D. (1987). Fundamental concepts in aquifer vulnerability pollution risk and protection strategy. In: W. van Duijvenbooden and H. G. van Waegeningh (Editors), *Vulnerability of Soils and Groundwater to Pollution, 38, TNO Committee on Hydrological Research*, The Hague, pp. 69-86.

Foster, S. S. D., Hirata, R., Gomes, D., D'Elia, M., and Paris, M. (2002). *Groundwater quality protection: a guide for water utilities, municipal authorithies, and environment agencies*. The World Bank, Washington, D.C., 103 pp.

Freeze, R. A. and Cherry, J. A. (1979). *Groundwater*. Prentice-Hall, Inc., Englewood Cliffs, New Jersey.

Frind, E., Molson, J. and Rudolph, D. (2006). Well vulnerability: a quantitative approach for source water protection. *Ground Water*, 44(5): 732-742.

Fritch, T. G., McKnight, C. L., Yelderman, J. C., and Arnold, J. G. (2000). Aquifer vulnerability assessment of the Paluxy aquifer, Central Texas, US, using GIS and a modified DRASTIC approach. *Environmental Management*, 25(3): 337-345.

GEAM (Associazione Georisorce é ambiente) (2005). Aquifer vulnerability and risk. *Proceedings of the 2nd Workshop, CNR-GNDCI*, Parma, Italy, September 2005.

GESAMP (1988). *Report of the Eighteenth Session, Paris 11-15 April 1988. GESAMP Reports and Studies No. 33,* United Nations Educational, Scientific and Cultural Organization, Paris.

Gogu, R. and Dassargues, A. (2000). Current trends and future challenges in groundwater vulnerability assessment using overlay and index methods. *Environmental Geology*, 39(6): 549-559.

Gogu, R. C., Hallet, V. and Dassargues, A. (2003). Comparison of aquifer vulnerability assessment techniques. Application to the Néblon River basin (Belgium). *Environmental Geology*, 44: 881-892.

Goldscheider, N. (2004). The concept of groundwater vulnerability. In: Zwahlen, F. (Editor), Vulnerability and risk mapping for the protection of carbonate (karst) aquifers, *Final Report COST Action 620*. European Commission, Directorate-General for Research, EUR 20912: 5-9.

Goldscheider, N. and Popescu, I. C. (2004). The European approach. In: Zwahlen, F. (Editor), *Vulnerability and Risk Mapping for the Protection of Carbonate (karst) Aquifers, Final Report COST Action 620*. European Commission Directorate-General for Research, EUR 20912: 17-21.

Goldscheider, N., Klute, M., Sturm, S., and Hotzl, H. (2000). The PI method: a GIS-based approach to mapping groundwater vulnerability with special consideration of karst aquifers. *Zeitschrift für Angewandte Geologie*, 463: 157-166.

Goodchild, M. F., Parks, B. O. and Steyaert, L. T. (Editors) (1993). *Environmental Modeling with GIS*. Oxford University Press, New York.

Goovaerts, P. (1997). *Geostatistics for Natural Resources Evaluation*. Oxford University Press, New York.

Goovaerts, P. (1999). Geostatistics in soil science: State-of-the-art and perspectives. *Geoderma*, 89: 1-45.

Gotway, C. A., Ferguson, R. B., Hergert, G. W., and Peterson, T. A. (1996). Comparison of kriging and inverse-distance methods for mapping soil parameters. *Soil Science Society of America Journal*, 60(4): 1237-1247.

Güler, C., Thyne, G. D., McCray, J. E., and Turner, A. K. (2002). Evaluation of graphical and multivariate statistical methods for classification of water chemistry data. *Hydrogeology Journal*, 11: 607-608.

Guo, Q., Wang, Y., Gao, X., and Ma, T. (2007). A new model (DRARCH) for assessing groundwater vulnerability to arsenic contamination at basin scale: a case study in Taiyuan basin, northern China. *Environmental Geology,* 52(5): 923-932.

Gurnell, A. M. and Montgomery, D. R. (Editors) (2000). *Hydrological Applications of GIS*. John Wiley and Sons Ltd., Chichester, UK, 176 pp.

Haertle, A. (1983). Method of working and employment of EDP during the preparation of groundwater vulnerability maps. *International Association of Hydrological Sciences Publication* 142: 1073-1085.

Harman, H. H. (1960). *Modern Factor Analysis*. University of Chicago Press, Chicago.

Herlinger, R. Jr. and Viero, A. P. (2006). Evaluation of contaminants retention in soils from Viama˜o District, Rio Grande do Sul State, Brazil. *Environmental Geology*, 50: 47-54.

Hoelting, B., Haertlé, T., Hohberger, K.-H., Nachtigall, K. H., Villinger, E., Weinzierl, W., and Wrobel, J.-P. (1995). *Konzept zur Ermittlung der Schutzfunktion der Grundwasserueberdeckung.– Geol. Jb., C, 63: 5-24; Hannover.* – [translated into English by the Federal Institute for Geosciences and Natural Resources: Concept for the Determination of the Protective Effectiveness of the Cover above the Groundwater against Pollution.– Ad-hoc Working Group on Hydrogeology, 28 p.; Hannover].

Horton, R. K. (1965). An index number system for rating water quality. *Journal–Water Pollution Control Federation*, 37: 300-305.

Hrkal, Z. (2001). Vulnerability of groundwater to acid deposition, Jizerske Mountains, northern Czech Republic: construction and reliability of a GIS-based vulnerability map. *Hydrogeology Journal*, 9: 348-357.

Ibe, K. M., Nwankwor, G. I. and Onyekuru, S. O. (2001). Assessment of ground water vulnerability and its application to the development of protection strategy for the water supply aquifer in Owerri, Southeastern Nigeria. *Environmental Monitoring and Assessment*, 67(3): 323-360.

Isaaks, E. and Srivastava, R. M. (1989). *An Introduction to Applied Geostatistics.* Oxford University Press, New York.

Jackson, J. E. (1991). *A User's Guide to Principal Components*. John Wiley and Sons, New York.

Jha, M. K., Chowdhury, A., Chowdary, V. M., and Peiffer, S. (2007). Groundwater management and development by integrated remote sensing and geographic information systems: Prospects and constraints. *Water Resources Management,* 21(2): 427-467.

Johnson, L. E. (2009). *Geographic Information Systems in Water Resources Engineering.* CRC Press, Boca Raton, 286 pp.

Journel, A. G. and Huijbregts, C. J. (1978). *Mining Geostatistics*. Academic Press, New York.

Jury, W. A. (1986). Spatial variability of soil properties. In: S. C. Hern and S. M. Melancon (editors), *Vadose Zone Modeling of Organic Pollutants*, Lewis publishers, Chelsea, pp. 245-269.

Jury, W. A., Russo, D., Sposito, G., and Elaod, H. (1987). The spatial variability of water and solute transport properties in unsaturated soil: I. *Analysis of property variation and spatial structure and statistical models.* Hilarda, 55: 1-32.

Kaiser, H. F. (1958). The varimax criterion for analytic rotation in factor analysis. *Psychometrika*, 23: 187-200.

Karanth, K. R. (1987). *Ground Water Assessment: Development and Management.* Tata McGraw-Hill Publishing Company Limited, New Delhi, pp. 720.

Kazakis, N. and Voudouris, K. (2011). Comparison of three applied methods of groundwater vulnerability mapping: A case study from the Florina basin, northern Greece. In: N. Lambrakis, Stournaras, G. and Katsanou, K. (Editors), *Advances in the Research of Aquatic Environment*, Vol. 2, Springer-Verlag, Berlin Heidelberg.

Kim, Y. J. and Hamm, S. Y. (1999). Assessment of the potential for ground water contamination using the DRASTIC/EGIS technique, Cheongju area, South Korea. *Hydrogeology Journal*, 7: 227-235.

Kitanidis, P. K. (1997). *Introduction to Geostatistics: Applications in Hydrogeology.* Cambridge University Press, New York, 249 pp.

Kitanidis, P. K. (1999). Geostatistics: Interpolation and inverse problems. In: J. W. Delleur (Editor-in-Chief), *The Handbook of Groundwater Engineering*, CRC Press, Florida, pp. 12-1 to 12-20.

Kouli, M., Lydakis-Simantiris, N. and Soupios, P. (2008). GIS-Based Aquifer Modeling and Planning Using Integrated Geoenvironmental and Chemical Approaches. In: L. F. Konig and J. L. Weiss (Editors), *Groundwater: Modeling, Management and Contamination.* Nova Science Publishers, Inc., pp. 1-61.

Kruseman, G. P. and de Ridder, N. A. (1990). Analysis and Evaluation of Pumping Test Data. *International Institute for Land Reclamation and Improvement, Publication No. 47,* 2nd ed., Wageningen, Netherlands.

Lake, I. R., Lovett, A. A. and Hiscock, K. M. (2003). Evaluating factors influencing groundwater vulnerability to nitrate pollution: developing the potential of GIS. *Journal of Environmental Management*, 68(3): 315-328.

Lasserre, F., Razack, M. and Banton, O. (1999). A GIS-linked model for the assessment of nitrate contamination in groundwater. *Journal of Hydrology*, 224(3-4): 81-90.

Lee, S. (2003). Evaluation of waste disposal site using the DRASTIC system in southern Korea. *Environmental Geology*, 44: 654-664.

Lermontov, A., Yokoyama, L., Lermontov, M., Machado, M. A. S. (2009). River quality analysis using fuzzy water quality index: Ribeira do Iguape river watershed, Brazil. *Ecological Indicators*, 9: 1188-1197.

Lo, C. P. and Yeung, A. K. W. (2003). *Concepts and Techniques of Geographic Information Systems.* Prentice-Hall of India Pvt. Ltd., New Delhi, 492 pp.

Loague, K. and Corwin, D. L. (1998). Regional-scale assessment of non-point source groundwater contamination. *Hydrological Processes*, 12(6): 957-965.

Loague, K., Bernknopf, R. L., Green, R. E., and Giambelluca, T. W. (1996). Uncertainty of groundwater assessments for agricultural regions in Hawaii, Review. *Journal of Environmental Quality*, 25(3): 475-490.

Longo, A., Andreo, B., Carrasco, F., Cucchi, F., Vìas, J. M., and Jimènez, P. (2001). Comparison of two contamination vulnerability maps obtained by the SINTACS method in two carbonate aquifers (S Spain). In: *Proceedings of the 7th Conference on Limestone Hydrology and Fissured Media.* Besançon, Francia, pp. 233-236.

Lynch, S. D., Reynders, A. G. and Schulze, R. E. (1997). A DRASTIC approach to ground water vulnerability in South Africa. *South African Journal of Science,* 93(2): 59-60.

Machiwal, D. and Jha, M. K. (2010). Tools and techniques for water quality interpretation. In: Krantzberg, G., Tanik, A., Antunes do Carmo, J. S., Indarto, A., and Ekdal, A. (Editors-in-Chief), Advances *in Water Quality Control,* Scientific Research Publishing, Inc., California, US, pp. 211-252.

Machiwal, D., Jha, M. K. and Mal, B. C. (2011). GIS-based assessment and characterization of groundwater quality in a hard-rock hilly terrain of western India. *Environmental Monitoring and Assessment*, 174(1-4): 645-663.

Machiwal, D., Jha, M. K. and Mal, B. C. (2013). Evaluating Spatio-Temporal Changes in Groundwater Quality of Precambrian Aquifer System in Udaipur District of Rajasthan. In: Das, S. (Editor), *Groundwater in Drylands of Rajasthan: Arwari Model of Management*, Memoir 82, Geological Society of India, Bangalore, pp. 146-157.

Margat, J. (1968). *Groundwater Vulnerability to Contamination*. Publication 68, BRGM, Orleans, France.

Marsily, G. de (1986). *Quantitative Hydrogeology: Groundwater Hydrology for Engineers.* Academic Press, CA, 440 pp.

Martinez-Bastida, J. J., Arauzp, M. and Valladolid, M. (2010). Intrinsic and specific vulnerability of groundwater in central Spain: the risk of nitrate pollution. *Hydrogeology Journal*, 18: 681-698.

Massone, H., Londoño, M. Q. and Martínez, D. (2010). Enhanced groundwater vulnerability assessment in geological homogeneous areas: a case study from the Argentine Pampas. *Hydrogeology Journal*, 18(2): 371-379.

Massone, H., Quiroz Londoño, M., Tomas, M., and Ferrante, A. (2007). Evaluación de la vulnerabilidad de acuíferos en cuencas de llanura periserranas. Estudio de caso, Balcarce, Provincia de Buenos Aires. (aquifer vulnerability assessment in inter-range basins. Balcarce, Buenos Aires Province as study case). *V Congreso Argentino de Hidrogeología*, vol., IAH, Paraná, Argentina, pp. 149-158.

Matheron, G. (1965). *Les Variables Regionalisèes et leur Estimation*. Masson, Paris, France.

Mathes, S. E. and Rasmussen, T. C. (2006). Combining multivariate statistical analysis with geographic information systems mapping: a tool for delineating groundwater contamination. *Hydrogeology Journal*, 14: 1493-1507.

McCutcheon, S. C., Martin, J. L. and Barnwell, T. O. (1993). Water Quality. In: D. R. Maidment (Editor-in-chief), *Handbook of Hydrology*, McGraw-Hill, Inc., New York, pp. 11.1-11.73.

McLay, C. D. A., Dragten, R., Sparling, G., and Selvarajah, N. (2001). Predicting groundwater nitrate concentrations in a region of mixed agricultural land use: a comparison of three approaches. *Environmental Pollution,* 115(2): 191-204.

Meinardi, C. R. and Beusen, A. H. W. and Bollen, M. J. S. and Klepper, O. and Willems, W. J. (1995). Vulnerability to diffuse pollution and average nitrate contamination of European soils and groundwater. *Water Science and Technology,* 31(8): 159-165.

Melloul, A. J. and Collin, M. (1998). A proposed index for aquifer water quality assessment: The case of Israel's Sharon region. *Journal of Environmental Management*, 54: 131-142.

Merchant, J. W. (1994). GIS-based groundwater pollution hazard assessment: a critical review of the DRASTIC model. *Photogrammetric Engineering and Remote Sensing,* 60(9): 1117-1128.

Meybeck, M. and Helmer, R. (1992). An Introduction to Water Quality. In: D. Chapman (editor), *Water Quality Assessments: A Guide to Use of Biota, Sediments and Water in Environmental Monitoring,* 2nd Edition, the

United Nations Educational, Scientific and Cultural Organization (UNESCO), the World Health Organization (WHO), and the United Nations Environment Programme (UNEP), E and FN Spon, UK, 609 pp.

Meybeck, M., Kimstach, V. and Helmer, R. (1992). Strategies for Water Quality Assessment. In: D. Chapman (editor), *Water Quality Assessments: A Guide to Use of Biota, Sediments and Water in Environmental Monitoring*, 2nd Edition, the United Nations Educational, Scientific and Cultural Organization (UNESCO), the World Health Organization (WHO), and the United Nations Environment Programme (UNEP), E and FN Spon, UK, 609 pp.

Mouser, P. J., Hession, W. C., Rizzo, D. M., and Gotelli, N. J. (2005). Hydrology and Geostatistics of a Vermont, US Kettlehole Peatland. *Journal of Hydrology*, 301(1-4): 250-266.

Murat, V., Rivera, A., Pouliot, J., Miranda-Salas, M., and Savard, M. M. (2004). Aquifer vulnerability mapping and GIS: a proposal to monitor uncertainty associated with spatial data processing. *Geofisica Interncional*, 43(4): 551-565.

Namgial, D. and Jha, M. K. (2009). Filtering techniques for quantifying tidal impacts on groundwater: A comparative analysis. *Current Science*, 96(7): 947-956.

National Research Council (NRC) (1993). *Groundwater Vulnerability Assessment: Predictive Relative Contamination Potential under Conditions of Uncertainty.* National Academy Press, Washington, DC.

Osborn, N. I., Eckenstein, E. and Koon, K. Q. (1998). *Vulnerability assessment of twelve major aquifers in Oklahoma. Technical Report 98-5,* Oklahoma Water Resources Board, Oklahoma City, OK, US.

Otto, M. (1998). Multivariate methods. In: R. Kellner, J. M. Mermet, M. Otto and Widmer H. M. (editors), *Analytical Chemistry*, Wiley-VCH, Weinheim, Germany, 916 pp.

Piscopo, G. (2001). *Groundwater vulnerability map, explanatory notes – Castlereagh catchment*. Centre for Natural Resources, NSW Department of Land and Water Conservation, New South Wales, Australia.

Polemio, M., Casarano, D. and Limoni, P. P. (2009). Karstic aquifer vulnerability assessment methods and results at a test site (Apulia, southern Italy). *Natural Hazards and Earth System Sciences*, 9: 1461-1470.

Popescu, I. C., Gardin, N., Brouyere, S., and Dassargues, A. (2008). Groundwater vulnerability assessment using physically-based modelling: from challenges to pragmatic solutions. In: *Calibration and reliability in*

groundwater modelling: credibility of modelling. *Proceedings of ModelCARE 2007 Conference*, Denmark, September 2007, IAHS Publications, 320, IAHS, Wallingford, UK.

Pradhan, S. K., Patnaik, D. and Rout, S. P. (2001). Water quality index for the ground water in and around a phosphatic fertilizer plant. *Indian Journal of Environmental Protection,* 21: 355-358.

Provencher, M. and Lamontagne, M. P. (1977). *Méthode de determination d'un indice d'appréciation de la qualité des eaux selon différentes utilisations*, Québec, Ministère des Richesses Naturelles, Service de la qualité des eaux.

Rahman, A. (2008). A GIS based model for assessing groundwater vulnerability in shallow aquifer in Algarh, India. *Applied Geography*, 28(1): 32-53.

Ramesh, S., Sukumaran, N., Murugesan, A. G., and Rajan, M. P. (2010). An innovative approach of Drinking Water Quality Index - A case study from Southern Tamil Nadu, India. *Ecological Indicators*, 10: 857-868.

Rao, P. S. C. and Alley, W. M. (1993). Pesticides. In: Alley, W. M. (Editor), *Regional Groundwater Quality*. Van Nostrand Reinhold, New York, pp. 345-382.

Robinson, T. P. and Metternicht, G. (2006). Testing the performance of spatial interpolation techniques for mapping soil properties. *Computers and Electronics in Agriculture,* 50: 97-108.

Rodgers, J. L. and Nicewander, W. A. (1988). Thirteen ways to look at the correlation coefficient. *The American Statistician*, 42: 59-66.

Rodriguez, R., Civita, M. and de Maio, M. (2003). Aquifer vulnerability and risk. *1st International Workshop, Proceedings, UNAM*, Guanajuato, Mexico, May 2003.

Rupert, M. G. (2001). Calibration of the DRASTIC ground water vulnerability mapping method. *Ground Water*, 39(4): 625-630.

Sánchez, E., Colmenarejo, M. F., Vicente, J., Rubio, A., García, M. G., Travieso, L., and Borja, R. (2007). Use of the water quality index and dissolved oxygen deficit as simple indicators of watersheds pollution. *Ecological Indicators*, 7: 315-328.

Sara, M. N. and Gibbons, R. (1991). Organization and Analysis of Water Quality Data. In: D. M. Nielsen (Editor), *Practical Handbook of GroundWater Monitoring,* Lewis Publishers, Michigan, US, pp. 541-588.

Schaefer, J. A. and Mayor, S. J. (2007). Geostatistics reveal the scale of habitat selection. *Ecological Modelling*, 209 (2-4): 401-406.

Schultz, M. T. (2001). A critique of EPA's index of watershed indicators. *Journal of Environmental Management*, 62: 429-442.

Secunda, S., Collin, M. L. and Melloul, A. J. (1998). Groundwater vulnerability assessment using a composite model combining DRASTIC with extensive agricultural land use in Israel's Sharon region. *Journal of Environmental Management*, 54: 39-57.

Shuhaimi-Othman, M., Lim, E. C. and Mushrifah, I. (2007). Water quality changes in Chini Lake, Pahang, West Malaysia. *Environmental Monitoring and Assessment*, 131: 279-292.

Simsek, C., Kincal, C. and Gunduz, O. (2006). A solid waste disposal site selection procedure based on groundwater vulnerability mapping. *Environmental Geology*, 49(4): 620-633.

Skidmore, A. K., Bijer, W., Schmidt, K., and Lalit Kumar, K. (1997). Use of remote sensing and GIS for sustainable land management. *ITC Journal*, 3 (4): 302-315.

Soltan, M. E. (1999). Evaluation of groundwater quality in Dakhla Oasis (Egyptian Western Desert). *Environmental Monitoring and Assessment*, 57: 157-168.

Stafford, D. B. (editor) (1991). *Civil Engineering Applications of Remote Sensing and Geographic Information Systems*. ASCE, New York.

Štambuk-Giljanović, N. (1999). Water quality evaluation by index in Dalmatia. *Water Research*, 33(16): 2440-3423.

Stark, S. L., Nuckols, J. R. and Rada, J. (1999). Using GIS to investigate septic system sites and nitrate pollution potential. *Journal of Environment and Health,* 61(8): 15-20.

Stempvoort, D. V., Ewert, L. and Wassenaar, L. (1992). AVI: A method for groundwater protection mapping in the prairie provinces of Canada. *Prairie Provinces Water Board Report*, 114, Regina, SK.

Stempvoort, D. V., Ewert, L. and Wassenaar, L. (1993). Aquifer vulnerability index: A GIS - compatible method for groundwater vulnerability mapping. *Canadian Water Resources Journal*, 18(1): 25-37.

Steube, C., Richter, S. and Griebler, C. (2009). First attempts towards an integrative concept for the ecological assessment of groundwater ecosystems. *Hydrogeology Journal*, 17(1): 23-35.

Stigter, T. Y., Ribeiro, L. and Carvalho Dill, A. M. M. (2006). Application of a groundwater quality index as an assessment and communication tool in agro-environmental policies: Two Portuguese case studies. *Journal of Hydrology*, 327: 578-591.

Suk, H. and Lee, K. K. (1999). Characterization of a ground water hydrochemical system through multivariate analysis: clustering into ground water zones. *Ground Water*, 37(3): 358-366.

Tesoriero, A. J., Inkpen, E. L. and Voss, F. D. (1998). Assessing groundwater vulnerability using logistic regression. *Paper from proceedings for the Source Water Assessment and Protection 98 Conference*, Dallas, TX, April, 1998, pp. 157-165.

Thapinta, A. and Hudak, P. F. (2003). Use of geographic information systems for assessing groundwater pollution potential by pesticides in Central Thailand. *Environment International*, 29: 87-93.

Thirumalaivasan, D., Karmegam, M. and Venugopal, K. (2003). AHP-DRASTIC: software for specific aquifer vulnerability assessment using DRASTIC model and GIS. *Environmental Modeling and Software*, 18: 645-656.

Tilahun, K. and Merkel, B. J. (2010). Assessment of groundwater vulnerability to pollution in Dire Dawa, Ethiopia using DRASTIC. *Environmental Earth Sciences*, 59(7): 1485-1496.

Todd, D. K. (1980). *Groundwater Hydrology*. 2nd edition, John Wiley and Sons, NY, pp. 111-163.

Tovar, M. and Rodriguez, R. (2004). Vulnerability assessment of aquifers in an urban-rural environment and territorial ordering in Leon, Mexico. *Geofisica Interncional*, 43(4): 603-609.

Umar, R., Ahmed, I. and Alam, F. (2009). Mapping groundwater vulnerable zones using modified DRASTIC approach of an alluvial aquifer in parts of central Ganga plain, Western Uttar Pradesh. *Journal of the Geological Society of India,* 73(2): 193-201.

USEPA (1991). *Guidance for water quality-based decisions: The TMDL process.* Assessment and Watershed Protection Division, United States Environmental Protection Agency (USEPA), Washington, D.C.

Vauclin, M., Vieira, S. R., Vachaud, G., and Nielsen, D. R. (1983). The use of cokriging with limited field observations. *Soil Science Society of America Journal*, 47: 175-184.

Vías, J. M., Andreo, B., Perles, M. J., and Carrasco, F. (2005). A comparative study of four schemes for groundwater vulnerability mapping in a diffuse flow carbonate aquifer under Mediterranean climatic conditions. *Environmental Geology*, 47(4): 586-595.

Vias, J. M., Andreo, B., Perles, M. J., Carrasco, F., Vadillo, I., and Jimenez, P. (2002). Preliminary proposal of a method for contamination vulnerability

mapping in carbonate aquifers. In: Carrasco, F., Duran, J. J. and Andreo, B. (Editors), *Karst and Environment*, Fundacion Cueva de Nerja.

Vías, J. M., Andreo, B., Perles, M. J., Carrasco, F., Vadillo, I., and Jimenez, P. (2006). Proposed method for groundwater vulnerability mapping in carbonate (karstic) aquifers: the COP method - Application in two pilot sites in Southern Spain. *Hydrogeology Journal*, 14: 912-925.

Vignolo, A., Pochettino, A. and Cicerone, D. (2006). Water quality assessment using remote sensing techniques: Medrano Creek, Argentina. *Journal of Environmental Management,* 81: 429-433.

Vrba, J. and Zaporozec, A. (Editors) (1994). Guidebook on Mapping Groundwater Vulnerability. *IAH International Contribution for Hydrogeology*, Volume 16/94, Heise, Hannover, 131p.

Wade, A. C., York, H. F., Morey, A. E., Padmore, J. M., and Rudo, K. M. (1998). The impact of pesticide use on groundwater in North Carolina. *Journal of Environmental Quality*, 27: 1018-1026.

Wang, Y., Merkel, B. J., Li, Y., Ye, H., Fu, S., and Ihm, D. (2007). Vulnerability of groundwater in Quaternary aquifers to organic contaminants: a case study in Wuhan City, China. *Environmental Geology*, 53: 479-484.

Webster, R. and Oliver, M. A. (2001). *Geostatistics for Environmental Science.* John Wiley and Sons, Toronto, Canada, 271 pp.

Werz, H. and Hötzl, H. (2007). Groundwater risk intensity mapping in semi-arid regions using optical remote sensing data as an additional tool. *Hydrogeology Journal*, 15: 1031-1049.

WHO (2006). *Guidelines for Drinking-Water Quality: First Addendum to Third Edition*. Vol. 1, Recommendations, World Health Organization (WHO), Geneva, Switzerland, 515 pp.

Wilding, L. P. (1985). Spatial variability: Its documentation, accommodation, and implication to soil surveys. In: D. R. Nielsen and J. Bouma (editors), *Soil Spatial Variability, Proceedings of Workshop of the ISSS and the SSSA,* Las Vegas, November 30-December 1, 1984, Pudoc. Wageningen, the Netherlands, pp. 166-194.

Wollenhaupt, N. C., Mulla, D. J. and Gotway Crawford, C. A. (1997). Soil sampling and interpolation techniques for mapping spatial variability of soil properties. In: F. J. Pierce and E. J. Sadler (editors), *The State of Site Specific Management for Agriculture,* American Society of Agronomy, Madison, Wisconsin, pp. 19-54.

Yin, L., Zhang, E., Wang, X., Wenninger, J., Dong, J., Guo, L., and Huang, J. (2013). A GIS-based DRASTIC model for assessing groundwater

vulnerability in the Ordos Plateau, China. *Environmental Earth Sciences*, 69(1): 171-185.

Zhou, J., Li, G., Liu, F., Wang, Y., and Guo, X. (2010). DRAV model and its application in assessing groundwater vulnerability in arid area: a case study of pore phreatic water in Tarim Basin, Xinjiang, Northwest China. *Environmental Earth Sciences*, 60(5): 1055-1067.

Zwahlen, F. (Editor) (2004). *Vulnerability and risk mapping for the protection of carbonate (karst) aquifers. Final Report (COST action 620)*, European Commission, Brussels, 315.

Chapter 9

FLOOD RISKS ANALYSIS IN A LITTORAL AFRICAN CITY: USING GEOGRAPHIC INFORMATION SYSTEM

Nkeki Felix Ndidi[1] and Ojeh Vincent Nduka[2]

[1]Department of Geography and Regional Planning,
University of Benin, Benin City, Nigeria
[2]Department of Geography and Regional Planning,
Delta State University, Abraka, Nigeria

ABSTRACT

Flood hazard has become the most frequent natural disaster and has provoked global responsiveness. Due to its devastating nature, many lives have been lost, natural ecology degraded, disrupted social and economic activities and destroyed properties worth billions of dollars. Such overwhelming effect is felt more in urban centers especially those located in coastal regions. Estimating flood risk was a complex multi-faceted problem due to the level and amount of knowledge in systematic disciplines such as geography, geomorphology, climatology, hydrology, hydraulic engineering and urban planning that need to be combined.

Presently, this problem has been surmount with the introduction of geographic information system (GIS) which when properly integrated with remote sensing technique, has the capability to transform the manner and way of modeling flood risk and extracting spatial information to support decision making processes.

The substantive objective of this chapter is to examine the formidability of using high resolution remote sensing data and GIS techniques to assess and identify flood prone areas before occurrence in Lagos State-large coastal city of Nigeria. The GIS-based flood risk methodology so-developed for a littoral urban region proved to be helpful in extracting flood prone areas based on elevation from SRTM digital elevation model (DEM) and proximity to source of hazard. Such risk areas were then classified into magnitudes of potential risk and five classes were identified-very high, high, moderate, low and very low. This extracted flood mask was further used to estimate the proportion of agricultural land and urban land likely to be affected in the event of a flood episode. To support grass root policy, the areal calculation was disaggregated into local government area territory. Furthermore, land use/ land cover data of the study region was extracted from Landsat image using a supervised classification method based on maximum likelihood algorithm. The extracted potential flood risk masks were overlaid on the land cover data so as to assess the likely impact of flood on the various land uses-agricultural land use and urban land use. In the same way, the identified flood prone area masks were entered into Google earth engine for the purpose of quick visual impression and mapping the flood vulnerable areas by neighborhood and road infrastructures. The five-class vulnerability feature was then overlaid on the local administrative map data loaded with the projected population figure of the study region. From here the vulnerable population was estimated by Local Government Area (LGA). The results of the study show that GIS technique is a formidable tool for flood risk analysis, mitigation and pre-hazard planning. This can be seen from the series of thematic maps that were generated which were used to develop a large GIS-assisted database. It is evident that the database so-generated will facilitate flood risk management and provide an effective framework that will support policy formulation.

1. INTRODUCTION

Floods have become the most frequent and widespread natural disaster which has claimed many lives, degraded natural ecology, disrupted social and economic activities, destroyed properties and farmlands worth billions of dollars (Nkeki et al., 2013; Taubenbock et al., 2011; Thieken, et al., 2014; Ologunorisa, 2006). Some examples are the 1972 Rapid City, South Dakota flood in the United States which claimed about 238 lives and caused millions of dollars in damage, the 1975 Banqiao dam flood in China which drowned about 26,000 people and caused another 140,000 death as a result of epidemic outbreak, the 1983 Pacific flood, northwest of the United States destroyed pro-

perties estimated to worth 1.1 billion dollars, Yangtze river flood of 1998 displaced 14 million people, claimed hundreds of lives and damaged properties worth billions of pounds.

Recent examples are the 2012 Thailand devastating flooding episode which flooded 65 of 77 Provinces of the territory and resulted in a total of 815 deaths, left about 13.6 million people homeless and submerged 20,000 square kilometers of farmland. The 2012 Niger-Benue river floods in Nigeria affected 14 of the 36 states in the country, displaced an estimated 1.3 million people, claimed about 431 lives and submerged over 1,525 square kilometers of farmland.

The devastating effect of flooding is felt more in urban centers especially those located in coastal regions. This is because, on the one hand, the terrain is generally low and the presence of numerous water bodies (such as lake, lagoon, river, creek, etc.) which are prerequisite and essential source of flooding. On the other hand, littoral cities are prominent centers of high population concentration and prosperous economic region.

The economic boom that characterized such cities further initiate high population density. Consequently, there is need for more space with respect to residential and other developmental purposes. To cope with this rapid growth and satisfy the need, developmental activities spring up sporadically around the available urban space. In most cases, along sea shoreline, low lying terrain, close to swamp, lagoon and on a river valley. The fact that urban planning regulations in most African cities are not keenly enforced further aggravate the issue of flooding and vulnerability.

In Nigeria littoral cities for instance, it is common to find developmental activities and structures erected along natural flow paths, near shoreline, floodplain and lowland areas. Such anthropogenic actions obstruct excess runoff and discharge in the case of river flooding which has been reported (Sanyal and Lu, 2004) to be a recurrent natural phenomenon in the humid, tropical and subtropical climatic regions, especially in the wet seasons.

Basically, three major types of flooding occur in African coastal cities-river flooding, coastal flooding and urban flooding. River flooding is induced by heavy rainfall, excess runoff, and discharge within the river valley and its destructive impact is a function of distance from natural channel. Coastal flooding is typically a function of storm surge, waves (driven by wind) and heavy rainfall. Urban flooding results when development is concentrated within or along stream channels (Nkeki et al., 2013).

The consequences and severity of flooding is graver in littoral cities compared to cities in the hinterland. Apart from submergence of urban pro-

perties, loss of lives, destruction of agricultural lands and crops, disruption of socioeconomic activities, environmental disfiguration, inflow into sewage (causing municipal pollution), it also leaves a long lasting contaminating effect such as the intrusion of salt water into the soil, surface water and groundwater reserve. This may pose serious ecological distortion and initiates a new level of epidemic outbreak, scarcity of potable water and destruction of arable land for agricultural purposes (leading to shortage of food).

The issue of flood risk can be understood and linked to two major factors-the flood hazard itself and vulnerability. Flood hazard is a potentially destructive weather induced physical incident that is characterized by its location, intensity, frequency and probability (Taubenbock et al., 2011). The second factor-Vulnerability, represent the system or phenomenon (e.g. people, specific ecological configuration, land use, urban system, political component etc.) that is directly or indirectly exposed to the disastrous effect of the natural hazard. Thus, in an urban center the impact of flooding weighs heavily on the demographic, physical, social, economic, ecologic and political compositions of the affected area. Although, flood hazard is climatologically driven, the drive for increase in productivity, uncontrolled urban sprawl and rapid population growth in such urban area upsurges the risk and susceptibility.

However, urban flooding is directly and indirectly a function of man's interaction with the physical environment. Such interaction involves designing and locating infrastructure, exploring and exploiting natural resources, concentration of population and urbanization (Hualou, 2011). Indirectly, these activities have arguably increased flood risk through climate change and directly through anthropogenic disturbances, obstruction and alteration of natural flow paths and floodplains.

Since flooding is imminent in urban areas, formulating management strategy is the primary approach to achieving sustainable development. This is the case for advanced countries were technological knowledge is high and the availability of funding to accomplish any set objective and project pertaining to flood hazard such as hazard preparedness, quick response, awareness and enlightenment-vital information on flood prone areas and the spatial extent.

This is critical for most developing countries in Africa were hazard preparedness is not foremost and the existing flood management policies and strategies (mostly outdated and ill-prepared) are not enforced and executed to the latter. In most cases, such strategic plans are dedicated and geared towards compensating flood ravaged communities and dealing with the aftermath.

In these countries, resources (finance, information) for developmental activities are limited owing to the unstable political system. Perhaps, this

explains why floods of equal magnitude cause more losses and damage in developing countries compared to developed nations who generally have well-structured monitoring and early warning system (Opolot, 2013). Flood disaster management is a huge capital intensive program due to the amount of spatial information required for risk prediction and assessment, especially when ground-based survey method is adopted. To maximize the limited financial resources (in developing countries), a sustainable and cost-effective method of extracting and generating required information is paramount.

The first step needed to carryout flood risk analysis and assessment is to identify the areas vulnerable to the hazard (Sanyal and Lu, 2004; Ishaya et al., 2009) and delineating these areas in a map. Initially, estimating flood risk was a complex multi-faceted problem because various knowledge in systematic disciplines such as geography, geomorphology, climatology, hydrology, hydraulic engineering and urban planning need to be combined.

The current advancement in geographic information system (GIS) and remote sensing techniques have revolutionized the method of modeling flood risk and extracting spatial information to support decision making processes and enacting of public policies. GIS technique allows the integration and synchronization of spatial data captured by space borne sensors orbiting the earth with demographic and socioeconomic data for the purpose of generating timely geospatial information for comprehensive risk mitigation planning (Tralli et al., 2005).

The primacy of GIS technology in the field of disaster management, especially flood related has been reported and adopted by contemporary spatial scientist (Nkeki et al., 2013; Sanyal and Lu, 2004; Taubenbock et al., 2011; Alaghmand, et al., 2010; Samarasinghe, et al., 2010; Tralli et al., 2005; Triglav-Cekada and Radovan, 2013; Opolot, 2013; Zhang et al., 2008; Wang, 2004; Nirupama and Simonovic, 2007; Zheng et al., 2008; Irimescu, et al., 2010).

The capability of GIS technology to visualize and analyze spatial and non-spatial data from diverse sources makes it a powerful platform for multilevel decision making and so greater credit should be given to its geovisualization capabilities (Nkeki, 2013a). The technique is able to generate series of maps that summarize vital information useful for decision making and spatial planning. A GIS help to manipulate remote sensing data in a spatial format and offer a friendly platform to integrate such dataset with non-spatial data to produce new maps.

These maps are essential components and constituents for developing a GIS database pertaining to disaster assessment and management. GIS database

comprise series of map layers that are geographically referenced as well as attributes that can be linked to such map layers by common identifier (Vine et al., 1997). Thus, each of the map layers contain, in most cases, one central geographic theme (thematic map) of the studied phenomenon. However, one of the fundamental merits of a GIS is its ability to synchronize several map layers for on-screen visual comparison and extraction of spatial relationships.

This chapter focuses on the formidability of using high resolution remote sensing data and GIS techniques to assess and identify flood prone areas (estimating population and infrastructure at risk) before occurrence in Lagos State-large coastal city of Nigeria, and develop a more accurate, easily replicated geo-based flood risk model for sustainable mitigation strategies and policy plans.

2. THE STUDY AREA

Administratively, Lagos is the smallest state in Nigeria, and on the other hand, this territory contains the largest urban center in the country and one of the largest coastal city in Africa. It is composed of 20 local government areas (LGA) of which 16 forms the high density metropolitan region.

Geographically, the region is located at the south-western edge of Nigeria in the West African sub-region between latitude 6°22'N to 6°41'N and longitude 2°42'E to 4°21'E (Figure 1a). It covers an overall area extent of approximately 3,829.84 km^2 with a perimeter of 454,328.4 meters, and water bodies of about 1,700 km^2.

With respect to the topographical settings, Lagos can be categorized into three major geographic regions: a low-lying coastal zone along the Atlantic Ocean, consisting of beaches; a broad inland depression and flat land (sloping gently from the hinterland to the sea) surrounding the Lagoon and stretching from the eastern boundary of the state to the western border of the country (between Nigeria and Benin Republic), this zone comprises series of marshlands and mangrove wetlands with elevation ranging from between 0 meter to 25 meters above sea level; three distinctive upland zones in the northern part of the state with elevation of 70 meters above sea level, the region's highest point is at Iroko and Olasore (Figure 1b). The Ogun River constitute the primary surface water (river) that drains the region and it empty's its water into the Lagos Lagoon. The state has a coastline of about 180 km.
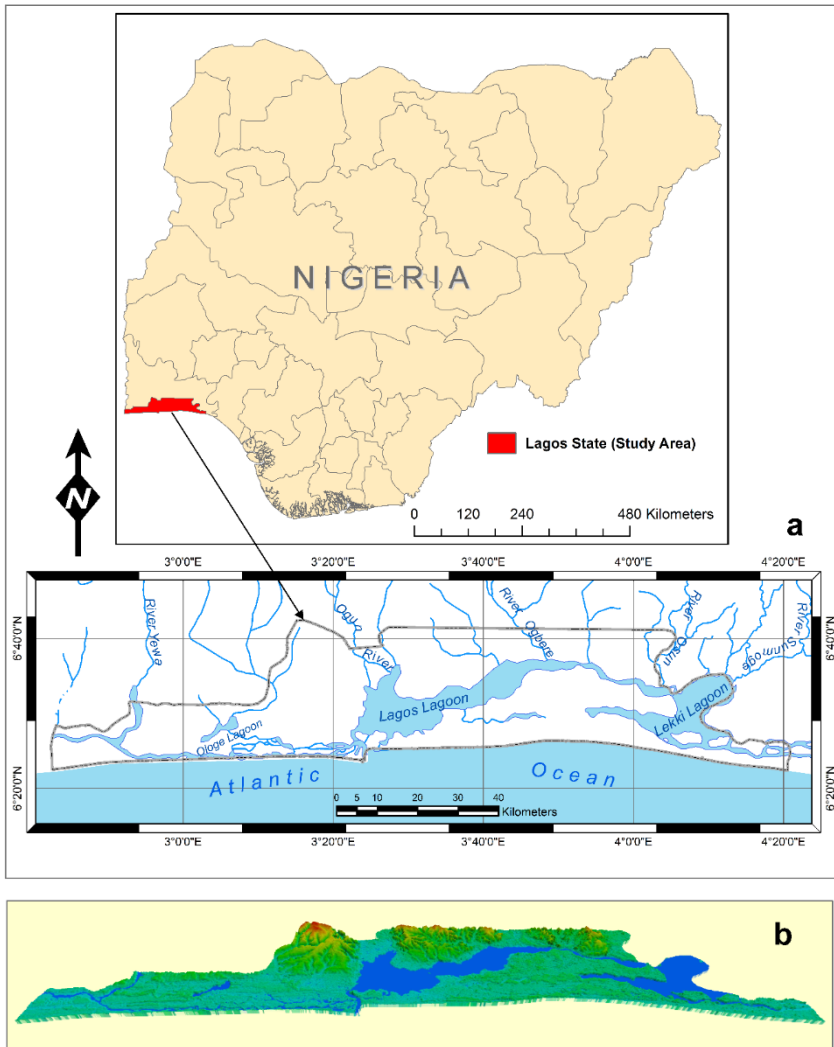
Figure 1. Location of the Study Area (a) the geographical position of Lagos State in Nigeria with its major water bodies (b) 3-D terrain model of the state.

Water bodies and wetlands cover over 40 percent of the overall land area of the state and additional 12 percent is subjected to seasonal flooding (BNRCC, 2012). The region falls within the tropical rain forest belt and the eco-zones are predominantly wetlands and rain forest. The vegetation types found outside the urbanized area are mostly secondary forest, mangrove swamps, freshwater swamps and cultivated crops.

Generally, the region is characterized by a deep and poorly drained soil. Further detail concerning the ecological regions of the state is presented in Table 1. The climate of the state is the wet equatorial type influenced by its nearness to the equator and the Gulf of Guinea.

Table 1. Lagos State ecological regions and their physical characteristics

Ecological region	Geology	Topography	Soil features	Eco-zone
Badagry, Ibeju-Lekki, Ojo, Lagos Island, Surulere, Eti-Osa and areas close to the coast	Deltaic basis and tidal flats	Nearly level plains of 1-2 % slope	Very deep, poorly drained and moderately well drained soils; sandy, sandy loamy or sandy clay loam surfaces over sandy clay, loam sub soils.	Wetland
Part of Ebutemetta, Mushin and Shomolu, Kosofe Agbowa, Ejinrin, parts of Epe and parts of Ikorodu like the Igbogbo areas.	Recent Alluvium	Nearly level to gently undulating plains of 2-4 % slope	Deep, well drained and deep poorly drained soils; sand, sandy loam, loamy sand or sandy clay loam surfaces over sand, sandy clay, sandy clay loam, clay loam or loamy sand sometimes gravel sub soils.	Wetland
Ikeja, part of Ebute-Metta, Mushin and Alimosho, Agege, Epe, part of Eredo, and part of Ejinrin.	Coastal Plain Sands (Alfisols)	Nearly level plains with 1-2% slope	Very deep well drained soils, loamy, sand, sandy loam or sandy clay loam surfaces over sandy clay loam, clay loam, sometimes gravel type sub soils.	Rain Forest
Part of Eredo towards Ijebu-Ode mainly the boundary of Lagos and Ogun States.	Transitional materials of sub-recent alluvium and coastal plain sands	Nearly level plains of 1-2% slope	Very deep to deep and moderately deep well drained and few imperfectly drained soils; sand, sandy loam, or loamy sand surfaces over sandy loam, sandy clay loam or gravel type sandy clay loam sub soils.	Rain Forest
Parts of Ikorodu leading to Shagamu.	Coastal Plain Sands	Gently undulating plains of 2-4%	Very deep well drained, and very deep poorly drained soils; sandy, sandy loam or sandy clay loam surfaces over sandy, loam, sandy clay, loam, sandy clay, or clay loam sub soils.	Rain Forest

Source: Adapted from FDALR (1995).

The interaction between the warm, humid maritime tropical air mass and the hot and dry continental air mass from the interior gives the region two contrasting seasons; a wet season, which usually lasts from April to October; and a dry season, which lasts from November to March (BNRCC, 2012). In the wet season, two rainfall peak periods are experienced-in the months of May to July and September to October. These peak periods are when acute flooding hazard usually occur in the state and this heightened by the poor surface drainage structure of the coastal lowlands (BNRCC, 2012). The mean annual rainfall for the state is roughly 1,657 mm with a consistently high temperature (about 30°C for the mean monthly maximum).

The actual population figure for Lagos State is disputed between the officially presented total by the National Population Commission of Nigeria in the 2006 census exercise (which is 9,113,605) and a far higher figure claimed by the state government (which is about 17.5 million, based on the parallel count conducted simultaneously by the state during the National Census exercise). In this chapter, the official 2006 National Census figure (9,113,605 people) is adopted. Despite this, the region remains one of the most populous and fast growing state in the country. At 3.2 growth rate, UNFPA population projection for the region is 11,867,082 and 12,252,970 in 2014 and 2015 respectively (http://nigeria.unfpa.org/lagos.html).

Using the UNFPA projected figure for 2014, the population density is currently about 3,098 persons per km^2. This has serious implication for the available urban land, management and the implementation of the existing urban design, because such uncontrolled growth has led to the development of slum villages and illegal structures and numerous disordered settlements.

Consequently, it has accelerated indiscriminate land reclamation, the encroachment of residential and economic activities into natural water paths, wetlands, river valleys and extremely low-lying lands and floodplains. For example, the Makoko slum water community that falls within the Yaba development area is completely resting on the waters of the Lagos Lagoon (Figure 2). Its population is estimated to have approached 85,840.

2.1. Flood Hazard in Lagos State

Over the years, flooding has become a major natural disaster ravaging Lagos State annually. The primary cause of floods in the region is heavy rainfall which increases the quantity of water discharged from rivers and lagoons thereby overflowing its channels and floodplains.

Figure 2. An aerial view of Makoko slum settlement on the Lagos Lagoon.

In 2010 and 2012, properties estimated to worth millions of Nigeria Naira were ravaged in Ikorodu axis as a result of the River Ogun persistent overflow and the heavy rainfall induced Atlantic Ocean rise forced the Lagos Lagoon waters to rise above its actual channel and flow into the River Ogun flood-plain. The flood water submerged and ravaged major roads and residential buildings (Figure 3).

It was reported (Akinsanmi, 2011) that River Ogun in October 2011 rose up to 4 meters as a result of the incessant rainfall in the south western part of the country (particularly Ogun State), this led to an overflow of the river into surrounding towns such as Mile 12, Owode-Onirin, Agiliti, Isheri North, Maji-dun, Egbeda etc. In 2013, Lekki, a high density activities area of Lagos State was affected by tidal flood. The flood water also found its way into Jakande Estate, Lekki Beach and Elegushi areas.

The Lagos State government have put numerous measures in place to check the hazard which include cleaning up of block municipal drainages, construction of canals and storm water channels, demolition of illegal structures (especially those located along stream channels), fortification of the beach line to mitigate the effect of ocean surge and coastal erosion, early flood warning and enlightenment campaign.

Figure 3. Major roads and residential properties damaged by floods in Lagos State.

Despite these efforts, the region still suffers from flood disaster annually (mostly in the wet season). The stark reality is that flooding in littoral cities with particularly reference to sub-Saharan Africa is difficult to prevent because of too numerous natural and anthropogenic factors.

The effect of climate change has further heightened the issue-increasing temperature and rainfall. The best practice is to reduce risk and vulnerability through permanent evacuation and relocation of activities from flood prone areas and declare such areas as unsafe zones for human inhabitation.

Hence, the flood prone areas must be identified spatially by producing well synthesized flood risk map and geospatial database system for sustainable development. A peculiar area with respect to flood frequency and magnitude, is the River Ogun floodplain. This floodplain is notorious for high degree of submergence (Figure 4) and its effect cut across many large surrounding communities such as Ikorodu, Ajegunle, Magodu, Mile 12, Owode-Elede, Ibeje, Oworonsoki, Ajelogo, Maiden, Agboyi, Odo-Ogun etc.

Studies have reported (Olajuyigbe et al., 2012 and Oyinloye et al., 2013) that the fundamental causes of perennial flood hazard in this floodplain are in two folds: the first is the release of excess water (accumulated from heavy

rainfall) from the Oyan dam constructed on the Oyan river, a tributary of River Ogun in Ogun State which is an operational regulation of the management to ensure safety and avoid dam failure; the second is the wave induced sea level rise which forces its waters into the Lagos Lagoon and consequently discharging into the floodplain and surrounding lowlands.

3. DATA

The application of GIS techniques in flood risk analysis and modeling requires a wide range of spatial dataset from different sources. Such dataset include high resolution space borne images collected with active earth observation system technology. Studies (Nkeki et al., 2013; Triglav-Cekada and Radovan, 2013; Townsend and Walsh, 1998) in the field of spatial sciences have shown that the utilization of this technology and GIS platform has become an integrated, well improved and reliable approach in disaster and risk management.

In this chapter, the Shuttle Radar Topography Mission (SRTM) remote sensing data was used to generate elevation components, and on the other hand, Landsat and Google earth datasets were used to assess the urban footprint and the land use physiognomies of the study region. The former, is a 90-meter spatial resolution digital elevation model (DEM) developed by SRTM.

Originally, this data is produced by National Aeronautics and Space Administration (NASA), and it has become a major advancement in digital terrain modeling and provides free and easy access to high quality elevation data for researchers worldwide (Nkeki and Asikhia, 2014).

Figure 4. Aerial view of flood hazard in River Ogun floodplain.

The latter, utilized the current Google earth engine database version 7.1.322 developed in October, 2013 and Landsat 8 2013 data captured with the Thermal Infrared Sensor.

The SRTM high resolution DEM with 3 arc-seconds of 90-meter resolution has been mosaiced into seamless (gapless) near-global coverage (up to 60 degrees north and south) making it one of the DEM with the wider coverage. The SRTM captured elevation in two spatial resolution- 30-meter and 90-meter. Only 90-meter spatial resolution data is available globally while 30-meter spatial resolution (1 arc-second) data is available for US territorial coverage alone. SRTM carries onboard its space shuttle specially modified radar device that collected elevation data on the 11-day mission in February 2000. However, it is a mosaiced elevation data delivered in 1 x 1 degree tiles and also in various raster formats acceptable by most GIS applica-tion. The digital data is freely available for download from US Geological survey's EROS data center's website.

SRTM dataset is usually delivered in a preprocessed form which involves filling in the voids (especially in Version 4.1) with improved hole-filling algorithm which make use of ancillary data sources. The mission uses a dual-antennae, single-pass interferometric synthetic aperture radar (INSAR) and operates at a wavelength of 5.6 cm (C-band). Landsat 8 (L8) became fully operational in April 11, 2013 and the satellite images the whole earth every 16 days in an 8-day offset from Landsat 7. Two optical sensors are onboard the earth observation instrument (L8)-the operational land imager (OLI) and the Thermal Infrared Sensor (TIRS).

Unlike other versions of Landsat data such as the Landsat multi-spectral scanner (MSS), Landsat thematic mapper (TM), Landsat enhanced thematic mapper plus (ETM+) with 4 bands, 7 bands and 8 bands respectively, L8 data is composed of 11 bands and it is acquired at 100-meter spatial resolution, which is resampled to 30-meter pixels in delivered data with 16-bit high quality pixel values of surface data, scaled to 55,000 grey levels. It captures an approximate scene size of 170 km north to south by 183 km east-west. The OLI sensor captures data in the visible, near infrared and shortwave infrared wavelength areas, including panchromatic band. The TIRS captures earth data in two long wavelength thermal infrared bands. The OLI has 12 meters circular error, 90 percent confidence and the TIRS is characterized with 41 meters circular error, 90 percent confidence (USGS, 2013).

Google earth engine is a powerful platform which combines the strength of Google search engine with satellite data, maps, terrain and 3D data to make both local and global geographic information available for end users (Nkeki,

2013b). Data from such system is high resolution images specifically adopted in this chapter for geovisualization and database creation.

The most recent Google earth engine (Google earth pro version 7.1.322) was used in this chapter because it captures current urban footprints that have taken place in the study region. Other vector data were downloaded from map library website such as the territorial boundary of Lagos State and the local administrative boundaries (polygons).

4. METHODOLOGY

Various GIS spatial analysis, extraction and image classification techniques were conducted to develop a flood risk modeling methodology that can easily be replicated (Figure 5). This was achieved majorly with the aid of ESRI ArcGIS version 10.1 and Google earth pro version 7.1.322 softwares.

The primary objectives of this chapter are to develop a comprehensive GIS driven methodology for flood risk analysis in a littoral mega city and to demonstrate the capability of using GIS technology to create a geodatabase system for flood risk management that contains spatially referenced information as the flood prone areas and their various risk magnitudes, estimated population and infrastructures at risk.

4.1. Extraction, Vectorization and Reclassification of Elevation Data

Elevation data is one of the principal datasets needed for GIS-based flood risk modeling. It is particularly useful for the generation of potential inundation extent and classification of risk zones.

It has been used by numerous researchers (Islam et al., 2001; Taubenbock et al., 2011; Nkeki et al., 2013; Townsend and Walsh, 1998; Sobowale and Oyedepo, 2013) to model flood risk and produce maps of potential flood prone areas. The SRTM high resolution DEM which has been spatially corrected and preprocessed to fill in the voids in the data were entered into ArcMap-ArcInfo environment for further processing.

Using the DEM assembly tool extension in the software, the series of 1-degree elevation data tiles were merged and resampled to create a composite grid hydro DEM.

The resulting raster image was then clipped to the shape and size of the study area (Figure 6a) with the 'extract by mask' tool of the spatial analyst tool box of the GIS software.
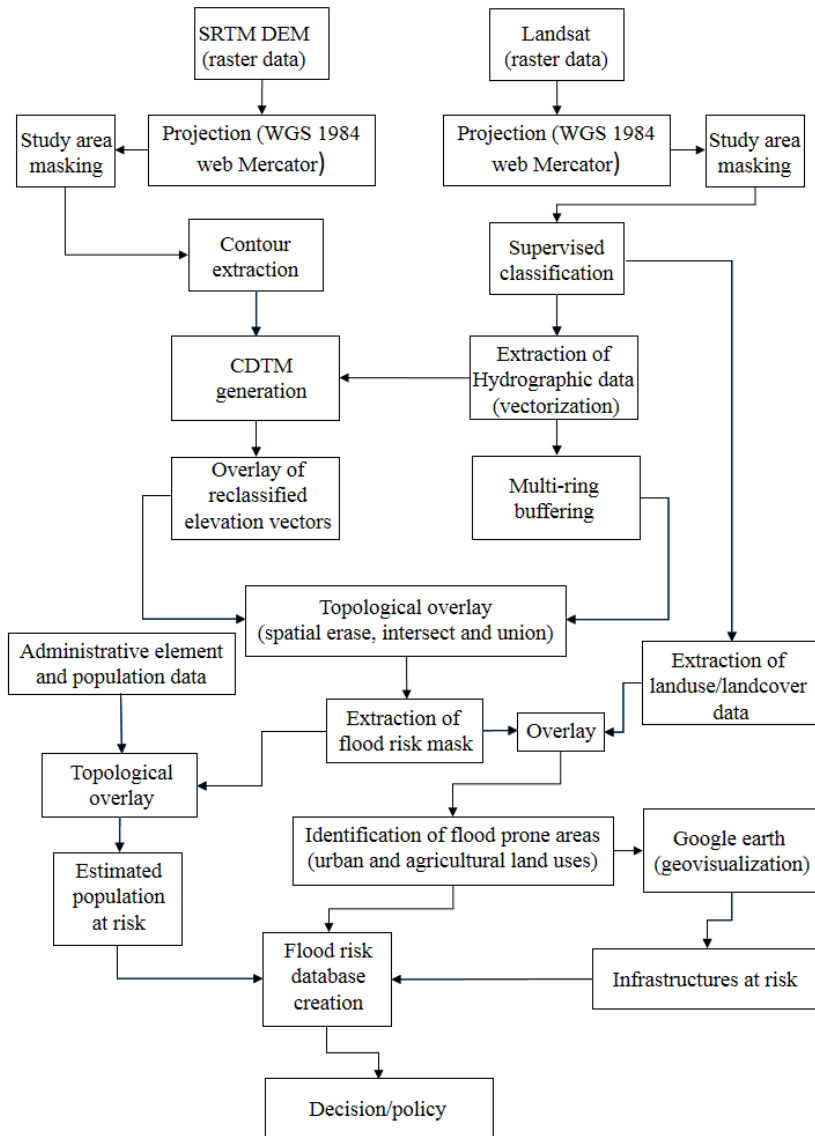
Figure 5. Methodological framework of GIS-based flood risk modeling.

In the process, the DEM was transformed from the original geographic coordinate system to projected coordinate system (applying the World Geodetic System (WGS) 1984 web Mercator). Hence, to ensure that the hydrological component of the DEM is correct and updated, the elevation data was leveled and reconditioned using the vecto-rized hydrological features (consisting of Lagoons and major rivers) extracted from the Landsat 8 imagery of 2013.

The hydrologically updated SRTM data was used to generate a classified digital terrain model (CDTM) through vectorization procedure. The fundamental reason for creating the vector-based CDTM is to aid the various forms of overlay operation (such as spatial intersect, union, erase, spatial join and identity) and calculate the spatial extent or area coverage.
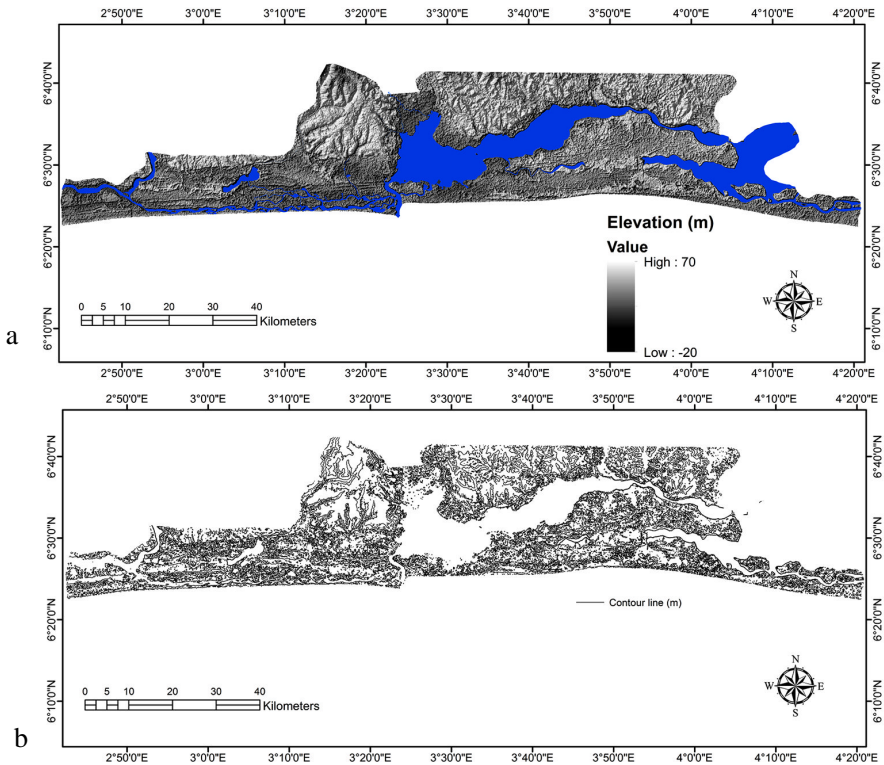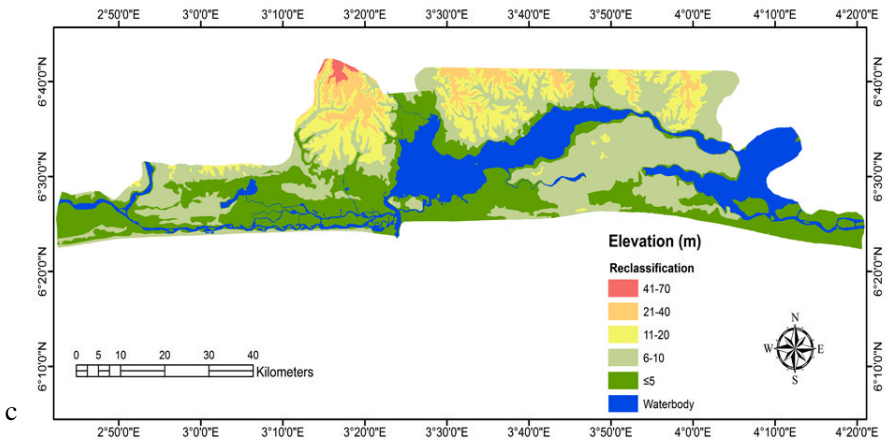
Figure 6. Processed elevation data of the study region: (a) Reconditioned DEM with vectorized hydrological constituents (in lapis lazuli blue); (b) Extracted contour lines with specified contour listing; and (c) Vector-based CDTM.

Also, to group the elevation of the region into classes of lowland and highland. To achieve this (generate CDTM), the DEM grid was subjected to spatial analyst surface algorithm to extract list of contour lines (Figure 6b).

The contour lines were further superimposed on the DEM data to assist and serve as a guide for on-screen digitalization. Thus, the final vector lines representing the boundaries of each elevation class were converted to polygons and 5 classes of elevation were identified-≤ 5m, 6-10m, 11-20m, 21-40m, and 41-70m above sea level (Figure 6c).

4.2. Land Use/Land Cover Classification

To estimate the urban footprints of the region for up-to-date flood risk management and assessment, a zero percent cloud-free Landsat imagery of 2013 (Figure 7a) was preferred because it is recent, noise-free and easy to classify. The Landsat data is intended for a land use/land cover detection analysis which will provide vital information on the actual urban extent.

The main purpose of this analysis is to detect the urban built-up area and agricultural lands in order to identify and calculate the areal extent potentially vulnerable to flooding hazard. For that purpose the Landsat raster image was classified after it was transformed from geographic coordinate system to

projected coordinate system using the WGS 1984 web Mercator and then clipped to the boundary of the study region.

To generate a land use/land cover map for the year 2013 of the region, a supervised image classification method was adopted using the maximum likelihood algorithm of ArcGIS. The training sample data were collected from the original (raw satellite image) Landsat imagery and used to create a spectral signature file which contains the identified five classes of land cover. The five classes that were selected are: built-up area (high density); built-up area; cultivated land; Forest; and water body (Figure 7b).
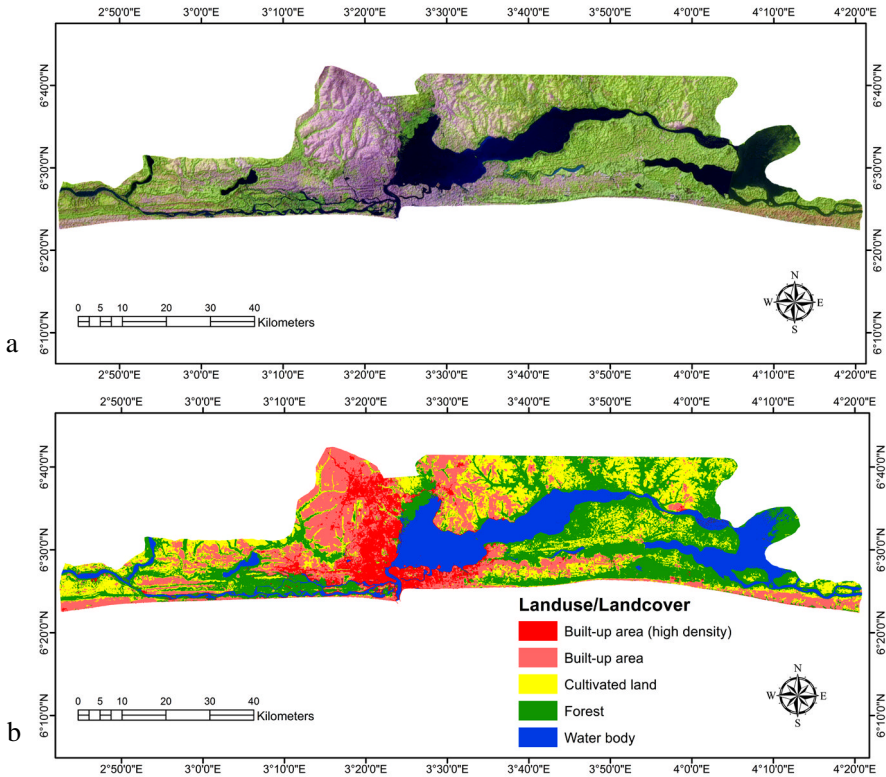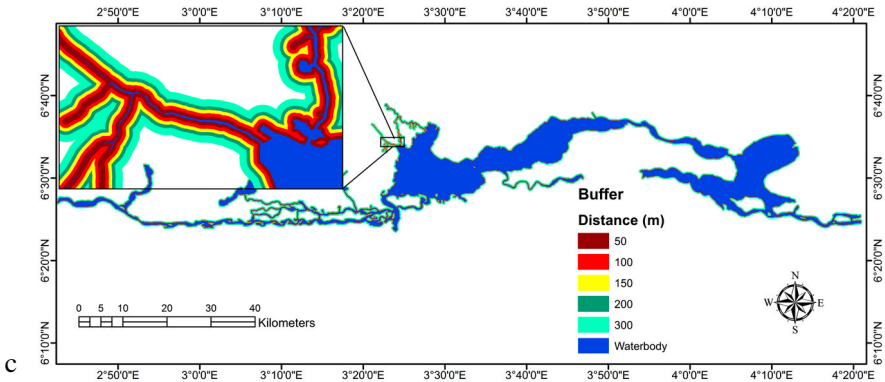
Figure 7. Processed Landsat imagery and its derivatives: (a) Raw Landsat data; (b) Extracted land use/land cover data; and (c) Five level multi-ring buffered hydrographic data of the region.

The reason for not selecting more classes is because urban footprints/ coverage is the primary concern in this chapter. The multivariate classification has an overall accuracy of 88 percent. This was calculated by generating 200 random points within the limit of the region's raster data in ArcMap and subsequently exported to Google earth so as to extract land use/land cover information which was later exported back to ArcMap for error matrix and accuracy assessment.

From the classified land use data, each of the parameters were converted to vector format to aid further analysis. The hydrographic feature was particularly extracted as vector so that spatial proximity analysis can be carried out on it. The extracted hydrographic parameter consisting of Lagos Lagoon, Lekki Lagoon, creeks and rivers was further edited by filling in the gaps. These are void created by dense vegetation cover in the Landsat imagery. A spatial proximity map was generated (Figure 7c) using this hydrographic data which involved applying a multi-ring buffer operation to identify specified distances from the water bodies.

4.3. Buffering Distance Selection

Determining the appropriate distance from the shoreline of water bodies to the hinterland is not universal especially across countries, organization and researchers. Some researchers (Adeniran et al., 2013; Oyinloye et al., 2013;

Oriola and Bolaji, 2012) in Nigeria adopted the 30-50 meters minimum setback presented by 1986 town and country planning regulation. This regulatory setback was enacted based on the physical appearance and architectural design of urban centers. In addition, the need to protect natural water bodies from pollution. It fails to take into consideration the general safety of the public with special reference to flooding. More importantly, when the regulation was passed (in 1986) the impact of climate change (rapid increase in annual rainfall and sea level rise) has not been intensely manifested as it is currently.

Others (Nkeki et al., 2013; Sobowale and Oyedepo, 2013; Ikusemoran et al., 2013) have used previous flooding extent captured by near real-time satellite sensors and documented reports to determine the distance or areal extent prone to flooding disaster. In the study region, there is no available or accessible recent satellite image of previous flood hazard, hence this chapter used reports and documentted evidence on previous flooding extent to estimate and calculate the buffer distances. The maximum recorded flood extent in the study region is roughly 200 meters from the sources of the hazard (which are the Ogun River and Lagos Lagoon). This was estimated based on the reported cases during the October 2011 and April 2013 flooding.

Also, report released by the Lagos State Government during the October 2011 flood disaster showed that the Ogun River rise above its normal level by 4 meters (Akinsanmi, 2011). Ogun River is the major tributary of the Lagos Lagoon and one of the primary source of flooding in the study area. This is because of the yearly release of excess accumulated water from the Oyan dam in Ogun State and the excess water stored in the Ikere gorge during wet season.

In the month of September annually when the dam experiences a peak flood volume of 4,270 million m^3 the average excess water of 8.5 meters depth is uncontrollably allowed to flow downstream causing havoc along its path (Sobowale and Oyedepo, 2013). However, it is assumed that before it gets to Lagos region, about half of the flood waters might have been absorbed and lost to the floodplain, thus the reported 4 meters rise. This information was used to estimate the maximum distance that such flood water would possibly submerge in the region relating it to the elevation of the adjacent land (Figure 8). The calculation shows that the approximate maximum distance likely to be inundated when the river rises by 4 meters above the normal level is 250 meters. Consequent upon this, the five-ring buffer distances that were selected are 50, 100, 150, 200 and 300 meters.
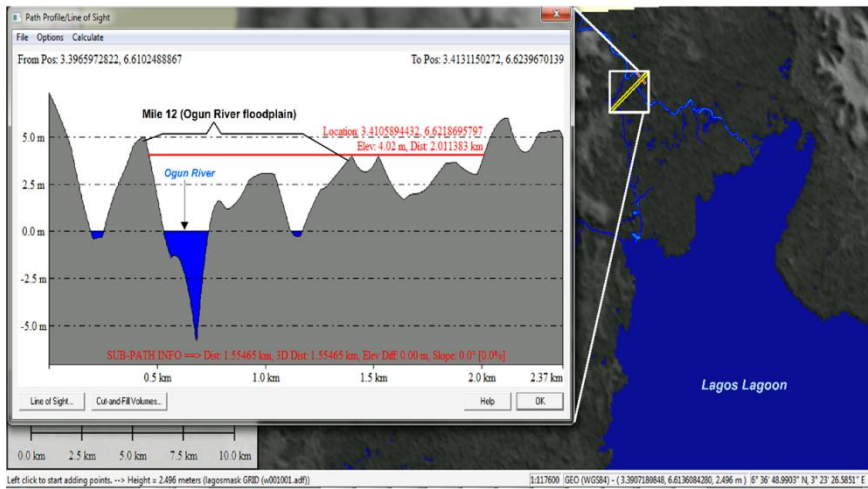
Figure 8. Cross profile of Mile 12 in the Ogun River floodplain showing the possible maximum inundate-distance when the river rises up to 4 meters above its normal level.

4.4. Extracting Potential Flood Risk Mask

Identification of areas having higher flood hazard potential is the most effective measure to mitigate the impact of the hazard and the first step to formulation of sustainable flood management strategy. The issue of creating a reliable flood hazard map (that show areas with high degree of susceptibility) is one of the foremost concern within the field of flood disaster management (Sanyal and Lu, 2004).

To map out the areas having high probability to be flooded, this chapter suggests that the likelihood for a hinterland to be flooded (as a result of rain induced excess runoff, waves etc.) is directly linked to the proximity of the hinterland to agent of flood (hydrographic features) and the closeness of such hinterland's elevation to the source water level. From the multi-ring buffered hydrographic data and the CDTM created in previous sections, a flood risk mask was generated through series of spatial analysis techniques-overlay intersect, spatial join, union and erase functions.

The categorization of the potential flood risk areas by magnitude was done based on the CDTM and proximity data (Table 2). This is because as noted by Nkeki et al., 2013, the devastating impact of flooding disaster decreases with increasing distance from the source river channel.

Table 2. Categorization parameters for potential flood risk by magnitudes

Risk magnitude	Elevation class (m)	Buffered distance (m)
Very high	≤5	50
High	0-5	100
Moderate	0-5	150
Low	6-10	200
Very low	6-10	300
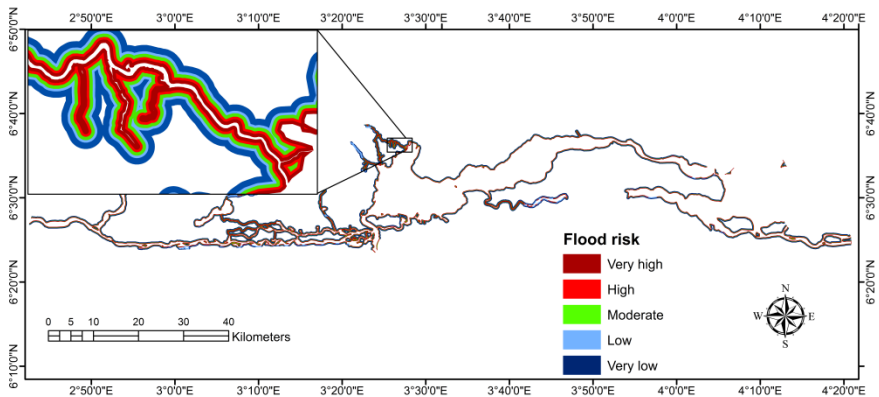
Figure 9. Spatial distribution of flood prone areas by magnitude in the study region.

Nonetheless, the so-generated flood risk mask (Figure 9) was overlaid on the land cover, administrative/population density dataset to detect and estimate vulnerable components such as urban land use and agricultural land use. Specific attention was focus on these land uses because they are high valued structures pertaining to flooding impact. Such land uses are economic and infrastructural based and also involve human lives, that is the reason behind their frequent use as a measure of quantifying flood damage and level of seriousness.

Linking elevation data, such as SRTM DEM with high spatial resolution, to hydrographic dataset and progressively aligning the resulting interplay with satellite derived land use data is a methodology that is likely to yield a more accurate result and produce a reliable flood risk map, database and modeling procedure compared to one derived ultimately from pure hydrological modeling. The major limitation of this method, typically rest on the accuracy of the adopted DEM dataset, land use data and the overall competency of the analysts. SRTM data and Landsat imagery have become paramount and most widely used datasets among contemporary researchers.

The latter was complemented with Google data based on its resolution and distinctiveness in displaying surface features. It is a better platform as a guide for the analyst to assess the degree of accuracy with respect to the training data collected and vulnerable features.

5. RESULTS AND DISCUSSION

In this section, the extracted flood risk mask were related to the susceptible features with the aim of creating a comprehensive flood risk GIS-based database system for the area. The susceptible features are the high-valued land uses-urban and agricultural areas. The former includes the population and infrastructures (roads and rail tracks) while the latter includes cultivated and arable lands.

5.1. Spatial Assessment and Analysis of Land Use Vulnerability

The result of supervised land use classification (Figure 7b) revealed that urban footprint extends as much as 1,092.7 km^2 covering 28.7 percent of the total area of Lagos State, out of this, higher density urban area covers 7.4 percent, cultivated land use occupies 22.3 percent and forest land 31.5 percent. The flood risk mask which has been classified into five levels of risk-very high, high, moderate, low and very low was superimposed (applying spatial intersect) on the land use map derived from remotely sensed data to visualize and quantify features exposed to flood hazard. Figure 10 shows the spatial distribution of vulnerability to flooding disaster on different land use classes. The overall areal extent in the land use map potentially exposed to flood hazard is roughly 296 km^2. From the perspective of high-valued land uses, such as urbanized area and arable area (which is basically the central focus of this chapter), the potentially endangered valued land covers approximately 107 km^2 which is about 36 percent of the total vulnerable area. Additionally, more than 7 percent of the overall urbanized area are susceptible to the hazard.

The results in Table 3 (extracted from the attribute table of the spatial analysis in ArcMap) show that more than 48 km^2 of the higher density urban land use is likely to be affected during flood scenario. Based on evidence from this analysis, serious urban activities are concentrated close to water bodies and in most cases, in extremely low lying terrain.
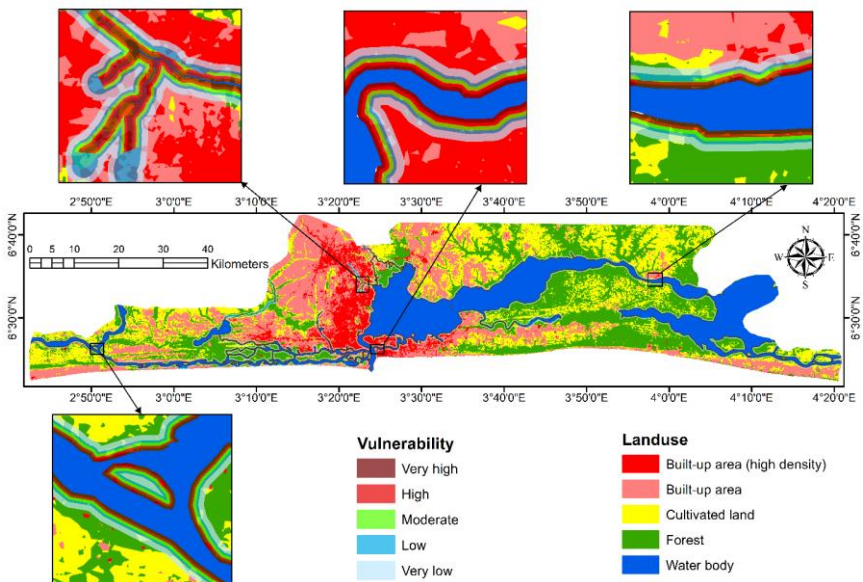
Note: To ensure a more alluring and visual integration among the parameters, the delineated flood risk areas were set to a transparency value of 30 percent.

Figure 10. Flood risk and land use vulnerability map of Lagos State.

Such high level concentration is found around the western and southern edges of the Lagos Lagoon. This is why among the high-valued land use classes, higher density urban area is more exposed to flooding disaster.

A cursory examination of Table 3 reveals that same character is manifest-ted within the vulnerability class of higher density urbanized land use catego-ry, i.e. the largest area of land (26.7 percent of the five classes) occupied by this land use category typically falls within the very high risk vulnerable class. It is therefore estimated that inundation extent will cover roughly 83 km^2 of building area within the urban space.

As revealed by the spatial analysis, over 24 km^2 (8.2 percent of the overall flood prone area) of agricultural land-including cropland and arable land is exposed to flood hazard. Though roughly half of this lies within the very low risk vulnerable class, it however exhibits grave implication for food security in the state.

This is due to the stark reality that the state is experiencing disconcert and hysterical population inflow leading to further urban expansion and conse-quently dwindling contiguous agricultural lands.

Table 3. Vulnerability class by different land use categories

Parameters			Land use exposed to flood risk (km^2)			
Proximity to source of hazard (m)	Elevation within buffer distance (m)	Vulnerability class	Urbanized area (higher density)	Urbanized area	Agricultural land	Forest
50	≤ 5	Very high	12.85 *(4.4)*	1.74 *(0.6)*	1.37 *(0.5)*	32.47 *(11.0)*
100	≤ 5	High	9.15 *(3.1)*	4.17 *(1.4)*	2.68 *(0.9)*	31.93 *(10.8)*
150	≤ 5	Moderate	6.28 *(2.1)*	5.28 *(1.8)*	3.26 *(1.1)*	30.00 *(10.1)*
200	6-10	Low	8.01 *(2.7)*	8.90 *(3.0)*	5.95 *(2.0)*	39.51 *(13.3)*
300	6-10	Very low	11.78 *(4.0)*	14.59 *(4.9)*	10.93 *(3.7)*	55.18 *(18.6)*
Total			48.07 *(16.3)*	34.68 *(11.7)*	24.19 *(8.2)*	189.09 *(63.8)*

Note: values in parentheses are the corresponding percentage values.

This can be deduced from the result of supervised classification (Figure 7b) which shows a pattern of intermediate or transitional relationship, where urban land use is engulfing agricultural lands and the latter, in turn encroa-ching into forest lands.

5.2. Spatial Analysis of Urban Infrastructural Vulnerability

Infrastructural vulnerability involves the road structure and rail track that are exposed to flooding hazard because they are found in the flood prone area of the region. These infrastructures have high economic value and are mostly susceptible to the hazard. For example, the asphalting of roads involve huge financial resources and it can easily be destroyed by insistent waterlogging.

On the other hand, road is the primary medium for accessibility in an urban space and when it is flooded, it eventually obstruct economic activities. Road infrastructure includes expressway, major and residential roads that are paved, while rail infrastructure includes active rail tracks. This were further group and reclassified as dual and single lane.

To map, visualize and estimate the length of road and rail track susceptible to flood disaster, the generated flood risk map (Figure 9) was set to 60 percent transparency and then converted to Keyhole Markup Language (KML) format. KML is an excellent format for sharing geographic data because it has the capability to compress graphic and non-graphic data either in raster, vector or both including their respective spatial references, symbology, etc. into one file.

The flood risk data in KML format (major format acceptable by Google earth) was entered into Google earth engine for progressive manipulation.

Through this synchronization, it was possible to spatially and visually map and estimate vulnerable infrastructures through line digitalization within the Google earth engine. This platform also present an accurate geovisualization capability which will support quick decision making. Figure 11 gives a clear visual impression of vulnerable areas, building and road infrastructure in Google earth.
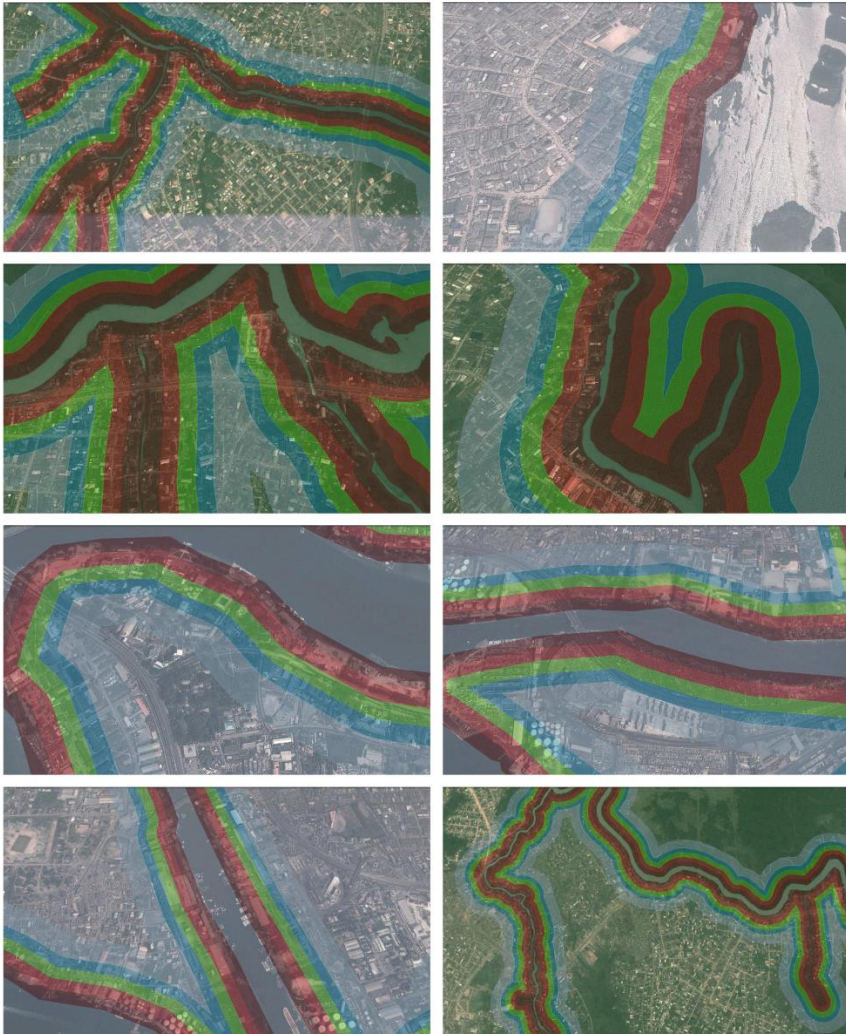
Figure 11. Satellite map of possible flood risk area and vulnerable infrastructures.

The images are clipped scene from Google earth engine which constitutes a major part of the generated database system. A fundamental benefit of this modeling method, which involve locally aligning a well-integrated, carefully and logically generated flood risk mask with high resolution remotely sensed data is that it is possible to track down a specific residential building, monument, hotel, administrative building, reli-gious or shopping complex, as the case may be, that lies within the risk zone.

From the perspective of interpretation, the result is highly simplified and visually alluring for policy makers who do not have expert knowledge in GIS and spatial analysis. Progressively, the vectorized road and rail network data-base was exported as KML file from Google earth engine to ArcMap as shape-file. This database was then overlaid (using spatial intersect technique) on the flood risk database to calculate the amount of accessibility infrastructures that are exposed to the disaster (Figure 12).

For the purpose of detailed visualization, Figure 12 was zoomed in on the most urbanized area of the state-Lagos Island, Eti-Osa, Surulere, Lagos Main-land, Apapa, Ajeromi-Ifelodun and Amuwo-Odofin administrative areas. The result of the spatial database integration shows that the overall length of road potentially at risk is 300.91 km. High priority infrastructure like dual carriage road has a total length of 54.5 km exposed to flooding disaster and this is about 18 percent of the overall length.
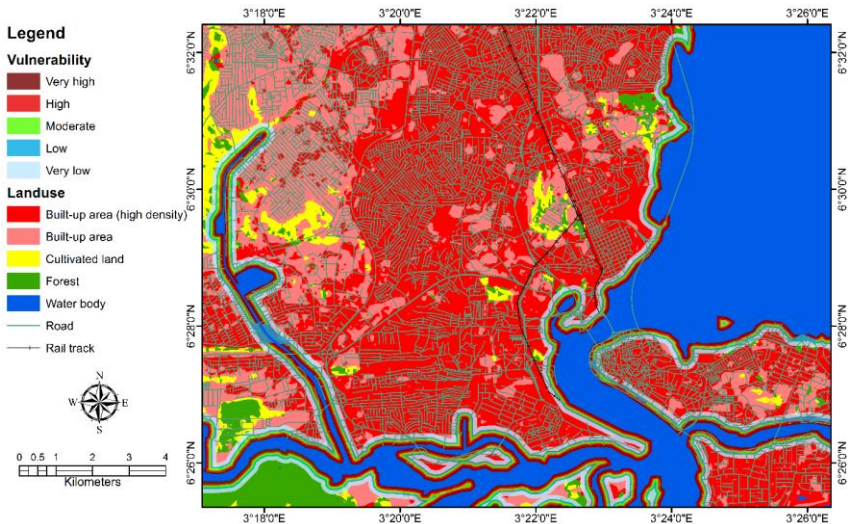
Figure 12. An integrated geo-database for assessing susceptible infrastructures.

Single carriage road has a total length of 246.41 km (81.9 percent) exposed to flood risk (Table 4). This information will greatly assist planners and decision makers on how to allocate resources pertaining to flood eventuality, the road category to be given first attention based on the carriage capacity and level of usage.

In addition, in a case of ad hoc mitigation plan and impact reduction, this information will be useful for prioritizing and selecting infrastructures serving areas of higher population concentration and high valued economic centers. For instance, the multiple dual carriage roads that connect the heavy density Lagos Mainland area with Lagos Island are of high economic value and high priority linkage because they connect the high density Islands to the other parts of the city.

Evidence from Figure 12 reveals that such accessibility infrastructures crosses the five-class potential risk zones at both sides (edge of Lagos Mainland and Island) for a distance running to 1.2 km. A total of 0.61 km of rail track in the region is vulnerable to the hazard, of this 6.4 percent lies within the low risk vulnerability class while 93.6 percent lies within the very low risk vulnerability class. These sections are the two railway terminals, located at the Lagos Mainland near the shoreline of the Lagos Lagoon (Figure 12).

5.3. Spatial Analysis and Estimation of Potentially Vulnerable Population

Susceptibility of population to flooding is the major propellent of studying flood disaster and finding mitigation measures. Hence, it has become a widely used concept in flood risk management and vulnerability assessment.

Table 4. Exposed road infrastructure by priority and vulnerability class

Vulnerability class	Length of road exposed to flood risk (km)	
	Dual carriage	Single carriage
Very high	8.07 *(2.7)*	17.51 *(5.8)*
High	13.77 *(4.6)*	27.32 *(9.1)*
Moderate	8.07 *(2.7)*	37.58 *(12.5)*
Low	9.89 *(3.3)*	60.32 *(20.0)*
Very low	14.73 *(4.9)*	103.68 *(34.5)*
Total	54.5 *(18.2)*	246.41 *(81.9)*

Note: values in parentheses are the corresponding percentage values.

However, quantifying and estimating population exposed to risk has become necessary and this has further raised another line of study-how to estimate vulnerable population to hazard with minimal error. The most popular method is the used of density data, which basically involves sharing the population equally across the specified areal territory.

A fundamental weakness of this procedure is that population is distributed evenly across the various land uses of the territory. Areas with no human settlement (such as forest, swamps and water bodies) are likewise assigned population value. Since population is generally known to reside within an urban structure, this chapter presented a better procedure that distribute population according to the urban structure using information from remotely sensed data. The maximum likelihood supervised classification data previously generated (Figure 7b) was disaggregated into various land uses and the urban footprint (areas covered with human settlements and other building structures) was extracted for further analysis.

To estimate the population potentially endangered by Local Government Area (LGA), the vectorized local administrative element represented by 20 polygons (corresponding with the LGAs of Lagos State) in ArcMap was loaded with population data for each of the polygons. To ensure a substantial level of accuracy in the estimation, the 2006 population census data for the 20 LGAs of the state was projected to 2013 parallel to Landsat data of 2013 from which the urban footprint was extracted. The growth rate of 3.2 prescribed by the national population commission was adopted for the projection.

A topological overlay of the GIS layer carrying administrative/population data and the urban footprint layer was performed based on attributes and features spatial join (Figure 13a). The urbanized area land use classes was merged and then superimposed on the flood risk magnitude map using spatial intersect. The new map so-generated captured and clipped out the urbanized areas within the potentially exposed LGA by vulnerability class (Figure 13b).

Figure 14 reveals that though Ikorodu is the fourth largest LGA after Epe, Badagry and Ibeju/Lekki, it has the largest settled area (over 139 km^2) in the state. In addition, 6 LGAs are at the verge of achieving 100 percent urban land coverage, these are Surulere, Agege, Ajeromi/Ifelodu, Ifako/Ijaye, Mainland and Mushin. The result shows that 15 LGAs are prone to flooding disaster in the state and a total of 14.587 km^2, 13.318 km^2, 11.559 km^2, 16.899 km^2 and 26.348 km^2 for very high, high, moderate, low and very low vulnerability classes respectively are exposed to flood hazard (Table 5). Among the flood prone 15 LGAs with an overall population of 8,423,846, an estimated total of 172,444 are vulnerable to the hazard.
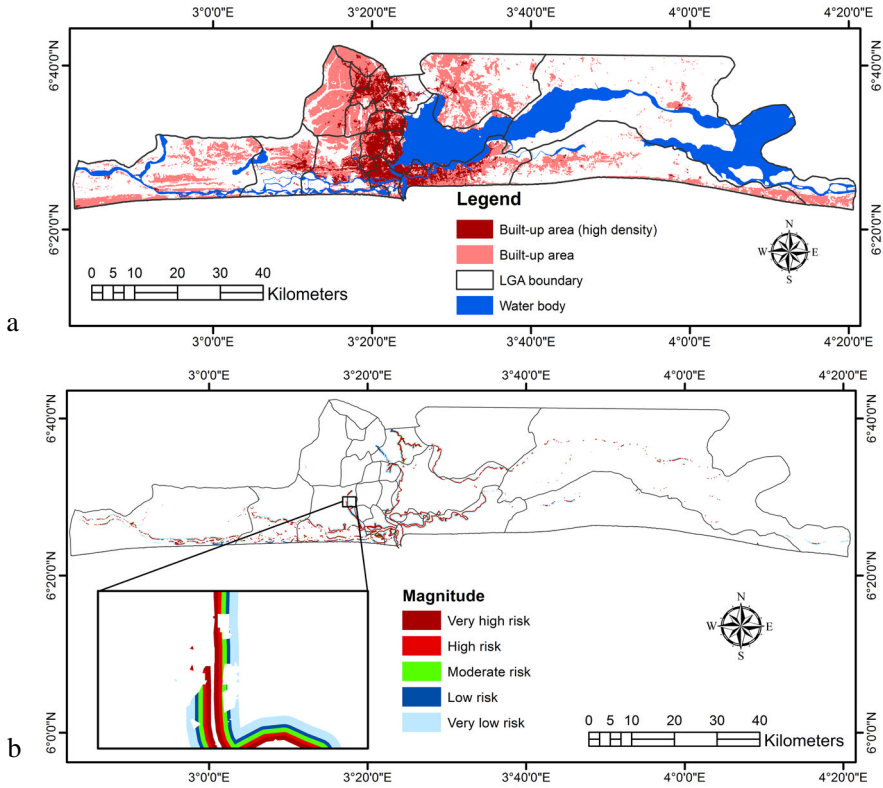
Figure 13. An integration of urban footprint and administrative data: (a) Overlay of extracted urbanized land use and local administrative/population data (b) Vulnerable urban land use by LGA.

The result shows that Kosofe LGA which lies within the Ogun River floodplain has the highest estimated number (44,227) of vulnerable people to flooding. This is about 26 percent of the entire vulnerable population by LGA. Followed by Amuwo-Odofin and Shomolu LGAs with vulnerable population of 24,253 (14.1 percent) and 22,493 (13.0 percent) respectively.

The final result of this analysis is the generation of a comprehensive flood risk geo-database system which contains both spatial and non-spatial data. In the database, a query system was built for quick and easy search of flood information for decision making processes.
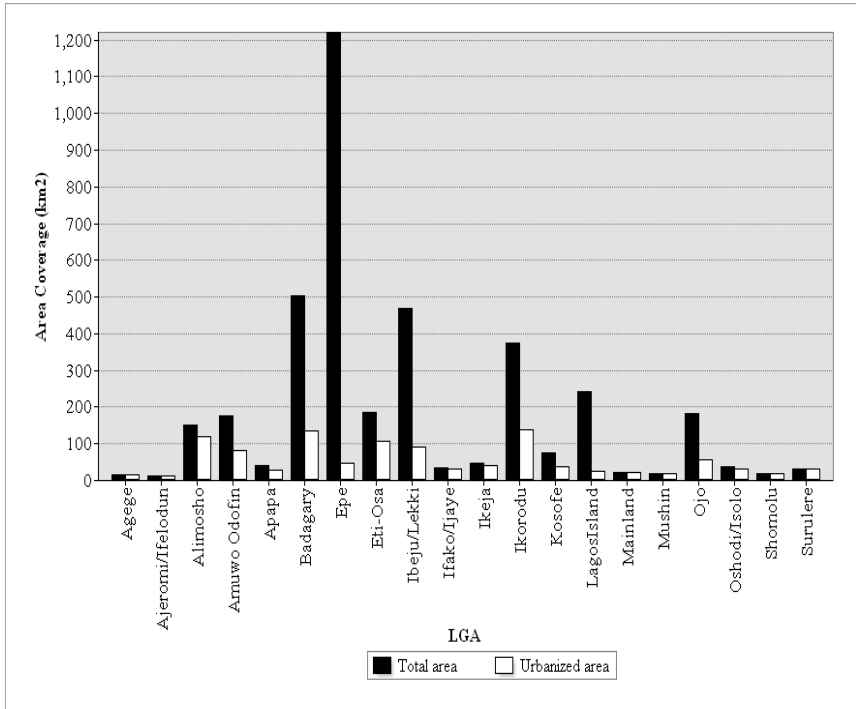
Figure 14. Side-by-side comparison of the administrative areal extent and urbanized area.

Table 5 provides basic planning information and this is a result of GIS-assisted query technique within the created geo-database. From this database system, it is possible to retrieve non-attribute information as it relates to its spatial constituent pertaining to a particular local administrative area and further narrowed down to specific vulnerability class.

However, the various derivatives and spatial information generated from this analysis demonstrate the capability of GIS-based system supported by multi-scale remote sensing and temporal data for mapping and identifying vital components exposed to the impact of flooding. The modeling methodology proposed in this chapter is beneficial for both local and holistic flood risk modeling and offers a significant degree of accuracy and simplification in contrast to pure hydrological flood risk and prediction model which has been criticized for its complexity with respect to the nature of data, preparation, rigorousness of procedure and computational time (Sanyal and Lu, 2004; Taubenbock et al., 2011).

Table 5. Urbanized areas and population at risk by LGA

LGA	Total area extent (km^2)	Urba-nized area extent (km^2)	Extent of risk area by vulnerability class (km^2)					Population distribution		
			Very high	High	Mode-rate	Low	Very low	Total popu-lation*	Popu-lation density	Popu-lation at risk
Ajeromi/ Ifelodun	11.82	11.56	0.004	0.020	0.030	0.041	0.113	856,869	74,103	3,020
Alimosho	150.38	120.11	0.000	0.000	0.000	0.005	0.038	1,645,094	13,696	69
Amuwo-Odofin	176.72	81.93	3.090	2.703	2.277	3.524	4.845	410,129	5,006	24,253
Apapa	42.31	29.07	2.089	1.951	1.735	1.612	2.881	277,994	9,563	15,415
Badagry	502.15	135.80	1.170	1.076	0.850	1.736	3.069	296,378	2,182	3,788
Epe	1,220.83	47.93	0.319	0.265	0.255	0.371	1.150	226,566	4,726	1,754
Eti-Osa	184.19	106.38	3.066	2.857	2.521	2.867	4.966	353,799	3,325	16,514
Ibeju/ Lekki	467.36	89.89	0.069	0.070	0.034	0.373	0.454	146,851	1,633	609
Ikeja	46.46	42.12	0.000	0.000	0.000	0.359	0.073	395,966	9,400	3,373
Ikorodu	375.32	139.16	0.417	0.435	0.398	0.400	0.834	658,148	4,729	1,895
Kosofe	75.28	38.55	1.131	1.113	0.965	2.003	2.214	851,204	22,077	44,227
Lagos Island	242.65	25.33	2.199	1.917	1.645	1.805	3.133	265,171	10,469	18,896
Mainland	23.13	21.05	0.079	0.093	0.098	0.112	0.274	777,104	36,923	4,121
Ojo	182.94	57.02	0.634	0.484	0.403	0.902	1.331	759,449	13,318	12,017
Shomolu	18.588	17.654	0.323	0.334	0.348	0.789	0.973	503,124	28,498	22,493
Total	3,720.028	855.554	14.587	13.318	11.559	16.899	26.348	8,423,846		172,444

*Projected population figures to 2013 from the 2006 national census data.

The fundamental strengths of this proposed method are simplification, lesser modeling time, wide range of application, rapid mapping of vital flood component and quick estimation of vulnerable population, infrastructures and environmental layout. In addition, the classification of vulnerability into five magnitudes offers a wide range of options for planners to explore and make multi-level decisions pertaining to flood hazard mitigation.

Remarkably, the assessment of exposed population and settled areas by grass root level will facilitate coordination between the tiers of government regarding policy making and intervention. The prime limitation of this framework is finding a suitable method with higher level of accuracy to estimate endangered population especially in developing African cities where population data is aggregated on large scale administrative elements; and neighborhood-based demographic data is lacking.

Conventional density estimation method which assumes the homogenous distribution of population over space often under-mine the fact that population

is majorly concentrated within urban space and other settled areas. To improve on this and possibly minimize this error, human footprints such as building activities and settlement structures which were extracted from temporal satellite data (and accurately checked with Google data) were used as a basis for calculating density. In other words, the primary human settled areas were included in the estimation.

Notwithstanding, even within the human settled areas population concentration is not homogenous, so care should be taken when using the estimated vulnerable population information because some areas may be over-estimated and some underestimated. This however, depend on the expected level of information needed.

On the one hand, if the purpose is to derive maximum degree of accuracy pertaining to the vulnerable population, (in most cases this is always a mirage because flood risk modeling is basically estimation and prediction), a comprehensive ground population count is recommended using the generated flood prone area map of the region. On the other hand, if the purpose is for substantial decision making and policy relevance, (mostly involving imminent and uncertain factors) it is most appropriate to know the correct pattern and dimension rather than the exact number of people (Taubenbock et al., 2011), thus this estimation method is preferred because it is based on up-to-date remote sensing data and statistical figures.

CONCLUSION

The most effective method of combating and mitigating the impact of flood disaster is to conduct a pre-risk assessment and identify vulnerable factors before a flooding episode. This is the case for more advanced countries of the world, but for developing countries especially those found in Africa region, the case is far from disaster preparedness. In these countries, with particular reference to Nigeria, public policies concerning flood management are oriented towards disaster alleviation and provision of aids.

Public decision makers and other governmental framework in Nigeria find it more convenient to setup ad hoc disaster emergency management agencies with huge financial budget instead of concentrating manpower, technical skills and available financial resources on potential flood impact assessment and mitigation. The reason for this mono-perspective policy is generally lack of well synthesized planning information.

GIS technique is a reliable tool for spatial planning based on the level and quality of information generated. Its ability to integrate multi-scale and multi-temporal data from diverse sources makes the platform a powerful force for contemporary development and problem solving.

The robustness of the GIS driven procedure prescribed in this chapter further demonstrates the quality and nature of its results. The series of maps produced and the database system generated are indispensable tools for decision makers, regarding flood management and risk analysis.

The results are well simplified especially for policy formulators who do not have strong knowledge for interpreting spatial data. This is promoted by its geovisualization capability which provide quick visual impression of the pattern and degree of vulnerability.

However, the results have a parallel link and application to public policies especially those related to urban and town planning in the study area. For example, evidence from this analysis point to the conclusion that urban planners need to revisit the water body setback policy. The flood mask generated through integrated procedures will be highly beneficial when the setback legislation is set for review. In addition, when decision makers decide to take a more drastic measure concerning the safety of the general public by relocating activities and residents from the floodplain and risk zones to risk free areas, the created database will serve as a guideline for such a project.

The identified flood prone areas, infrastructures and population based on vulnerability class provide range of options and will undoubtedly assist in priority ranking. The integration of the flood risk data with Google map will help to explore building structures and track down residences (including their spatial location) that are exposed to a particular risk magnitude. Such spatially synchronized database would facilitate campaign and enlightenment program by presenting basic spatial information on flood risk and vulnerability. This can be done by collaborating with Google map makers to upload the flood mask data to the internet through their map server from where individuals can access it at any point and time.

REFERENCES

Adeniran, O., Alagbe, A. and Aboderin, O. (2013). Delineation of flood vulnerable zones and disaster risk management along Asa River: A GIS Approach. FIG Working Week-Environment for Sustainability, Abuja, Nigeria.

Akinsanmi, G. (2011). Lagos communities flooded as Ogun River rises 4m. *This Day News Live*, www.thisdaylive.com/articles/lagos-communities-flooded-as-ogun-river-rises-4m/101132.

Alaghmand, S., Abdullah, R., Abustan, I., and Vosoogh, B. (2010). GIS-based River Flood Hazard Mapping in Urban Area (A case study in Kayu Ara River Basin, Malaysia). *International Journal of Engineering and Technology*, vol. 2, No. 6, pp. 488-500.

BNRCC-Building Nigeria's Response to Climate Change (2012). Towards a Lagos State Climate Change Adaptation Strategy. Report prepared for the Commissioner of Environment, Lagos State http://nigeriaclimatechange.org/docs/lasAug2012.pdf.

FDALR-Federal Department of Agriculture and Land Resources (1995). Reconnaissance Soil Survey of Nigeria. *Final Report of the Ministry of Agriculture and Natural Resources*, Abuja, Nigeria.

Hualou, L. (2011). Disaster Prevention and Management: A Geographical Perspective. *Disaster Advances*, vol. 4, No. 1, pp. 3-5.

Ikusemoran, M., Dami, A. and Maryah, U. M. (2013). GIS based sssessment of flood risk and vulnerability of communities in the Benue floodplains, Adamawa State, Nigeria. *Journal of Geography and Geology*, vol. 5, No. 4, pp. 148-160. doi:10.5539/jgg.v5n4p148.

Irimescu, A. Craciunescu, V. Stancalie, G., and Nertan, A. (2010). Remote Sensing and GIS Techniques for Flood Monitoring and Damage Assessment Study Case in Romania. *4th International Scientific Conference BALWOIS*, Ohrid, pp. 1-10.

Ishaya, S., Ifatimehin, O. O. and Abaje, I. B. (2009). Mapping Flood Vulnerable Areas in a Developing Urban Centre of Nigeria. *Journal of Sustainable Development in Africa*, vol. 11, No. 4, 2009, pp. 180-194.

Islam, M. M. and Sadu, K.: 2001, Flood damage and modelling using satellite remote sensing data with GIS: Case study of Bangladesh. In: Jerry Ritchie et al. (Eds.), *Remote Sensing and Hydrology 2000*, (pp. 455-458). Oxford, IAHS Publication.

Nirupama, N. and Simonovic, S. P. (2007). Increase of Flood Risk due to Urbanization: A Canadian Example. *Natural Hazards*, vol. 40, pp. 25-41.

Nkeki, F. N. (2013a). Living near high-voltage power lines: GIS-based modeling of the risk in Nigeria's Benin region. *Applied GIS*, vol. 9, No. 1, 1-20.

Nkeki, F. N. (2013b). The risk of living near power lines: GIS modeling approach. Saarbruxken, Deutschland, Germany: Lambert Academic Publishing.

Nkeki, F. N. and Asikhia, M. O. (2014). Mapping and geovisualizing topo-graphical data using geographic information system (GIS). *Journal of Geography and Geology*, vol. 6, No. 1, pp. 1-13. doi:10.5539/jgg.v6n1p1.

Nkeki, F. N., Henah, P. J. and Ojeh, V. N. (2013). Geospatial techniques for the assessment and analysis of flood risk along the Niger-Benue Basin in Nigeria. *Journal of Geographic Information System*, vol. 5, No. 2, pp. 123-135. doi:10.4236/jgis.2013.52013.

Olajuyigbe, A. E., Rotowa, O. O. and Durojaye, E. (2012). An assessment of flood hazard in Nigeria: The case of Mile 12, Lagos. *Mediterranean Journal of Social Sciences*, vol. 3, No. 2, pp. 367-377.

Ologunorisa, E. T. (2006). *Flood Risk Assessment and Management in Nigeria: Perspective from the Niger Delta*. Makurdi, Nigeria: Selfers Edu-cational books.

Opolot, E. (2013). Application of Remote Sensing and Geographical Informa-tion Systems in Flood Management: A Review. *Research Journal of Applied Sciences, Engineering and Technology*, vol. 6, No. 10, pp. 1884-1894.

Oriola, E. and Bolaji, S. (2012). Urban flood risk information on a river catchment in a part of Ilorin Metropolis, Kwara State, Nigeria. *Informa-tion and Knowledge Management*, vol. 2, No. 8, pp. 70-84.

Oyinloye, M., Olamiju, O. I. and Ogundiran, A. (2013). Environmental Impact of Flooding on Kosofe Local Government Area of Lagos State, Nigeria: A GIS Perspective. *Journal of Environment and Earth Science*, vol. 3, No. 5, pp. 57-66.

Oyinloye, M. A., Olamiju, O. I. and Oyetayo, B. S. (2013). Combating flood crisis using GIS: Empirical evidences from Ala River Floodplain, Isikan area, Akure, Ondo State, Nigeria. *Communications in Information Science and Management Engineering*, vol. 3, No. 9, pp. 439-447.

Samarasinghe, S. M. J. S., Nandalal, H. K., Weliwitiya, D. P., Fowze, J. S. M., Hazarika, M. K., and Samarakoon, L. (2010). Application of remote sensing and GIS for flood risk analysis: A case study at Kaluganga River, Sri Lanka. *International Archives of the Photogrammetry, Remote Sensing and Spatial Information Science*, vol. 38, No. 8, pp. 110-115.

Sanyal, J. and Lu, X. X. (2004). Application of Remote Sensing in Flood Management with Special Reference to Monsoon Asia: A Review. *Natural Hazards*, vol. 33, pp. 283-301.

Sobowale, A. and Oyedepo, J. A. (2013). Status of flood vulnerability area in an ungauged basin, southwest Nigeria. *International Journal of Agricultu-*

ral and Biological Engineering, vol. 6, No. 2. pp. 28-36. doi:10.3965/j. ijabe.20130602.004.

Taubenbock, H., Wurm, M., Netzband, M., Zwenzner, H., Roth, A., Rahman, A., and Dech, S. (2011). Flood risks in urbanized areas-multi-sensoral approaches using remotely sensed data for risk assessment. *Natural Hazards and Earth System Sciences*, vol. 11, No. 2, pp. 431-444. doi:10. 5194/nhess-11-431-2011.

Thieken, A. H., Mariani, S., Langfield, S., and Vanneuville, W. (2014). Preface: Flood resilient communities managing the consequences of flooding. *Natural Hazards and Earth System Sciences*, vol. 14, No. 1, pp. 33-39. doi:10.5194/nhess-14-33-2014.

Townsend, P. A. and Walsh, S. J. (1998). Modeling floodplain inundation using an integrated GIS with radar and optical remote sensing. *Geomorphology*, vol. 21, pp. 295-312.

Tralli, D. M., Blom, R. G., Zlotnicki, V., Donnellan, A., and Evans, D. L. (2005). Satellite remote sensing of earthquake, volcano, flood, landslide and coastal inundation hazards. *Journal of Photogrammetry and Remote Sensing*, vol. 59, pp. 185-198 doi:10.1016/j.isprsjprs.2005.02.002.

Triglav-Cekada, M. and Radovan, D. (2013). Using volunteered geographical information to map the November 2012 floods in Slovenia. *Natural Hazards and Earth System Sciences*, vol. 13, pp. 2753-2762 doi:10.5194/ nhess-13-2753-2013.

USGS-US Geological Survey (2013). Landsat 8. Fact sheet 2013-3060, pp. 1-4. http://pubs.usgs.gov/fs/2013/3060/pdf/fs2013-3060.pdf.

Vine, M. F., Degnan, D. and Hanchette, C. (1997). Geographic Information Systems: Their use in environmental epidemiologic research. *Environmental Health Perspectives*, vol. 105, No. 6, pp. 598-605.

Wang, Y. (2004). Seasonal change in the extent of inundation on floodplains detected by JERS-1 Synthetic Aperture Radar data. *International Journal of Remote Sensing*, vol. 25, 2497–2508.

Zhang, H., Ma, W. and Wang, X. (2008). Rapid urbanization and implications for flood risk management in hinterland of the Pearl River Delta, China: The Foshan study. *Sensors*, vol. 8, No. 4, pp. 2223-2239.

Zheng, N., Takara, K., Tachikawa, Y., and Kozan, O. (2008). Analysis of vulnerability to flood hazard based on land use and population distribution in the Huaihe River Basin, China. *Annuals of Disaster Prevention Research Institute*, vol. 51, No. 2, pp. 83-91.

Chapter 10

USE OF REMOTE SENSING AND GIS FOR GROUNDWATER POTENTIAL MAPPING IN CRYSTALLINE BASEMENT ROCK (SABODALA MINING REGION, SENEGAL)

I. Mall[*], M. Diaw, H. D. Madioune, P. M. Ngom and S. Faye

Department of Geology/Faculty of Sciences and Technology/UCAD
Dakar, Senegal

ABSTRACT

Detection of favorable zones for sustainable groundwater supply in terrains underlying by crystalline rocks needs to integrate two approaches: Remote Sensing and GIS. Landsat ETM+ images are processed by using ERDAS IMAGINE 9.2 and ASTER images by ArcGIS 9.3. Parameters controlling groundwater accumulation such as: rainfall, lineaments, lithology, slopes, and drainage network are evaluated in terms of 5 potential classes namely: very good potentials, good; moderate; low and very low potential and integrated in the GIS tool. The resulting map shows that 5% of the study area presents a very good groundwater potential and this part is mainly concentrated in the south part of the study area and on the MTZ, very low potentials constitute 13%

---

[*] Ibrahima.mall@ucad.edu.sn.

of the area located essentially in the north part of the study area and particularly on granites. Combination of results generated by the GIS with NDVI and the borehole productivities shows that, generally good groundwater potentials are well correlated with high vegetal activities in dry season except in areas affected by forest fires which are frequent in the region. High borehole productivities (11.5 -30m^3/H) are observed in zone presenting high groundwater potential resulting from the GIS tool and very low borehole productivities (0.6-2.5m^3/H) are shown in the north part of the study area corresponding to the low and very low groundwater potentials. Good, moderate and low groundwater potentials represent respectively 18, 33 and 30% of the total investigated surface area. This integrated approach combining Use of RS, GIS and hydrodynamic parameters such as borehole productivities can contribute to improve Knowledge of groundwater resources investigation in context of hard rock aquifers of the south-eastern of Senegal and can reduce the high rates of failed wells. So, RS and GIS can be used as an efficient tools for assessing groundwater potential at large scale.

Keywords: Remote Sensing, GIS, groundwater, NDVI, Lineaments, crystalline rocks, Senegal

I. INTRODUCTION

In the sub-saharian regions, water storage issues have been increasingly difficult to tackle especially in regions where, the aquifers are located in crystalline rocks. The Sabodala region (Kédougou kéniéba Inlier in Senegal) like many parts of basement regions belongs to the field of Birimian basement rocks characterized by discontinuous aquifers. The hydrogeological system is constituted by weathered and fractured aquifers which are depending on tectonic structuration and climatic effects on rock formations. However, availability of groundwater resources is limited and therefore water issues in Sabodala constitute a great concern to supply population with fresh water due to the boreholes low yield and the high unsuccessful rates of drilling. Localization of favorable drilling zones for sustainable groundwater supply in crystalline rock terrain needs to integrate two approaches: Remote Sensing (RS) and geographic information systems (GIS). Many authors demonstrated the usefulness of the application of GIS and RS on natural resources management and monitoring. According to Ismail (2011), the use of satellite based RS has made it possible to map large areas with greater accuracy for various resources assessment and management. Teeuw (1995) proposed an

integrated approach of RS and GIS techniques to improve the site selection for borehole drilling in the Volta basin of northern Ghana. The application of GIS technology allows swift organization, quantification and interpretation of large quantities of hydrogeological data with more accuracy and minimal risk of human error (Pinder 2002). For Sisay (2007), Remote sensing technique provides an advantage of having access to large coverage, even in inaccessible areas. It is rapid and cost-effective tool in producing valuable data on geology, geomorphology, lineaments, slope, etc. that helps in deciphering groundwater potential zone. A systematic integration of these data with follow up of hydrogeological investigation provides rapid and cost effective delineation of groundwater potential zones. Despite the extensive research and technological advancement, the study of groundwater has remained more risky, as there is no direct method to facilitate observation of water below the surface. Its presence or absence can only be inferred indirectly by studying the geological and surface parameters.

The Birimian formations which are the most representative formations are gold bearing formations like in most part of the West African craton. The geological formations are mainly made up of basalts, andesite, rhyodacites of gabbros, peridotites and volcanic-sedimentary rocks intruded by granites (Bassot, 1966). These formations, which have been repeatedly deformed and metamorphosed in low amphibolite facies and green schists facies by granite intrusions are often overlaid by a thick lateritic mantle, and this latter covers more than 2/3 of the geological strata which outcrops sometimes at the riverbeds. The weathering profiles show thickness as much as twenty meters with different horizons. Also the alluvium thickness can reach few meters at the riverbeds. A new cartography of Birmian formations (Théveniaut & al 2010) identified that two groups and three suites are present in eastern Senegal, these are:

- Volcano-sedimentary Groups of Mako and Dialé-Dalema;
- Magmatic suites of Sandikounda-Soukouta, Saraya and Boboti.

The hydrographic network comprises the Gambia River and Falémé River, both fed by Fouta Djalon in Guinea. The tributaries of these rivers are non-perennial and dry up during the dry season (Camus & Debuisson, 1964). The area is characterized by a dry season from October to April-May and a rainy season which usually starts at the end of April and continues until October with a maximum rainfall in August. The yearly average rainfall is about 1200 mm per year at the Kédougou station (Mall. 2009). Hydrogeological context of

the study area is characterized by fractured, discontinuous and semi-continuous aquifers which are represented by the weathered fringe of hard rocks with yields varying from 0.6 to 30 m³/H and high unsuccessful drilling rates (Diouf, 1999).

Figure 1. Location map of the study area.

II. METHOD AND TOOLS

Landsat ETM+ (2010) images were respectively processed using Erdas IMAGINE 9.2 and ASTER images, by Arc GIS 9.3. Landsat images were filtered for highlighting lineaments by low pass band (3x3 filter) and directional filtering (Sobel filter 7x7). The processing of ASTER images were carried out in Arc GIS 9.3 by spatial analyst tools with the Hydrology module in order to generate the drainage network and Slopes. So, lineament density and drainage density are carried out by using Line Density tool that calculates the density of linear features in the neighborhood of each output raster cell. Density is calculated in units of length per unit of area. All input rasters were generated, reclassified, weighted and overlaid using Weighted Overlay module. The Reclassification tools provide an effective way to compute the conversion. Each class value in an input raster is assigned a new value based on an evaluation scale. These new values were computed from the original input raster values. Each input raster is weighted according to its importance or its percent influence. The weight is a relative percentage, and the sum of the percent influence weights must equal 100. Changing the evaluation scales or the percentage influences can change the results of the weighted overlay analysis (Silverman,. 1986). The output data were combined in the model with parameters controlling groundwater accumulation such as rainfall, and lithology (Al Saud., 2010, Hossam., & al, 2011). These parameters were evaluated in terms of 5 potential classes namely: very good potentials potential, good; moderate; and low potential and very low and weighted from 1 to 9 prior to integrate them into the GIS tools. All the thematic maps, such as: rainfall, geology, lineament density, geology, slope, drainage density, were converted to raster format followed by assigning respective theme weight and class rank as shown in (Table.1). Each raster map is reclassify into five classes of potentiality, ranging from very good potentials to very low potentials passing through to the moderate, good and low potentials. The weighted overlay analysis was performed "Spatial Analyst Module" of ArcGIS 9.3 (Mehnaz, 2011), with integration of all the most influencing parameters controlling groundwater storage in the study area. NDVI (Normalized Difference Vegetation Index) from Landsat (ETM+, April 2010) was calculated from Landsat Bands NIR (ETM4+) and Red (ETM3+) and formula is given in (equation. 1). The NDVI is used to analyze Remote Sensing measurements to assess the presence of live green vegetation. In areas of a shallow water table, the presence of live green vegetation indicates the availability of groundwater during summer and hence NDVI is highly

important (National Remote Sensing Agency 2008). In this study, groundwater productivity in boreholes combined with NDVI are used as a validation method of the results given by the GIS tool.

II.1. Rainfall
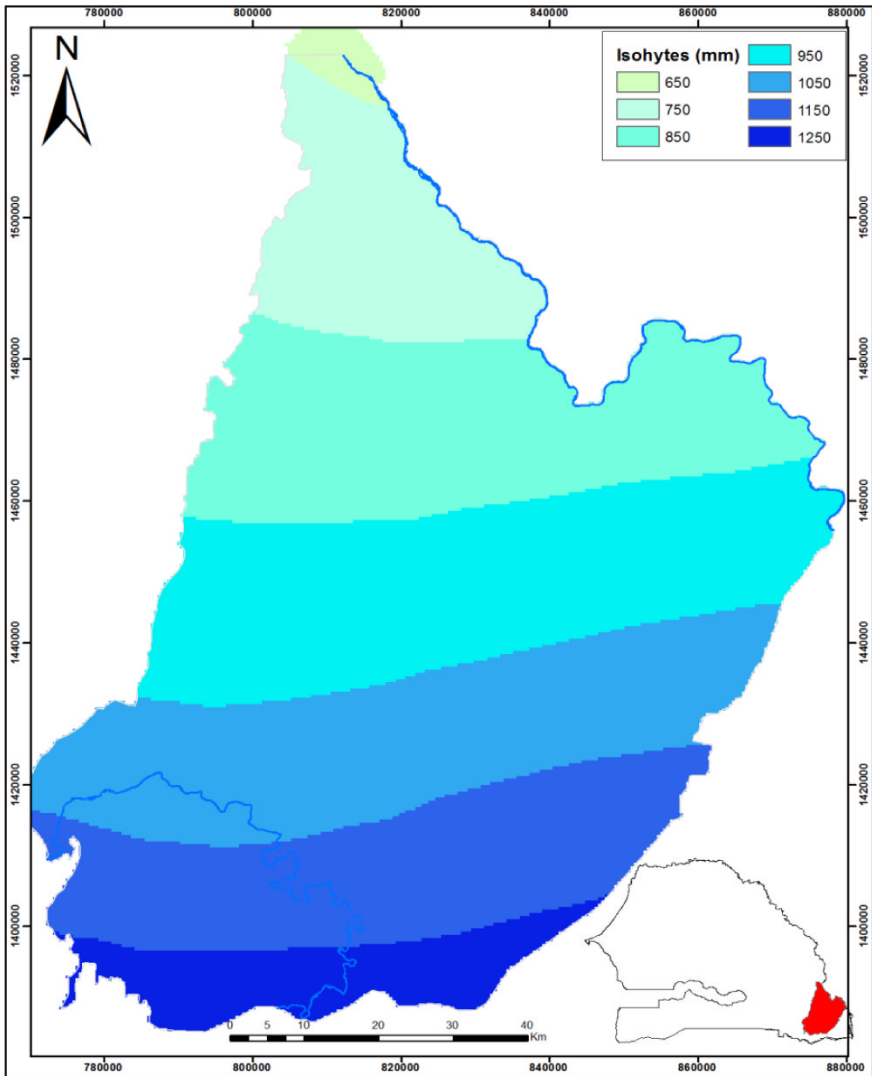
Figure 2. Isohyets distribution in the study area (MEPNBRLA, 2009).

Table 1. Classification of influencing factors on groundwater storage

Class Weighted parameters	Very Good 9	Good 7	Moderate 5	Low 3	Very low 1
Rainfall 30%	2,7 1250-1150mm	2,1 1150-950mm	1,5 950-850mm	0,9 850-750mm	0,3 750-650mm
Lineaments 25% Lenght Km/Km²	2,25 38-48	1,75 28-38	1,25 19-28	0,75 9,5-19	0,25 0-9,5
Geology 20%	1,8 Gabbros	1,4 Volcano-clastic	1 Schiste	0,6 Granite	0,2 Basalte
Slope 15%	1,35 0-1%	1,05 1-2%	0,75 2-3%	0,45 3-5%	0,15 5-35%
Drainage 10% Lenght Km/Km²	0,9 0-1	0,7 1-1,8	0,5 1,8-2,7	0,3 2,7-3,6	0,1 3,6-4,5

It is the most important parameter in groundwater recharge. In the area, rainfall is concentrated mainly in rainy season which starts at the end of April and continues until the end of October in the south part of the study area. By cons in the northern part, rains start later in late June and usually stop at the beginning of October. Maximum precipitation is recorded in August in the two climatic provinces. The sector is characterized by a rainfall gradient change from south to north (Mall. 2009). This is shown by a spatial distribution of isohyets that increase from north to south with the 1250 mm isohyet observed in south of Kédougou and 650 mm isohyet in the north part of the area. This contrast between climatic provinces reflects a difference in the structure of vegetal communities. The southern part is the domain of forest with a high density of vegetation sometimes associated with gallery forests that follow the meandering of rivers. Nevertheless, going towards the north part of the study area, the forest gives way to savannah dominated by thorny vegetation well adapted to drought conditions.

II.2. Geology

Type of geological formation is an important factor in the development of water reserve in crystalline basement. Their petrography determines the type of weathering profile that develops on it. Thus, the thickness of the regolith is much higher on basic rocks than granites and schists as it develops more clay on basic rocks than on granites. However, the granites are much more resistant to weathering and mechanical disintegration than other rock types. So granites could become good aquifer if they are affected by faulting. By cons become

less if they are unstructured because of the high granites resistivity to weathering due to high contents of quartz in their petrographic structures. Basic rocks and schists may have good potential aquifer due to their altered upper part often very well developed. This regolith especially has a capacitive function that plays an important role in deferred groundwater recharge and therefore may be a useful aquifer for hand dug wells. So, the most interesting potentials are recorded at ultra-basic rocks and in carbonate formations. Volcano-sedimentary can be a good aquifer with a good groundwater potential. However, schists present a moderate potential and low potential are found on granites and acid volcanic rocks.

II.3. Lineaments

They have been subject of several studies in the West Africa (Biémi, Engelec, Kouamé, Savadogo Savané). Their involvement in the research area conducive to the implementation of drilling is well established today. On satellite imagery, lineaments correspond to image discontinuities and are expressed by the juxtaposition or layering simple physiographic elements or composite varied natures (morphology, hydrography, vegetation, surface difference in tone ...) where, different parties are rectilinear relationship or slightly curvilinear (Kouamé, 1999). On the ground there are the lithological discontinuities (contact between different formations) or structural (fault, joint, dyke…) (GRONAYES et al.). Four major lineament directions are noted in the region. The N60-N50 directions (Fig. 5) are the most representative with respectively 10.8% and 10.5% of total lineament length followed by the N170-N180 and N0-N10 and finely the N100 direction that represents about 8% of the total lineament length. The preponderance of the N60 and N50 is essentially due to a regional tectonic accident called main transcurrent zone (MTZ) which represents a regional shear zone that affected the whole region.

II.4. Slope

The plain occupies most part of the area and the terrain is often marked by plateaus covered by a thick lateritic mantle. Slopes are higher especially in the southern west part of Kédougou in vicinity of Mako and in the center of the study area where they can reach 32% (Fig. 6). The north side of the study area land becomes relatively flat with few elevations and gentle slope near the

Falémé River. The elevations are more important in the south of the study area. This configuration of the geomorphology makes the terrains in the southern part, more conducive to runoff than infiltration, therefore less favorable to groundwater storage.
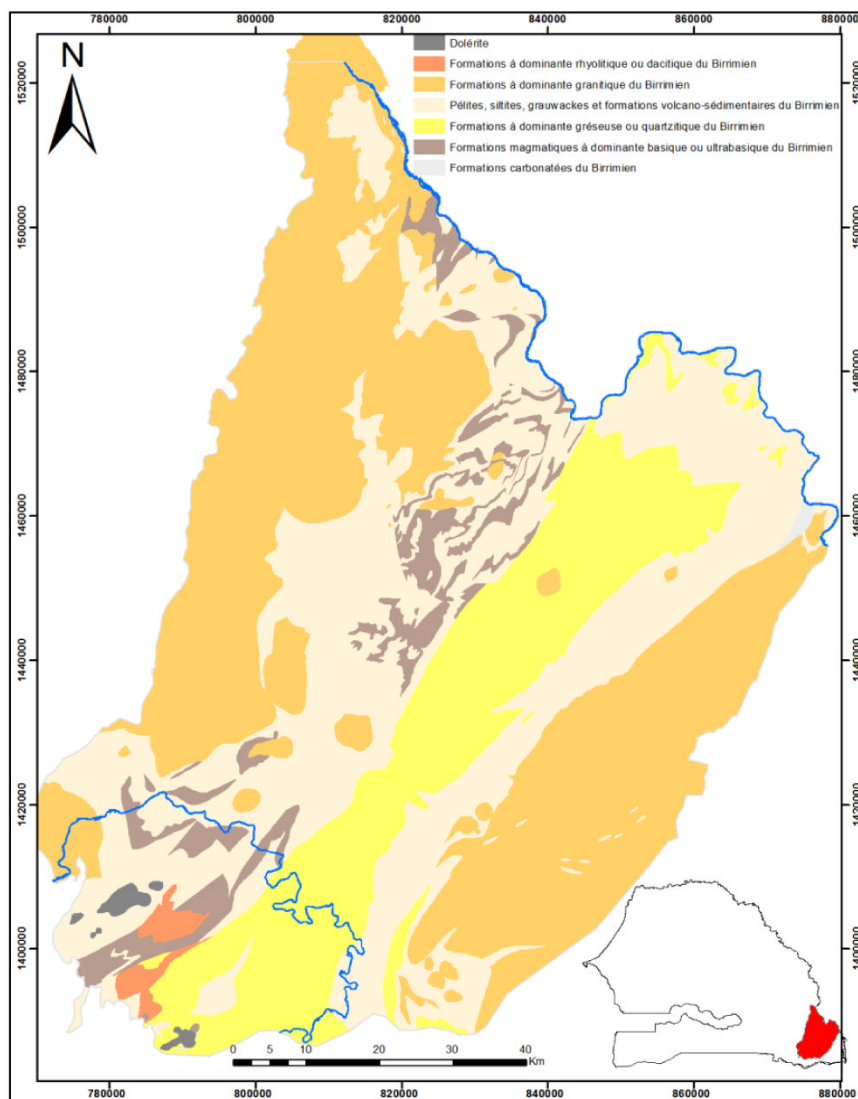
Figure 3. Hydrogeological units map (Wuilleumier & al 2010).
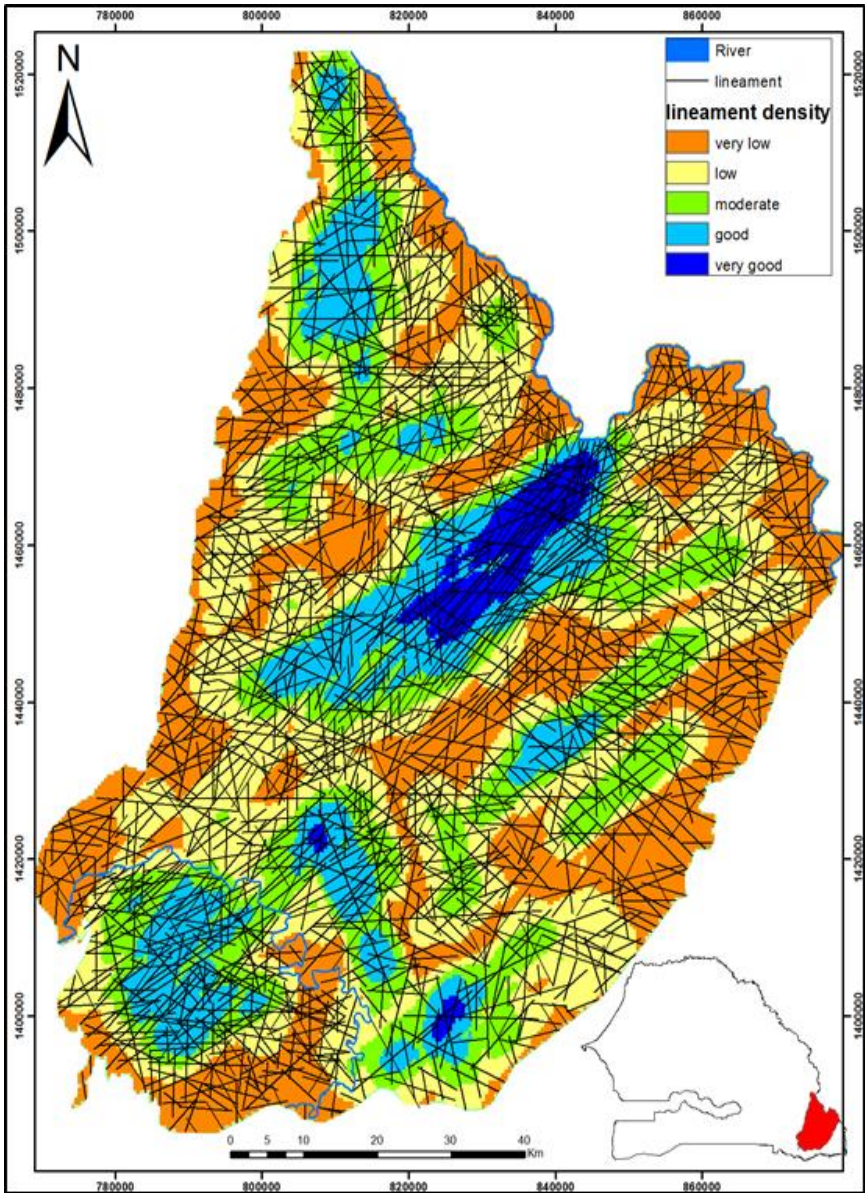
Figure 4. Lineaments and lineament density map.
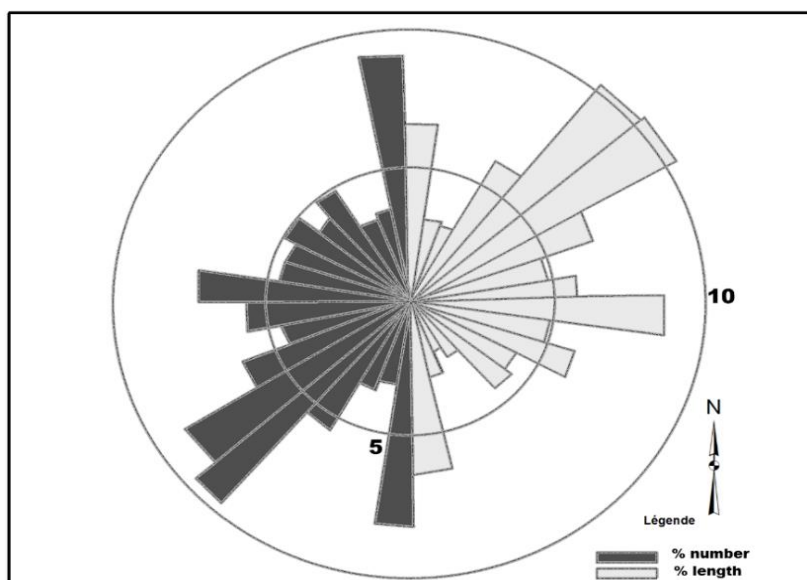
Figure 5. Rose diagramm of lineament orientations.

II.5. Drainage Network

Drainage network is a factor which depends essentially on watershed physiography including: its shape, size, slopes, geological formations etc. Like slope, the drainage network is inversely proportional to groundwater storage. An important drainage network means, a higher runoff that reduces groundwater storage capacity. In the study area, impermeable nature of the hard rock formations explains a very high density of the drainage network, which essentially corresponds to intermittent streams that dry up earlier as of January. However, if the topographical conditions are favorable (low slope) these gullies which accompany the riverbeds, can constitute substantial groundwater reserves with low lateral extension at the scale of villages.

$$\text{NDVI} = \frac{ETM4 - ETM3}{ETM4 + ETM3} = \frac{NIR - RED}{NIR + RED} \qquad \text{(Eq. 1)}$$

Nearly all satellite Vegetation indices employ this difference to quantify the density of plant growth on the Earth: near infrared minus visible radiation divided by near-infrared radiation plus visible radiation.
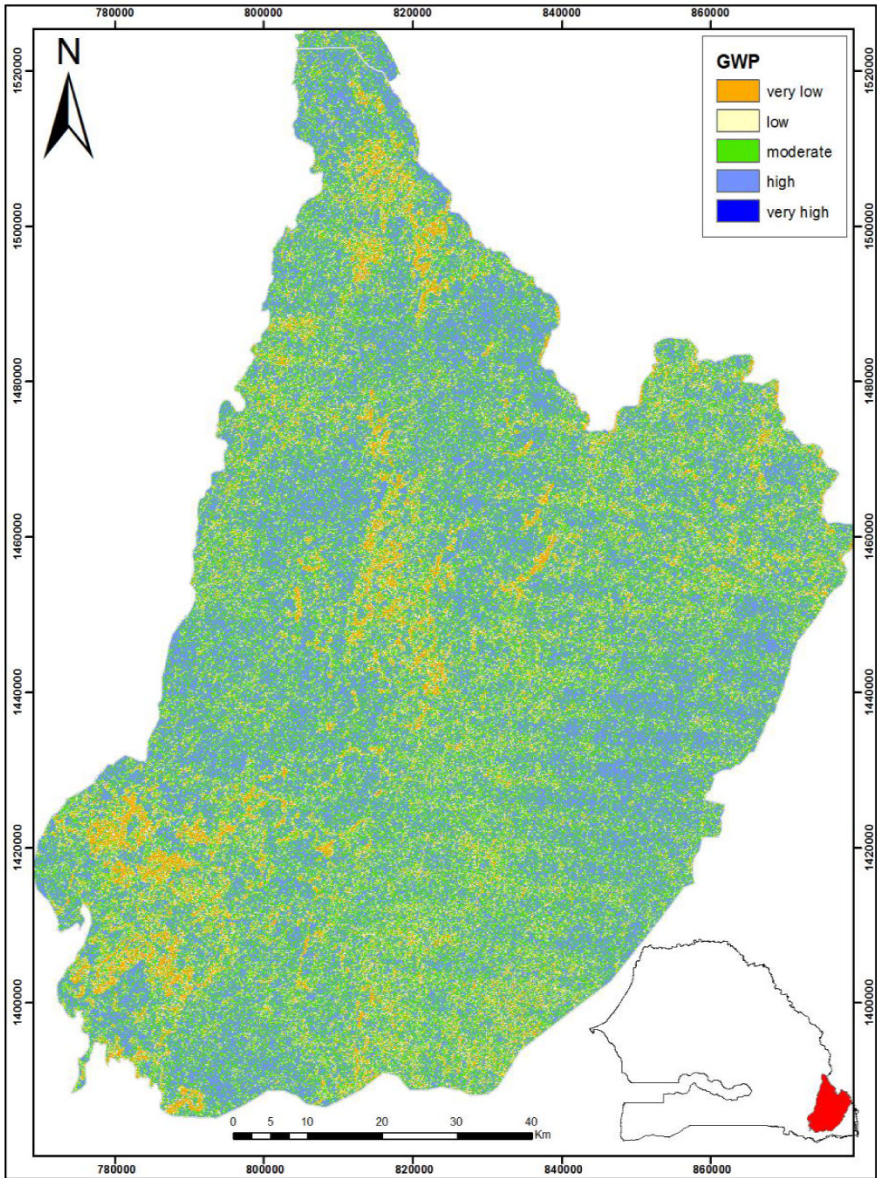
Figure 6. Slope distribution in the study area.
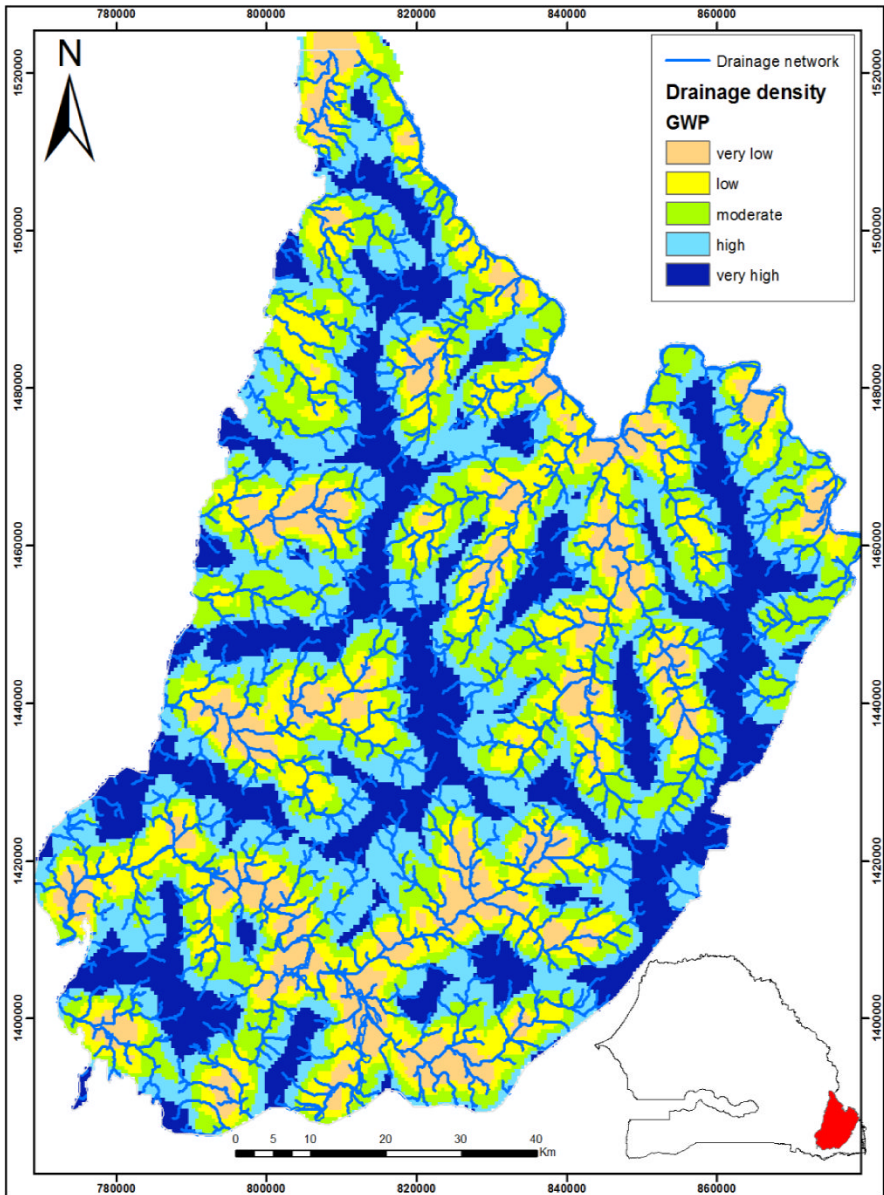
Figure 7. Drainage network and density.

II.6. Organization Diagram of Integrated Parameters in the GIS
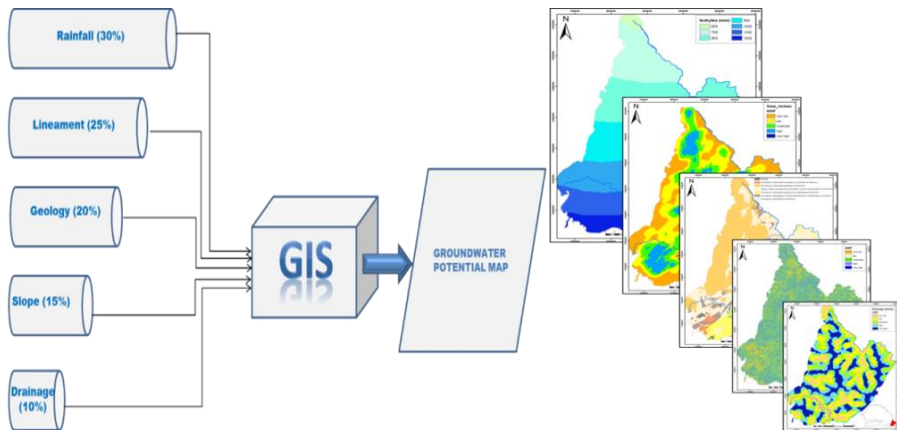
Figure 8. Integrated parameters (Rainfall, lineament density, Geology, Slope, Drainage density) and their percentage weights.

III. RESULTS AND DISCUSSION

Integration of the weighted parameters into a GIS platform infers a groundwater potential map with five potentiality classes in the study area ranking from very high potential groundwater zones to very low. It is noted that, high potential zone is located in the South of Sabodala mining region contrasting to the northern part where groundwater potential is low due to decrease in rainfall and type of lithology formations made up of granites essentially. The output map (Fig. 9) resulting from GIS combination of different parameters (rainfall, lineaments, geology, slope, drainage network) shows a map of five potential aquifer zones (Fig. 9) ranging from zones with very high potential to zones with very low potential. Thus about 5% of the investigated area has a very good potential. These zones are mostly found in the south of the area situated in the southern part of the Gambia River watershed between 1250 to 1150mm isohyets and on the main transcurrent zone (MTZ). However, zones presenting a very good potential are also noted in the sector located between isohyets 1150 to 850 mm, which are isolated zones and can be found on the south part of the Saraya's granite (south and east of the Saraya city), south of Kanouméry village and its immediate surroundings. Very good potential is also localized in the volcano-sedimentary

formations (South Massamassa village) and Mouran village. In the North part of the study area only few sectors present very good potential are found at Kossanto and south of Makana village (south of Sabodala village). Very good and good groundwater potential zones are associated with intensive fracture system that provokes a high secondary permeability. Good potential zones occupy 18% of the study area and surround zones characterized by very good potential. Most of these zones is localized in south of the 850mm isohyet, however, some relics with good potential are noted in some sectors in the Northern part of the isohyet 850mm. The NDVI results, calculated from Landsat images April, 2010 (end of the dry season) (Fig.10), show that the very good and the good potential zones are well correlated with zones which show high vegetal activities. Very low potential zones and low potential zones correspond to zones where, vegetal activity is very low as noted in major part of granites (Sandikounda Soukouta and Saraya) and the northern part of the sector above the isohyet 850mm (Fig.10). However, this good correlation between the high intensity of vegetal activity and very good and good potential zone does not exist in the northern part of the study area in vicinity of Soreto village and this, could be related to xerophytic nature of vegetal communities which are adapted on drought conditions and can maintain their activities at a high level with a low soil moisture. This indicates that at this advanced period of dry season, vegetal activity is essentially supported by groundwater resources.

So, the NDVI can be a good indicator of groundwater presence but, its use must require some caution because of deforestation and recurrence of fires bush in the area during advanced dry season. These phenomena can mask the intensity of vegetal activity in zones characterized by a low plants density. Also we must take into account the depth of water table. Low vegetal activity can be found in zones where, depth of water table exceeds 20m even though, the results of GIS indicate sometimes a very good aquifer potential in these zones, that is the case of the southern part of Mouran village. Borehole productivities are also taking into account and show that, high borehole productivities (about 11.5 to 30 m^3/H) are observed in zone presenting high groundwater potential resulting from GIS processing and very low well productivities are shown in the north part of the study area corresponding to the low and very low groundwater potential with productivities ranging from 0.6 to 2.5 m^3/H. The results proved that, the north part of the study area

appears as a poor zone for groundwater storage if we take into account the results of GIS and the borehole productivities.
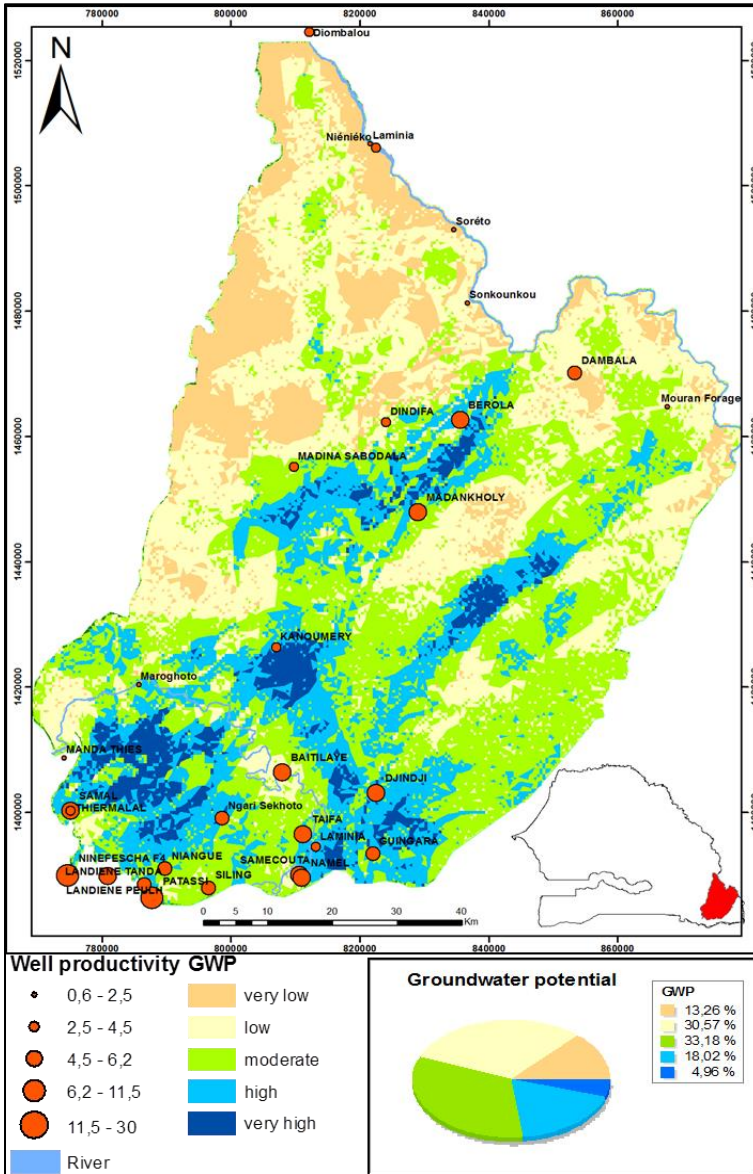
Figure 9. Groundwater potential map.
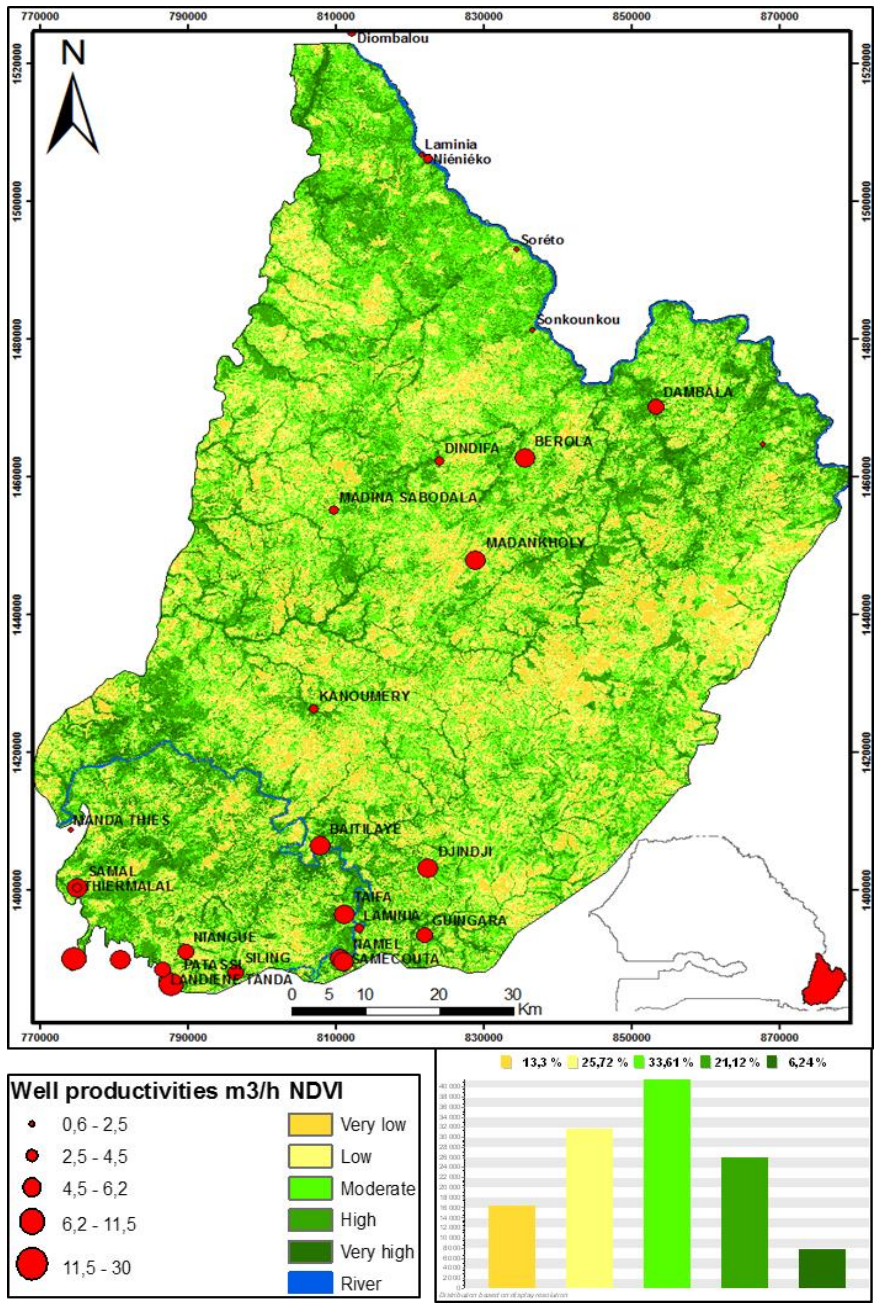
Figure 10. NDVI (Landsat image 04/2010).

CONCLUSION

Integration of different parameters that influence on groundwater storage is helpful to find out the best place for drillings and thus to reduce the rates of unsuccessful wells. The resulting map shows that 5% of the study area presents Very high groundwater potential storage that is mainly concentrated in the south part of the study area and on the MTZ, very low potential constitutes 13% of the area is located essentially in the north part of the study area and particularly on granites. Combination of results generated by the GIS with NDVI and wells productivities shows that, generally good aquifer potentials are well correlated with high vegetal activities in advanced dry season except in areas affected by forest fires which are frequent in the region. High borehole productivities are observed in zone presenting high groundwater potential resulting from GIS application and very low borehole productivities are observed in the north part of the study area corresponding to the low and very low groundwater potential. These important results can be an efficient indicator that helps decision makers to better manage their drilling projects and minimize the high rates of failed boreholes. Therefore, use of RS and GIS contributes to improve Knowledge of groundwater resources investigation in context of hard rock aquifers of south-eastern of Senegal and can be used as an efficient tool for assessing groundwater potential at large scale.

ACKNOWLEDGEMENTS

REFERENCES

Bassot J.P. 1966. Etude géologique du Sénégal oriental et de ces confins Guinéo-maliens. *Mem. Bur. Rech. Géol. Min.,* Paris, 40, 322p.

Biémi J. 1992. *Contribution à l'étude géologique, hydrogéologique et par télédétection des bassins* versants sub-sahéliens du socle précambrien d'Afrique de l'Ouest : Hydrostructurale, hydrodynamique, hydrochimie et

isotopie des aquifères discontinus de sillons et aires granitiques de la haute Marahoué (Côte d'Ivoire). Thèse d'Etat, Univ. Abidjan, 480 p.

Camus H. & Debuisson. J 1964. *Etude hydrologique des terrains anciens du Sénégal oriental.* Campagne 1962-1963. Rapport ORSTOM, n°114, Paris 434p.

Diouf. S. 1999. Hydrgéologie en zone de socle cristallin et cristallophyllien du Sénégal oriental. *Application de la méthode électrique 1D et 2D à la localisation et à la caractérisation des aquifères du batholite de Saraya et ses environs.* Thèse de doctorat de 3ecycle. Univ. C.A.D. de Dakar, 86p.

Engaenc. M (1978) : Méthode d'étude et de recherche de l'eau souterraine des roches cristallines. *Pub. CIEH, Ouagadougou,* Vol, 1,2, 3, 652p.

Hossam H. Elewa & Atef A. Qaddah. Groundwater potentiality mapping in the Sinai Peninsula, Egypt, using remote sensing and GIS-watershed-based modeling. *Hydrogeology Journal* (2011) 19: 613–628.

http://earthobservatory.nasa.gov/Features/MeasuringVegetation/measuring_ve getation_1.php.

Ismail Jasmin & P. Mallikarjuna 2011. Review: Satellite-based remote sensing and geographic information systems and their application in the assessment of groundwater potential, with particular reference to India. *Hydrogeology Journal* (2011) 19: 729–740.

Kouamé K. F. 1999. *Hydrogéologie des régions de montagne : Apports des données de télédétection et des méthodes statistique et fractale à l'élaboration d'un système d'information hydrogéologique a référence spatiale des aquifères discontinus du secteur Man-Danané* (ouest de la cote d'ivoire). Thèse de 3ème Cycle Université de Cocody.

Mashael Al Saud 2010: Mapping potential areas for groundwater storage in Wadi Aurnah Basin, western Arabian Peninsula, using remote sensing and geographic information system techniques. *Hydrogeology Journal* (2010) 18: 1481–1495.

Mavrantza O, Argialas D. *An object-oriented image analysis approach for the identification of* geologic lineaments in a sedimentary geotectonic environment.

Mehnaz Rashid & Mahjoor Ahmad Lone & Shakeel Ahmed 2011. Integrating geospatial and ground geophysical information as guidelines for groundwater potential zones in hard rock terrains of south India. *Journal, Environ Monit Assess.*

MEPNBRLA, 2009. Ministère de l'environnement, de la protection de la nature, des bassins de rétention et des lacs artificiels (MEPNBRLA):

Annuaire sur l'environnement et les ressources naturelles du Sénégal – deuxième édition, mai 2009.

Pinder GF 2002. *Groundwater modeling using geographical information system.* Wiley, New York.

R. K. Prasad N. C., Mondal Pallavi Banerjee., M. V. Nandakumar., V. S. Singh. 2007. Deciphering potential groundwater zone in hard rock through the application of GIS. *Journal, Environ Geol.*

Ramli M. F, Yusof. N, Yusoff. M. K, Juahir. H, Shafri, H. Z. M. 2009. Lineament mapping and its application in landslide hazard assessment: a review. *Journal Bull Eng Geol Environ.*

Savadogo A. N. 1984. *Géologie et hydrogéologie du socle cristallin de Haute Volta – Etude régionale du bassin versant de la Sissili.* Thèse d'Etat, Univ. Grenoble 1, Institut Dolomieu, 350 p.

Savané I. 1997. Contribution à l'étude géologique et hydrogéologique des aquifères discontinus du socle cristallin d'Odienné (Nord-Ouest de la Côte d'Ivoire). *Apports de la télédétection et d'un Système d'Information Hydrogéologique à Référence Spatiale.* Thèse d'Etat, Univ. Abidjan, 386 p.

Silverman, B. W. 1986. Density Estimation for Statistics and Data Analysis. New York: Chapman and Hall, 1986.

Sisay L. 2007. *Application of Remote Sensing and GIS for Groundwater Potential Zone Mapping in Northern.* Ada'a Plain (Modjo Catchment). Addis Ababa University, Addis Ababa – 1176; 77p.

Teeuw RM 1995. Groundwater exploration using RS and a low cost GIS. *Hydrogeol J* 3:21–30.

Théveniaut, H., Ndiaye, P.M., Buscail, F., Couëffé, R., Delor, C., Fullgraf, T., Goujou, J.-C., 2010b. Notice explicative de la carte géologique du Sénégal oriental à 1/500 000. Ministère des Mines, de l'Industrie, de l'Agro-Industrie et des PME, Direction des Mines et de la Géologie, Dakar.

Wuilleumier, A., Mall, I. et Ndiaye, P.M., 2010a. Carte hydrogéologique à 1/500 000 du Sénégal oriental. Ministère des Mines, de l'Industrie, de l'Agro-Industrie et des PME, Direction des Mines et de la Géologie, Dakar.

Wuilleumier, A., Théveniaut, H., Mall, I. et Ndiaye, P.M., 2010. Notice explicative de la carte hydrogéologique à 1/500 000 du Sénégal oriental, Ministère des Mines, de l'industrie, de l'agro-industrie et des PME, Direction des Mines et de la Géologie.

INDEX

C

D

G

H

Q

T